# Environment of West Antarctica, Potential CO2-Induced Changes: Report of a Workshop Held in Madison, Wisconsin, 5-7 July 1983 (1984)

Pages
248

Size
8.5 x 10

ISBN
0309325331

Committee on Glaciology; Polar Research Board; Commission on Physical Sciences, Mathematics, and Resources; National Research Council

# Environment of West Antarctica: Potential $CO_2$–Induced Changes

## Report of a Workshop Held in Madison, Wisconsin 5-7 July 1983

**Committee on Glaciology**
**Polar Research Board**
**Commission on Physical Sciences, Mathematics, and Resources**
**National Research Council**

**NATIONAL ACADEMY PRESS**
**Washington, D.C. 1984**

NOTICE: The project that is the subject of this report was approved by the Governing Board of the National Research Council, whose members are drawn from the councils of the National Academy of Sciences, the National Academy of Engineering, and the Institute of Medicine. The members of the committee responsible for the report were chosen for their special competences and with regard for appropriate balance.

This report has been reviewed by a group other than the authors according to procedures approved by a Report Review Committee consisting of members of the National Academy of Sciences, the National Academy of Engineering, and the Institute of Medicine.

The National Research Council was established by the National Academy of Sciences in 1916 to associate the broad community of science and technology with the Academy's purposes of furthering knowledge and of advising the federal government. The Council operates in accordance with general policies determined by the Academy under the authority of its congressional charter of 1863, which established the Academy as a private, nonprofit, self-governing membership corporation. The Council has become the principal operating agency of both the National Academy of Sciences and the National Academy of Engineering in the conduct of their services to the government, the public, and the scientific and engineering communities. It is administered jointly by both Academies and the Institute of Medicine. The National Academy of Engineering and the Institute of Medicine were established in 1964 and 1970, respectively, under the charter of the National Academy of Sciences.

Support for the conduct of this workshop and the preparation of this report was provided by the $CO_2$ Research Division of the Department of Energy under grant DE-FG01-ER-G0013.

Copies available in limited quantity from

Polar Research Board
2101 Constitution Avenue, N.W.
Washington, D.C. 20418

Printed in the United States of America

## Committee on Glaciology

Mark F. Meier (Chairman), U.S. Geological Survey, Tacoma, Washington
Colin B. Bull, Ohio State University
Gordon F. N. Cox, U.S. Army Cold Regions Research and Engineering Laboratory
Joan Gosink, University of Alaska, Fairbanks
Anthony J. Gow, U.S. Army Cold Regions Research and Engineering Laboratory
Michael Herron, Schlumberger-Doll Research
William D. Hibler, U.S. Army Cold Regions Research and Engineering Laboratory
John Kreider, Arctec, Inc.
Richard Moore, University of Kansas, Lawrence
Ronald I. Perla, Environment Canada
Uwe Radok, University of Colorado, Boulder
Richard C. J. Somerville, Scripps Institution of Oceanography

Ex officio
David Male, Chairman, Committee on Snow and Ice, American Geophysical Union

Agency Liaison Representatives
Thomas J. Gross, $CO_2$ Research Division, Department of Energy
G. Leonard Johnson, Arctic Programs, Office of Naval Research
Ned A. Ostenso, National Oceanic and Atmospheric Administration
Edward P. Todd, Division of Polar Programs, National Science Foundation

Staff
W. Timothy Hushen, Executive Secretary
Bertita E. Compton, Staff Officer
Muriel A. Dodd, Administrative Assistant

## Polar Research Board

Charles R. Bentley (Chairman), University of Wisconsin, Madison
W. Lawrence Gates, Oregon State University
Ben C. Gerwick, Jr., University of California, Berkeley
Richard M. Goody, Harvard University
Arnold L. Gordon, Lamont-Doherty Geological Observatory of Columbia University
Hans O. Jahns, EXXON Production Research Company
Philip L. Johnson, Lamar University
Arthur H. Lachenbruch, U.S. Geological Survey, Menlo Park
Louis J. Lanzerotti, Bell Laboratories
Chester M. Pierce, Harvard University
Juan G. Roederer, University of Alaska, Fairbanks
Robert H. Rutford, University of Texas, Dallas
John H. Steele, Woods Hole Oceanographic Institution
Ian Stirling, Canadian Wildlife Service
Cornelius W. Sullivan, University of Southern California

Ex Officio
Jerry Brown, Chairman, Committee on Permafrost
Mark F. Meier, Chairman, Committee on Glaciology
James H. Zumberge, U.S. Delegate to Scientific Committee on Antarctic Research of the International Council of Scientific Unions

Agency Liaison Representatives
Thomas J. Gross, $CO_2$ Research Division, Department of Energy
G. Leonard Johnson, Arctic Programs, Office of Naval Research
Ned A. Ostenso, National Oceanic and Atmospheric Administration
Edward P. Todd, Division of Polar Programs, National Science Foundation

Staff
W. Timothy Hushen, Executive Secretary
Bertita E. Compton, Staff Officer
Muriel A. Dodd, Administrative Assistant

## Commission on Physical Sciences, Mathematics, and Resources

# Participants in the Workshop on Potential $CO_2$—Induced Changes in the Environment of West Antarctica

H. van Loon (Chairman), National Center for Atmospheric Research
U. Radok (Convenor), University of Colorado, Boulder
S. F. Ackley, U.S. Army Cold Regions Research and Engineering Laboratory
C. R. Bentley (Chairman, Polar Research Board), University of Wisconsin, Madison
David H. Bromwich, Ohio State University
W. F. Budd, University of Melbourne
Andrew M. Carleton, Arizona State University, Tempe
W. T. Hushen (Staff Director, Polar Research Board), National Research Council
H. Lettau, University of Wisconsin, Madison
D. W. S. Limbert, British Antarctic Survey
C. Lorius, Laboratoire de Glaciologie
D. R. MacAyeal, University of Chicago
M. F. Meier (Chairman, Committee on Glaciology), U.S. Geological Survey, Tacoma, Washington
Olav Orheim, Norsk Polar Institute
Claire L. Parkinson, National Aeronautics and Space Administration
W. S. B. Paterson, Heriot Bay, British Columbia, Canada
Michael E. Schlesinger, Oregon State University
W. Schwerdtfeger, University of Wisconsin, Madison
Albert J. Semtner, Jr., National Center for Atmospheric Research
K. E. Trenberth, University of Illinois, Urbana
N. Young, University of Melbourne

# Preface

To respond to a series of questions posed by the $CO_2$ Research Division of the Department of Energy about the probable effects of increasing levels of atmospheric $CO_2$ on precipitation, summer temperatures, and ocean heat flux of West Antarctica, the Polar Research Board's Committee on Glaciology organized a workshop in July 1983 at the University of Wisconsin, Madison. This report includes the 12 presentations made at that workshop, summarizes the thrust of workshop discussion, and presents the Committee's initial responses to the questions together with its recommendations.

Because the topic is complex and the development of realistic models has been hampered by the lack of adequate field data, the Committee on Glaciology views this workshop as a beginning--the initiation of a dialogue between those engaged in modeling and those engaged in collection of data to better acquaint each group with the needs and problems of the other. As this report goes to press, plans are already in progress for a second workshop that will also be organized by the Committee on Glaciology and supported by the Department of Energy. The objective will be to explore further the relationship between land ice and sea level, in particular, the exchange of water between land ice and oceans over the past century and predictions for the future based on present models of the impact of increased atmospheric $CO_2$ on climate.

It is the Committee's hope that the report of the July 1983 Workshop will stimulate discussion, new questions, and increased research in this critically important field.

Mark F. Meier
Chairman, Committee on Glaciology

Charles R. Bentley
Chairman, Polar Research Board

# Acknowledgments

The Committee on Glaciology and the workshop participants wish to express their appreciation for the superb facilities provided by the Geophysical and Polar Research Center of the University of Wisconsin, Madison, and their particular gratitude to Alison Mares for the assistance she so graciously provided throughout the meeting.

The Committee also acknowledges with gratitude the support provided by the $CO_2$ Research Division of the Department of Energy, grant DE-FG01-ER-G0013, for the planning and conduct of the workshop.

# Contents

# 1. Executive Summary

It has been suggested that a rapid reduction of the ice mass of West Antarctica leading to a drastic rise in sea level might occur as a consequence of $CO_2$-induced warming. In this report, the climatic factors that provide the principal external forcing for the glacial ice of West Antarctica are examined, but the hypothesized dynamic mechanisms that could lead to a reduction of the ice mass in response to a change in the internal forcing are not dealt with explicitly.

In July 1983, the Workshop on Potential $CO_2$-Induced Changes in the Environment of West Antarctica, organized by the Committee on Glaciology for the Polar Research Board, National Research Council, was held in Madison, Wisconsin. Topics discussed included historical changes of atmospheric carbon dioxide and other environmental variables, changes of the polar ice sheets, knowledge of the present environment of West Antarctica, model simulations of the present environment, and model predictions of potential $CO_2$-induced changes.

A background discussion dealt with similarities and differences between environmental changes during the last glaciation and changes during the last hundred years, as reflected in ice cores. Of particular interest is the evidence of rapid changes in $CO_2$ concentration, especially during and at the end of the last glacial maximum. However, interpretation of the ice-core features will require further experimental work with ice-sheet and climate models. Preliminary modeling of the long-term behavior of the major ice sheets suggests that fluctuations of the Antarctic Ice Sheet appear to be induced in part by sea level changes caused by growth or decline of Northern Hemisphere ice sheets.

The existing West Antarctic environment is inadequately described by the available observations. This conclusion holds both for the general atmospheric and oceanic circulations and for their specific manifestations: the mass and energy balances of the inland ice sheet, the ice shelves, and the surrounding sea ice. In turn, the incomplete observational data create major uncertainties in assessing the validity of simulations of the West Antarctic environment by numerical models.

Atmospheric models have succeeded in reproducing qualitatively the broad patterns of pressure and temperatures for the Southern Hemisphere. However, there are systematic quantitative errors in the modeled surface temperatures over Antarctica and in the pressure of the

subtropical high-pressure belt and the subpolar trough. Corresponding deficiencies exist in the model representations of more complex features such as storms, including their numbers, regions of formations, and tracks.

Ocean models clearly require finer resolution in order to simulate crucial processes such as the thermohaline circulation and the formation of water masses affecting the large ice shelves. Models of the southern sea ice have given realistic results when driven by atmospheric and oceanographic forcing; in coupled simulations, on the other hand, inadequacies of the atmospheric and oceanic models used so far have resulted in less accurate simulation of sea-ice extent and very poor simulation of interannual changes.

Existing model predictions for strongly enhanced atmospneric $CO_2$ suggest only slightly higher summer temperatures and a moderate increase in precipitation for West Antarctica, together with an augmented production of Circumpolar Deep Water, which would affect the outer reaches of the large ice shelves. When translated into ice-shelf/ice-sheet dynamics, such changes produce conflicting trends. These will only be reconciled by improved ice-shelf/ice-sheet models and tuning with additional measurements from key regions. Therefore, with the present state of knowledge, quantitative predictions for the future of West Antarctica cannot be made with confidence.

The workshop recognized that opportunities to collect environmental data in Antarctica are sparse and the costs are high. In order to augment the existing set of data, the workshop therefore recommended:

- Establishment of an archive of all pertinent Antarctic data that can still be recovered, in which emphasis would be placed on certain periods, from individual years to weeks, at times when unusually large amounts of data were collected or when significant weather or oceanographic events occurred.

Recommendations of the workshop on testing and improving model simulations of the atmospheric environment include:

- Model validation studies, such as expanding model comparisons to additional variables, comparing computer and observed cyclogenesis and cyclone tracks, comparing simulated and measured surface energy balances over Antarctica, comparing simulated and measured snow and ice mass balances, extending comparisons to as many models as possible, and developing simulations of the interannual variability.
- Model sensitivity studies, including examining the pressure errors to see if they are due to the method for reducing to sea level, explaining the tendency to underestimate the Antarctic circumpolar trough, analyzing the effect of too smooth or too low topography on temperature and precipitation, and determining whether the less frequent cyclogenesis in certain regions results from the prescribed topography.
- Atmosphere-ocean simulations of $CO_2$-induced climate change, including improving control simulations (present climate) for sea ice and snow; analyzing the statistical significance of the simulations,

and studying the effects of simulated climate changes on the ice, snow, and water balance and on other major features such as the ice sheet and ice shelves.

- Testing model simulations of the oceanic environment, using finer-resolution ocean models and a sea ice-model that incorporates only the most essential physics; a specific strategy is proposed on page 26.

While such improved model experiments are being developed, there is great need for observations that could reveal current changes of the West Antarctic environment. The workshop recommended:

- Testing of predictions through new measurements and monitoring, including the establishment of new weather stations on Peter I Island, in the open and ice-covered ocean, and on the ice sheet; systematic observations of sea ice properties from ice breakers and research vessels; strain and velocity measurements and measurements to locate the grounding zone for ice streams draining the West Antarctic Ice Sheet; core drilling through the Filchner-Ronne Ice Shelf, and through the inland ice to clarify the history of the West Antarctic Ice Sheet back into the last interglacial; observations combined with theory and modeling on the calving process, and on the back stress exerted by shelves on the ice sheet; monitoring of features that might give early warning of effects predicted by the models, including a carefully planned set of physical and chemical measurements in the ocean; observations of sea-ice structural changes, and continuous monitoring of temperature and pressure trends; and satellite measurements, using radar or laser altimeters, to detect changes in ice-sheet elevation.

The assimilation of these data and focused modeling would be greatly aided by additional workshops and by a newsletter reporting all relevant research achieved and in progress.

# 2. Introduction

The current rise in $CO_2$ in the atmosphere will cause a rise in air temperature, which in turn may cause a rise in sea level due to the melting of glacial ice. This rise in sea level will be relatively manageable in the next century unless, as some scientists have suggested, the warming triggers a rapid reduction in the ice mass of the West Antarctic Ice Sheet. In order to assess the possibility that this could happen, two kinds of studies are required. First, the external climate factors that influence the West Antarctic Ice Sheet--mainly precipitation, summer temperature, and oceanic heat flux--need to be known. Second, the dynamic response of the ice sheet/ice stream/ice shelf system to changes in this external forcing needs to be understood. This report, and the workshop on which it is based, addresses the first of these tasks.

In response to a request from the Department of Energy, the Committee on Glaciology of the National Research Council's Polar Research Board organized the Workshop on Potential $CO_2$-Induced Changes in the Environment of West Antarctica, which was held at the Geophysical and Polar Research Center (C. R. Bentley, Director) of the University of Wisconsin, Madison. In its charge to workshop participants, the Committee on Glaciology called on them to address:

> ...regional changes in the precipitation, summer temperatures, and ocean heat flux of West Antarctica to be expected from increased atmospheric $CO_2$ concentrations....

The principal objectives of the workshop were to assist theoreticians and modelers in understanding the physical systems and to inform them about the data already available. In turn, field scientists would have a better idea of the data needed to improve models and would be better able to identify gaps in knowledge.

The following specific questions and suggestions were prepared for workshop consideration by T. J. Gross, $CO_2$ Research Division of the Department of Energy.

1. How adequate are climate model simulations in representing present conditions? (Variables, resolution, etc.) What additional variables should be calculated by general circulation models that might

be of use? Do inadequacies of present simulations affect model predictions elsewhere on the globe?

2. What information, including resolution and accuracy, is required to determine the sensitivity of the Antarctic ice sheet/ice shelves/sea ice to warming?

3. How can equilibrium climate model results be applied to analysis of time-dependent ice dynamics? (It is not foreseen that global climate models will be run in 400-year transient calculations; equilibrium results will have to be interpolated, if that is possible.)

4. What is the priority list for model improvements (ocean dynamics, sea ice, atmosphere, etc.)?

5. How can the use of global and regional models to improve simulations be coordinated?

6. What can be done to improve coordination between model and observational studies?

7. What should be done to encourage more individuals and groups to give these issues higher priority?

Consensus responses to these questions appear in the concluding chapter of the report.

It was suggested that in addressing most of these issues, the Antarctic problem might be subdivided into several nonexclusive domains:

1. Atmospheric conditions affecting the Antarctic ice cap/ice shelves.
   - a. Summer temperatures
   - b. Precipitation and storm frequency
   - c. Energy-balance components (including radiation, evaporation, etc.)
   - d. Other variables and processes
2. Ocean/atmosphere conditions affecting sea ice
   - a. Extent and thickness of sea ice, seasonal variations
   - b. Wind-induced breakup of sea ice
   - c. Energy-balance components affecting the thermodynamics of sea-ice formation
   - d. Ocean temperatures, bottom-water formation
   - e. Stratification (salinity, temperature, etc.)
   - f. Large-scale and local ocean dynamics
   - g. Ice accretion on the bottom of sea ice
   - h. Other variables and processes
3. Glaciological conditions affecting atmosphere and oceans
   - a. Albedo
   - b. Thermal conductivity
   - c. Density
   - d. Leads and polynyas
   - e. Other variables

In each of the domains, the workshop participants might consider the appropriate variables and parameters, comparisons of models with observations, sensitivity studies, and the like.

With this guidance, the workshop participants adopted the following five-point organization for the workshop agenda:

- Background: $CO_2$ and ice sheets
- Reviews of the present environment of West Antarctica
- Model simulations of the present Antarctic environment
- Model-predicted changes for increased atmospheric $CO_2$ and their critical assessment
- Conclusions, recommendations, and answers to the suggested questions

The presentations made by individual participants were supported with prepared statements that are included as attachments to this summary of the points made in the presentations and in the wide-ranging discussion.

# 3. Background: $CO_2$ and Ice Sheets

## 3.1 CHANGES IN CLIMATE AND $CO_2$ INFERRED FROM ANTARCTIC ICE CORES (see Attachment 1, by C. Lorius)

Most data from Antarctic ice cores on changes in $CO_2$, climate, aerosols, and ice thickness relate to East Antarctica, with the exception of those obtained at Byrd Station. These cores have been intensively studied for the most recent glaciation and for the last hundred years. Although radically different in most other respects, during both these periods changes of the order of 30 percent in the (inferred) concentration of atmospheric $CO_2$ occurred. The newest analyses show that at the end of the ice age (Figure 1), and even near the height of the glaciation, changes in concentration ranging from 200 to 340 ppm (the present value) occurred within intervals of the order of $10^3$ years or less. Ice cores obtained from Greenland, of higher temporal resolution, suggest that the fluctuations occurred in times of only $10^1$ to $10^2$ years (Stauffer et al. 1984). In recent times the concentration appears to have reached a minimum of around 260 ppm 100 years ago, at the start of the industrial revolution, an amount that is significantly lower than that so far assumed in models of the different $CO_2$ reservoirs (Raynaud and Barnola 1984). But whereas the $CO_2$ increase at the end of the last glaciation was accompanied by stable isotope changes, suggesting temperature rises of the order of 8-10°C at the surface of the ice sheet and somewhat smaller changes above the surface inversion, the recent $CO_2$ increase has occurred without a clear Antarctic temperature trend. A marked decrease in aerosol loading from the ice ages to the Holocene also has no modern equivalent; it has been attributed to significantly lower (30-50 percent) wind speeds in the Holocene. By contrast, evidence that accumulation rates became around 25 percent larger in the Holocene offers a parallel (albeit of a different time scale) to a 30 percent increase in Antarctic precipitation during 1965-1975 over the values that prevailed during 1955-1965. Analyses of total gas content in various cores suggest no major differences in ice thickness, except for a coastal belt from the ice age to today. More cores are needed, especially from West Antarctica, to secure data that might explain these agreements and contrasts and to establish the relative timing of the changes in different features.

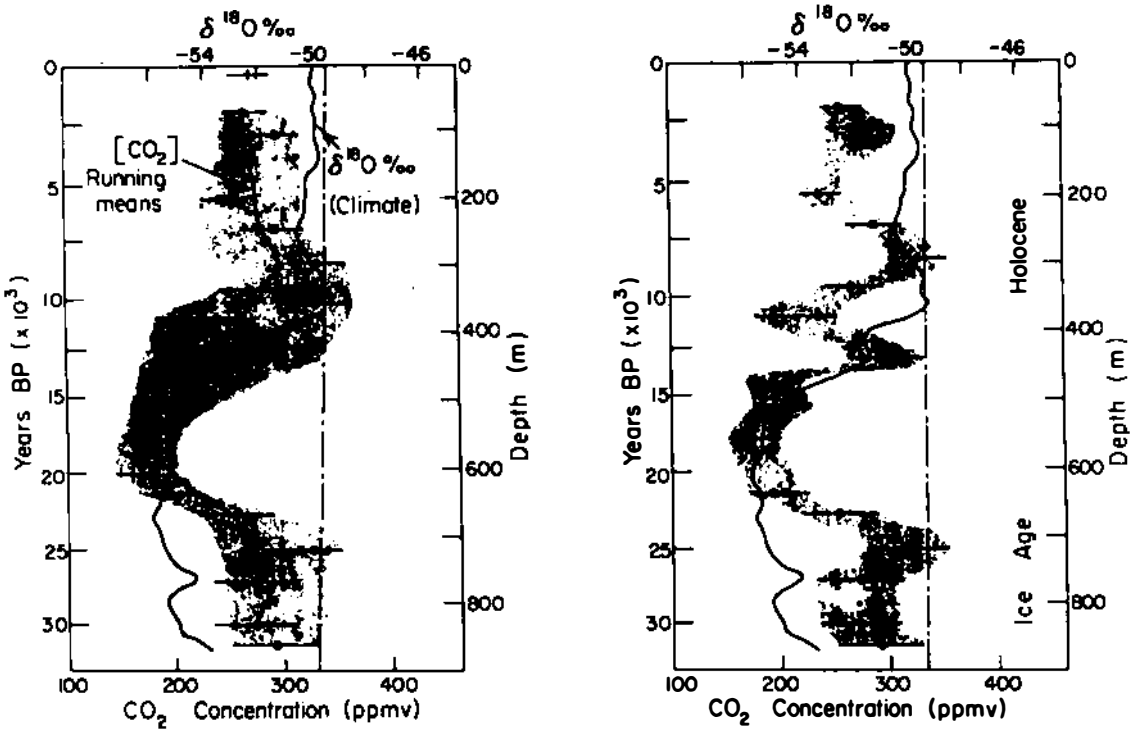


**Figure 1.** $CO_2$ concentrations and stable isotope content in the Dome C ice core plotted as a function of age and depth (meters of ice). For the $CO_2$ concentrations, two "extreme" ranges of variation are shown. The left one takes into account measurements performed also on another Antarctic core. The right one, based only on Dome C results, suggests shorter-term natural fluctuations. Solid line ($\delta^{18}O$) relates to air temperature at the time of snow condensation. (Original data from Delmas et al. 1980.) (See also Attachment 1.)

## 3.2 CHANGES IN CLIMATE AND THE ICE SHEET INFERRED FROM ICE-SHEET MODELING (W. F. Budd)

Various model experiments have demonstrated that changes in the great northern ice sheets could have resulted from orbital variations in insolation at key latitudes and reactions of the earth's crust, plus precipitation changes produced by the ice sheets themselves. A recent series of experiments has used the resulting changes in sea level as forcing for models of the Antarctic Ice Sheet (Figure 2). The result is a global glaciation/sea-level sequence that is in accord with the ocean-sediment record and provides an example of the recurrence of major interglacials at 100,000-year intervals, which has characterized the last 500,000 years. This sequence could offer yet another explanation of the 100,000-year "cycle" that is absent from the orbital frequencies. A major problem for achieving realistic model shapes and extents for the Antarctic Ice Sheet is inadequate understanding of the basal sliding of the large ice streams, which produces high velocities

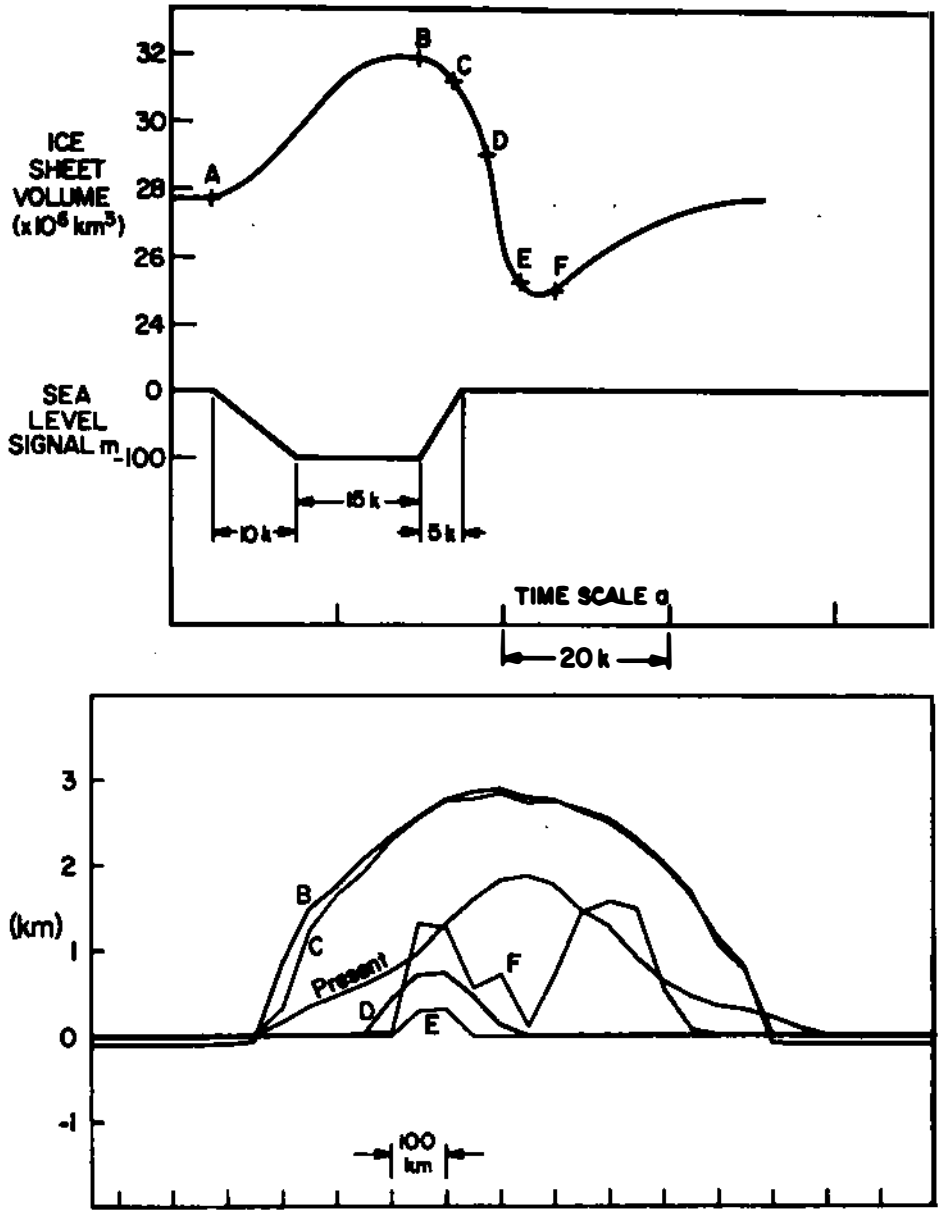


**Figure 2. Three dimensionally modeled reaction of the Antarctic Ice Sheet to a sea level change produced by the growth and decline of the Northern Hemisphere ice sheets. (Top) Curve 1 shows assumed sea-level change; curve 2 gives the change in the total Antarctic ice volume. (Bottom) Curves show the changing surface elevation of a cross section corresponding to the different stages of the total volume change (curve 2). (From Smith 1984.)**

for small gravitational downstream forces (balanced by equally small base and perhaps lateral and longitudinal stresses). Planned velocity measurements on the West Antarctic ice streams flowing into the Ross Ice Shelf are expected to clarify this feature.

# 4.
# Reviews of the Existing West Antarctic Environment

## 4.1 VARIABILITY OF THE ATMOSPHERIC CIRCULATION AT THE SURFACE OF THE SOUTH PACIFIC OCEAN IN SUMMER (see Attachment 2, by H. van Loon)

Weather systems dominating the South Pacific in summer were illuminated for the first time since the opening of the Panama Canal by the daily weather reports from whaling ships during the summers of 1955-1958. The last of these summers was marked by a warm "El Nino" event in the tropical eastern Pacific, so that despite its brevity, the record covers a wide range of conditions. The mean thermal and flow patterns exhibit the marked semiannual oscillation first fully reported by Schwerdtfeger (1970) (Figure 3)--a polar trough pulsation or pressure seesaw between the Antarctic continent and the Southern Ocean. The features of subsequent years with good observational cover need to be viewed against that background. Both the 1973-1974 summer and the First GARP Global Experiment (FGGE) year, 1979, were marked by relatively low pressures over the continent and high pressures over the oceans, whereas the summer of 1976-1977 had abnormally low pressure over the oceans and high pressure over Antarctica. In the 1976-1977 summer, another warm event occurred in the equatorial Pacific, with lower-than-normal pressure in the Pacific subtropical high and higher-than-normal pressure over Australasia, whereas in 1973-1974 the converse pressure distribution was found. Undoubtedly, the sea surface temperature at the equator in the Pacific is associated with the circulation in temperate and high southern latitudes.

The cyclonic depressions that affect the weather of West Antarctica in summer come from middle and even subtropical latitudes in the eastern Indian Ocean and western Pacific. The mean geostrophic wind between 35°S and 55°S ("zonal index") undergoes large short-term and interannual changes, and a similarly high synoptic variability is found around the West Antarctic coast. This makes the existing short records inadequate for testing the mean features of model simulations. However, the possibility exist that some of the essential eddy features are correctly modeled.

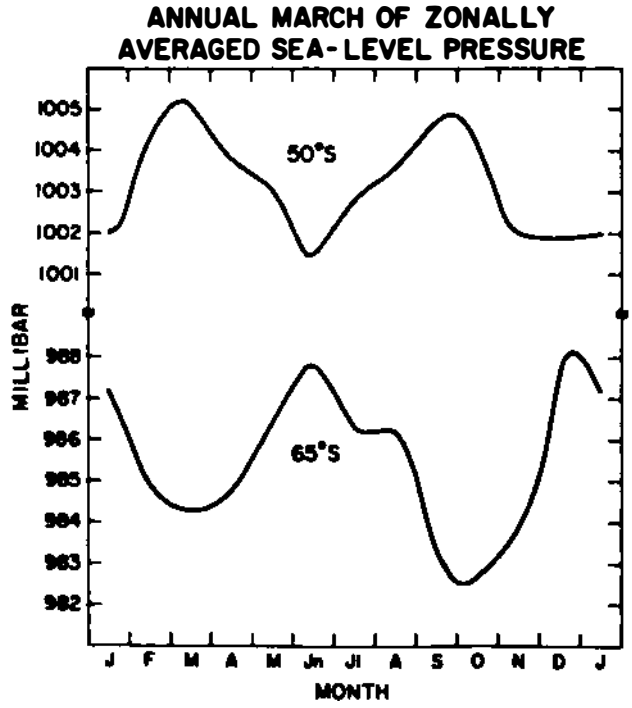


Figure 3. The semiannual pressure oscillation of the Antarctic region. (See also Attachment 2.)

## 4.2 THE ATMOSPHERIC CIRCULATION AFFECTING THE WEST ANTARCTIC REGION IN SUMMER (see Attachment 3, by K. E. Trenberth)

The circulation of the midtroposphere of West Antarctica in summer can be described by statistics based on the daily constant pressure level charts of the Australian Weather Service for the period 1972-1980. The main patterns are broadly zonal, with a ridge in the Australian sector (the most pronounced blocking region of the Southern Hemisphere) and rather uniform thermal gradients in the lower troposphere between 30° and 70°S. This uniform pattern hides a considerably more interesting eddy reality, which the variability of geopotential heights shows to be dominated by the sequence of highs and lows and, on a somewhat lower frequency, by blocking episodes.

Interannual variability and pronounced longer-term fluctuations are prominent features of the Southern Hemisphere circulation. The different circulation regimes that exist in different years and decades provide clues to the kinds of natural extremes that can occur and give indications of the kinds of changes than may well accompany a $CO_2$ warming. For example, in the summer of the FGGE year (1978-1979), the jet stream was displaced poleward by 3° (Figure 4), with a polar trough

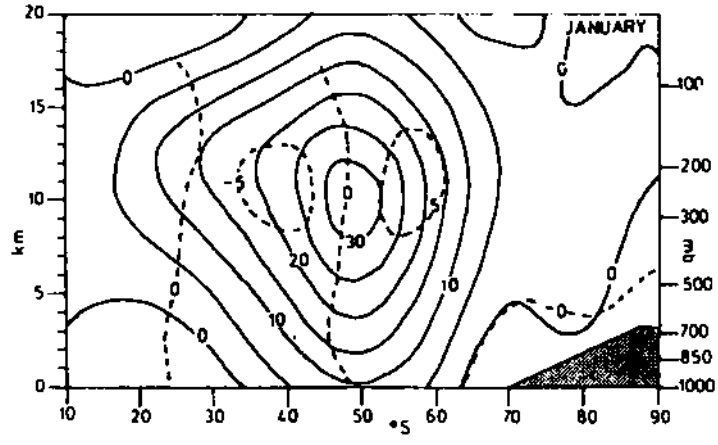


Figure 4. Meridional cross section of the zonally averaged wind (m $s^{-1}$) for January 1979. The dashed contours give the differences from the means for 1973-1978. (See also Attachment 3.)

much deeper than its (9-year) average. A particularly marked contrast existed between the summers of 1976-1977 and 1978-1979; the former had weak zonal flow, whereas the westerlies were strong in the latter. The main jet was displaced southward by 6° latitude in 1978-1979 relative to 1976-1977, and this displacement was accompanied by a corresponding shift in the high-latitude storm tracks. In 1978-1979 this displacement led to high-temperature extremes at stations as distant from one another as McMurdo, Halley Bay, and South Pole.

Although there are difficulties with the available data, longer-term trends are also clearly evident in the circulation over and around Antarctica. The high level of natural variability will make any $CO_2$ effects difficult to isolate.

## 4.3 WEST ANTARCTIC SEA ICE (see Attachment 4, by S. F. Ackley, and Attachment 12, by Claire L. Parkinson)

Sea ice plays many roles in the present environment of West Antarctica. In addition to the classical ice-albedo feedback, consideration must be given to the changes accompanied by formation of sea ice on the oceanic pycnocline and, over longer periods, on the temperatures of the deep ocean. Moreover, the free northern edge of the pack-ice belt is the site of interactions with atmosphere and ice-free ocean on scales ranging from the subsynoptic to the hemispheric.

The sea ice in the western Weddell Sea, the Amundsen-Bellingshausen Seas, and the Ross Sea first received continuous surveillance with the

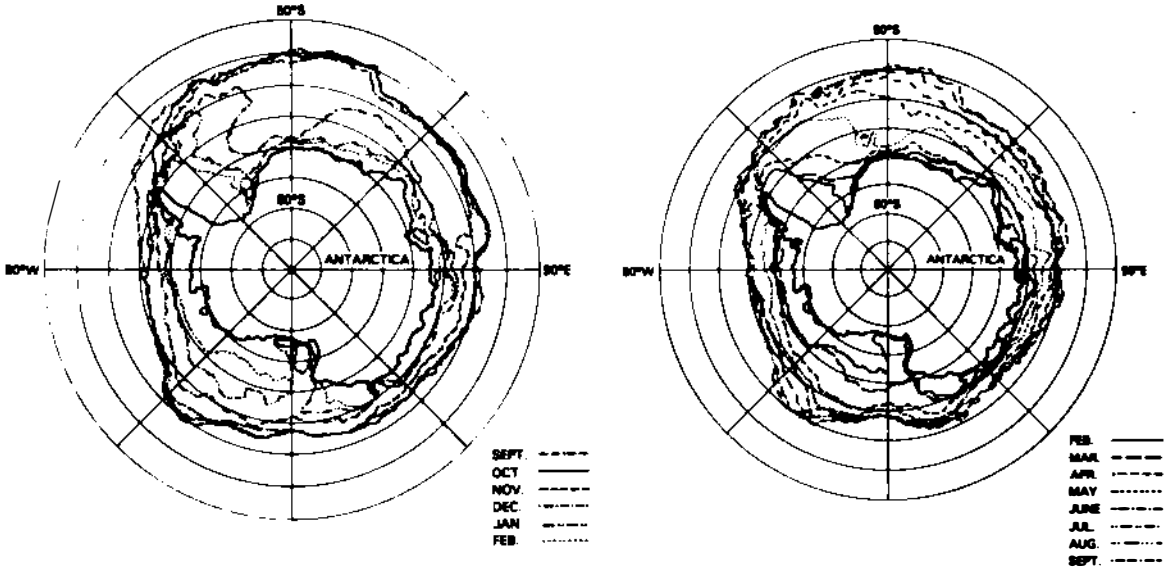


**Figure 5. Average monthly ice limits 1973-1976, from Nimbus 5 ESMR data. (See also Attachment 12.)**

electrical scanning microwave radiometer (ESMR) on the Nimbus 5 satellite during 1973-1976 (Figure 5). The analysis of these data (Zwally et al. 1983) shows that after the spring and summer months, most of the residual Antarctic sea ice, covering about $4 \times 10^6$ km$^2$, is found around West Antarctica. At the time of the maximum extent, the Amundsen-Bellingshausen sector, which has the smallest seasonal variation, accounts for 20 percent of the West Antarctic sea ice; the Weddell Sea contains about one half, and the Ross Sea, the remaining 30 percent.

The sea-ice covers of both the Ross and Weddell seas exhibit a relatively precipitous decline during the months from November through January. The life of the winter ice cover in the Weddell Sea may be prolonged by its advection along the Antarctic Peninsula to lower latitudes, where it is quickly melted (Figure 6).

Ice conditions in the Weddell Sea are now somewhat better known than those in the Ross and Amundsen-Bellingshausen seas, where information on drift comes solely from the tracks of two ships trapped in the ice in 1897-1899 (Belgica) and 1915-1916 (Aurora). New data on the small-scale structure of the Ross Sea ice pack have recently been obtained by airborne laser profiling, but a great need remains for observations of ice characteristics from all ships encountering the pack ice on resupply voyages and in biological projects.

The interannual variation over the period of satellite surveillance shows no clear trend in ice extent. A decrease in the mid-1970s was temporary, being both preceded and followed by larger ice covers. Interannual changes have varied in different sectors: the maximum ice area of the Ross Sea increased from 1973 through 1975, then decreased in 1976, whereas the ice cover of the Weddell Sea shrank from 1973 to

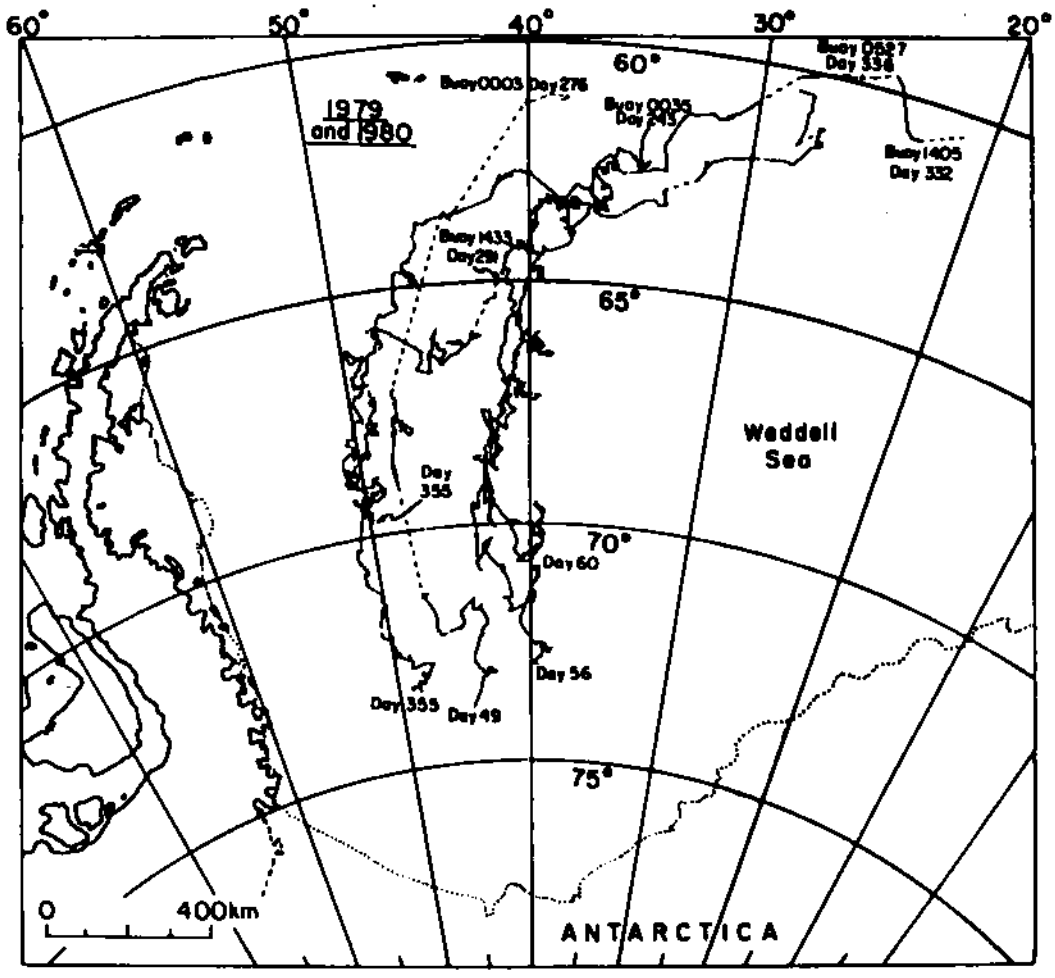


**Figure 6. The drift of Weddell Sea ice. (See also Attachment 4.)**

1974, and again from 1975 to 1976, but increased from 1974 to 1975 (see Zwally et al. 1983).

The satellite data also provide some idea of ice concentrations and ice types, but as noted by the recent Meeting of Experts on the Role of Sea Ice in Climate Variations,[1] there is an urgent need for ground truth observations and measurements to verify the results of remote sensing and to establish a fuller picture of the structural, dynamic, and thermodynamic characteristics of Antarctic sea ice.

[1]Organized in Geneva, Switzerland, in June 1982, by the World Meteorological Organization together with the Joint Scientific Committee of the World Climate Research Program and the Committee for Climatic Changes in the Ocean.

## 4.4 ASSOCIATED CHANGES IN WEST ANTARCTIC CYCLONE ACTIVITY AND SEA ICE (see Attachment 5, by Andrew M. Carleton)

An analysis of early satellite photos by Schwerdtfeger and Kachelhoffer (1973) showed that the latitude belt dominated by Southern Ocean depressions moves north and south with the seasonal expansion and contraction of the pack ice. More recently, the developmental stages of the depressions could be distinguished from details of their cloud "signatures." It was found that in winter, the peak frequency of cyclogenesis coincides broadly with the location of the ice edge, which then is close to frontal zones in both the atmosphere and the ocean. In summer, cyclogenesis largely occurs well north of the ice edge in the region where the meridional temperature gradient in the lower troposphere has its maximum (Figure 7).

The decay of depressions ("cyclolysis") occurs preferentially in the embayments of West Antarctica where the sea ice exhibits its highest variability. In the Ross and Amundsen seas, to the west of the region with the greatest number of cyclones, the ice tends to be advected toward the equator, and the ice extent changes interannually with the strength of a mean cyclonic circulation over that region. In the Weddell Sea the relationship between the strength of the atmospheric mean circulation and the extent of the sea ice is less close, suggesting that the dominant effects on the sea ice come from the oceanic gyre. Some differences in cyclonic activity have been noted between the years when the Weddell Sea Polynya was present or absent, but the number of these contrasting years is too small to draw firm conclusions.

In the discussion, examples of cyclone tracks running along the ice edge were noted, as were others that extended across the pack ice into the center of West Antarctica (Figure 8). It was suggested that analysis of cyclone intensity, separate from that of cyclonic numbers, is needed. Such analysis could use statistical relationships in terms of cloud signature features established by Streten and Troup (1979).

## 4.5 PRECIPITATION REGIME OF WEST ANTARCTIC ICE SHEET (see Attachment 6, by David H. Bromwich)

Solid precipitation, which predominates in Antarctica, is difficult to measure in the windy conditions of the region. For glaciological purposes the net snow accumulation (which includes also the effects of drift, rime and hoar frost formation, and evaporation) is the crucial parameter. However, the vortices (Figure 8) giving rise to precipitation are of interest in their own right, as environmental features represented in models and likely to undergo systematic changes in nature.

Apart from the Antarctic Peninsula, the only coastal observations in West Antarctica are those recently started at Russkaya, where upper-air observations would be particularly valuable. Precipitation is deduced from surface mass balance measurements at a few widely scattered sites (Little America, Byrd, Ellsworth, and the stations in

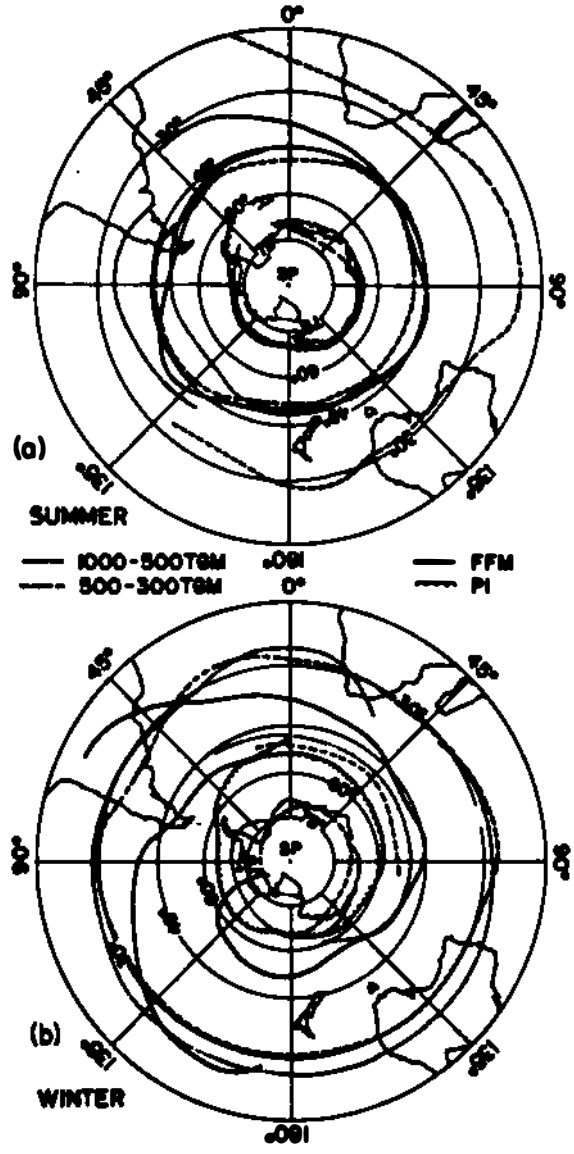


**Figure 7. Surface frontal frequency maxima (FFM), 1000- to 500-mbar and 500- to 300-mbar thickness gradient maxima (TGM), and pack-ice limits (PI) for summer. (From Taljaard 1972, Figure 8.9.)**

the Antarctic Peninsula). In principle, these net accumulation records can be extended into the past by data from pits and boreholes. The average mass gain of the ice sheet constructed from such data is in broad agreement with the moisture flux across the periphery of the ice sheet, as calculated from radiosonde observations by Rubin and Giovinetto (1962), Lettau (1969), and Bromwich (1979).

Information on the mechanisms of Antarctic precipitation can be drawn from a few detailed series of accumulation measurements made during the International Geophysical Year (IGY) and isolated later

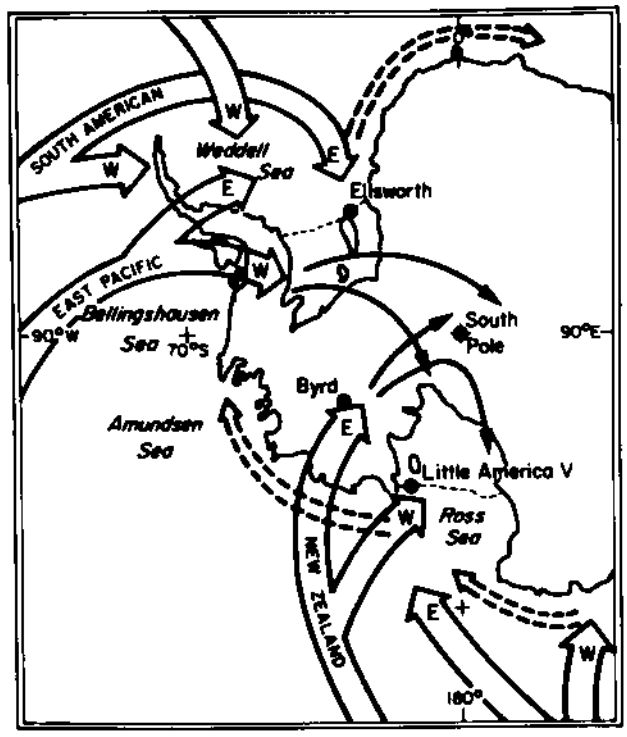


**Figure 8. Tracks of sea level (double arrows) and 700-mbar (single arrows) vortices during 1958. (After Rubin and Giovinetto 1962.) (See also Attachment 6.)**

years. Examples of the latter are the measurements made by Dingle at Byrd during 1962 and at Plateau Station during 1967, and the fully published Japanese measurements at Syowa and Mizuho. The IGY measurements for the summers 1956-1957 and 1957-1958 are especially valuable in view of the concurrent synoptic analysis for the southeastern Pacific (see also Section 4.1). Vickers (1966) analyzed the synoptic circumstances of the major precipitation episodes in the IGY and established their space and time scales. That work and the budget analysis of Bromwich (1979) have shown that a substantial part of the total mass gain accumulates during a small number of precipitation events, in contrast to East Antarctica, where precipitation is more continuous.

An intriguing feature of the West Antarctic oceanic precipitation regime noted by Loewe (1957) is its tendency to shower-type precipitation. The relative frequency of showers reported from the southeast Pacific and South Atlantic is 28 percent; this amount decreases to 22 percent for the South Indian Ocean and falls as low as 10 percent between 135°E and the entrance to the Ross Sea. The synoptic mechanisms producing these contrasts merit further investigation.

## 4.6 WEST ANTARCTIC TEMPERATURE RELATIONSHIPS AND THE NOMINAL LENGTHS OF SUMMER AND WINTER SEASONS (see Attachment 7, by D. W. S. Limbert)

West Antarctic temperature regimes are now quite well defined by the records kept since the IGY. Key stations in the present context are Faraday (Argentine Islands) and Byrd (in the center of West Antarctica). Their seasonal and annual temperatures lack any significant correlation; however, the Byrd temperatures throughout the year are strongly correlated with those measured at McMurdo, and there appears to be a moderate correlation between Faraday and Macquarie Island in the southwest Pacific. Lag correlations suggest that anomalies of the summer temperatures at McMurdo may be influenced by anomalies in spring temperatures at Faraday, perhaps through the westward drift of coastal sea ice. On an annual basis, however, the correlation is higher in the opposite direction.

Temperature anomalies along the Antarctic Peninsula can be deduced to some extent from the incidence of four synoptic patterns that, depending on the latitude of the polar trough, place a station into easterlies or westerlies, into the trough itself, or into the col between two high-pressure regions. For Faraday, the easterly type of situation appears to have come into dominance during the 1970s, with higher-than-average temperatures in all seasons.

The relative lengths of the summer and winter seasons are important for understanding changes in the production of sea ice. They can be defined physically by the absence or presence of a surface inversion, which is also reflected in the daily maximum temperatures. In this way, it was found that the high temperatures of the 1970s at Faraday resulted primarily from the early end and late start of the winter season.

The estimation of temperature trends (Figure 9) must take into account local effects and is limited by the relatively short periods during which temperatures have been observed. Proxy indicators that can be used to extend the instrumental records include, in addition to the stable isotopes in ice cores (see Section 3.1), a statistical relationship between the annual rate of net accumulation and the annual mean temperatures, first established by Mellor (1963). In this way it becomes apparent that changes in Antarctic temperature trends in the last 100-200 years have been within the range of natural variability. In particular, the warming trend of the early 1970s has been reversed in more recent years. Few long-term data from West Antarctica exist; deployment of additional automatic weather stations is an urgent need.

## 4.7 SURFACE MELT ON ANTARCTIC ICE SHELVES (see Attachment 8, by W. S. B. Paterson)

Melting on Antarctic ice shelves (Figure 10) represents an environmental feature of special interest for assessing the vulnerability of the ice shelves to $CO_2$-induced polar warming. Such meltwater generally does not represent a mass loss; it percolates into

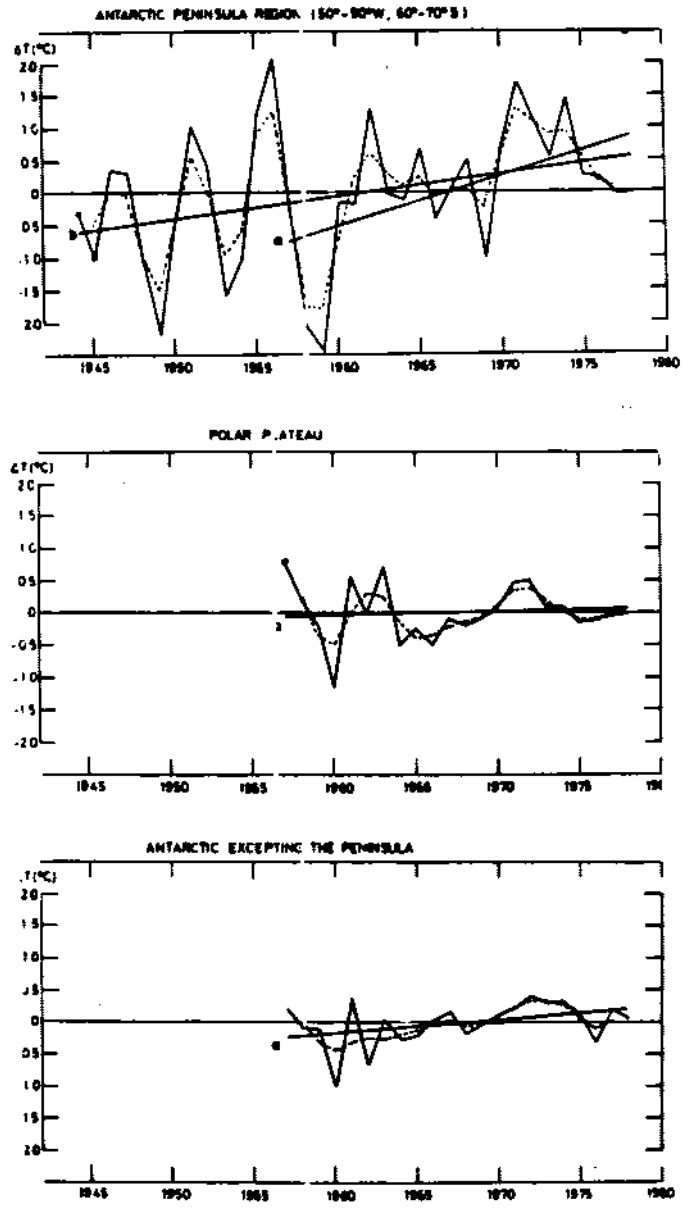


**Figure 9. Antarctic temperature trends. Symbol "a" marks regression lines from 1956-1978; "b" marks regression line for entire peninsula record. (See also Attachment 7.)**

the firn and by refreezing warms the upper layer of the ice shelf more rapidly and efficiently than can be done by conduction in firn at temperatures below melting. If the increase in near-surface firn temperatures were of the order of 5°C, it could affect a large part of the flat ice-shelf surface. The main effect of the temperature increase would be to increase the ice-shelf spreading and calving rates, but the penetration of the warming into the interior of the ice

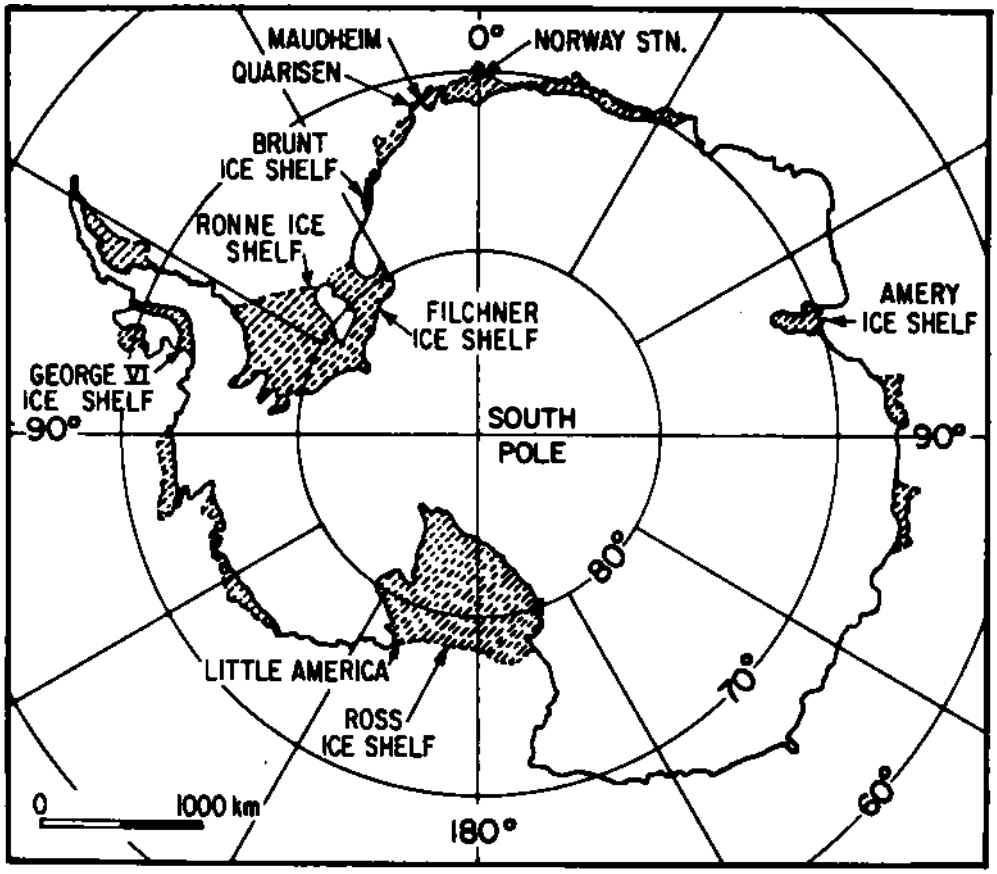


**Figure 10. The principal ice shelves of Antarctica. (See also Attachment 8.)**

shelf would take considerable time, if only because the heated top layer is continually lost to the sea by calving.

A first estimate of the present occurrence of surface melt on ice shelves can be based on a small number of detailed temperature observations. Present temperatures exceeding -6°C during the summer months might qualify for melting according to some $CO_2$ scenario, but the amount of melt would depend on the energy balance and could change radically if intermittent snowfalls restore the surface albedo to around 85 percent from the lower value of a melting surface and delay the resumption of melt.

The first detailed ice-shelf record of meltwater percolation was obtained from an ice core extracted from the Maudheim Ice Shelf, at a latitude of 71°S, and showed that up to 15 percent of the annual mass accumulation was melted and frozen in some years; however, hardly any melt occurred in the years of direct instrumental observations (1950-1952). Further west in the same latitude on the George VI Ice Shelf, the entire winter snow melts in summer, and some meltwater runs off to the sea. Further south, at Little America (78°S), on the edge of the Ross Ice Shelf, positive surface air temperatures during four

sets of summer months (November through February) failed to occur in one summer and existed for as many as 137 hours in another. This amount would rise to around 1,400 hours, or half of the entire summer, if ambient air temperatures of the ice shelf rose by 4°C. More definite results need to be derived from detailed surface energy balance calculations, including the effects of advection, for which Lettau (1977) has provided a highly sophisticated "climatonomy" procedure. It was suggested that useful clues might be provided by icebergs that have reached the warmer waters north of the Antarctic Convergence.

The probable effects of an increased concentration of atmospheric $CO_2$ on the major ice shelves include increased surface mass balance, due to increased precipitation; increased surface melting, which will not represent appreciable loss of mass; increased surface temperature, which will, in time, increase the spreading rate and tend to thin the shelf; and increased basal melting, which will remove the warmest ice and decrease the mean temperature, possibly tending to decrease the spreading rate and thicken the shelf. A numerical model that treats ice flow and heat transfer simultaneously will be needed to estimate the relative importance of these different effects.

# 5.
# Model Simulations of the Present Antarctic Environment

## 5.1 ATMOSPHERIC GENERAL CIRCULATION MODEL SIMULATIONS OF THE MODERN ANTARCTIC CLIMATE (see Attachment 9, by Michael E. Schlesinger)

Antarctic features can be extracted from the published results for at least six different models. The polar regions in most cases were not of primary interest, and comparison of the realism achieved by different simulations for the Antarctic region is rendered difficult by the different map projections used and by the absence of consistent displays. Therefore, for this workshop, a special effort was made to obtain the relevant information from the various modelers and to convert it to a common and comparable form. Features examined were the sea-level pressure, surface air temperature, precipitation rate, and synoptic characteristics (cyclogenetic regions and tracks of storms). Illustrations presented here show only examples of the results that are presented more completely in Attachment 9.

The sea-level pressure fields simulated with prescribed realistic sea surface temperatures generally show the Antarctic low-pressure trough in the observed position, with mean pressures higher than observed, especially in winter (Figure 11). It was pointed out, however, that the current synoptic charts tend themselves to be in error over the pack-ice belt and in the "barrier wind" regions of the western Weddell and Ross seas.

The model pressures also are generally too high over the Antarctic continent, although this may represent in part an artifact involving reduction to a nonexistent sea level from the prescribed smoothed surface elevations. More relevant comparisons could possibly be made for the 500-mbar surface, but the necessary model data generally have not been reported.

The observed surface air temperature field is well matched by most models over the Southern Ocean, where the sea surface temperature is given its climatological value (Figure 12). The surface air temperatures given by the models over the Antarctic continent are generally too warm; they could perhaps be interpreted as applying to some level inside the surface inversion, but it is not clear that the correct magnitude of the surface heat and moisture exchanges is being achieved.

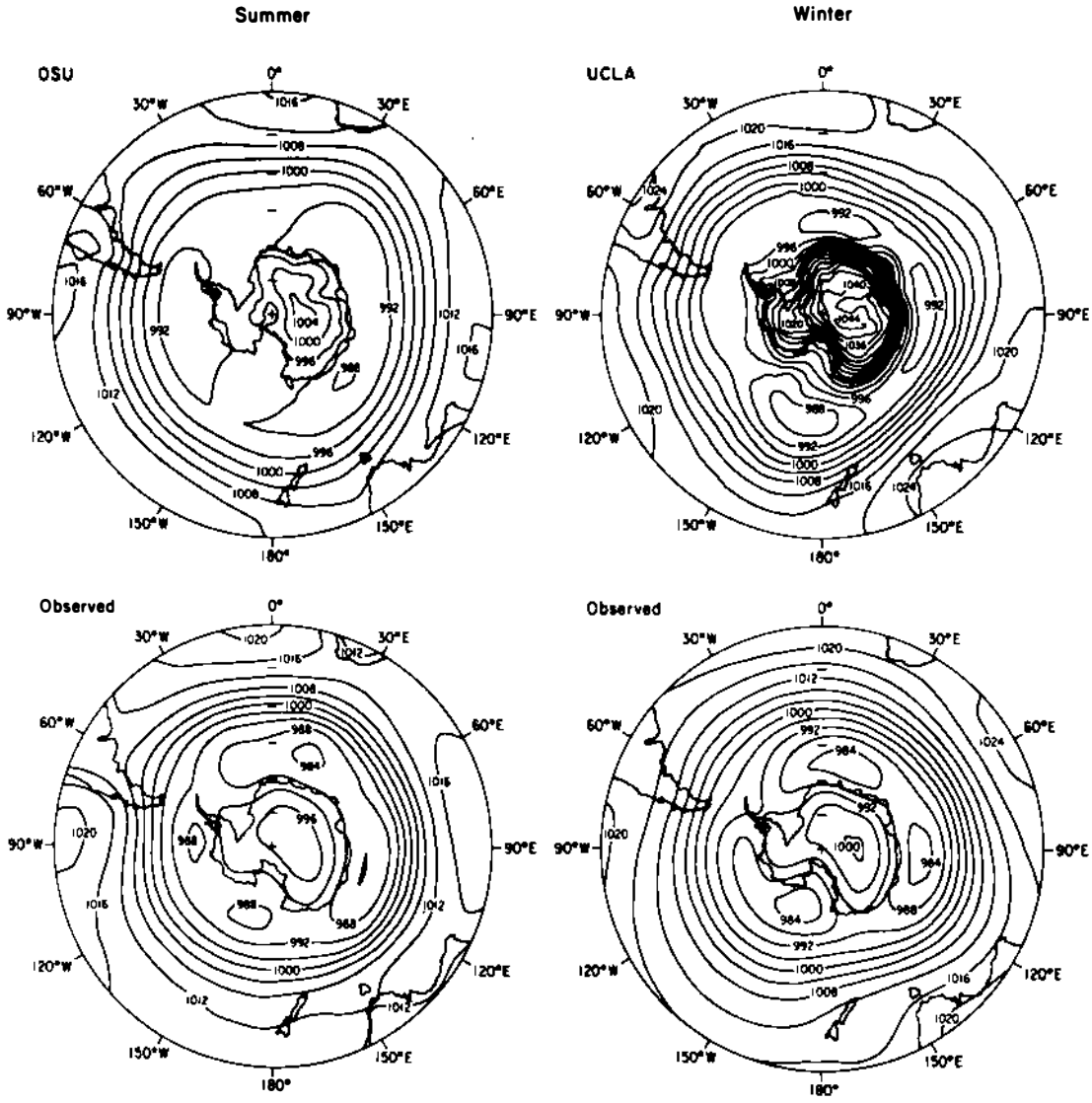


**Figure 11. The simulated and observed Southern Hemisphere sea-level pressure (mbar) for summer and winter. The mean January sea-level pressure simulated by the OSU[1] model is shown for summer, and the mean July sea-level pressure simulated by the UCLA[2] model is shown for winter. The observed January and July sea-level pressures are shown based on Taljaard et al. (1969), as tabulated by Schutz and Gates (1971, 1972).**

[1] Oregon State University, Climatic Research Institute, Corvallis.
[2] University of California, Los Angeles, Department of Atmospheric Sciences.

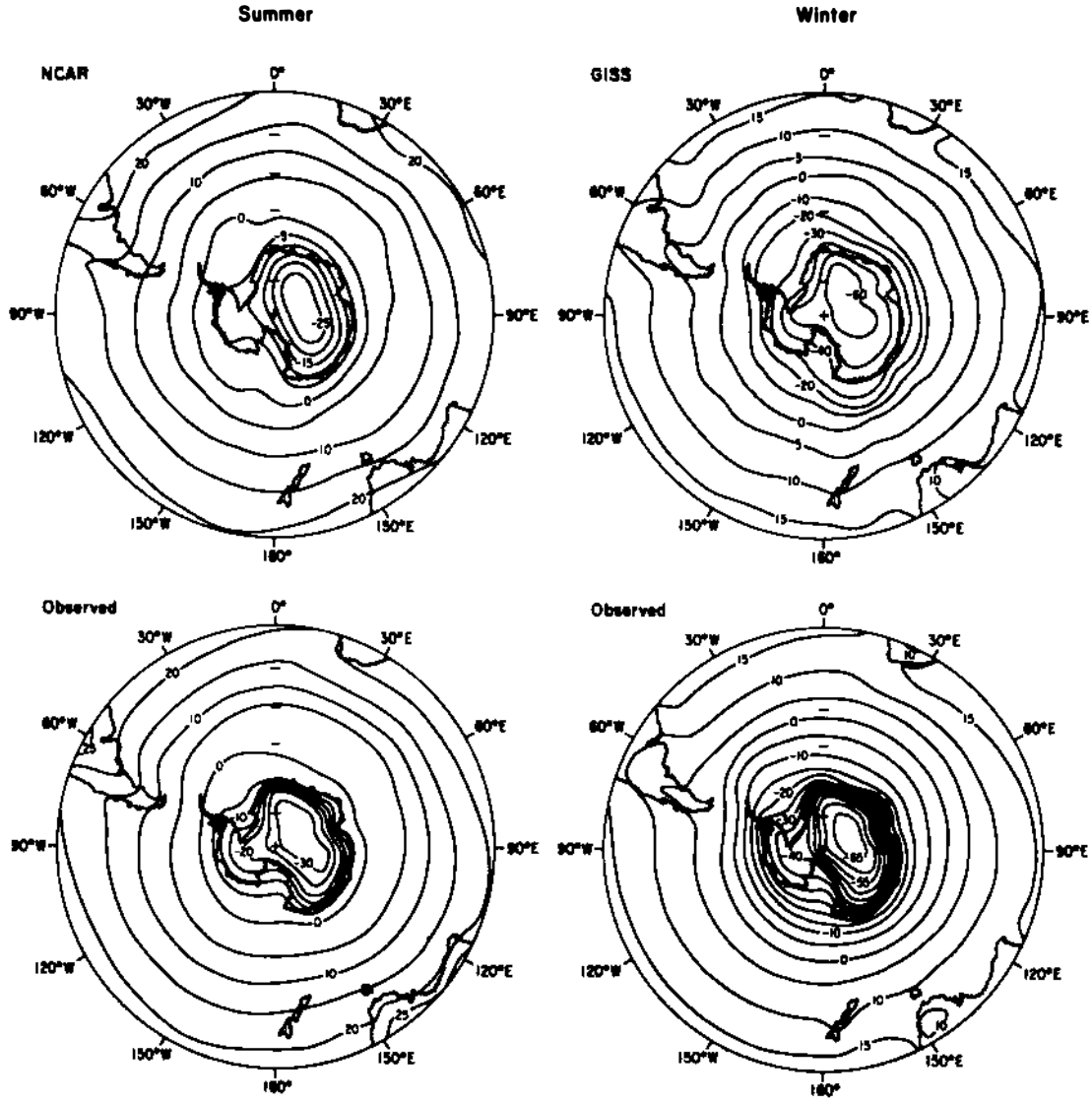


**Figure 12. The simulated and observed Southern Hemisphere surface air temperatures (°C) for summer and winter. The mean January temperature simulated by the NCAR[1] model is shown for summer, and the mean July temperature simulated by the GISS[2] model is shown for winter. The observed January and July temperatures are shown based on Taljaard et al. (1969) as available from the NCAR archive (Jenne 1975).**

[1] National Center for Atmospheric Research, Boulder, Colorado.
[2] NASA Goddard Space Flight Center Institute for Space Studies, New York.

The simulated precipitation amounts over the continent are generally larger than the climatological values (Figure 13). However, the latter are generally uncertain, and comparisons in terms of model and observed moisture budgets might prove more conclusive.

The most sophisticated and informative comparisons concern the formation and movement of synoptic systems, which, in their aggregate, give rise to the monthly mean features of pressure, temperature, and precipitation. The model simulations generally fail to reproduce some important cyclogenetic regions (e.g., east of South America and south of Australia) and create spurious ones, especially near the coast of Antarctica. Moreover, the number of simulated storms tends to be significantly smaller than that observed.

The overall conclusion that the existing atmospheric models do not provide adequate simulations of the present West Antarctic climate should be qualified by stressing the inadequate climatology that exists for the region and the limited information obtainable from simple comparison of simulated and "observed" mean fields. This qualification underlines the need for increased attention to synoptic features, both when assessing model simulations and when describing the West Antarctic environment.

## 5.2 ON MODELING THE OCEANIC ENVIRONMENT OF WEST ANTARCTICA, INCLUDING $CO_2$-INDUCED CHANGES

(see Attachment 10, by Albert J. Semtner, Jr.)

Although the majority of simulations of Antarctic climate have been conducted with prescribed sea surface temperatures (SST) and sea-ice distributions, there are an increasing number of simulations in which SST and sea ice are predicted. These simulations, like those described in the preceding section, are being carried out with a hierarchy of ocean/sea-ice models varying from a "swamp" ocean, with zero heat capacity and no heat transport, to the oceanic general circulation model (GCM), which is the counterpart of the atmospheric GCM in comprehensiveness and complexity. Such sophisticated representations of the ocean can simulate the formation of intermediate-depth and deep-water masses by global-scale circulations and regional processes that are closely linked to the formation and decay of sea ice and to basal melting of the large ice shelves of West Antarctica. Coupled ocean-atmosphere GCM simulations of the Antarctic sea ice are discussed in Section 5.4.

Circulation patterns matching the observed distribution of water masses have been simulated with a baroclinic model of the world ocean using a 200-km grid (Cox 1975) (Figure 14). That resolution is inadequate for reproducing the observed mesoscale variability of the Antarctic Ocean circumpolar current, which must be included implicitly through diffusion coefficients. Simulations with this model and coarser resolutions must necessarily prescribe unrealistically large coefficients. Probably, progress must be sought in the opposite direction, with finer-resolution models that also include a stability-dependent formulation of vertical heat flux and some

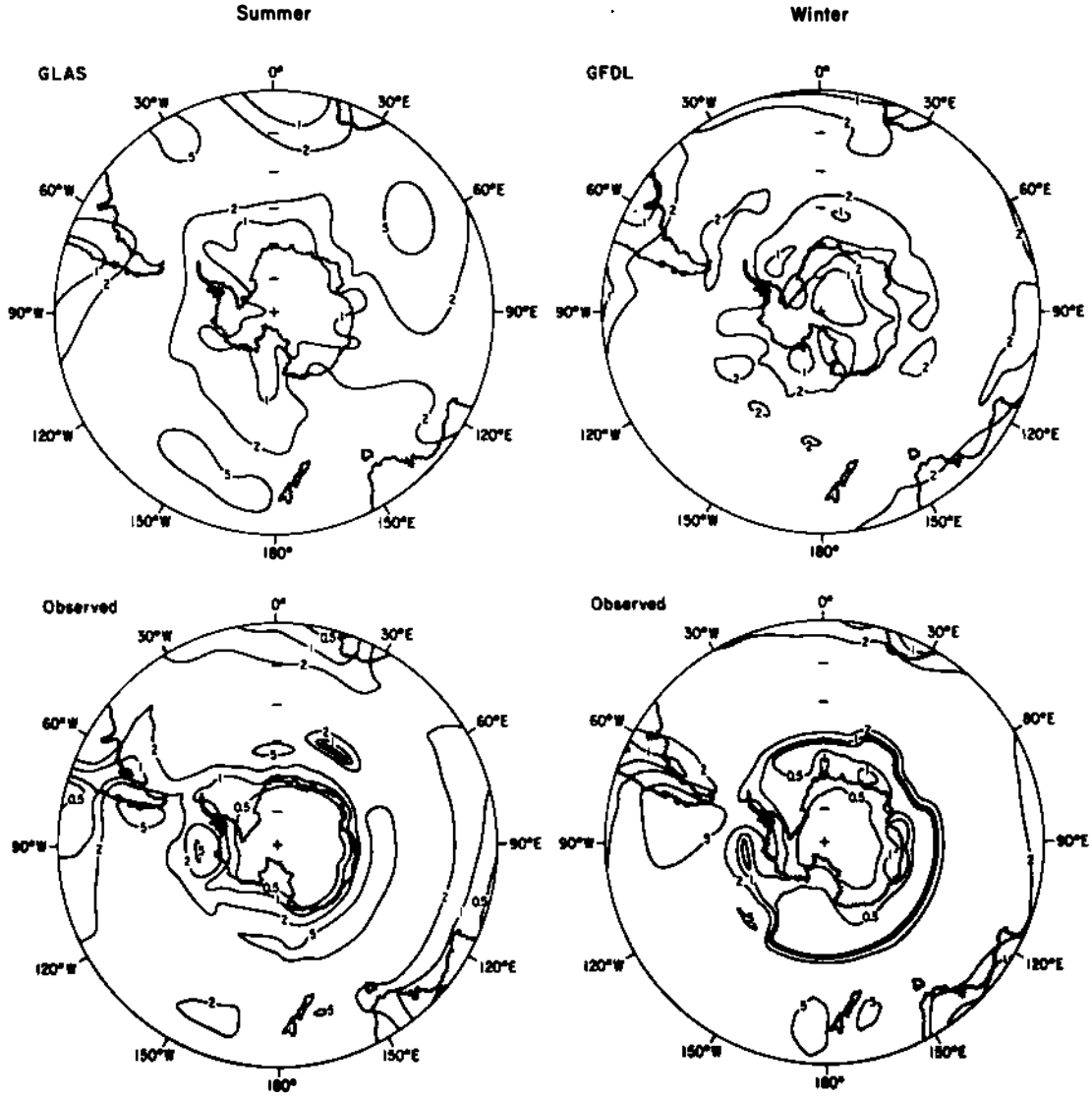


**Figure 13. The simulated and observed Southern Hemisphere precipitation rate for summer and winter. The mean February precipitation rate simulated by the GLAS[1] model is shown for summer, and the mean July precipitation rate simulated by the GFDL[2] model is shown for winter. The observed January and July precipitation rates are shown based on Jaeger (1976).**

[1] NASA Goddard Space Flight Center Laboratory for Atmospheric Sciences Modeling and Simulation Facility, Greenbelt, Maryland.
[2] Geophysical Fluid Dynamics Laboratory/NOAA, Princeton, New Jersey.

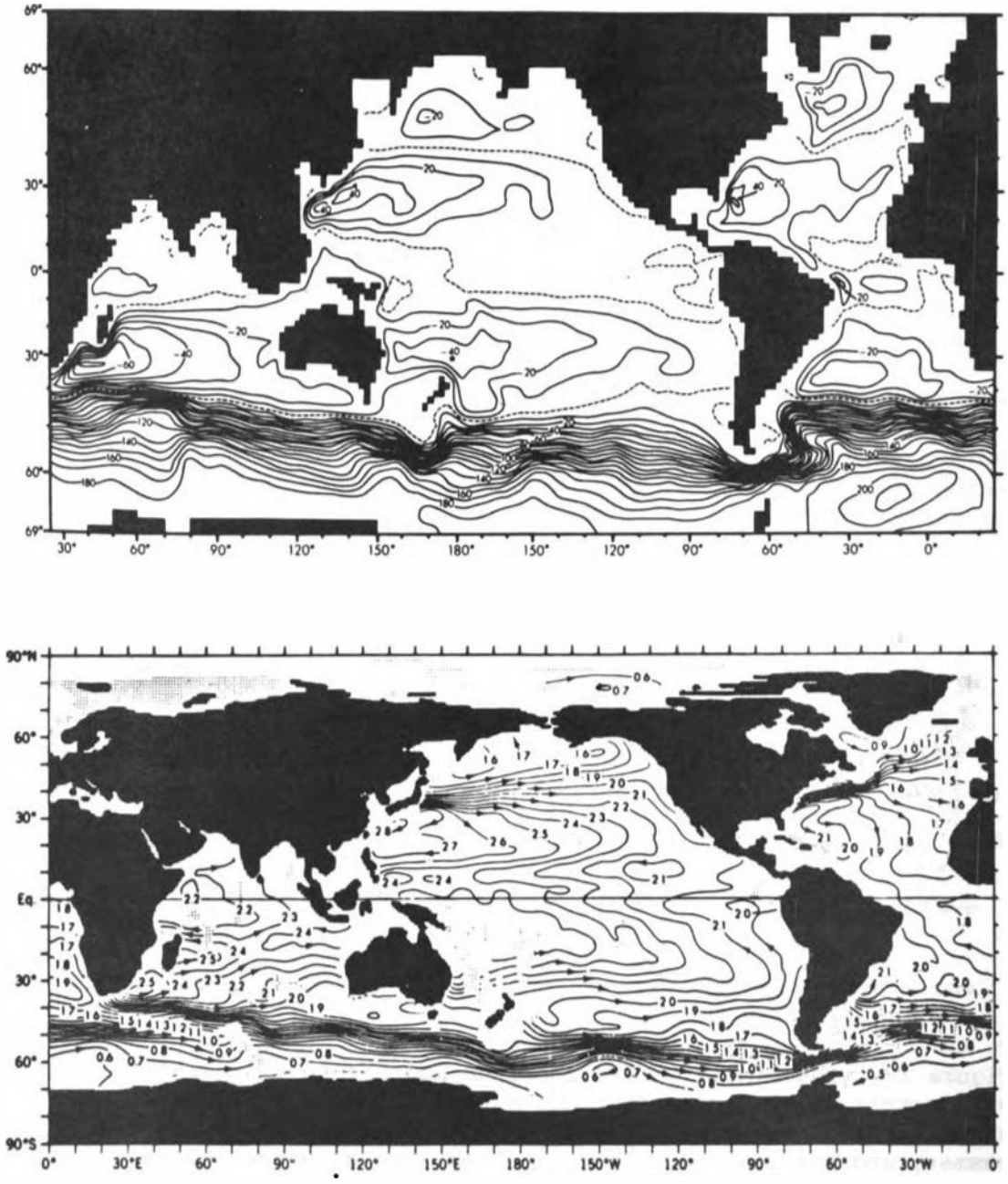


**Figure 14. (Top) Streamlines of mass transport from the model of Cox (1975) and (bottom) surface streamlines inferred from the observed density field (After Levitus 1982.) (See also Attachment 10.)**

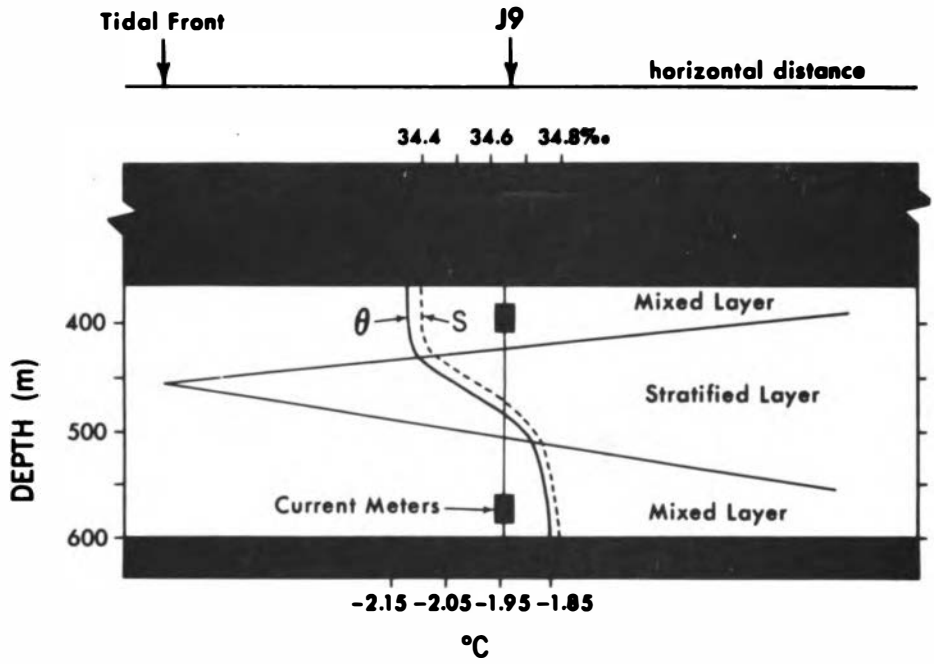


**Figure 15. The temperature and salinity stratification below the J9 borehole through the Ross Ice Shelf. (See also Attachment 11.)**

representation of special processes. Recent successful simulations of the circulation over the Arctic shelf provide guidance for model experiments that would define the background for a detailed description of what takes place under the large ice shelves at present and in conditions of increased $CO_2$.

## 5.3 POTENTIAL EFFECT OF $CO_2$ WARMING ON SUB-ICE-SHELF CIRCULATION AND BASAL MELTING (see Attachment 11, by D. R. MacAyeal)

The heat transfer below ice shelves represents a key problem for any assessment of West Antarctica's responses to environmental changes. The present circulation below the Ross Ice Shelf has recently been modeled within the constraints imposed by hydrographic observations along the ice-shelf front and through the water column below a single point on the ice shelf, the J9 borehole (Figure 15). The model describes two separate circulation systems that act at different levels and exert their principal effects in different parts of the sub-ice-shelf cavity. One circulation involves relatively warm, high-salinity shelf water, which produces melting in the narrowing cavity near the grounding line and returns to the Ross Sea as "deep ice shelf water" at depths below 400 m. The other circulation occurs at higher levels and involves warm offshore water, which produces melt near the ice-shelf front and returns as "shallow ice shelf water" at depths of the order of 200 m. The reality of these concepts can be demonstrated with the $\delta^{18}O/^{16}O$ values of the water masses that

result from mixing with the low-δ fresh water derived from the glacial ice of West Antarctic origin.

The model produces the necessary heat transfer near the root of the ice shelf by tidal wave turbulence but does not yet provide the full penetration needed to sustain the shallow circulation mode, although its main inflow is placed where it is actually observed to occur (northeast of Roosevelt Island). If these mechanisms can be confirmed by further measurements planned for the ice front, the model will be able to deduce the changes in the basal melt rate from the changes predicted or observed in the production and properties of the different water masses involved.

In the discussion it was emphasized that the effects on the ice shelf of changes in the basal melt rate themselves require careful quantitative formulation; this point is considered in Section 6.

## 5.4 MODELED AND OBSERVED SEA-ICE VARIATIONS IN THE SOUTHERN OCEAN (see Attachment 12, by Claire L. Parkinson, and Attachment 4, by S. F. Ackley)

Modeled and observed sea-ice variations in the Southern Ocean hold the keys to several linked problems of the West Antarctic environment. These include the possible steering of storms by the pack-ice edge, the dependence of water-mass production on the extent and concentration of the sea ice, and the downward transfer of $CO_2$ by the thermohaline circulation associated with the growth of sea ice. Moreover, changes in the timing of the Southern Hemisphere sea-ice maximum have been shown to magnify year-to-year fluctuations of the Southern Hemisphere energy balance (Fletcher 1969).

In addition to the thermodynamics of ice growth and decay, based on the energy fluxes incident at the upper and lower ice surfaces, five major stresses acting on the sea ice need to be modeled; these result from air and water currents, the Coriolis acceleration, the dynamic topography of the ocean, and the internal resistance of the ice. Most existing parameterizations have been developed from Arctic data and for Arctic conditions; only recently have the ice characteristics of Antarctica (to the extent that they are known) become the objects of modeling experiments.

The major differences between the numerics in the various sea-ice models lies in the sophistication characterizing the formulation of ice dynamics, which has ranged from a nonlinear viscous-plastic rheology (Hibler and Ackley 1983) to a complete disregard of the ice dynamics (Washington et al. 1976). An intermediate formulation (Parkinson and Washington 1979) calculates ice velocity with a restricted momentum equation, then adjusts velocities in regions of excessive convergence to account for internal ice resistance. The need for limiting the complexity of sea-ice parameterizations for coupled model experiments lends special interest to the possibility that the ice flow could be adequately represented with even further simplifications, perhaps by assuming the ice speed to be a fixed fraction of the geostrophic wind speed and the ice direction to be a fixed turning angle from the

geostrophic wind direction. On the other hand, formulations may need to become more complicated, as Hibler (1984) argues: in order to capture the effect of increasing $CO_2$, it may be essential to take into account little-known features of the Antarctic ice, such as the state of its snow cover, its thickness distribution, and its structural composition, especially its content of ice formed under turbulent conditions (frazil).

Simulations carried out so far with observed or climatological ocean-atmosphere forcing (Figure 16) have succeeded in reproducing the maximum sea-ice export from the Weddell Sea and the observed asymmetric pattern of sea-ice distribution around Antarctica, including even the autumnal development in the Weddell Sea of an ice tongue, which subsequently encircles a thermodynamically controlled open-water area, the Weddell Sea Polynya. An additional simulation that would be of great interest might use the 1979 (FGGE) observations to explain why the polynya did not form in that year.

In all these simulations the reverse effects exerted by the sea ice on the atmosphere and the ocean only appeared implicitly in the observed or climatological forcing, about which there is considerable uncertainty. Observations by Ackley in the Weddell Sea have shown that the temperatures on the Australian synoptic charts (determined by linear interpolation between the FGGE buoys and coastal observations) were at times as much as 10°C too high in the pack-ice zone. Such flaws in the atmospheric data provide additional reasons for desiring properly coupled atmosphere-ocean-ice models.

Coupled atmosphere-ocean-ice models, however, generally have not yet achieved realistic sea-ice distributions. This shortcoming appears to result mainly from excessively high simulated ocean and atmospheric temperatures, which in one simulation were reduced by increasing the prescribed cloudiness. The principal problems are perhaps the coarseness of the ocean-model grid and the inadequate representation of processes such as the stress-curl-related heat transport and the overturning in the thermohaline circulation.

## 5.5 RESULTS OF AUSTRALIAN ICE SHEET/OCEAN/ATMOSPHERE MODELING (W. F. Budd)

In a broad program of field observations and diagnostic modeling, Australian workers have addressed specific aspects of the Southern Ocean and Antarctic climate.

### Atmospheric General Circulation Model Simulations with Different Continental Topographies, Boundary-Layer Parameterizations, and Sea-Ice Extent

Parallel experiments were carried out with a "rough" and a "smooth" Southern Hemisphere topography, both with and without the Antarctic ice cap. The rough and smooth topographies approximated the continents by Fourier fits with 15 and 30 components. The rough topography is more subject than the smooth to the well-known "ringing" effect in spectral

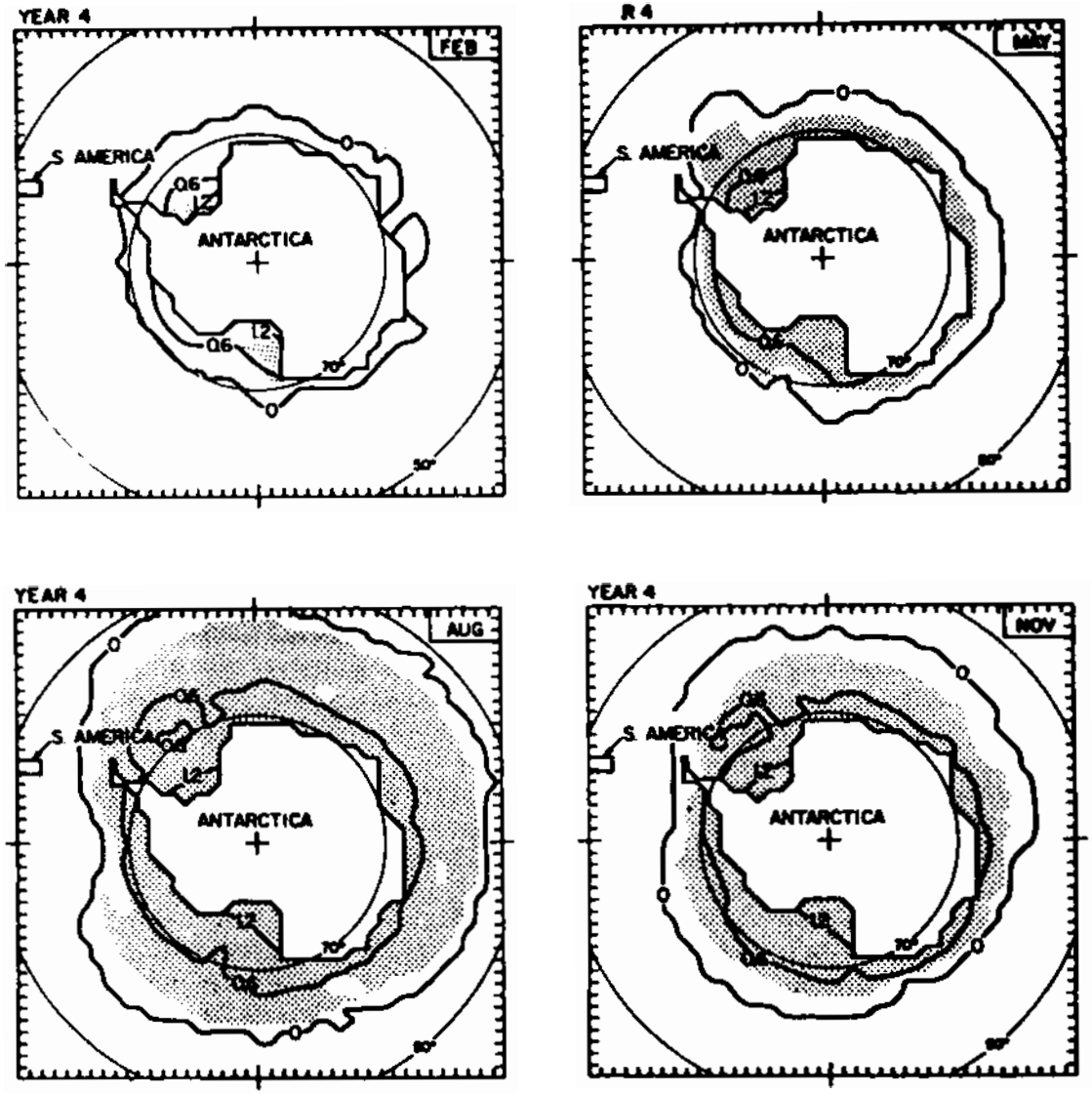


**Figure 16. Sea-ice thickness (in meters) and limits simulated with a dynamic/thermodynamic sea-ice model; in the stippled areas the ice concentration exceeds 90 percent. (After Parkinson and Washington 1979.) (See also Attachment 12.)**

models, producing below-sea-level land at the edges of elevated regions in spectral models. Each configuration was used for a series of sensitivity experiments, with different precisions, initiation procedures, boundary-layer parameterizations, and cloud and ice albedos, for July and January as well as for the months of maximum (September) and minimum (March) sea ice.

The results of the last of these experiments have been published (Simmonds 1981). Others can be assessed by considering the impact of changes in the model topography and other model assumptions on the

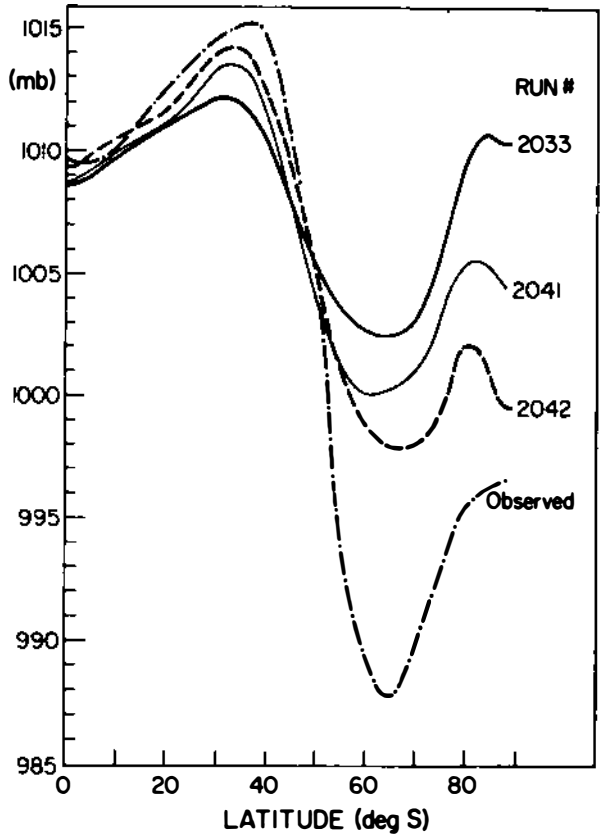


**Figure 17. Observed and modeled meridional profiles of mean sea-level pressure for January. Run 2033: Standard model run with "rough" topography (15 wave numbers). Run 2041: As run 2033 but with Monin-Obukhov boundary layer. Run 2042: As run 2041 but allowing for latitude dependence of cloud albedos. (From Simmonds 1981.)**

polar trough and on the tropospheric temperature profile over the ice sheet. The rough ice-cap topography, when used in the basic GCM, weakened both the subtropical ridge and the polar trough pressure in comparison with the accepted climatology. Introducing a Monin-Obukhov boundary layer, or allowing the albedos of the clouds at different levels their observed changes with latitude, resulted in mean pressures closer to those observed (Figure 17).

The main effect of systematically lowering the ice-sheet surface in the model was to move the entire free-atmosphere temperature profile by a few degrees toward higher temperatures and to weaken the marked surface inversion found for high elevations. The simulated surface temperatures remained considerably above those observed.

## Antarctic Sea-Ice and Ocean Heat Budgets

The results of the Antarctic sea-ice and ocean heat flux measurements have been summarized by Allison et al. (1982). The open water near the Antarctic coast gains heat by radiation around midsummer but starts cooling through turbulent exchanges by early February. After the sea ice has formed, the radiation heat loss from the surface is approximately balanced by conduction through the ice until the ice breaks up and the water is again heated strongly by radiation.

The temperature profiles in the ocean suggest that a substantial amount of heat is brought to the ice by oceanic advection. The water temperatures rise from -1.8° to -1°C through most of the depths by the end of February. At the coastal site of these measurements the salinity shows a slight decrease with the onset of basal melt; a much larger one is produced a little later by the runoff of meltwater from the ice sheet.

## The Southern Ocean as a $CO_2$ Sink

The annual march of the atmospheric $CO_2$ concentrations at Mawson falls by more than 1 ppm below the corresponding one for South Pole Station for the months February through June because of the increased intake of $CO_2$ by the cold ocean prior to the formation of sea ice. The resulting thermohaline circulation then carries the $CO_2$ down into the bottom water. An intriguing implication of the process follows from the fact that the traverse time is about 15 years and is of the same order of magnitude as the lag between an increase in human-induced $CO_2$ and the rise in the global atmospheric concentration (Budd 1982). In these circumstances a stabilization of the $CO_2$ production rate might enable the ocean to catch up after about 15 years and go into a steady state, with a larger flux rate corresponding to the higher global atmospheric content of $CO_2$.

# 6. Model-Predicted Changes for Increased Atmospheric $CO_2$ and Their Critical Assessment

The results of numerous atmospheric GCM experiments for substantially increased concentrations of atmospheric $CO_2$ have been reported by Schlesinger (1982, 1983), who reviewed their Antarctic features for the workshop. The GCM simulations generally show warming increasing from the tropics to the poles and varying with season and longitude. The uncertainties of global-scale predictions tend to be accentuated in regional predictions.

Only one of the experiments, that of Manabe and Stouffer (1980), has been reported in sufficient detail to provide predictions of the summer temperature changes and annual precipitation changes for West Antarctica that are of interest here. Other models may suggest a somewhat higher global temperature rise for equivalent changes in $CO_2$. For a quadrupling of present $CO_2$ concentrations, summer temperature increases of the order of from 2° to 3°C were predicted by the Manabe and Stouffer model for the West Antarctic Ice Sheet; increases exceeding 5°C were found north of the Ross Ice Shelf, and values as large as 8°C on the highest parts of East Antarctica, which remain very cold even then. The annual precipitation rate was predicted to rise generally by less than 20-cm water equivalent, with a small area of 30-cm rise east of the Filchner Ice Shelf and actual decreases on the Amundsen and Bellingshausen seas.

These predictions for a rather extreme $CO_2$ change, a quadrupling of $CO_2$, can hardly be described as dramatic but ought to be checked with others that could be extracted from unpublished results.

The modeling of ocean changes likely to arise from increased atmospheric $CO_2$ was reviewed by Semtner. The few simulations made so far suggested that sea surface temperature rises of the order of 5°C would result from a doubling of atmospheric $CO_2$; more results will become available from coupled ocean-atmosphere experiments at Geophysical Fluid Dynamics Laboratory (GFDL), National Center for Atmospheric Research (NCAR), and Oregon State University. A prerequisite for establishing correct patterns in the Antarctic will be the use of fine-resolution models, which are also needed to simulate the present Southern Ocean circulation and transfers. However, some broad predictions have been made for potential related changes that might arise in the Antarctic sea ice and below the large ice shelves.

The key role in this context is played by the temperature of the relatively warm and saline Circumpolar Deep Water (CDW) found below the pycnocline of the Southern Ocean. According to Gordon (1983), the CDW temperature rises from 0.5°C in the Weddell Sea to 1.5°C in the Amundsen and Bellingshausen seas and recently underwent a 0.4° decrease in the Weddell Sea following the light-ice winters of the early 1970s, which lowered the static stability of the pycnocline. The $CO_2$-induced surface warming, increased precipitation, and reduced windiness, however, all could increase the stability. Gordon (1983) has estimated that, as a result, the temperature of the CDW would rise by 0.25°C in the Weddell Sea and by 0.5°C in the Amundsen and Bellingshausen seas.

The warmer water can be expected to increase the melt rate produced by the shallow circulation below the West Antarctic Ice Shelves, according to MacAyeal. The consequences for the ice-shelf dynamics were outlined by Paterson. The increased melt would remove the warmest ice and might stiffen the ice shelf against both deformation and calving. On the other hand, increased surface melting might have the opposite effect. At least on intermediate time scales, it is not clear whether the combination of warmer air and warmer ocean would sustain or weaken the ice shelves. Moreover, Budd pointed out that the transfer of ocean heat to the base of an ice shelf is limited because of the limited time spent by the water under the ice, judging by measurements on the Amery Ice Shelf.

Changes resulting for the southern sea ice from $CO_2$-induced global warming have been modeled by Parkinson and Bindschadler (1984) by prescribing temperature rises of different magnitudes. The results calculated with the Parkinson and Washington (1979) model establish hemispheric and regional values of the latitudinal displacement of the ice edge per degree (Celsius) temperature change. But in reality, the presence of sea ice exerts strong control on the temperature, and the ice extent is modulated also by changes in wind, which result from the temperature anomalies. Ackley pointed out that this relationship explains how thermodynamically created positive anomalies in the maximum extent of sea ice can be followed by dynamically produced negative anomalies in the minimum extent, as well as regional differences. The observed interannual variations in extent of sea ice have been as large as $3.5 \times 10^6$ $km^2$ and suggest that the signal-to-noise ratio of the southern sea-ice extent may not be large enough to provide a useful tool to detect the early development of $CO_2$ effects (see Parkinson, Attachment 12).

# 7.
# Conclusions and Recommendations

## 7.1 PRESENT ENVIRONMENT OF WEST ANTARCTICA

The existing climatic conditions of West Antarctica are inadequately defined by available observations. Antarctic communications at the best of times are haphazard, so the routine meteorological data often fail to enter the global telecommuniation system and standard meteorological archives. Many specialized observations made both at stations and, especially, on traverses have never reached a collection or archive. Yet all these observations were made at great expense and are as unique and irreplaceable as are the historical ship observations that have been the object of an international archiving project of the World Meteorological Organization (WMO).

Recommendation: Establishment of an archive of all pertinent Antarctic data that can still be recovered. Emphasis would be placed on certain periods, from individual years to weeks, at times when unusually large amounts of data were collected, or when significant weather or oceanographic events occurred.

The year of the IGY and subsequent years should receive special attention, for in this period there was a disproportionate increase in the rate at which observations were made and in the variety of data collected, as well as an end to the classical thoroughness of reporting of expeditionary results in monographs. Together with the archiving of past Antarctic data, the collecting and archiving of current and future data should be reorganized to ensure the continued growth of complete and high-quality observational records readily accessible to climate researchers.

These broad recommendations cover also a top priority contribution that the Scientific Committee on Antarctic Research (SCAR) nations are being asked to make to the World Climate Research Program (Allison 1983). But even the best conceivable climatology of Antarctica will be based on short observational series fragmented by the closing and reopening or relocating of stations. When the high interannual variability of the polar climate is added to this discontinuity, an adequate climatology in the conventional sense becomes at best a distant goal. This situation accounts for the continued reference to

individual years in the earlier discussion of the Antarctic circulation (see Section 4).

Instead, in developing the Antarctic archives, special weight should be placed on covering periods ranging from individual years down to weeks when the vagaries of logistics provided fuller-than-usual data or when significant weather events took place. Outstanding examples are the FGGE year, 1979, and the summers of 1955-1956, 1956-1957, 1957-1958, and part of 1958-1959, when observations from the whaling ships in the southeast Pacific adequately described the synoptic systems over the Southern Ocean; during the last two of these summers the most intense observational effort ever was proceeding on the ice sheet. Of more recent data, the digitized series of Australian weather charts since 1972 deserve to be included in the archive and should be supplemented by complete records of hourly to six-hourly meteorological observations made at manned and automatic stations and on ships. These observations are needed to clarify precipitation processes and the creation of stable isotope changes in ice cores.

As controls on the Australian charts, microfilmed or digitized synoptic charts of the other Southern Hemisphere weather services should be archived for the same period. Useful historical map series were prepared by the South African Weather Bureau for 1951-1963 and by the International Antarctic Analysis Center in Melbourne, Australia, for the 1960s. But it is important to remember that, except for isolated brief periods (such as the summers of 1955-1956 to 1957-1958, and the FGGE year, 1979), all Southern Hemisphere weather charts had to be constructed from quite inadequate observations.

Other large groups of data that should be brought together into an Antarctic archive are the individual upper-air temperatures and winds observed by the steadily shrinking radiosonde network of Antarctica and the full range of satellite data, obtained with visible, infrared, and microwave radiation sensors.

Finally, two extremely important requirements of an Antarctic data archive should be reiterated: adequate quality control and easy access for users. Although integral features of any archive, they must be especially stressed here, for they seem to present particular problems in relation to Antarctic data.

## 7.2 MODEL SIMULATIONS OF THE PRESENT ATMOSPHERIC ENVIRONMENT OF WEST ANTARCTICA

A realistic rendering of the present environment of West Antarctica by models of its atmosphere, ocean, and ice is an essential prerequisite for any credible prediction of $CO_2$ effects. Basic problems include how to incorporate the earth's surface topography in the models and how to determine the natural variability of climate in the models. In some cases treating the polar regions and the entire Southern Hemisphere as areas of secondary interest has permitted the models to be tuned for better performance in regions of prime interest--the Northern Hemisphere middle latitudes and the tropics. To settle the many

questions raised about West Antarctica in the $CO_2$ debate, the Southern Hemisphere should now become the focus of the models.

A specific strategy for improving the atmospheric general circulation models (AGCMs) should have the following components (see also Attachment 9).

Recommendation: Model Validation Studies (How well do AGCMs simulate the present Antarctic climate?)

1. Expand the comparison of the model simulations to include the variables in the free atmosphere such as temperature, winds, moisture, and clouds.
2. Compare the models' simulated cyclogenesis/cyclone tracks with observations, for example, by the method proposed by Trenberth (see Attachment 3).
3. Compare the components of the surface energy budget (solar radiation, upward and downward longwave radiation, sensible and latent heat fluxes) simulated by the models over West Antarctica with observations.
4. Compare the components of the snow and ice budgets simulated by the models (snowfall, sublimation, melting) for West Antarctica with observations.
5. Extend all comparisons to as many AGCMs as possible.
6. Because of the large year-to-year fluctuations in the circulation around Antarctica, develop simulations not only of the mean fields but also of the level of interannual variability.

Recommendation: Model Sensitivity Studies (How are the AGCM simulation errors produced/corrected?)

1. Determine whether sea-level pressure errors over Antarctica are due to an erroneous method of reduction to sea level or represent an error in the distribution of mass.
2. Determine why most models underestimate the intensity of the Antarctic circumpolar trough and why most improvements in this feature result in the generation of an "Arctic circumpolar trough."
3. Determine whether the larger-than-observed surface air temperatures and/or precipitation rates over Antarctica are the result of the prescribed orography being too low in elevation and/or too smooth.
4. Determine whether the less frequent cyclogenesis off the east coast of South America, southeast of Africa, and south of Australia is the result of the prescribed orography for those continents.

Recommendation: Atmosphere-Ocean Model Simulation Studies of $CO_2$-Induced Climate Change (How do models simulate $CO_2$-induced climate changes?)

1. Comprehensively document the models' simulations of the present climate, which are used as the controls for the enhanced $CO_2$ climates, with particular attention to sea ice and snow.

2. Perform studies to ascertain the statistical significance of the models' simulated climate changes.

3. Analyze the models' statistically significant climate changes (if necessary, extend the length of the simulations to obtain statistically significant results) to determine:

a. The role of the predicted changes in ice and snow in the warming and the acceleration of the hydrological cycle.

b. The effects of the climate change on the unpredicted ice components such as the West Antarctic Ice Sheet and ice shelves.

## 7.3 MODEL SIMULATIONS OF THE OCEANIC ENVIRONMENT OF WEST ANTARCTICA

As a general requirement, the use of finer-resolution ocean models was emphasized as the development most likely to lead to improved realism. In particular, the use of such models would help to define more precisely the processes contributing to the melting below ice shelves. Realistic model representations of Antarctic sea ice need above all new observational data, as well as a consensus trade-off between physical completeness and computation time requirements. For the extended coupled experiments with atmospheric and oceanic GCMs that lie ahead, the sea-ice parameterizations will have to be reduced to the most essential physics.

Recommendation: Studies to test model simulations of the oceanic environment. A specific strategy for improving model representations of the Southern Ocean and predictions of oceanic responses to increasing atmospheric $CO_2$ should involve the following steps (see also Attachment 10).

1. Begin with a regional model having intermediate grid size (100 km).

2. Parameterize eddy effects, as suggested by eddy-resolving quasi-geostrophic studies, with realistic coefficients for the horizontal ($A_H$,$A_M$) and vertical ($K_H$,$K_M$) eddy diffusion of heat (H) and momentum (M).

3. Allow $K_H$ to depend on the buoyancy frequency (N) or on the Richardson number (Ri).

4. Use primitive equations with prognostic temperature and salinity and the nonlinear equation of state.

5. Specify an idealized (but not zonally symmetric) geometry. Provide adequate vertical resolution ($\geq$10 levels).

6. Include an indented deep continental shelf (Weddell Sea), a partially blocked channel (Drake Passage), and topography (Scotia Ridge).

7. Prescribe seasonally varying, zonally symmetric wind forcing.

8. Idealize the treatment of surface energy fluxes.

9. Include thermodynamic-dynamic ice cover and (melting-freezing) ice shelves.

10. Specify the temperature and transport of the North Atlantic deep water (NADW) in some fashion.

11. With such a model, try to reproduce known aspects of the general circulation (especially the formation of Antarctic bottom water (AABW) and the transport of the Antarctic circumpolar current (ACC).

12. To predict potential oceanic consequences of increased atmospheric $CO_2$, consider effects of increased surface heating and precipitation, following Gordon (1983); effects of a reduction in NADW transport, following Rooth (1982); and effects of a change in wind forcing.

## 7.4 MODEL PREDICTIONS THROUGH NEW MEASUREMENTS AND MONITORING OBSERVATIONS

With these proposed developments and changes, the atmospheric and oceanic models can be confidently expected to advance from their already considerable achievements in matching the broad features of the global climatic system to more faithful simulations of its regional manifestations. This progress will also lead to firmer predictions of what the rise in atmospheric $CO_2$ concentrations might or might not do to the West Antarctic environment. Although some of the gaps in the present sketchy pictures of the West Antarctic environment could be closed by the analyses of existing data suggested in Section 7.1, there is an urgent need for additional measurements and observations to define essential features for the models to reproduce and project into the future. Detailed requirements have been spelled out in recommendations of recent documents of the Polar Research Board (1983) and its Committee on Glaciology (1983).

Recommendation: New measurements and monitoring to test model prediction. In addition to further ice coring and continued monitoring of the sea-ice extent and concentration, this should include the following:

1. Automatic weather stations should be established at key island locations such as Peter I Island, in the open and ice-covered ocean and on the ice sheet. Such an expansion of the present network should be coordinated with the emerging Tropical Ocean/Global Atmospheric (TOGA) project, which will form the second main theme of the World Climate Research Program.

2. Systematic observations should be made, from icebreakers and biological research vessels, of sea-ice properties (thickness, concentration, frazil content, etc.), especially in the Amundsen and Bellingshausen seas.

3. Strain and velocity measurements are needed for the ice streams discharging into the Ross Ice Shelf.

4. Changes in the positions of the ice-shelf grounding lines need to be monitored.

5. Core drilling through the West Antarctic Ice Sheet is needed to establish its history, at least as far back as the last interglacial, and through the Filchner-Ronne Ice Shelf to clarify

resemblances to and differences from the Ross and Amery sub-ice-shelf circulations.

6. Observational and modeling studies should be undertaken of ice-shelf calving and of the back stresses exerted by the ice-shelf embayment and by the discharge of ice streams.

7. Of special importance in the $CO_2$ context will be the monitoring of features that might give an early warning of effects predicted by the models. As pointed out earlier, the large interannual variability of the southern sea ice may make it necessary to look for clear signals in the ice structure rather than simply in the extent of sea ice. Temperatures observed at Antarctic stations and field sites, and especially on Antarctic and sub-Antarctic islands, should be continuously monitored, together with synoptic trends as represented by the pressure variability patterns at different levels in the atmosphere. A rigorously planned set of oceanographic observations is needed.

8. Satellite measurements of changes in the elevation of the ice-sheet surface are urgently needed. These methods are fast approaching technical feasibility and represent another monitoring tool of great value, for they will give the space-time integrated response of the ice sheet itself.

Performing even a part of these recommended measurements and observations would bring many of the outstanding questions about potential $CO_2$-induced changes in the environment of West Antarctica substantially closer to solution.

The most urgent question posed by such changes--the response of the $2 \times 10^6$ $km^3$ of ice stored above sea level in the West Antarctic Ice Sheet--was not on the agenda of the workshop. Nevertheless, most of the deliberations had a bearing on that question and provided implicit answers to it. A major uncertainty is where increased surface and basal melting would cause the ice shelves to stiffen and thicken or soften and thin. Another major uncertainty concerns potential ice-sheet surges. Preliminary indications are that the ice streams primarily involved are maintaining their present fast movement in approximate balance with the ice-sheet accumulation. In other words, the ocean is gaining roughly as much mass in the form of icebergs as it is losing by evaporation, which provides the accumulation feeding ice streams. It remains to be determined whether the ice streams could change to an unbalanced mode of flow if regional temperatures and accumulation rates were to increase by amounts of the order predicted for higher atmospheric $CO_2$ concentrations. No new facts emerged to challenge the conclusion that substantial responses of the glacial ice are likely to take at least several centuries to develop (Thomas et al. 1979; Bentley 1982, 1983; Revelle 1983).

## 7.5 CONSENSUS ANSWERS TO DOE QUESTIONS

The participants formulated the following answers to the questions proposed for workshop consideration by T. J. Gross, of the $CO_2$ Research Division.

1. How adequate are climate model simulations in representing present conditions (variables, resolution, etc.)? What additional variables could be calculated by general circulation models that might be of use? Do inadequacies of present simulations affect model predictions elsewhere on the globe?

The simulations of regional features by general circulation models are generally quite inadequate; for example, they have invariably yielded temperatures and pressures that are substantially higher than those observed in key regions. Some of the discrepancies are difficult to judge precisely from the limited results, a problem that could be considerably eased by generating difference plots. Eddy statistics for atmospheric simulations would be especially valuable for getting at the basic cause of the discrepancies and for clarifying episodic processes that create precipitation, surface melt, and sea-ice changes.

Many of the inadequacies of the Antarctic simulations probably arise from the simplistic modeling of sea-ice and ice-sheet boundary-layer processes. Other shortcomings could perhaps represent, in part, the price paid for improved simulations of Northern Hemisphere conditions with models that use the Southern Hemisphere more as a tuning device than as important in its own right. In the long term, however, improvements in the representation of the Southern Hemisphere will allow better simulation of global climate features, which cannot be achieved until the Southern Hemisphere representations are improved.

2. What information, including resolution and accuracy, is required to determine the sensitivity of the Antarctic ice sheet/ice shelves/sea ice to warming?

Present models of ice sheets that could be used to assess their sensitivity to warming require, above all, measurements of the sliding and deformation rates of the larger ice streams of Antarctica and Greenland. More information is also needed on the mass balance and the topography of surface and bedrock of large areas of Antarctica.

Present models of ice shelves that could be used to assess their sensitivity to warming require, above all, realistic estimates of the surface and basal heating that would result from higher atmospheric temperatures. The surface heating must be established by modeling the regional atmospheric circulation of the warmer scenario, while the basal heating must be derived by modeling the expected production rate of the major water masses involved in the sub-ice-shelf circulation systems. Hydrographic measurements are also needed to further substantiate details of the circulation system, especially for the Filchner-Ronne Ice Shelf.

Present models of sea ice that could be used to assess its sensitivity to warming require, most of all, observations on the present thickness distribution and structural properties of Antarctic sea ice, especially for the Bellingshausen and Amundsen seas. Also desirable is consolidation of existing models into one model combining the most essential physics with maximum simplicity for use in long-term, coupled ocean-atmosphere experiments.

The resolution and accuracy of the various new measurements recommended are in the ranges of 30 km and 10 percent, respectively, but need to be assessed separately for each variable in the light of existing logistic capabilities and opportunities. Satellites already provide essential microwave data on sea ice and promise information on the ice-sheet surface accumulation. Satellite laser and radar systems may soon be able to detect minute changes in the ice-sheet surface elevation, a key factor for interpreting changes in sea level.

3. How can equilibrium-climate model results be applied to analysis of time-dependent ice dynamics?

This is a special case of "asynchronous coupling," a strategy widely used in ocean-atmosphere modeling. Its pitfalls are discussed in papers by Harvey and Schneider (in press, and unpublished manuscript). In experimental ocean-atmosphere modeling tests, they found that holding atmospheric temperatures constant while computing oceanic temperatures led to very large errors; these errors were considerably reduced by fixing, instead, the turbulent fluxes between the ocean and the atmosphere. The conclusion is that much testing will be needed to establish the potential errors that any particular coupling scheme might introduce in climate/ice-sheet simulations.

4. What is the priority for model improvements (ocean dynamics, sea ice, atmosphere, etc.)?

Ocean dynamics: Finer resolution is needed to simulate water-mass production and deep-convection processes. A detailed program for model development appears in Section 7.3.

Sea ice: The main need is for a model of intermediate complexity, retaining the essential physics for long-term simulations with observed and model-derived forcing.

Atmosphere: A detailed program for improving the atmospheric models is given in Section 7.2.

Ice sheets: The dynamics of ice streams and their interactions with the slow-moving adjacent ice and with terminal ice shelves await more nearly adequate modeling, but this development depends to some extent on new data.

5. How can the use of global and regional models to improve simulations be coordinated?

The necessary "nested grid" techniques have been developed in other contexts (severe storms, tropical cyclones, air pollution). Their adaptation to the West Antarctic problems such as surface melting in the ice shelves, episodal precipitation, sudden changes in the sea-ice distribution, and the like presents no intrinsically new problems and could be undertaken as a part of implementing the strategies for model improvement suggested in Sections 7.2 and 7.3.

**6. What can be done to improve coordination between model and observational studies and what should be done to encourage more individuals and groups to give these issues higher priority?**

Workshops such as this one are excellent means of coordinating such studies. Seminar series by those engaged in making observations should be sponsored in modeling establishments to increase awareness of the data that are available. An informal periodical making known current work and new results, similar to the Tropical Ocean-Atmosphere Newsletter that has been prepared and distributed for some years by NOAA's Pacific Marine Environment Laboratory, could be a valuable coordinating tool.

# References

Allison, I. (ed.), 1983. Basis for an Action Plan on Antarctic Climate Research. Report of the SCAR Group of Specialists on Antarctic Climate Research. Scientific Committee on Antarctic Research, Cambridge, United Kingdom.

Allison, I., C. M. Tivendale, G. J. Akerman, J. M. Tann, and R. H. Wills, 1982. Seasonal variations in the surface energy exchanges over antarctic sea ice and coastal waters. Annals of Glaciology, 3, 12-16.

Bentley, C. R., 1982. Response of the West Antarctic Ice Sheet to $CO_2$-Induced, Climatic Warming: A Research Plan. Carbon Dioxide Effects Research and Assessment Program, Volume II. Part I. DOE/EV/10019-02. U.S. Department of Energy, Washington, D.C.

Bentley, C. R., 1983. The West Antarctic Ice Sheet: diagnosis and prognosis. In Proceedings, Carbon Dioxide Research Conference. National Technical Information Service, U.S. Department of Commerce, Springfield, Virginia.

Bromwich, D. H., 1979. Precipitation and accumulation estimates for West Antarctica, derived from Rawinsonde information. Ph.D. dissertation, Department of Meteorology, University of Wisconsin, Madison.

Budd, W. F., 1982. The role of Antarctica in Southern Hemisphere weather and climate. Australian Meteorological Magazine, 30, 265-272.

Committee on Glaciology, 1983. Snow and Ice Research. An Assessment. National Academy Press, Washington, D.C.

Cox, M. D., 1975. A baroclinic numerical model of the world ocean; preliminary results. In Numerical Models of Ocean Circulation (pp. 107-120). National Academy of Sciences, Washington, D.C.

Delmas, R., J. M. Ascencio, and M. Legrand, 1980. Polar ice evidence that atmospheric $CO_2$ 20,000 years BP was 50% of present. Nature, 284 (5722), 155-157.

Fletcher, J. O., 1969. Ice Extent on the Southern Ocean and its Relationship to World Climate. Report RM-5793. Rand Corporation, Santa Monica, California.

Gordon, A. L., 1983. Comments about the ocean role in the antarctic glacial ice balance. In Proceedings, Carbon Dioxide Research Conference (pp. IV. 75-IV. 86). National Technical Information Service, U.S. Department of Commerce, Springfield, Virginia.

Harvey, L. D. D. and S. H. Schneider, unpublished manuscript. Sensivitity of transient climate response to ocean model formulation, Part I: Experiments with a globally averaged model. Submitted to Journal of Geophysical Research.

Harvey, L. D. D. and S. H. Schneider, in press. Sensitivity of internally generated climate oscillations to ocean model formulation. In A. Berger, J. Imbrie, J. Hays, G. Kukla, and B. Saltzman (eds.), Milankovitch and Climate: Understanding the Response to Orbital Forcing. D. Reidel, Dordrecht, The Netherlands.

Hibler, W., 1984. On the role of sea ice dynamics in the $CO_2$ problem. In Climatic Processes and Climatic Sensitivity. Maurice Ewing Volume 5. Geophysical Monograph 29. American Geophysical Union, Washington, D.C.

Hibler, W. and S. F. Ackley, 1983. Numerical simulation of the Weddell Sea pack ice. Journal of Geophysical Research, 88 (C5), 2873-2887.

Jaeger, L., 1976. Monatskarten des Niederschlags fur die ganze Erde. Berlin Deutscher Wetterdienstes, 139, 38 pp.

Jenne, R. L., 1975. Data Sets for Meteorological Research. NCAR Technical Note NCAR-TN/IA-111 (194 pp.). National Center for Atmospheric Research, Boulder, Colorado.

Lettau, B., 1969. The transport of moisture into the Antarctic interior. Tellus, 21, 331-340.

Lettau, H., 1977. Climatonomical modeling of temperature response to dust contamination of antarctic snow surfaces. Boundary Layer Meteorology, 12, 213-229.

Levitus, S., 1982 Climatological Atlas of the World Ocean. NOAA Professional Paper 13 (173 pp). U.S. Department of Commerce, Rockville, Maryland.

Loewe, F., 1957. Precipitation and evaporation in the Antarctic. In M. P. van Rooy (ed.), Meteorology of the Antarctic (pp. 71-89). South African Weather Bureau, Pretoria.

Manabe, S. and R. J. Stouffer, 1980. Sensitivity of a global climate model to an increase of $CO_2$ concentration in the atmosphere. Journal of Geophysical Research, 85, 5529-5554.

Mellor, M., 1963. Remarks concerning the Antarctic mass balance. Polarforschung, 5, 179-180.

Parkinson, C. L. and R. A. Bindschadler, 1984. Response of Antarctic sea ice to uniform atmospheric temperature increases. In Climate Processes and Climate Sensitivity, Maurice Ewing Volume 5. Geophysical Monograph 29. American Geophysical Union, Washington, D.C.

Parkinson, C. L. and W. M. Washington, 1979. A large-scale numerical model of sea ice. Journal of Geophysical Research, 84, 151-172.

Polar Research Board, 1983. Research Emphases for the U.S. Antarctic Program. National Academy Press, Washington, D.C.

Raynaud, D. and J. M. Barnola, 1984. The $CO_2$ record in ice cores, a reconstruction of the atmospheric evolution between 18,000 y. B.P. and 1850 A.D. Annals of Glaciology, 5.

Revelle, R. 1983. Probable future changes in sea level resulting from increased atmospheric carbon dioxide, In Changing Climate (pp. 443-448). National Academy Press, Washington, D.C.

Rooth, C., 1982. Hydrology and ocean circulation. Progress in Oceanography, 11, 131-149.

Rubin, M. J. and M. B. Giovinetto, 1962. Snow accumulation in central West Antarctica as related to atmospheric and topographic factors. Journal of Geophysical Research, 67, 5163-5170.

Schlesinger, M. E., 1982. A review of climate models and their simulation of $CO_2$-induced warming. International Journal of Environmental Studies, 20, 103-144.

Schlesinger, M. E., 1983. A Review of Climatic Model Simulations of $CO_2$-Induced Climatic Change. Report 41. Climatic Research Institute, Oregon State University, Corvallis.

Schutz, C. and W. L. Gates, 1971. Global Climatic Data for Surface, 800 mb, 400 mb: January. R-915-ARPA (180 pp.). The Rand Corporation, Santa Monica, California.

Schutz, C. and W. L. Gates, 1972. Global Climatic Data for Surface, 800 mb, 400 mb: July. R-1029-ARPA (180 pp.). The Rand Corporation, Santa Monica, California.

Schwerdtfeger, W., 1970. The climate of the Antarctic. In H. E. Landsburg (ed.), World Survey of Climatology. Volume 14 (pp. 253-355). Elsevier, New York.

Schwerdtfeger, W. and J. Kachelhoffer, 1973. Frequency of cyclonic vortices over the Southern Ocean in relation to the extension of pack ice melt. Antarctic Journal of the United States, 8(5), 234.

Simmonds, I., 1981. The effects of sea ice on a general circulation model of the Southern Hemisphere. In I. Allison (ed.), Sea Level, Ice, and Climatic Change. IAHS Publication 131 (pp. 193-206). International Association of Hydrological Sciences, Geneva.

Smith, I. N., 1984. Ph.D. dissertation, University of Melbourne, Melbourne, Australia.

Stauffer, B., H. Hafer, H. Oeschger, J. Schwarder, and U. Siegenthaler, 1984. Atmospheric $CO_2$ concentrations during the last generation. Annals of Glaciology, 5.

Streten, N. A. and A. J. Troup, 1979. A synoptic climatology of satellite-observed cloud vortices over the Southern Hemisphere. Quarterly Journal of the Royal Meteorological Society, 99, 56-72.

Taljaard, J. J., 1972. Synoptic meteorology of the Southern Hemisphere. In C. W. Newton (ed.), Meteorology of the Southern Hemisphere. Meteorological Monograph 13 (35) (pp. 139-213). American Meteorological Society, Boston, Massachusetts.

Taljaard, J. J., H. van Loon, H. L. Crutcher, and R. L. Jenne, 1969. Climate of the Upper Air: Southern Hemisphere. Volume 1. Temperatures, Dew Points and Heights at Selected Pressure Levels. NAVAIR 50-1C-55. Naval Weather Service Command, Washington, D.C.

Thomas, R. H., T. J. O. Sanderson, and K. E. Rose, 1979. Effect of climatic warming on the West Antarctic Ice Sheet. Nature, 277, 355-358.

Vickers, W. W., 1966. A study of ice accumulation and tropospheric circulation in West Antarctica. In M. J. Rubin (ed.), Studies in Antarctic Meteorology. Antarctic Research Series 9 (pp. 135-176). American Geophysical Union, Washington, D.C.

Washington, W. M., A. J. Semtner, Jr., C. L. Parkinson, and L. Morrison, 1976. On the development of a seasonal change sea-ice model. Journal of Physical Oceanography, 6, 679-685.

Washington, W. M., A. J. Semtner, Jr., G. A. Meehl, D. J. Knight, and T. A. Mayer, 1980. A general circulation experiment with a coupled atmosphere, ocean sea ice model. Journal of Physical Oceanography, 10, 1887-1908.

Zwally, H. J., C. L. Parkinson, and J. C. Comiso, 1983. Variability of Antarctic sea ice and changes in carbon dioxide. Science, 220 (4601), 1005-1012.

# Appendix A: Workshop Presentations

## ATTACHMENT 1

## DATA FROM ANTARCTIC ICE CORES ON $CO_2$, CLIMATE, AEROSOLS, AND CHANGES IN ICE THICKNESS

C. Lorius
Laboratoire de Glaciologie et Geophysique
de l'Environement, Grenoble, France

Analyses of polar ice cores have yielded a number of parameters that provide proxy data on climatic changes and on important factors that may influence them (Table 1). In particular, the isotopic composition ($\delta$) of the ice is an indicator of temperature change, the amount of impurities is linked with aerosol concentration, and the amount and composition of entrapped air reflect the ice thickness and atmospheric composition.

Although the transfer functions used for such reconstructions require some refinement, appropriate information has already been obtained from Antarctic ice cores on time scales covering the climatic transition from the late glacial maximum (LGM) to the Holocene and the last 100 years or so. Both these periods are characterized by a significant and comparable increase in carbon dioxide ($CO_2$), but climatic parameters and other forcing factors show very different changes.

### THE LATE GLACIAL MAXIMUM/HOLOCENE TRANSITION

#### Climate

One inland ice record from West Antarctica (Byrd) and two from East Antarctica extend back to the LGM (Figure 1). The isotopic shift associated with the deglaciation varies from 5 to 7 percent; after correction for change of the mean isotopic composition (+1.6 percent) of the ocean due to the melting of the ice (mainly from the Northern Hemisphere) and using available empirical and theoretical transfer functions, the isotopic data suggest a mean temperature change of about 8°-10°C. These figures apply to surface conditions (Lorius et al. 1984) and assume no drastic change of the ice thickness. Theory (Robin 1977) and comparison of $\delta$ and dust indices from the Dome C ice core with other continental and marine $^{14}C$-dated records suggest that accumulation may have been lower by about 25 percent during the LGM.

Table 1. Ice Cores as Sources of Environmental Proxy Data

| Atmosphere | Snow and Ice |
|---|---|
| **Climate** | |
| Temperature, relative humidity | Isotopic composition ($\delta^{18}O$, $\delta D$) |
| Precipitation | Thickness of accumulated layers |
| **Atmospheric Environment** | |
| Composition of the atmosphere | Ice-bubble composition |
| Aerosol concentrations | Concentration and composition of impurities |
| Intensity of marine, continental volcanic, anthropogenic, and extraterrestrial sources | |
| Atmospheric transport | |
| **Ice-Sheet Thickness** | |
| Surface elevation | Total gas content |

## Carbon Dioxide

$CO_2$ concentrations have been measured on the Dome C (Delmas et al. 1980) and Byrd (Neftel et al. 1982) ice cores. Although there is some scatter in the data (Figures 2 and 3), which could reflect both experimental problems and natural fluctuations, some features are clearly apparent: $CO_2$ concentrations are of the order of 200 parts per million by volume (ppmv) during the LGM; a mean value for the Holocene is about 270 ppmv. Possible explanations involve changes in the marine biological productivity (Broecker 1983; McElroy 1983) or in the reef-building activity (Berger 1982) in connection with the rise in sea level; possible modification in the oceanic circulation may also play a primordial role (Stauffer et al. 1984; Broecker 1983). As the ice-bubble composition may integrate a rather large time interval, the existence of a possible time lag between $CO_2$ and the $\delta$ climatic record has still to be established. This problem is complicated because of the existence of large fluctuations over short-term intervals and several step changes in atmospheric $CO_2$ variation (Raynaud and Barnola 1984). Nevertheless, the change in atmospheric

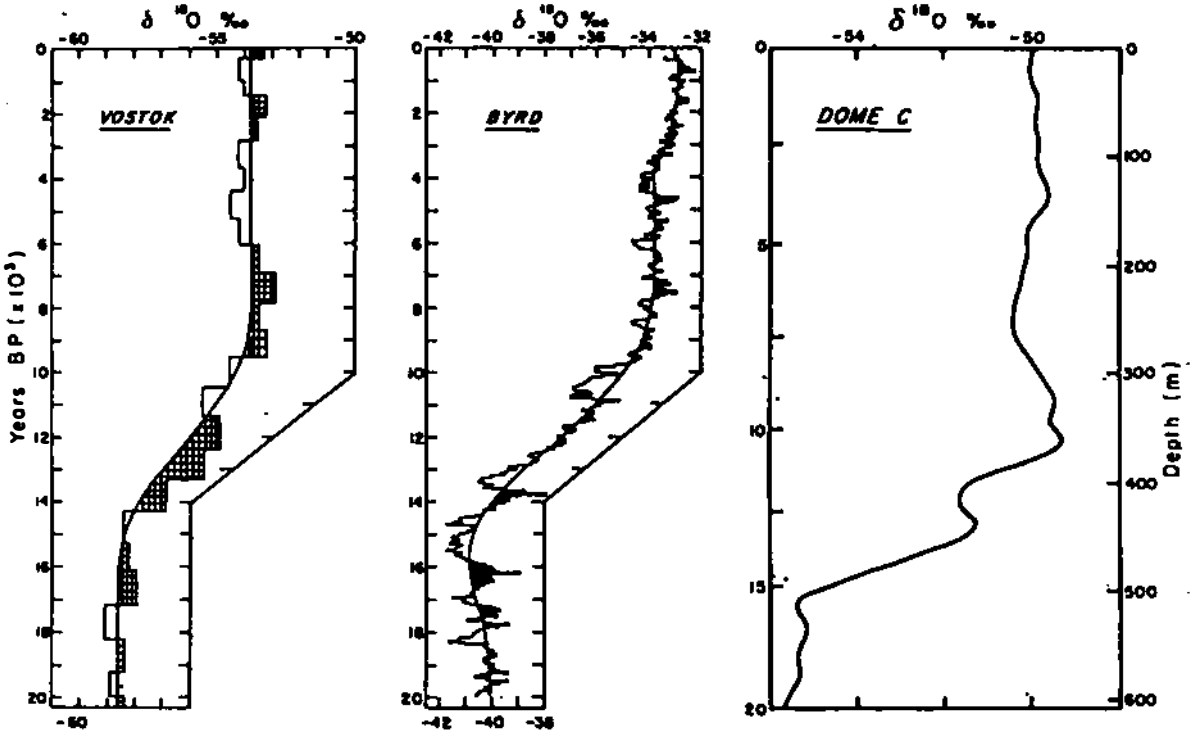


Figure 1. Antarctic isotopic ($\delta^{18}O$) profiles over the last 20,000 years: Vostok (from Barkov et al. 1977), Byrd (from Johnsen et al. 1972), and Dome C (from Lorius et al. 1979).

$CO_2$ concentration may have contributed significantly to the amplitude of the climatic warming.

## Aerosols

Another striking feature of the three LGM ice-core records is the very large load of atmospheric aerosols at this time (Cragin et al. 1974; Petit et al. 1981; Thompson and Mosley-Thompson 1981; de Angelis et al. in press). A large increase of the flux of continental dust in the atmosphere (up to about x20) is then observed; marine aerosol concentrations are about x5 with respect to mean Holocene concentrations (Figure 4). These high values have been interpreted by increased (possibly up to 1.4-2 times greater) wind speeds modulated by desert and area of sea-ice extent. The large-scale atmospheric circulation increase is probably due to a greater latitudinal temperature gradient (CLIMAP Project 1981). It has been estimated that the total LGM atmospheric dust load was about 5 or 6 times larger when compared with the Holocene (Royer et al. in press); this atmospheric dust could have affected the radiation balance and significantly reduced the temperature change observed in Antarctica during the deglaciation. Although some layers of volcanic ash have been observed in the Byrd ice core, they are likely to be of local origin; present

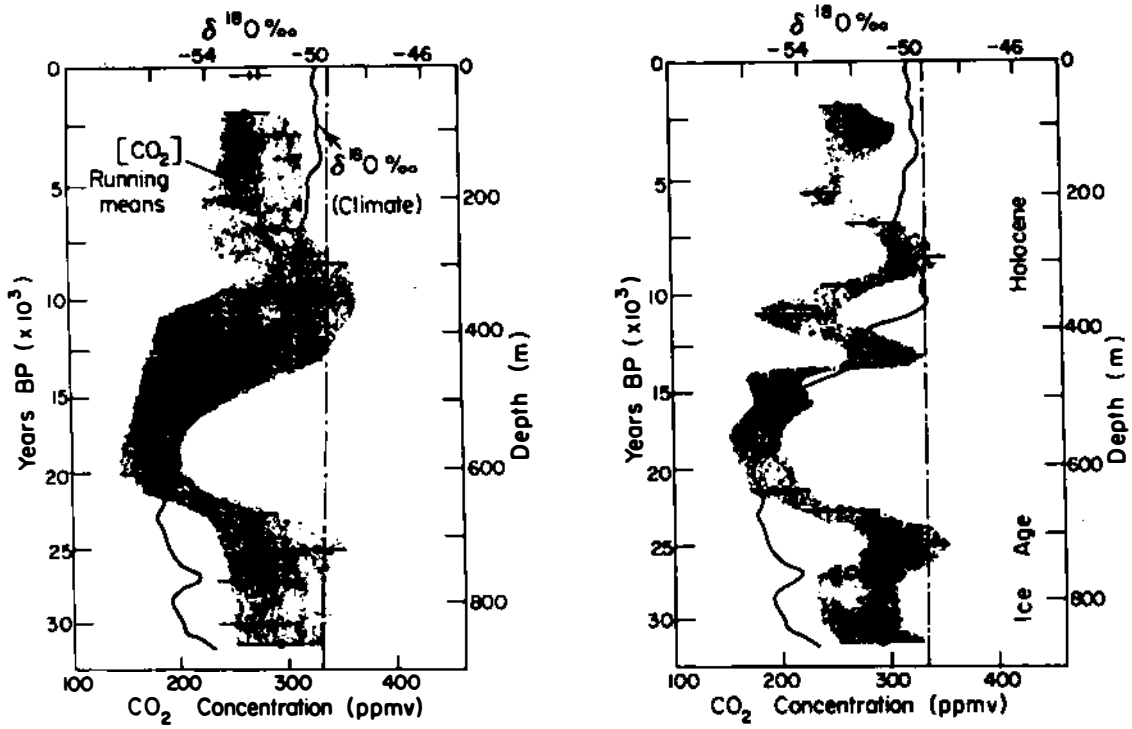


Figure 2. $CO_2$ concentrations and stable isotope content in the Dome C ice core plotted as a function of age and depth (meters of ice). For the $CO_2$ concentrations, two "extreme" ranges of variation are shown. The left one takes into account measurements performed also on another Antarctic core. The right one, based only on Dome C results, suggests shorter-term natural fluctuations. (Original data from Delmas et al. 1980.)

evidence suggests that the volcanic dust loading over Antarctica was not higher during the LGM.

## Ice Thickness

As previously mentioned, the amount of air entrapped in the ice depends on the elevation (atmospheric pressure) at which the ice was formed. A few available data from Byrd (see Raynaud and Whillans 1982, Figure 3) and Vostok (Korotkevich et al. in press) indicate no drastic change of inland ice thickness during the deglaciation. The data suggest, in fact, a slightly thinner (100-200 m) central West and East Antarctic, in disagreement with some ice-sheet reconstructions. Results from coastal sites of East Antarctica indicate thicker (400-500 m) LGM ice (Budd and Morgan 1977; Young et al. 1984). A slight thickening of central West Antarctica between the LGM and the Holocene could have been induced by an increase in the rate of snow accumulation, while coastal areas may have thinned under the influence of increases in sea level and temperature.

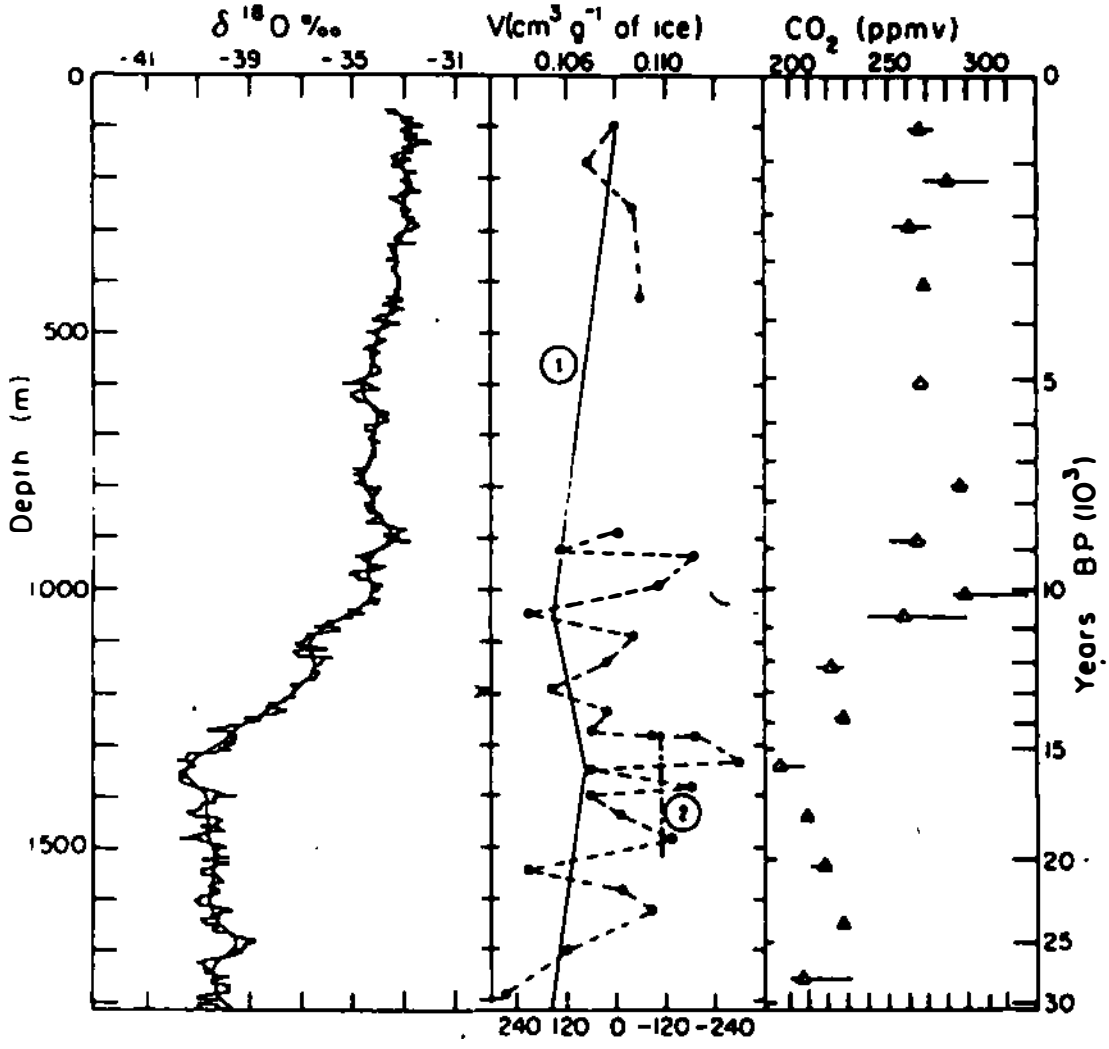


Figure 3. Stable isotope content (from Johnsen et al. 1972), total gas content (from Raynaud and Whillans 1982), and $CO_2$ concentrations (from Neftel et al. 1982; Oeschger et al. 1982); profiles obtained at Byrd Station. For the gas-content record, the difference between line 1 (expected value assuming stable conditions) and line 2 (mean measured values around the LGM) suggests that the Byrd area was then slightly lower than now.

## THE LAST CENTURY RECORD

### Carbon Dioxide

Recent measurements performed on the Dome C and Byrd ice cores indicate (Barnola et al. 1983) that between about 800 and 2500 years B.P., a period prior to the significant anthropogenic perturbation, the $CO_2$ concentration was of the order of 260 ppmv (see Figure 5). Further

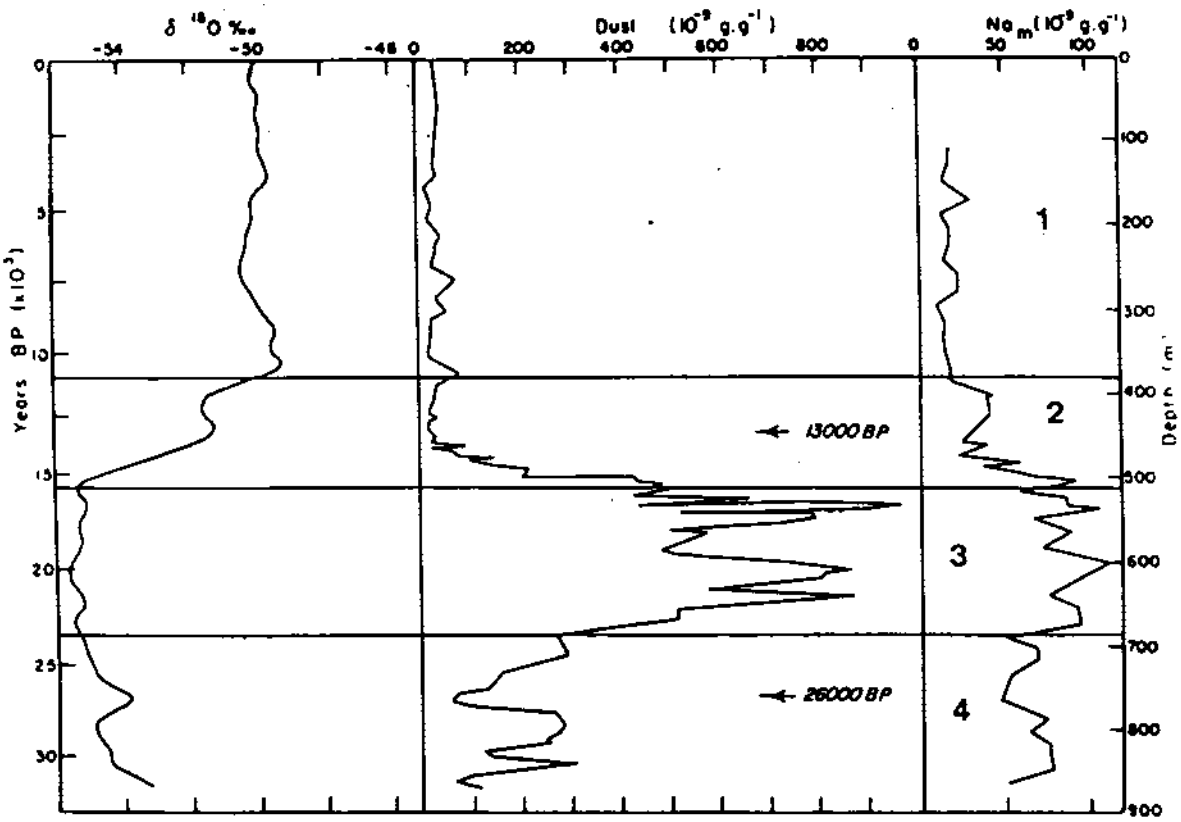


**Figure 4. Smoothed stable isotope content, dust, and Na marine concentrations profiles for the Dome C ice core plotted as a function of age and depth (meters of ice). (From de Angelis et al.1982.) Numbers indicate the different climatic stages.**

**study of another core (D 57, Raynaud and Barnola 1984) suggests the existence of slight natural variations prior to about 1850; a "preindustrial" value of 260 ppmv has also been obtained from this detailed East Antarctic record. This figure should be compared with the $CO_2$ concentration measured today in the atmosphere, 340 ppmv; the preindustrial value obtained from ice cores is significantly lower than the one (about 295 ppmv) generally used for modeling the present $CO_2$ increase (Lorius and Raynaud 1983) and to explain global temperature changes from various forcing factors.**

## Climate

**Extensive Antarctic meteorological data do not extend back prior to 1957 (see Attachment 7, by D. W. S. Limbert). Some longer isotope-climatic time series records are being determined but are not yet available. A detailed δ profile obtained at South Pole (Jouzel et al. 1983) shows a rather good correlation with meteorological data**

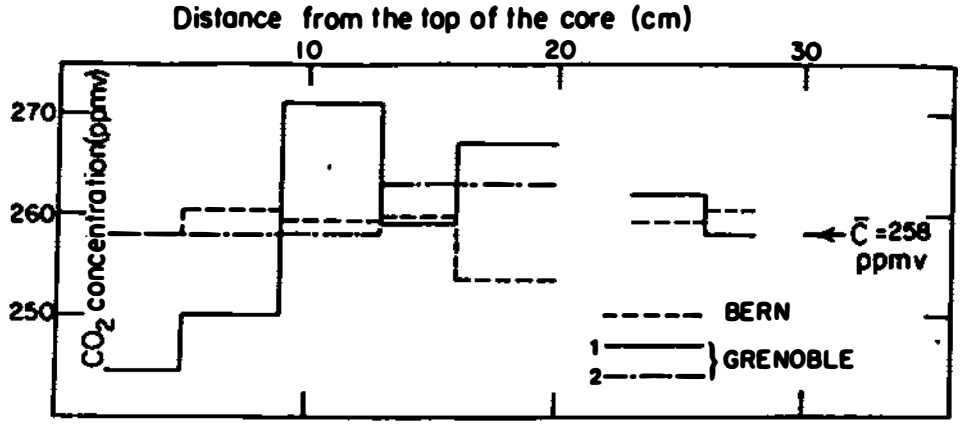


Figure 5. $CO_2$ concentrations measured on a core section from Dome C (depth is 132.9 m below the surface). (From Barnola et al. 1983.)

observed over the last 20 years; the isotopic profile (Figure 6) suggests a slight warming from about 1890 to 1945, followed by a cooling up to about 1960 and less negative temperatures since then. Data from West Antarctica are not yet available, but the Dome C record (Petit et al. 1981) does not show identical features. No clear δ-T trend over the last century can currently be established from available data, possibly because of a weak "temperature signal/isotopic noise" ratio; it is also possible that different parts of Antarctica experienced different behaviors over this time scale, as suggested by changes over the recent decades (see Attachment 2, by H. van Loon, and Attachment 7, by D. W. S. Limbert).

Accumulation time series can also be obtained from dated ice cores, although accumulation differs from precipitation due to the influence of various factors (snow drift, topographic features, sublimation, etc.). Accumulation records over the last century, obtained at South Pole, show different results (see Figure 7 and Giovinetto and Schwerdtfeger 1966; Mosley-Thompson 1980; Jouzel et al. 1983), which may result from uncertainties in dating or local effect, as the studied sites are different. A high interannual and areal variability may possibly account for the observed discrepancies. Accumulation data are also available from Little America and Byrd, both in West Antarctica, prior to 1958. No secular trend is obvious (Gow 1968). More data are available over the last decades. From radioactive fallout, which characterizes the 1955 and 1965 summer layers in Antarctica, it has been shown (Pourchet et al. in press) that all over Antarctica the accumulation increased by about 30 percent (in a range of from 10 to 92 percent) between about 1975 and 1965 when compared with the decade 1955-1965. The studied stations in West Antarctica include South Pole, the Antarctic Peninsula (James Ross Island), and 21 sites from the Ross Ice Shelf (Clausen and Dansgaard 1977).

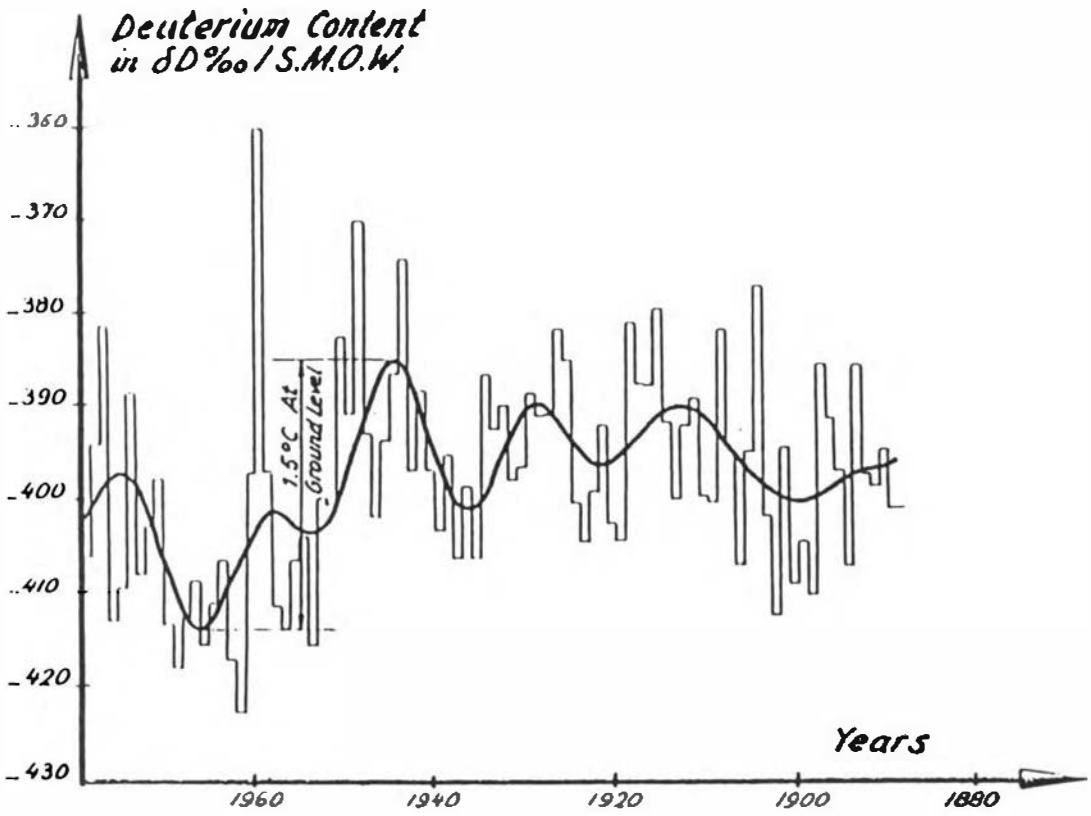


**Figure 6. South Pole: isotopic (δD) profile observed over the last century with indication of the smoothed estimated temperature change at ground level. (From Jouzel et al. 1983.)**

## Aerosols

**There is no indication of a significant secular trend for the loading of atmospheric aerosols over Antarctica. Short-term fluctuations may be connected with atmospheric transport changes, but the major concentration peaks are associated with specific volcanic events (Figure 8) (Delmas and Boutron 1980). Although this finding should be valid over all of Antarctica, most of the available data are from the eastern part.**

## Ice Thickness

**No clear changes in ice thickness over the last century have been identified.**

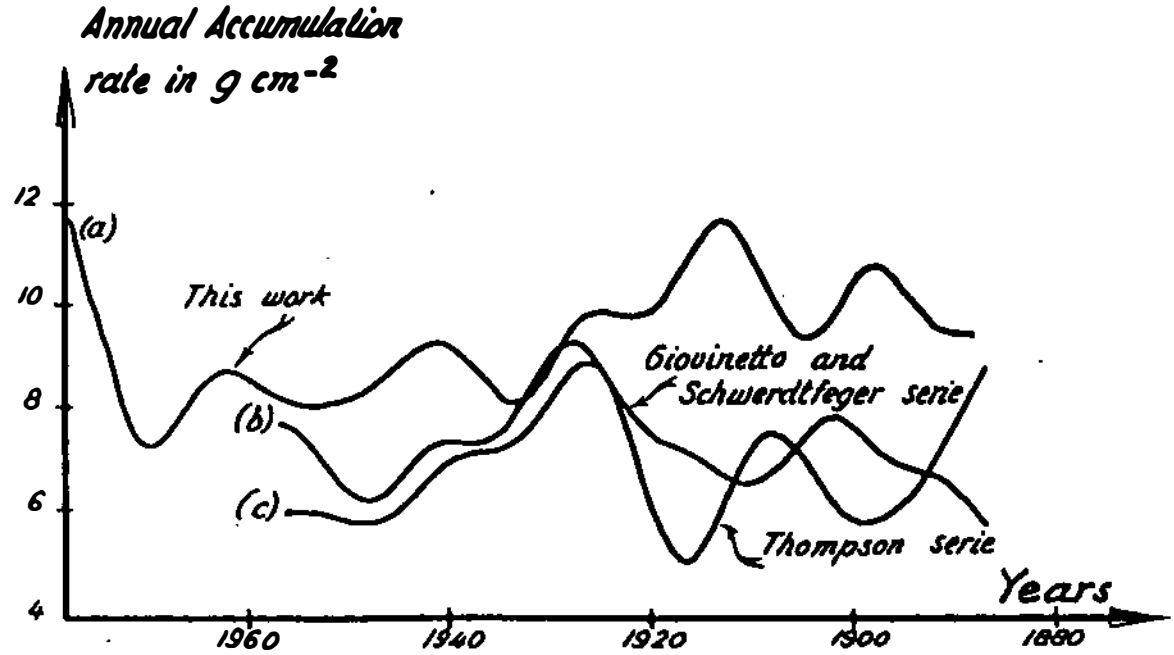


**Figure 7. South Pole: smoothed accumulation data versus time. (From Jouzel et al. 1983; Mosley-Thompson 1980; and Giovinetto and Schwerdtfeger 1966.)**

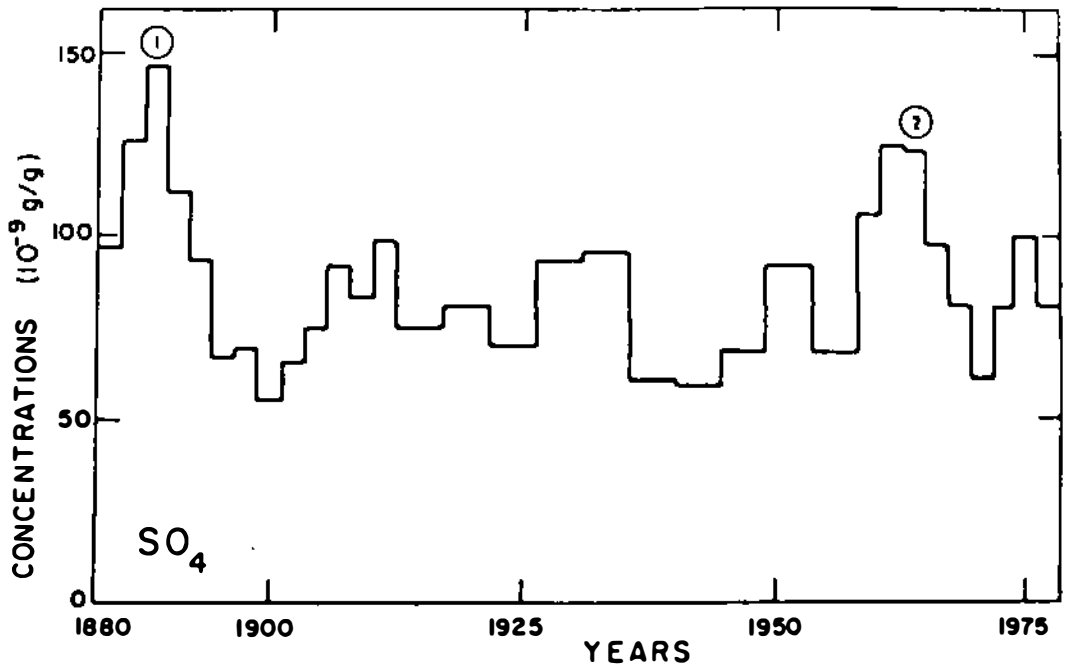


**Figure 8. Dome C: Profile of $SO_4^=$ concentrations over the last century. $SO_4^=$ is one of the major ions of Antarctic aerosols. No trend is apparent, but high values reflect the large volcanic eruptions of Krakatoa (1) and Mount Agung (2).**

## CONCLUSIONS

When dealing with potential $CO_2$-induced changes in the environment of West Antarctica, it seems appropriate to examine proxy data obtained from ice cores. They show that for two different time intervals during the last 20,000 years the atmospheric $CO_2$ concentration increased by about 30 percent; changes in the Antarctic environment were very different in the two time intervals, as summarized in Table 2, which outlines the apparent "$CO_2$-climate paradox."

The following conclusions are drawn in regard to the apparent contradiction between $CO_2$ and climatic environmental changes observed in the past in Antarctica.

- Available Antarctic ice-core data do not indicate the existence of a trend in the environment associated with the recent $CO_2$ increase. However, more ice-core data are needed, in particular for West Antarctica, to document recent changes of $CO_2$ and other forcing factors and climatic parameters in order to get a better assessment.
- The present absence of an observed trend could also result from various other causes: existence of a low signal-to-noise ratio in the records, due to a high interannual variability; insufficiencies in the proxy data transfer functions; overestimation of the $CO_2$ impact (in particular, for high latitudes) obtained from climate models; and damping and lag effects due to the thermal response of the ocean.
- Ice-core proxy data indicate that a $CO_2$ increase similar to that of the last century (about 30 percent) happened during the last deglaciation. The cause of this change is not yet clear, but the long time interval involved (about 5000 years) may be of importance, as the

Table 2. Antarctic Ice-Core Data on Past $CO_2$ and Environmental Changes

| Characteristic | LGM-Holocene Transition | Last Century |
|---|---|---|
| Time scale, years | 5,000 | 100 |
| $CO_2$ increase | x1.3 | x1.3 |
| Other trace gases | ? | ? |
| Aerosols | x6 | |
| Temperature, °C | + 8-10 | No systematic trend depicted |
| Ice thickness | Slight thickening inland; coastal thinning | No detected change |

oceans (chemistry, circulation, rise in sea level associated with the melting of Northern Hemisphere ice sheets) may have had an effect. The contribution of $CO_2$ to the large climatic and environmental changes then observed is difficult to assess, inasmuch as other forcing factors such as aerosol concentrations also show major variations. Central West Antarctica apparently remained relatively stable. A much longer time series, extending to the previous interglacial (about 125,000 years ago), may provide useful information by establishing an overall picture of a complete climatic cycle and by documenting a period possibly analogous to future conditions.

- The complexity of the real climate system points out the need to combine both the modeling and the diagnostic approaches for a better assessment of $CO_2$ impact.

Current environmental glaciological data would be useful to check GCM output data over West Antarctica. Correct simulation of past climate (i.e., during the LGM) would provide a critical test of the climate models, giving confidence to $CO_2$-impact studies. Conversely, a reasonable modeling of Antarctic parameters would be of great value to help calibrate the ice records, to extend the validity of single-site studies, and to understand past changes that have been observed.

## REFERENCES

Barkov, N. I., F. G. Gordienko, Ye. S. Korotkevich, and V. M. Kotlyakov, 1977. The isotope analysis of ice cores from Vostok station (Antarctica), to the depth of 950 m. In Proceedings of the International Union of Geodesy and Geophysics Symposium, Grenoble. IAHS Publication 118 (pp. 382-387). International Association of Hydrological Sciences, Geneva.

Barnola, J. M., D. Raynaud, A. Neftel, and H. Oeschger, 1983. Comparison of $CO_2$ measurements by two laboratories on air from bubbles in polar ice. Nature, 303, 410-413.

Berger, W. H., 1982. Increase of carbon dioxide in the atmosphere during deglaciation: the coral reef hypothesis. Naturwissenschaften, 69, 87-88.

Broecker, W. S., 1983. Ocean chemistry and circulation changes at the close of glacial time. Geochimica et Cosmochimica Acta, 46 (10), 1689-1705.

Budd, W. F. and V. I. Morgan, 1977. Isotopes, climate and ice sheet dynamics from core studies on Law Dome, Antarctica. In Proceedings of the International Union of Geodesy and Geophysics Symposium, Grenoble. IAHS Publication 118 (pp. 312-321). International Association of Hydrological Sciences, Geneva.

Clausen, H. B. and W. Dansgaard, 1977. Less surface accumulation on the Ross Ice Shelf than hitherto assumed. In Proceedings of the International Union of Geodesy and Geophysics Symposium, Grenoble. IAHS Publication 118 (pp. 172-173). International Association of Hydrological Sciences, Geneva.

CLIMAP Project, 1981. Seasonal reconstructions of the earth's surface at the last glacial maximum. In R. Cline (ed.), Map and Chart Series MC 26. Geological Society of America, Boulder, Colorado.

Cragin, J. H., M. M. Herron, C. C. Langway, and G. Klouda, 1974. Interhemispheric comparison of changes in the composition of atmospheric precipitation during the late Cenozoic era. In J. M. Dunbar (ed.), Polar Oceans. Proceedings of the Polar Ocean Conference, Montreal (pp. 617-671). Calgary Arctic Institute of North America, Calgary, Alberta, Canada.

de Angelis, M., J. Jouzel, C. Lorius, L. Merlivat, J. R. Petit, and D. Raynaud, 1982. Ice age data for climate modelling from an Antarctic (Dome C) ice core. In A Berger (ed.), Proceedings of the Symposium on New Perspectives in Climate Modelling, Ninth General Assembly of the European Geophysical Society, Leeds. Elsevier, New York.

de Angelis, M., M. Legrand, J. R. Petit, N. I. Barkov, and Ye. S. Korotkevich, in press. Soluble and insoluble impurities along the 950 m deep Vostok ice core (Antarctica): Climatic implications. Journal of Atmospheric Chemistry.

Delmas, R. and C. Boutron, 1980. Are the past variations of the stratospheric sulfate burden recorded in central antarctic snow and ice layers? Journal of Geophysical Research, 85 (C10), 5645-5649.

Delmas, R., J. M. Ascencio, and M. Legrand, 1980. Polar ice evidence that atmospheric $CO_2$ 20,000 years BP was 50% of present. Nature, 284 (5722), 155-157.

Giovinetto, M. V. and W. Schwerdtfeger, 1966. Analysis of a 200 year snow accumulation series from the South Pole. Archiv fuer Meteorologie Geophysiks und Bioklimatologie Series A, 45, 227-250.

Gow, A., 1968. Deep Core Studies of the Accumulation and Densification of Snow at Byrd Station and Little America V, Antarctica. CRREL Research Report. U.S. Army Cold Regions Research and Engineering Laboratory, Hanover, New Hampshire.

Johnsen, S. J., W. Dansgaard, H. B. Clausen, and C. C. Langway, 1972. Oxygen isotope profiles through the Antarctic and Greenland ice sheets. Nature, 235, 429-434.

Jouzel, J., L. Merlivat, J. R. Petit, and C. Lorius, 1983. Climatic information over the last century deduced from a detailed isotopic record in the South Pole snow. Journal of Geophysical Research, 88 (C4), 2693-2703.

Korotkevich, Ye. S., V. N. Petrov, N. I. Barkov, and V. Y. Lipenkov, in press. Vertical structure of the Antarctic ice sheet and paleogeographic interpretation of the data obtained.

Lorius, C. and D. Raynaud, 1983. Record of past atmospheric $CO_2$ from tree-ring and ice core studies. In W. Bach, A. Crane, A. Berger, and A. Longhetto (eds.), Carbon Dioxide: A Text on Current Views and Developments in Energy/Climate Research. D. Reidel, Dordrecht, The Netherlands.

Lorius, C., L. Merlivat, J. Jouzel, and M. Pourchet, 1979. A 30,000-yr isotope climatic record from Antarctic ice. Nature, 280, 644-648.

Lorius, C., D. Raynaud, J. R. Petit, J. Jouzel, and L. Merlivat, 1984. Late glacial maximum-Holocene atmospheric and ice thickness changes from Antarctic ice core studies. Annals of Glaciology, 5.

McElroy, M. B., 1983. Marine biological controls on atmospheric $CO_2$ and climate. Nature, 302, 328-329.

Mosley-Thompson, E., 1980. 911 Years of Microparticle Deposition at the South Pole: A Climatic Interpretation. Report 73 (pp. 1-133). Institute of Polar Studies, Ohio State University, Columbus.

Neftel, A., H. Oeschger, J. Schwander, B. Stauffer, and R. Zumbrunn, 1982. Ice core sample measurements give atmospheric $CO_2$ content during the past 40,000 yrs. Nature, 295, 220-223.

Oeschger, H., B. Stauffer, A. Neftel, J. Schwander, and R. Zumbrunn, 1982. Atmospheric $CO_2$ content in the past, deduced from ice-core analyses. Annals of Glaciology, 3, 227-232.

Petit, J. R., M. Briat, and A. Royer, 1981. Ice age aerosol content from East Antarctic ice core samples and past wind strength. Nature, 293, 391-394.

Pourchet, M., F. Pinglot, and C. Lorius, in press. Some meteorological applications of radioactive fallout measurements in antarctic snow. Journal of Geophysical Research.

Raynaud, D. and J. M. Barnola, 1984. The $CO_2$ record in ice cores, a reconstruction of the atmospheric evolution between 18,000 y. B.P. and 1850 A.D. Annals of Glaciology, 5.

Raynaud, D. and I. M. Whillans, 1982. Air content of the Byrd core and past changes in the West Antarctic ice sheet. Annals of Glaciology, 3, 269-273.

Robin, G. de Q., 1977. Ice cores and climatic change. Philosophical Transactions of the Royal Society, London, Series B, 280, 143-168.

Royer, A., M. de Angelis, and J. R. Petit, in press. A 30,000 yr record of physical and optical properties of microparticles from an East Antarctic ice core and implications for paleoclimate reconstruction models. Climatic Change.

Stauffer, B., H. Hofer, H. Oeschger, J. Schwander, and U. Siegenthaler, 1984. Atmospheric $CO_2$ concentrations during the last glaciation. Annals of Glaciology, 5.

Thompson, L. G. and E. Mosley-Thompson, 1981. Microparticle concentration variation linked with climatic change: evidence from polar ice cores. Science, 212, 812-814.

Young, N. W., D. Raynaud, M. de Angelis, J. R. Petit, and C. Lorius, 1984. Past changes of the Antarctic ice sheet in Adelie Land as deduced from ice core data and ice modelling. Annals of Glaciology, 5.

## ATTACHMENT 2

# VARIABILITY OF ATMOSPHERIC CIRCULATION AT THE SURFACE OF THE SOUTH PACIFIC OCEAN IN SUMMER

H. van Loon
National Center for Atmospheric Research,
Boulder, Colorado

Since the opening of the Panama Canal in August 1914, few ships cross the Pacific Ocean south of the subtropical high, and as whaling is not permitted in the South Pacific, few observations are available for synoptic and climatological studies. The following remarks on the variability in that ocean are principally based on the three summers 1955-1956, 1956-1957, and 1957-1958, when whaling was permitted to allow a better coverage of observations for the International Geophysical Year (IGY). Over Antarctica proper there are, unfortunately, not enough stations outside the Antarctic Peninsula for a detailed study.

The water temperature at 200 m (Figure 1) outlines the currents in the Antarctic Ocean and has many of the characteristics of the temperature distribution in the troposphere of the southern summer. The different geographical traits of the Weddell and Ross seas influence the strength and extent of the ocean currents in the sub-Antarctic. Thus cold water in the Weddell gyre is deflected eastward and northeastward by the Antarctic Peninsula, creating a zone of weak south-north temperature contrast in the Atlantic and Indian oceans between 50°S and Antarctica. The tongue of cold water northeast of the Ross Sea is considerably smaller and somewhat warmer, and the zone of weak gradient is of modest size and much farther south. The gradient in the westerlies is correspondingly weaker in the Pacific than in the two other oceans, and its maximum is closer to the continent.

This zonal asymmetry is reflected in the mean-pressure map (Figure 2), where the trough of low pressure lies about 5° latitude nearer the pole in the Pacific than in the Atlantic and Indian oceans and where the meridional gradient of pressure is weakest in the Pacific. It should be noted that the point of lowest pressure (central low) in the trough varies from one summer month to another and from one summer to another, as indicated by the solid circles in Figure 2. A central low on a long-term mean-pressure map is strictly a product of averaging and not a fixed feature. The same may be said of the strong westerlies found on all mean-pressure maps of the Southern Hemisphere, in the sense that daily maps (Figure 3) contain many single vortices in addition to troughs reaching into the subtropics and ridges extending to the Antarctic.

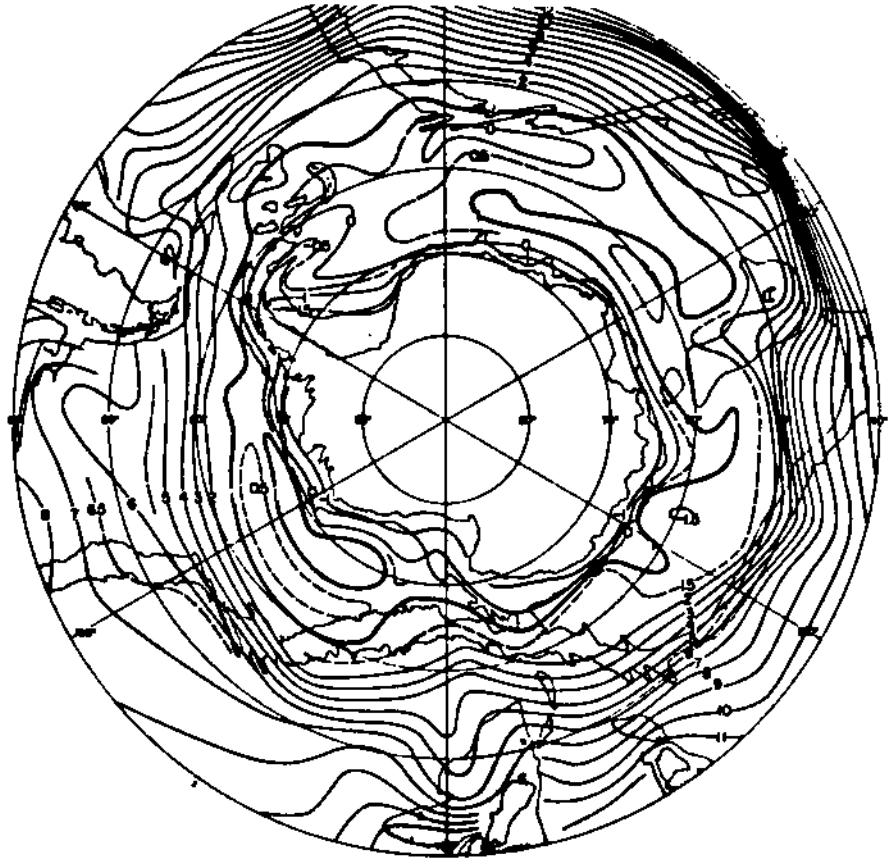

Figure 1. Water temperature at a depth of 200 m. (Adapted from Gordon and Goldberg 1970.)

Cyclones dominate in high latitudes; they originate in middle latitudes (Figure 4), some even farther north, and travel mainly toward the east and southeast. Most of those that are important to the weather over West Antarctica in summer are born in the western Pacific and south and southwest of Australia, whereas those that move through the Drake Passage or cross the Peninsula come from the central and eastern Pacific. Anticyclones are comparatively rare at higher latitudes.

The strength of zonal circulation changes frequently. The changes can be described by the Zonal Westerly Index, which is the zonal geostrophic wind between 35°S and 55°S (Figure 5). The index ranges between 1 and 12 m $s^{-1}$ in the South Pacific Ocean during the two summers shown in the illustration, and the changes are often quite sudden and large. The average is high, however, and was considerably higher in the summer of 1955-1956 than in 1956-1957.

In addition to irregular changes from month to month in middle and high latitudes, there is a seasonal cycle in the sea-level pressure that is dominated by the half-yearly wave. In middle latitudes (Figure 6) the wave has its maxima in the transitional seasons, and in the

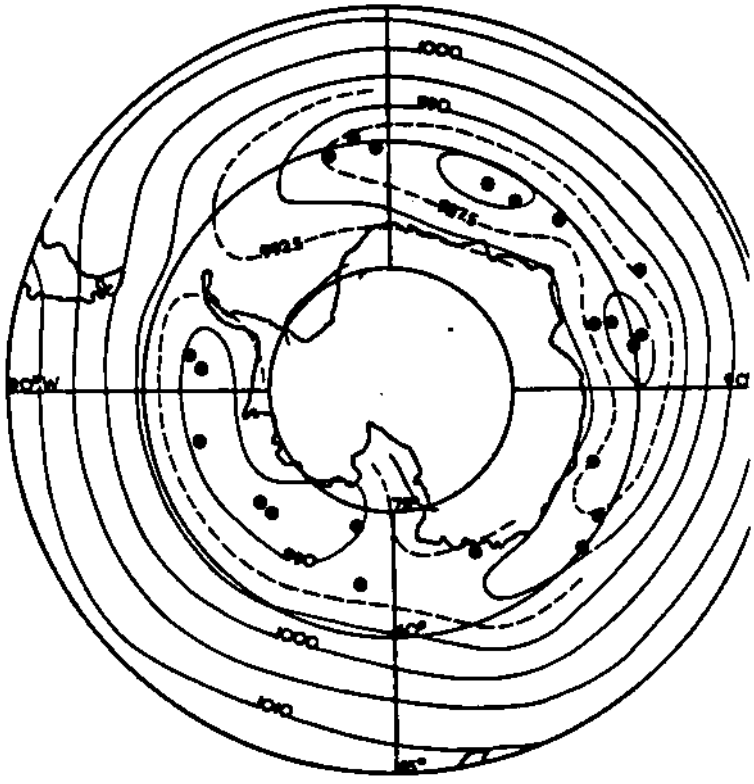

Figure 2. Sea-level mean pressure of the months January, February, and December 1956 and January and February 1957. The solid circles are the positions of the monthly mean pressure minima in the five single months. (See van Loon 1962.)

polar regions the maxima are in the extreme seasons. Consequently, the zonal geostrophic wind between the two zones varies with an appreciable half-yearly cycle during which it is strongest in March/September and weakest in June/December. The half-yearly wave is associated with changes in the position of the Antarctic trough, which brings it north in June and December and south to the Antarctic coast in March and September (Figure 7). While it is farthest north it is also weakest, whereas it is deepest when it is near Antarctica (van Loon 1972). Therefore, on the average, one must consider a deepening and movement to the south of the trough through the southern summer, from December to March.

The most common pattern (eigenvector one) of interannual variation of sea-level pressure in middle and high southern latitudes is one where the pressure anomalies are of opposite sign in middle and high latitudes (Figures 8 and 9). This pattern is, in turn, reflected in large interannual variations in the westerlies and in the polar easterlies.

The Southern Oscillation, which varies on a scale of several years, affects Australasia and the South Pacific Ocean more than any other place on the Southern Hemisphere (Figure 10). This is one of the

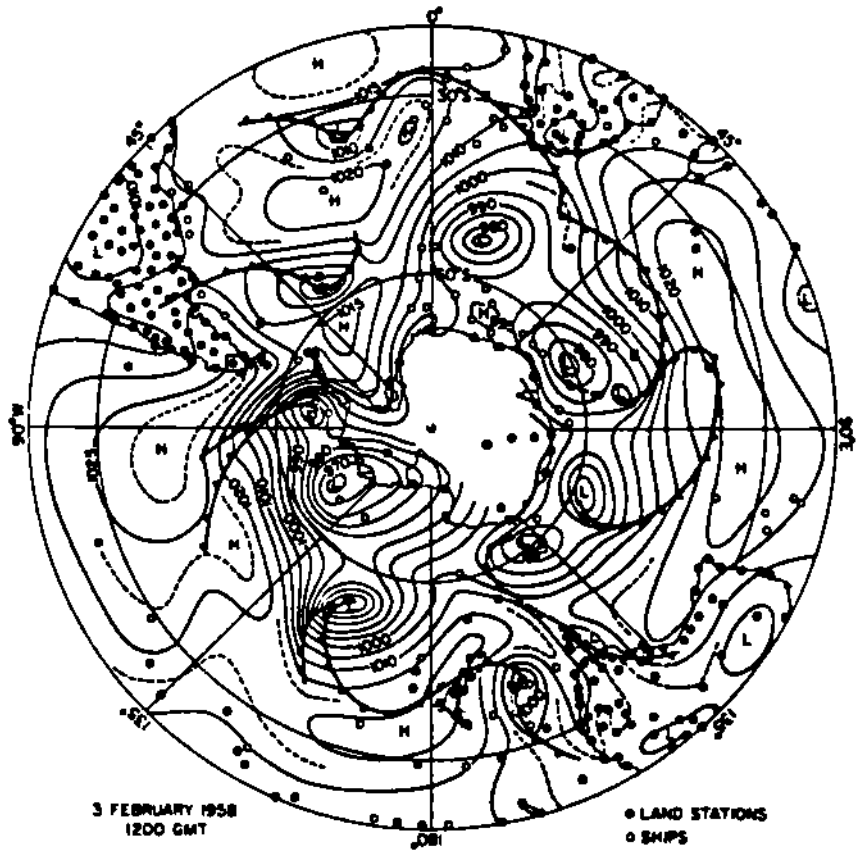


Figure 3. Synoptic map of 3 February 1958, 1200 GMT. Land and island stations are shown as dots, ships as circles.

reasons why the interannual variability of monthly sea-level pressure is higher in these two regions than elsewhere (Figure 11).

Finally, one should consider trends on a longer time scale. Figure 12 shows the linear trend of surface air temperature for an arbitrary 18-year period. Note that the trends occur on a large spatial scale, which suggests that they are associated with (not necessarily large) changes in the quasi-stationary waves.

The middle and high latitudes in the South Pacific Ocean are probably the regions where least is known about the circulation of the atmosphere. There are no long series of observations that will allow us to assess the natural variability of the climate there and, thus, to separate a climate-change signal from the interannual noise. Therefore, it is also impossible to judge whether the model simulations, which have little in common with the fairly well-established mean features, might be within the possible range of mean states of the circulation.

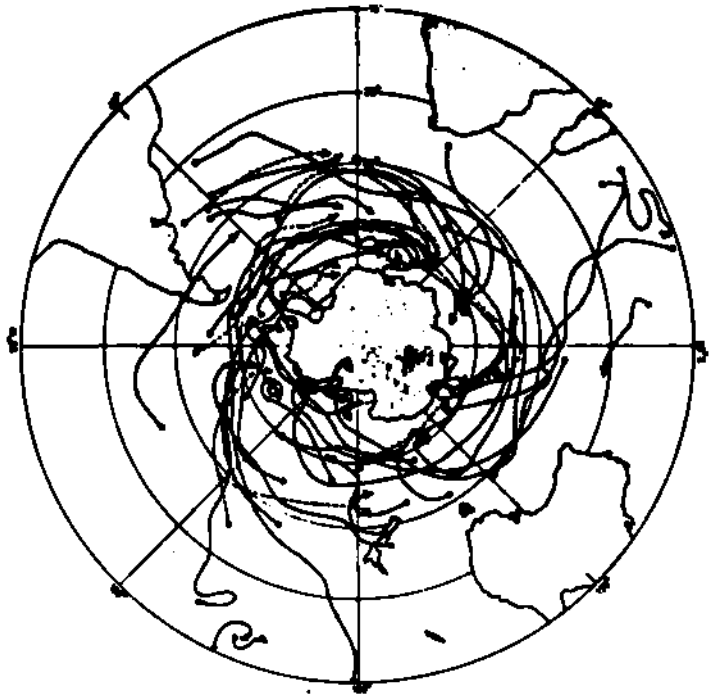

**Figure 4. Cyclone tracks with 24-hour positions for January 1958. (See Taljaard and van Loon 1963.)**

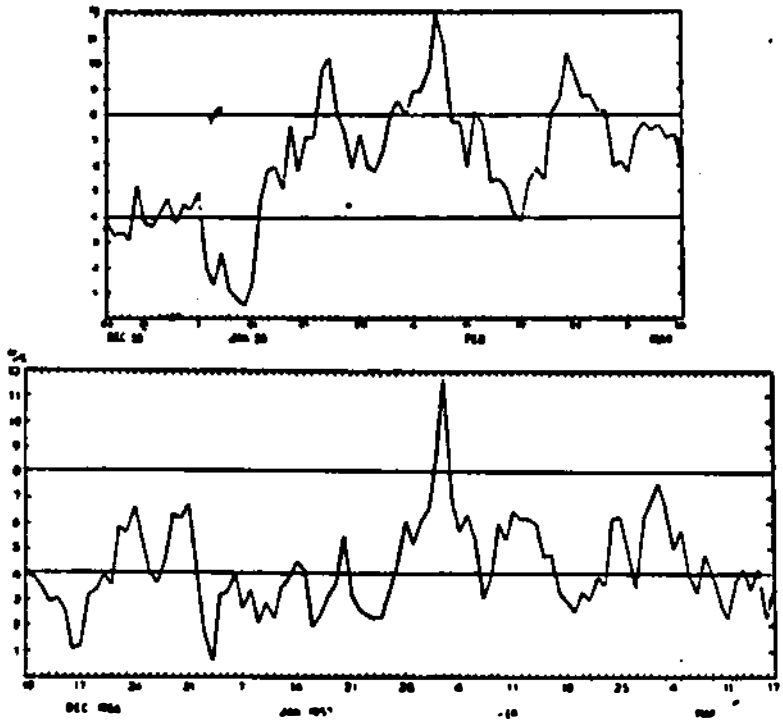

**Figure 5. Daily Zonal Westerly Index (m $s^{-1}$) between 35°S and 55°S in the Pacific Ocean for the summers of 1955/1956 and 1956/1957 (From van Loon 1960.)**

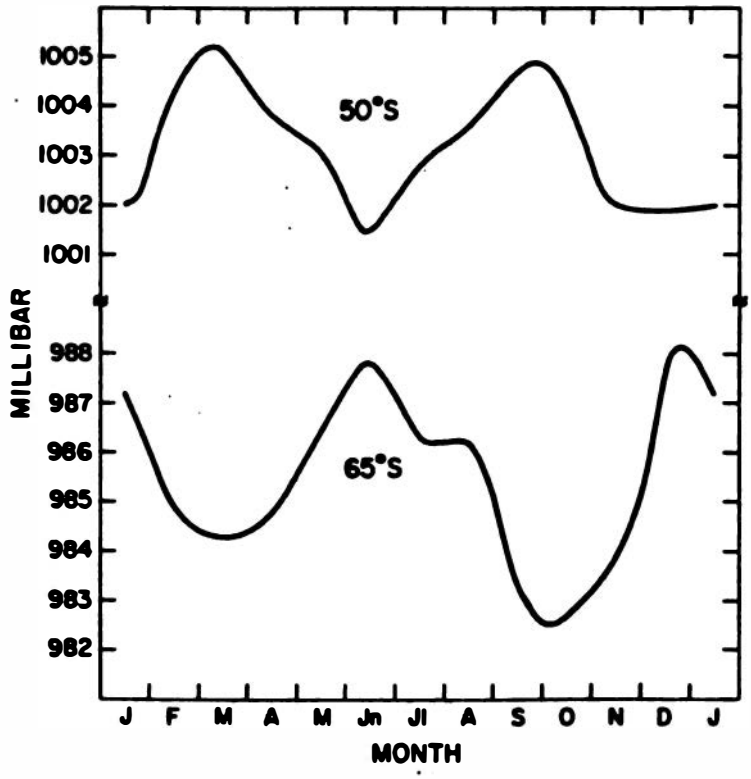


**Figure 6. Mean annual curves of zonally averaged sea-level pressure at 50°S and 65°S.**

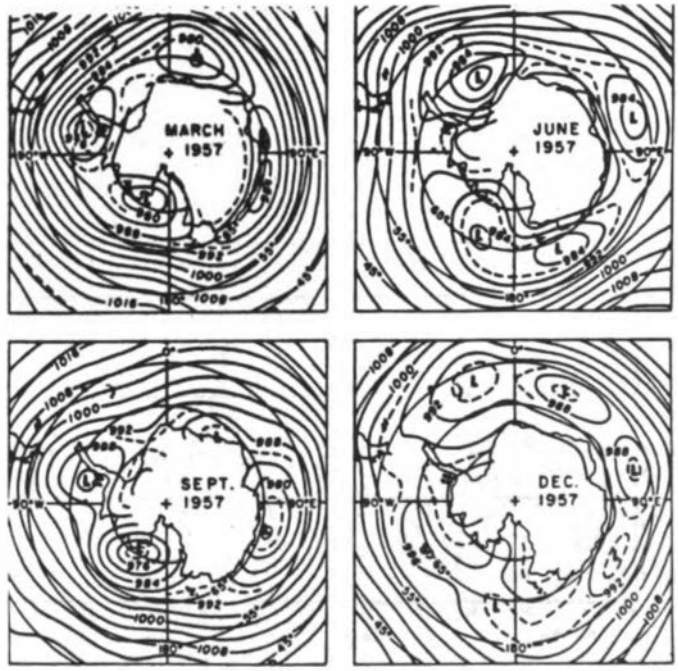


**Figure 7. Mean sea-level pressure in March, June, September, and December of 1957. (From van Loon 1967.)**

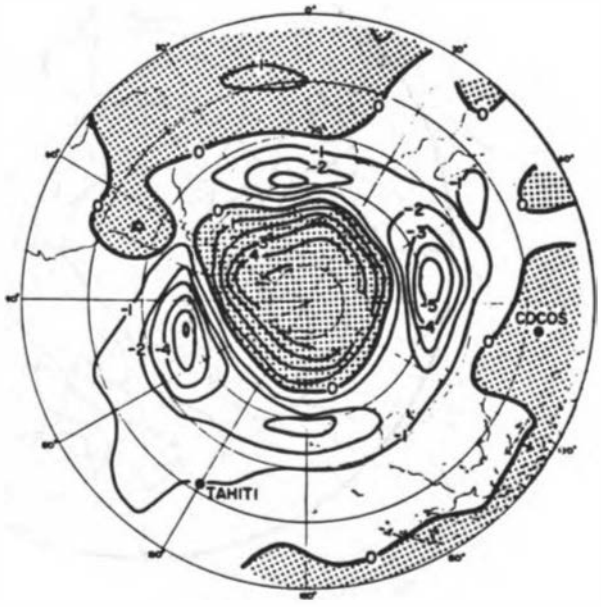


**Figure 8. Deviation from the mean of the sea-level pressure in December, January, and February of 1976-1977. (From van Loon and Rogers 1981.)**

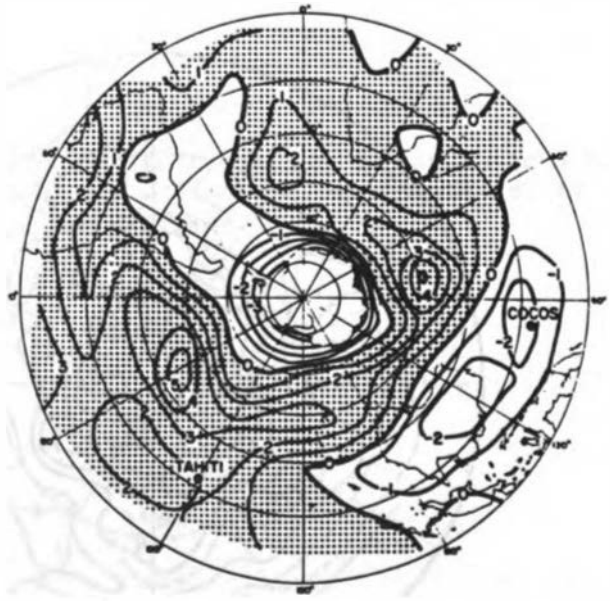


**Figure 9. Deviation from the mean of the sea-level pressure in December, January, and February of 1973-1974. (From van Loon and Rogers 1981.)**

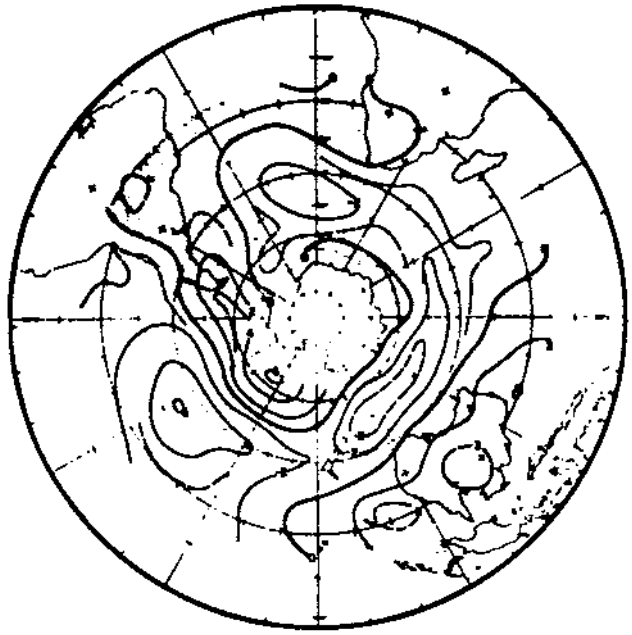

**Figure 10. The difference in sea-level pressure in summer between the extremes of the Southern Oscillation. (From van Loon and Madden 1981.)**

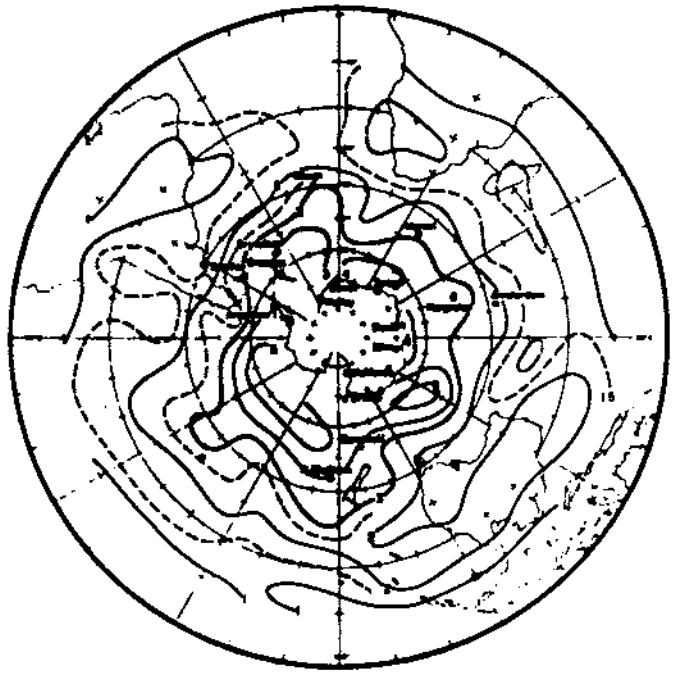

**Figure 11. The standard deviation of monthly mean sea-level pressure in January, based on daily synoptic maps for 12 years.**

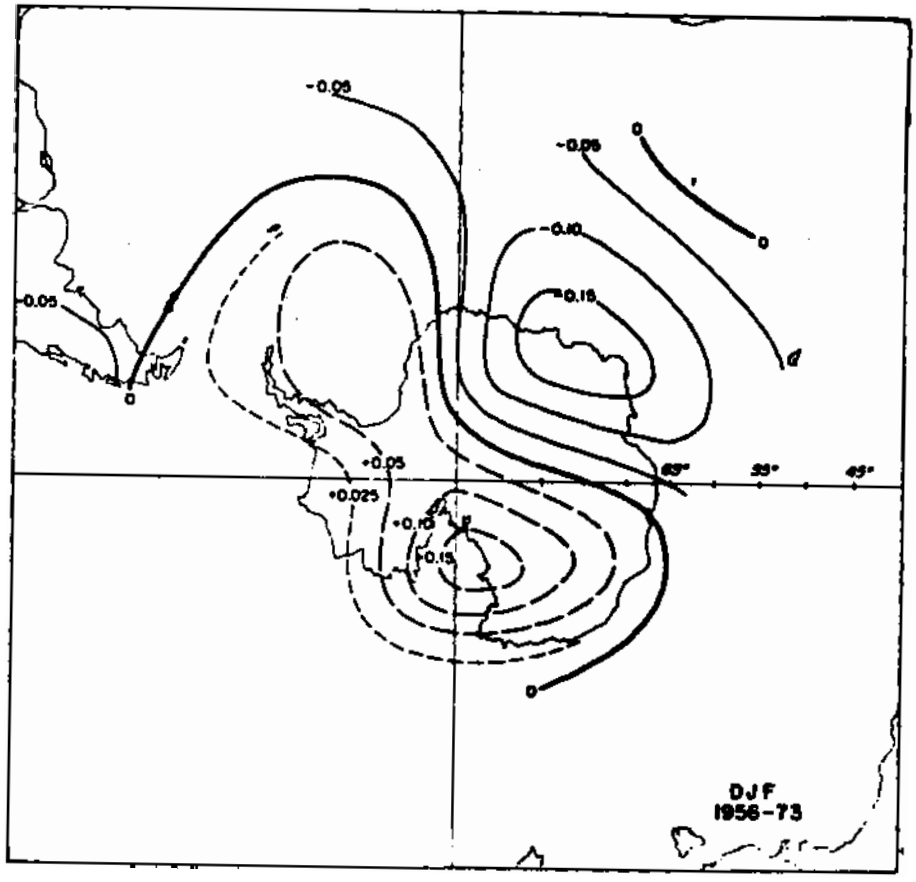


**Figure 12. Linear trend of surface air temperature in summer between 1956 and 1973. Based on all island and continental stations south of 40°S. (From van Loon and Williams 1977.)**

## REFERENCES

Gordon, A. L. and R. D. Goldberg, 1970. Circumpolar characteristics of Antarctic waters. Antarctic Map Folio Series 13, (pp. 1-5, plus maps). American Geographic Society, New York.

Taljaard, J. J. and H. van Loon, 1963. Cyclogenesis, cyclones and anticyclones in the Southern Hemisphere during summer 1957-1958. NOTOS, 12, 37-50.

van Loon, H., 1960. Features of the atmospheric circulation in the South Pacific Ocean during the whaling seasons 1955-1956 and 1956-1957. In Antarctic Meteorology (pp. 274-280). Pergamon, London.

van Loon, H., 1962. On the movement of lows in the Ross and Weddell Sea sectors in summer. NOTOS, 11, 47-50.

van Loon, H., 1967. The half-yearly oscillations in middle and high southern latitudes and the coreless winter. Journal of Atmospheric Science, 24, 472-486.

van Loon, H., 1972. Pressure in the Southern Hemisphere. Meteorological Monographs, 35 (13), 59-86.

van Loon, H. and R. A. Madden, 1981. The Southern oscillation. Part I. Monthly Weather Review, 109, 1150-1162.

van Loon, H. and J. C. Rogers, 1981. Remarks on the circulation over the Southern Hemisphere in FGGE and on its relation to the phases of the Southern Oscillation. Monthly Weather Review, 109, 2255-2259.

van Loon, H. and J. Williams, 1977. The connection between trends of mean temperature and circulation at the surface. Part IV. Monthly Weather Review, 105, 636-647.

# ATTACHMENT 3

# THE ATMOSPHERIC CIRCULATION AFFECTING THE WEST ANTARCTIC REGION IN SUMMER

K. E. Trenberth
University of Illinois, Urbana

## INTRODUCTION

These remarks focus on what is known and what needs to be determined about the circulation in the free atmosphere of the Southern Hemisphere in summer as it affects the West Antarctic Ice Sheet. It is clear that West Antarctica cannot and should not be treated in isolation. Changes in the mean flow over the Southern Hemisphere are accompanied by changes in storm tracks, weather regimes, the incidence of blocking anticyclones, and other synoptic features, all of which have an impact on the heat fluxes and precipitation in the region of interest. Therefore, a brief summary is provided of the mean flow and the characteristics of the stationary and transient eddies that are related to such things as storm tracks and blocking. The kinds of contrasting flow regimes that can occur are examined by looking at interannual variability, and evidence for trends in the circulation is considered.

## MEAN FLOW

A meridional cross section of the zonal mean wind in January is shown in Figure 1. The general features of the relatively strong (>30 m $s^{-1}$) winds at 200 mb should be noted (in contrast to climatologies based solely on station data). The mean geopotential height field and its zonally asymmetric component at 500 mb, given in Figures 2a and 2b for January, show, in spite of the dominance of the zonally symmetric component of the flow, that there are significant stationary waves. However, the latter have an equivalent barotropic structure and do not contribute significantly to poleward heat fluxes. The mean 1,000- to 500-mb thickness field (Figure 3) reveals a very broad meridional temperature gradient south of 30°S.

The regional aspects of Figure 1 are brought out in the mean westerly wind component at 500 mb for the entire summer season in Figure 4. Strongest winds occur over the Indian Ocean, and mean flow over Antarctica is generally quite weak.

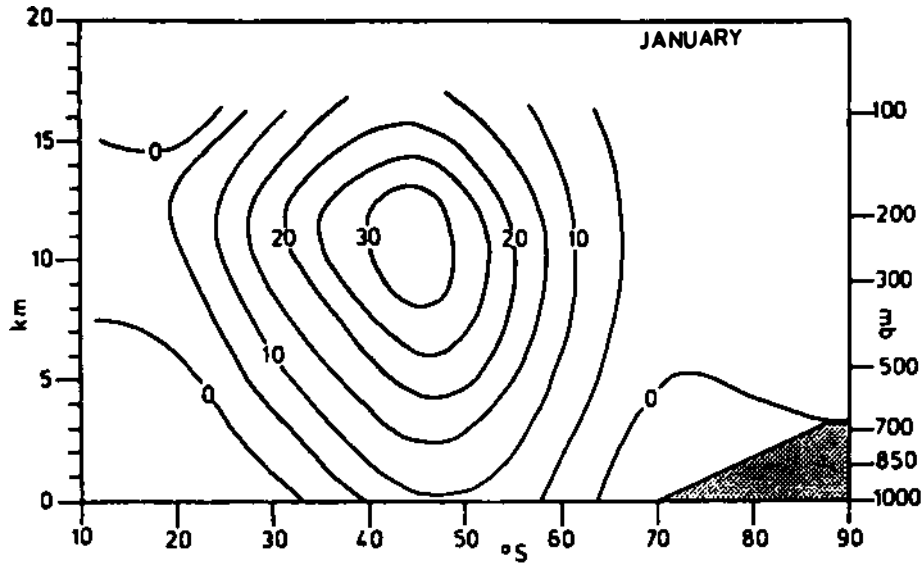


**Figure 1. Meridional cross section of the 6-year mean zonally averaged geostrophic wind (m $s^{-1}$) for January 1973-1978 (From Trenberth in press).**

## EDDY STATISTICS, STORM TRACKS, AND BLOCKING

The circulation in the Southern Hemisphere as a strong zonal mean component, and transient eddies play a much larger role than in the Northern Hemisphere. This role is most readily examined by considering variance and covariance eddy statistics. The high-frequency (periods less than about a week) eddies are transient baroclinic disturbances that tend to be organized into storm tracks and are clearly revealed by the eddy statistics.

Figure 5 shows the standard deviation of the geopotential height at 500 mb, and Figure 6 shows the variance of the north-south component of the wind. Both reveal maxima along about 50°S at all longitudes, which delineates the main storm track in summer. It occurs 5°-10° south of the strongest winds (Figure 4). Circulation statistics for a single summer (1980-1981) derived from analyses made by the European Centre for Medium Range Weather Forecasts provided further evidence for this finding (Figure 7). Again, the storm track lies along about 50°S, as identified by the maxima in $v'^2$ (Figure 7e), about 5° south of the 250-mb jet (Figure 7a). It coincides with maximum vertical ($\omega'T'$) and horizontal ($v'T'$) fluxes of heat (Figures 7b, 7c, and 7d) that are associated with baroclinic disturbances.

Although both cyclonic and anticyclonic disturbances are included in the storm tracks defined by eddy statistics, synoptic evidence (Figure 8) also supports that interpretation. The eddy statistics have the advantage that they measure both the frequency and intensity of disturbances, unlike most conventional synoptic indices.

A spectral breakdown of the variance and covariance fields reveals that not only are the transient high-frequency baroclinic eddies

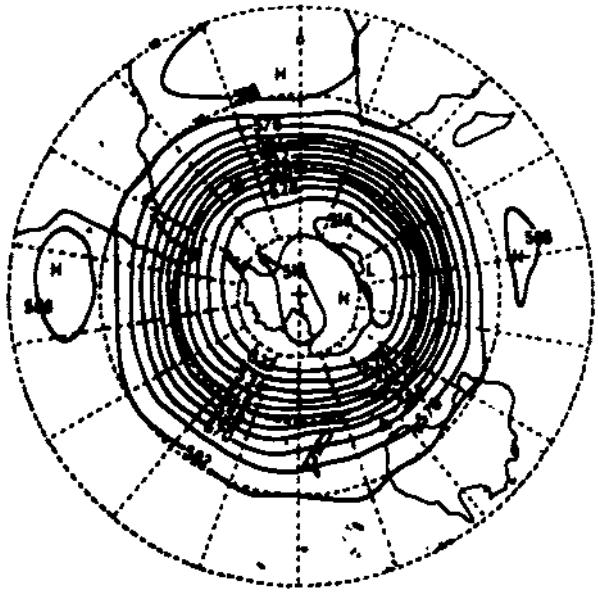

**Figure 2a. Mean geopotential height fields at 500 mb (dam) for January. (From Trenberth 1979.)**

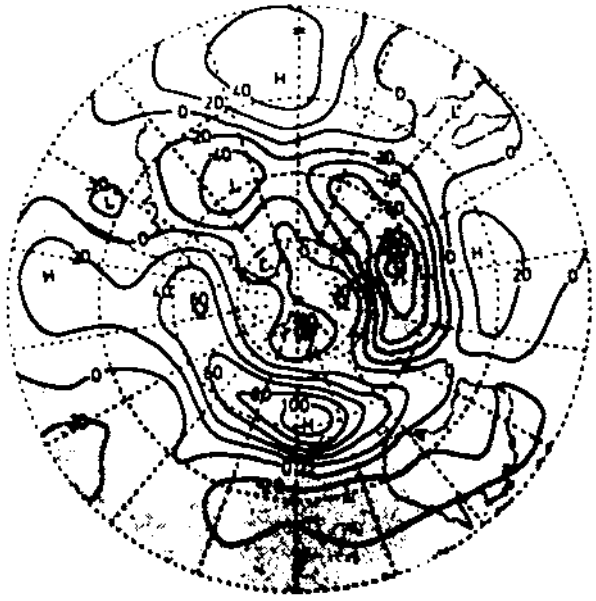

**Figure 2b. Mean zonally asymmetric component of the 500-mb geopotential height $\overline{z}^*$ (gpm) for January. (From Trenberth 1980.)**

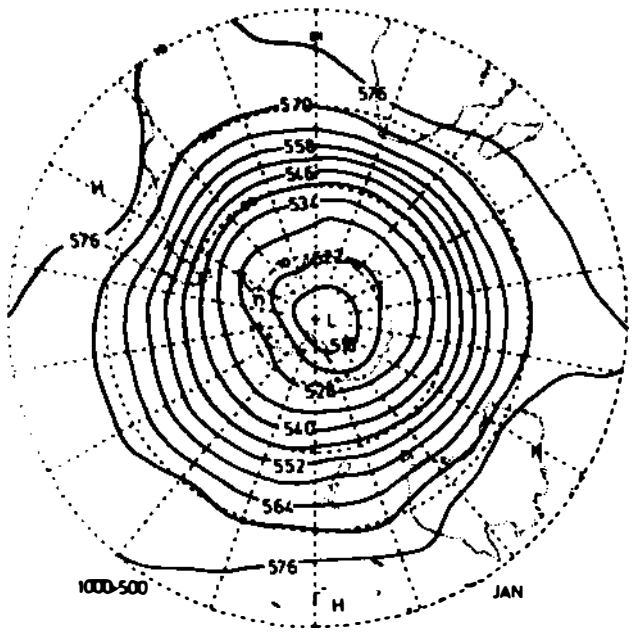


**Figure 3. 1,000- to 500-mb thickness field for January. (From Swanson and Trenberth 1981.)**

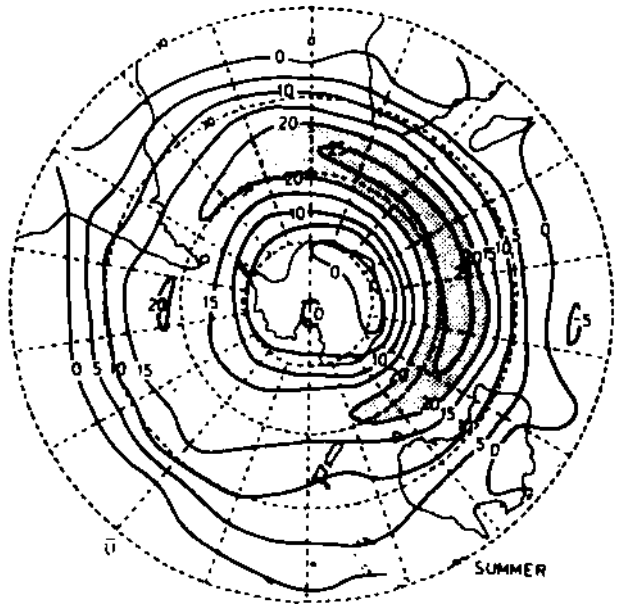


**Figure 4. Mean geostrophic westerly wind component $\bar{u}$ at 500 mb for the 128-day summer season (m $s^{-1}$). Values greater than 20 m $s^{-1}$ are shaded. (From Trenberth 1982.)**

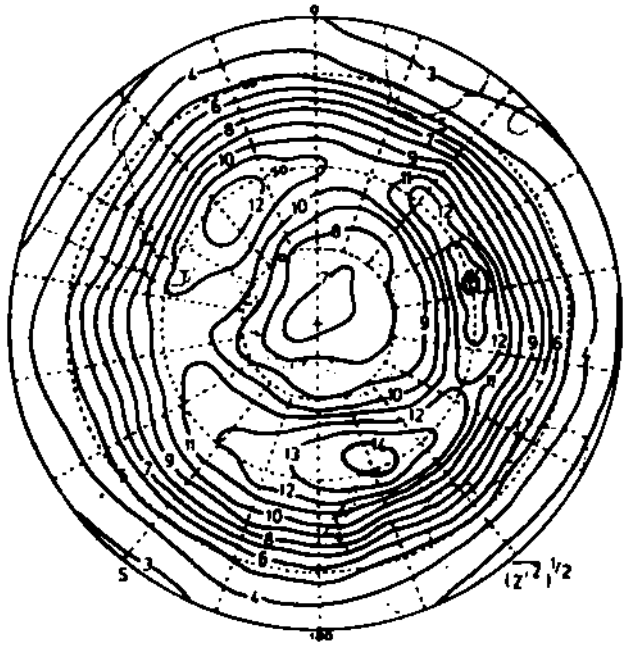

Figure 5. Standard deviations of the departures from the long-term mean of the geopotential height $(\overline{z}'^2)^{1/2}$ for summer (gpdam). Values greater than 14 gpdam are shaded. (From Trenberth 1982.)

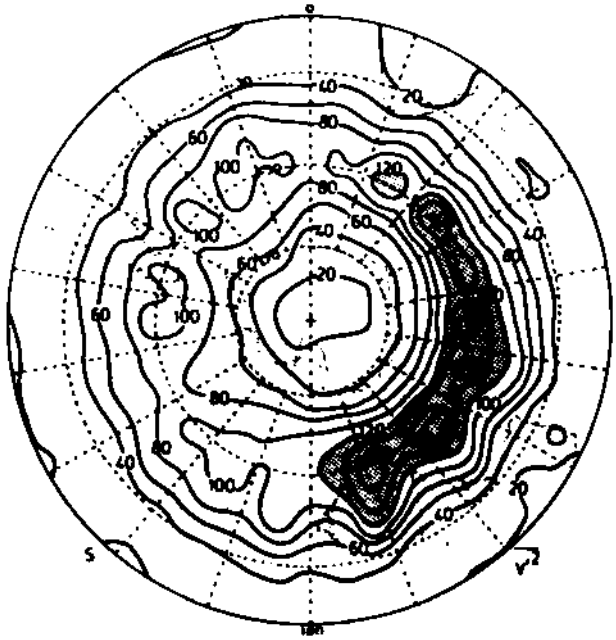

Figure 6. Variance of the northward component of velocity $\overline{v}'^2$ in $m^2\ s^{-2}$ for summer. Values greater than 120 $m^2\ s^{-2}$ are shaded. (From Trenberth 1982.)

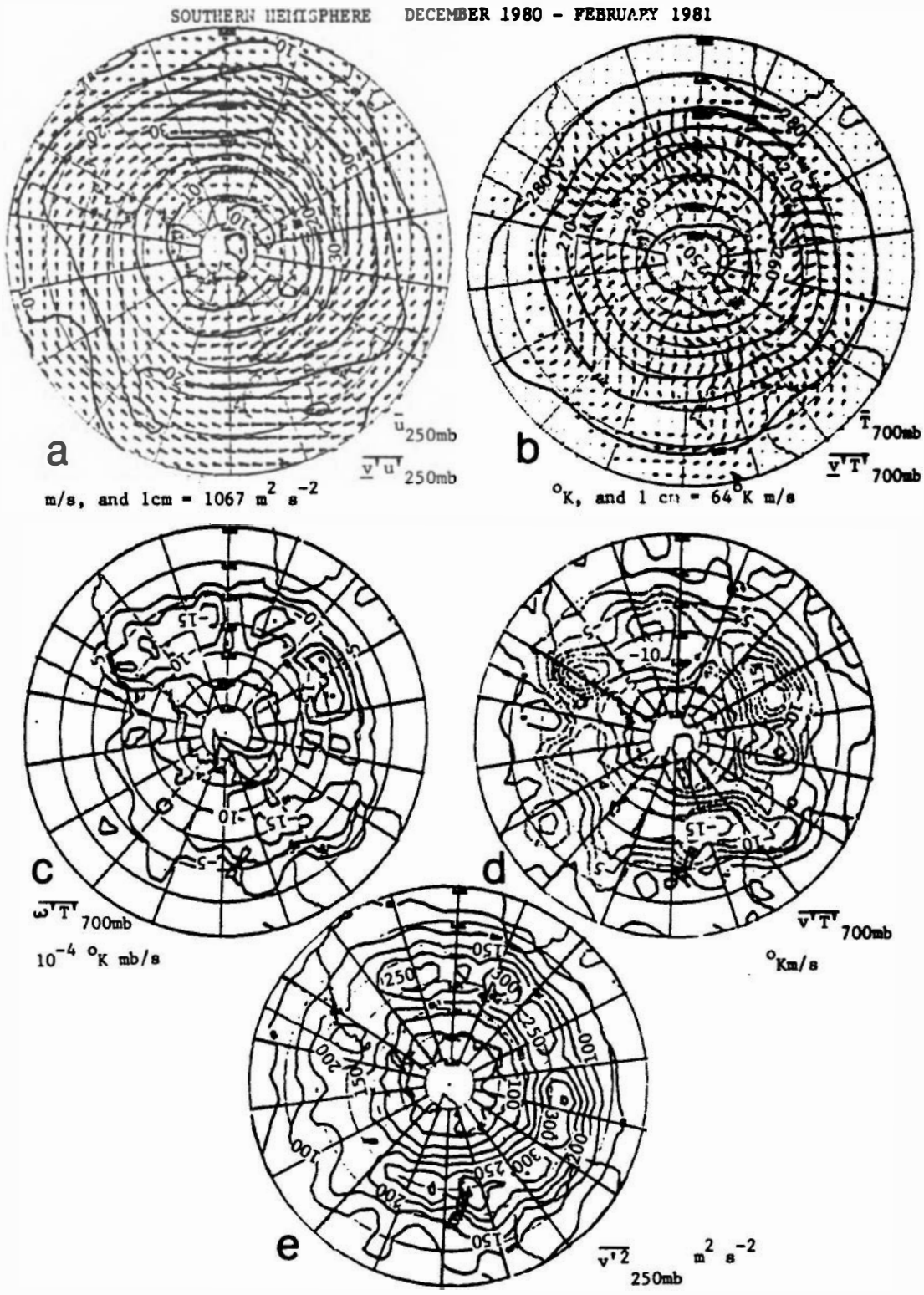


**Figure 7. Summer 1980-1981 circulation statistics (adapted from White 1982.)**

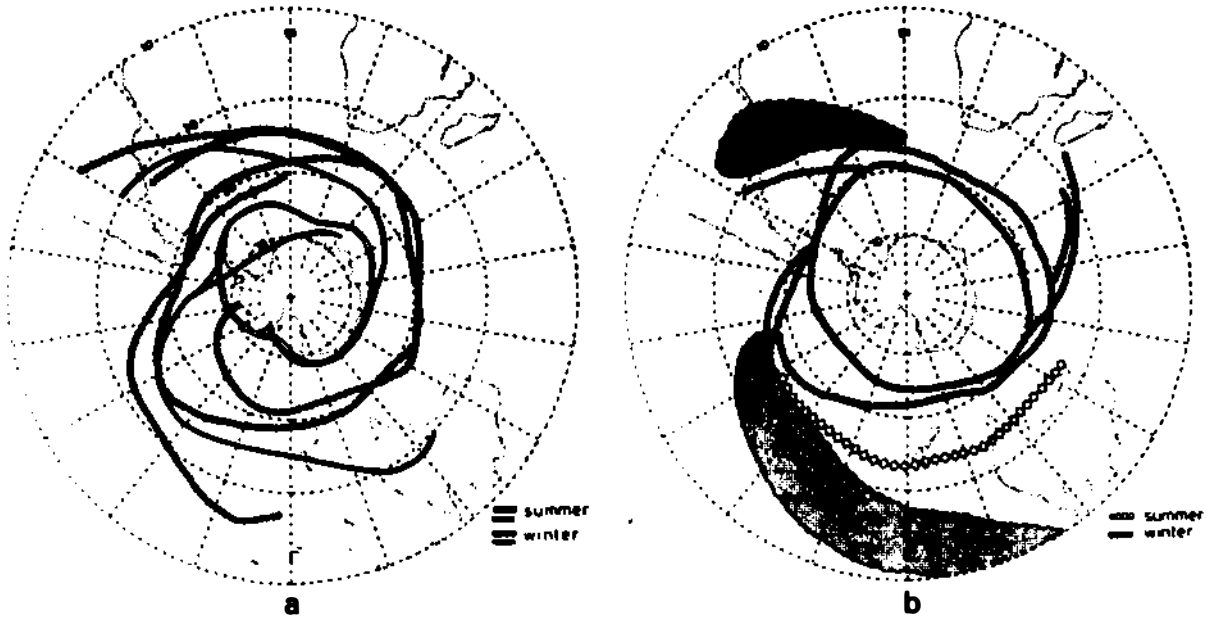


Figure 8. The location of maximum occurrences of various phenomena related to the frequency of storms in the Southern Hemisphere. (a) The frontal frequency maxima (FFM) for winter (solid circles) and summer (open circles), and the maximum frequency of low centers for winter (solid line) and summer (open line).
(b) The semipermanent cloud bands in the Southern Hemisphere are shown by the shaded area, and the scalloped outline depicts the annual mean values with a >30 percent frequency of 5-day average mosaics having axes of major cloud bands within a 5° latitude x 10° longitude square. Also shown are the axes of the maximum occurrence of the "early development (W.A.B.) type" vortices for summer (open circles) and winter (solid circles) and the axis of the "frontless cutoff F/G type" vortices in winter (open diamonds). (From Trenberth 1981a,b.)

important but that lower-frequency fluctuations are also contributing to these patterns. Figure 9 divides the geopotential variance into contributions from the 2- to 8-day period high-frequency baroclinic eddies and the lower-frequency 8- to 64-day period fluctuations. The latter are of comparable importance but tend to be concentrated more into the regions south of New Zealand, southeast of South America, and with a residual in the Indian Ocean. The former two regions are preferred areas in the Southern Hemisphere for blocking anticyclones to form and persist.

Further evidence for the incidence of blocking-type phenomena in summer is shown in Figures 10a and 10b, which give the numbers of disturbances at each point exceeding a certain threshold for a given number of days. The disturbance is defined as the departure from the mean annual cycle, and consequently, positive and negative departures balance overall. However, anticyclonic anomalies tend to last slightly

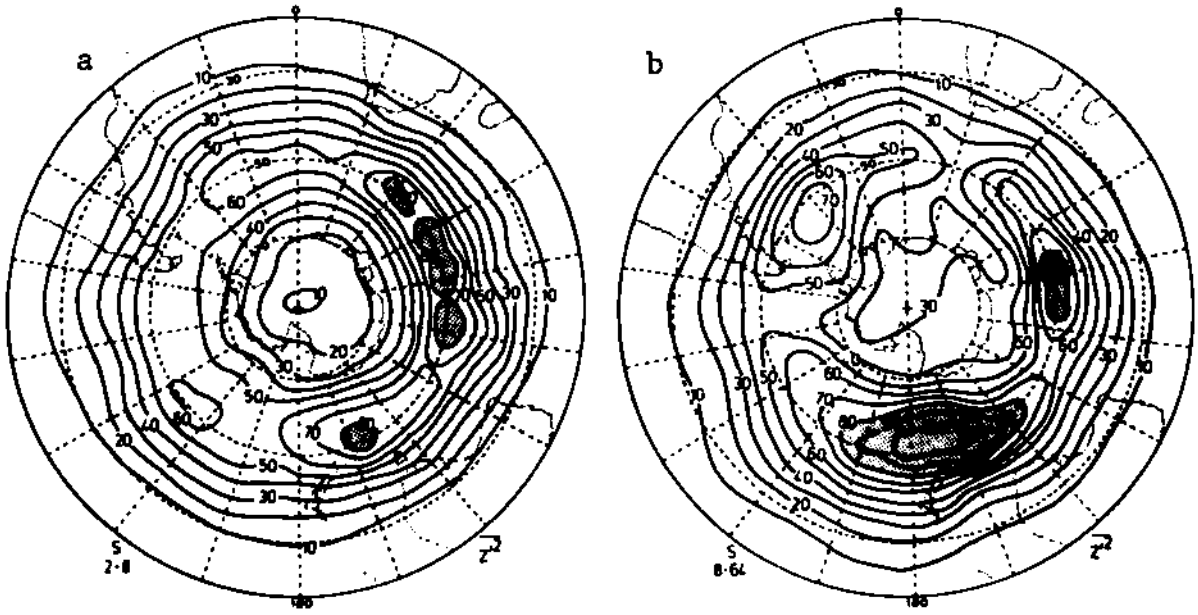


Figure 9. The spectral bands of geopotential height variance in gpdam$^2$. (a) Two- to eight-day band in summer; (b) 8- to 64-day band in summer. Values greater than 80 gpdam$^2$ are shaded. (From Trenberth 1982.)

longer than the cyclonic anomalies, for the latter are more likely to be interrupted by small-scale transient disturbances. At 1,000 mb (Figure 10a), the count of disturbances exceeding $\pm$50 gpm for 5 days or more is shown. At 500 mb (Figure 10b), the threshold has been increased to $\pm$100 gpm. Of special note for West Antarctica would be any change in the incidence of the blocking southeast of South America.

## INTERANNUAL VARIABILITY

Several studies have now shown that interannual variability of the circulation in the Southern Hemisphere is large, apparently larger than in the Northern Hemisphere. For example, the circulation throughout the First GARP Global Experiment (FGGE) year was quite anomalous. The mean meridional cross section of the wind for January 1979 is shown in Figure 11, together with the departure from the long-term mean of Figure 1. The anomalies, in excess of $\pm$5 m s$^{-1}$, correspond to a poleward shift of the jet by about 3° latitude.

The two summers over the past decade that appear to differ most are 1976-1977 and 1978-1979, the FGGE summer. The departures of $\bar{u}$ at 500 mb from the mean field of Figure 4 are given in Figure 12. We note the roughly opposite character of the anomalies of order 2-4 m s$^{-1}$. We further note the predominantly zonal character of anomalies, so that most of the contrast in circulation is revealed by the zonal means. Other studies have shown large interannual variability in the zonal mean winds year round, with a tendency for opposite fluctuations to

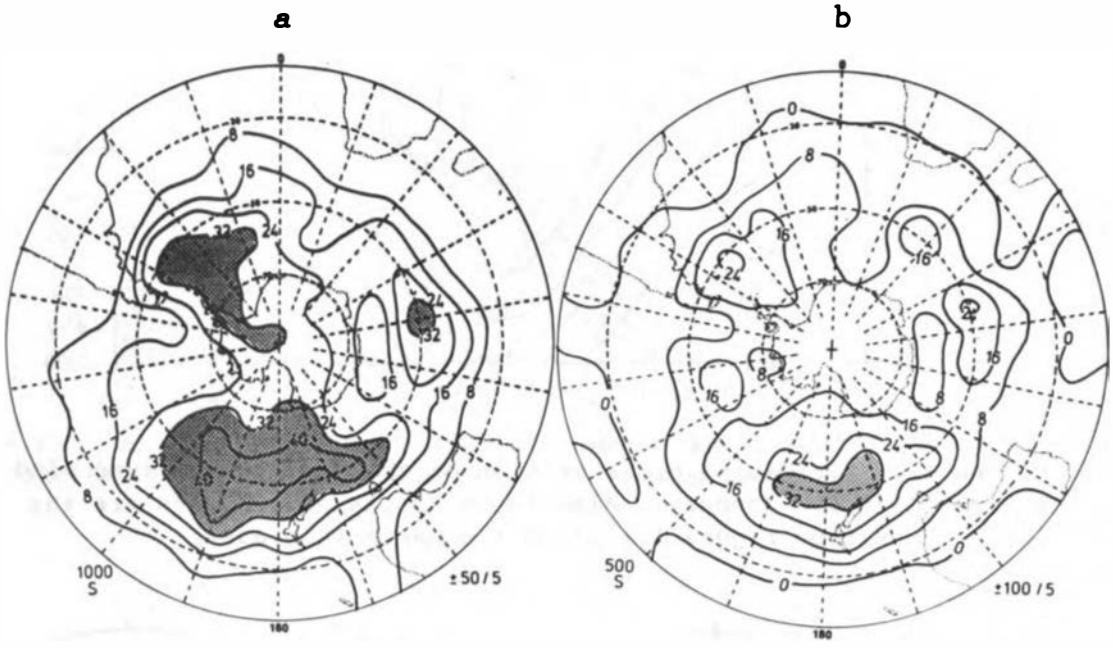


**Figure 10. Count of the number of cases per decade persisting for 5 days or more exceeding the thresholds (a) ±50 gpm in summer at 1,000 mb and (b) ±100 gpm in summer at 500 mb. (From Trenberth and Swanson 1983.)**

occur about 12° further north or south. For example, Figure 13 shows a negative correlation between $\bar{u}$ at different latitudes over the Pacific sector of the hemisphere.

An examination of the eddy statistics for the two opposite summer circulation regimes reveals a corresponding shift in the storm tracks. Figure 14 shows the differences at 500 mb in $[\bar{u}]$, the high-frequency part of $[\overline{z'^2}]$, $[\overline{v'^2}]$ (both measures of the storm track activity), and the tendency of the zonal mean wind due to convergence of momentum by the transient eddies (related to $\overline{u'v'}$) into the storm tracks. The pattern is systematic and internally consistent and corresponds to a poleward shift in the jet and storm tracks of ~6° latitude in going from 1976-1977 to 1978-1979.

It would be most useful to know just what changes were encountered over Antarctica corresponding to these contrasting summers. At Halley Bay (the only station "near" West Antarctica for which observations were published in Monthly Climatic Data for the World), the main contrast occurred between the Decembers, where December 1976 had heights higher than December 1978 by 131 gpm at 850 mb and 180 gpm at 500 mb. The regional eddy statistics show a much higher level of activity in the 1978-1979 summer through the Drake Passage and over the

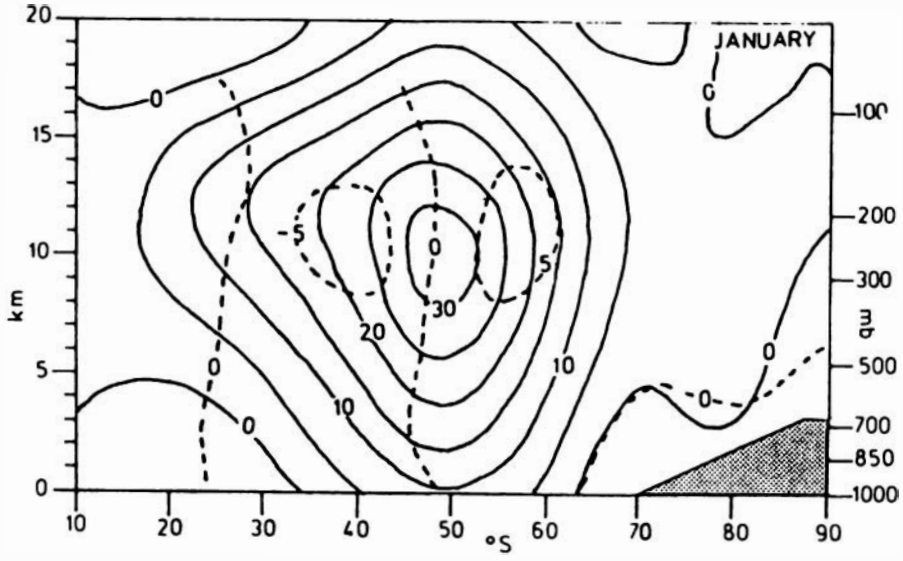


**Figure 11. Meridional cross section of the zonally averaged wind (m $s^{-1}$) in 1979 for January. Also shown as dashed contours are the differences from Figure 1. (From Trenberth in press.)**

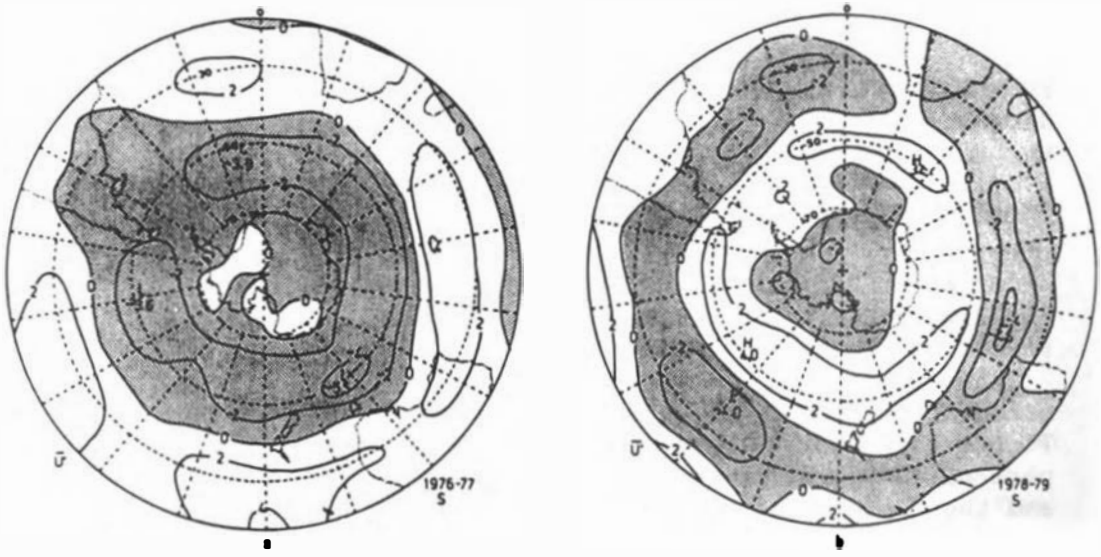


**Figure 12. Departures from the mean field of Figure 4 of the ū field for the summer of (a) 1976-1977 and (b) 1978-1979 (m $s^{-1}$). Negative departures are shaded. (From Trenberth in press.)**

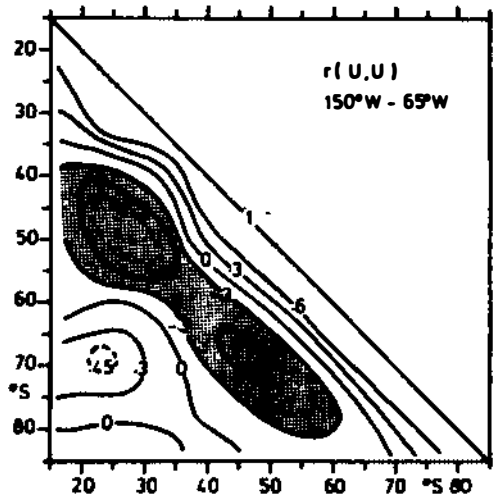


**Figure 13. Correlations between the 90° sector zonal mean $\bar{u}$ fields at different latitudes for the Pacific Ocean. (From Trenberth 1981b.)**

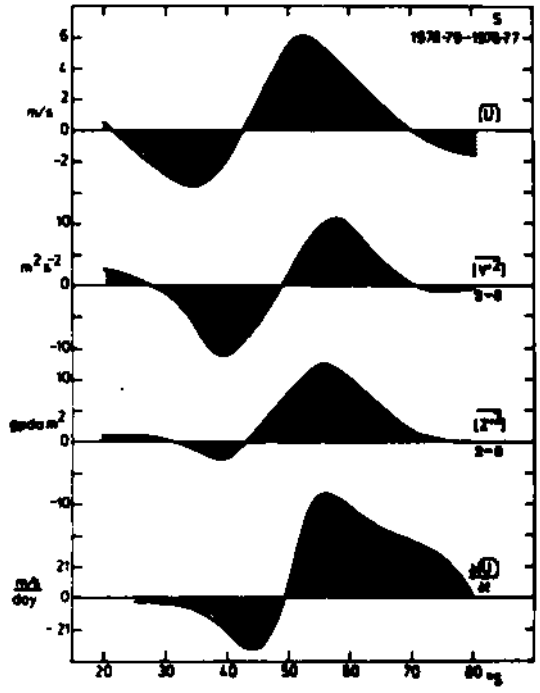


**Figure 14. Differences between zonal mean quantities for the summers of 1978-1979 minus 1976-1977. Shown from top to bottom are $[\bar{u}]$, m $s^{-1}$; $[\overline{v}'^2]$ in the 2- to 8-day band, $m^2$ $s^{-2}$; $[\overline{z}'^2]$ in the 2- to 8-day band gpdam$^2$; and the eddy convergence of momentum contribution to $\partial[\bar{u}]/\partial t$, m $s^{-1}$/day. (From Trenberth in press.)**

Antarctic Peninsula. In fact, during late December 1978 record-high surface temperatures were experienced over much of Antarctica associated with two warm air intrusions. These produced temperatures above 0°C at Halley Bay (+2.5°C on 28 December) and up to +9.6°C at McMurdo Sound, and at the South Pole, temperatures reached a record high of -13.6°C on 26 December. The detailed synoptic description of this period is given by Sinclair (1981).

## TRENDS

Owing to the rather short record, it is difficult to determine definitive trends over Antarctica. However, it seems clear from the available record that large-amplitude, long-period fluctuations have been occurring. Figure 15 shows the individual January mean surface pressures at the South Pole and geopotential heights at 500 mb at the South Pole and McMurdo Sound. The linear trend of +3.7 gpm/year at the South Pole is also shown. This figure is modified from the one given by Trenberth (1979) by including values at the Pole revised as

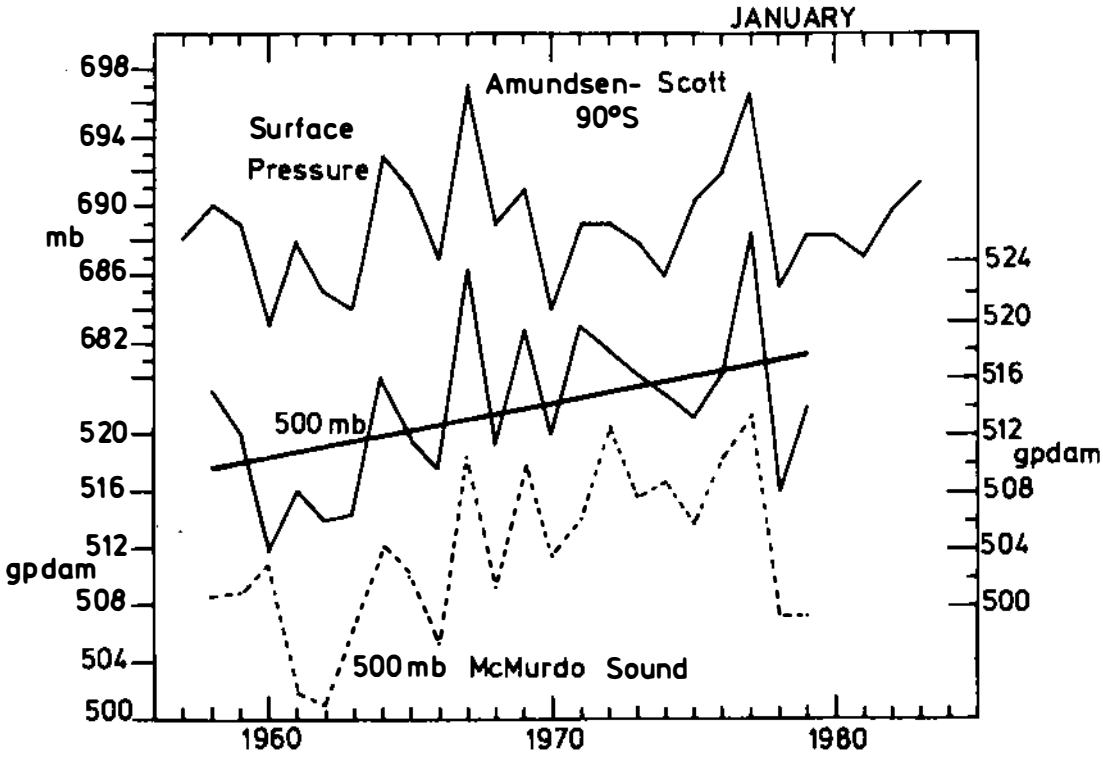


Figure 15. Series of month mean values for January at the South Pole (solid curves), surface pressure top (scale at left) and 500-mb height (scale at right), and at McMurdo Sound (78°S, 60°E) 500-mb height (dashed curve, scale at left). A linear trend line is also fitted to the Pole 500-mb height series.

suggested by Schwerdtfeger (1981). Data have been obtained from several sources, and it is disconcerting to find unexplained discrepancies between some values. However, the upward trend is also clearly evident at McMurdo Sound. It is less apparent in the station pressure at the Pole. Of special note in this figure is the range of 224 gpm in the January mean 500 mb height at the Pole. Since the corresponding range in surface pressures is 14 mb (about 147 gpm; 1 mb ~10.5 mb in January at the Pole), the low-level thickness between the surface and 500 mb has evidently also contributed significantly to the fluctuations. With such large natural variability, statistics over a limited period cannot be considered highly stable.

A further idea of the trends in the upper atmosphere can be obtained by contrasting sets of means over two different periods. Thus, we have contrasted the May 1972 to January 1978 period with the atlas means of Taljaard et al. (1969), which effectively cover the period 1957-1966. Some of the apparent trends that emerge are spurious and arise from different techniques of analysis and the like, but over Antarctica, as shown in Figure 15, the trends are mostly real for this period. The trends at 850 mb, 500 mb, and for the thickness layer are given in Figures 16a-16c. Almost certainly, these changes are not due to any changes in $CO_2$; therefore, they compound the difficulty of detecting any long-term significant trends associated with $CO_2$.

## CONCLUSIONS

This brief review focused on the general circulation of the Southern Hemisphere in middle and high latitudes in summer because of a strong conviction that any changes in climate induced by increases in $CO_2$ cannot be treated in a local framework. However, there is a dearth of detailed knowledge of the local circulation in the immediate vicinity of West Antarctica. Rawinsonde stations no longer exist in that area. Even the nearby stations like Amundsen-Scott at the South Pole and McMurdo are generally missing from Monthly Climatic Data for the World. At Halley Bay, which has reported more regularly over the past few years, many days are missing (in each of the months from March to July 1982 there were from 15 to 18 days missing in each reported monthly "mean" value). The status of the obervations in this region of the world appears to be deplorable.

A good set of observations is needed to validate models of the Southern Hemisphere circulation, and unfortunately, the model simulations to date are not good. It seems, in particular, that the effects of the cold, high, and highly reflective Antarctic continent appear to be poorly understood and not extensively explored.

In spite of the overall zonal symmetry of the circulation, especially in summer, there are planetary waves in the Southern Hemisphere that have an impact on the preferred regions of blocking and the distribution of storm tracks. The latter are also closely tied to the location of the mean jet stream. They all seem to be linked to the distribution of the Antarctic continental mass itself and to the associated surrounding sea ice and distribution of sea surface

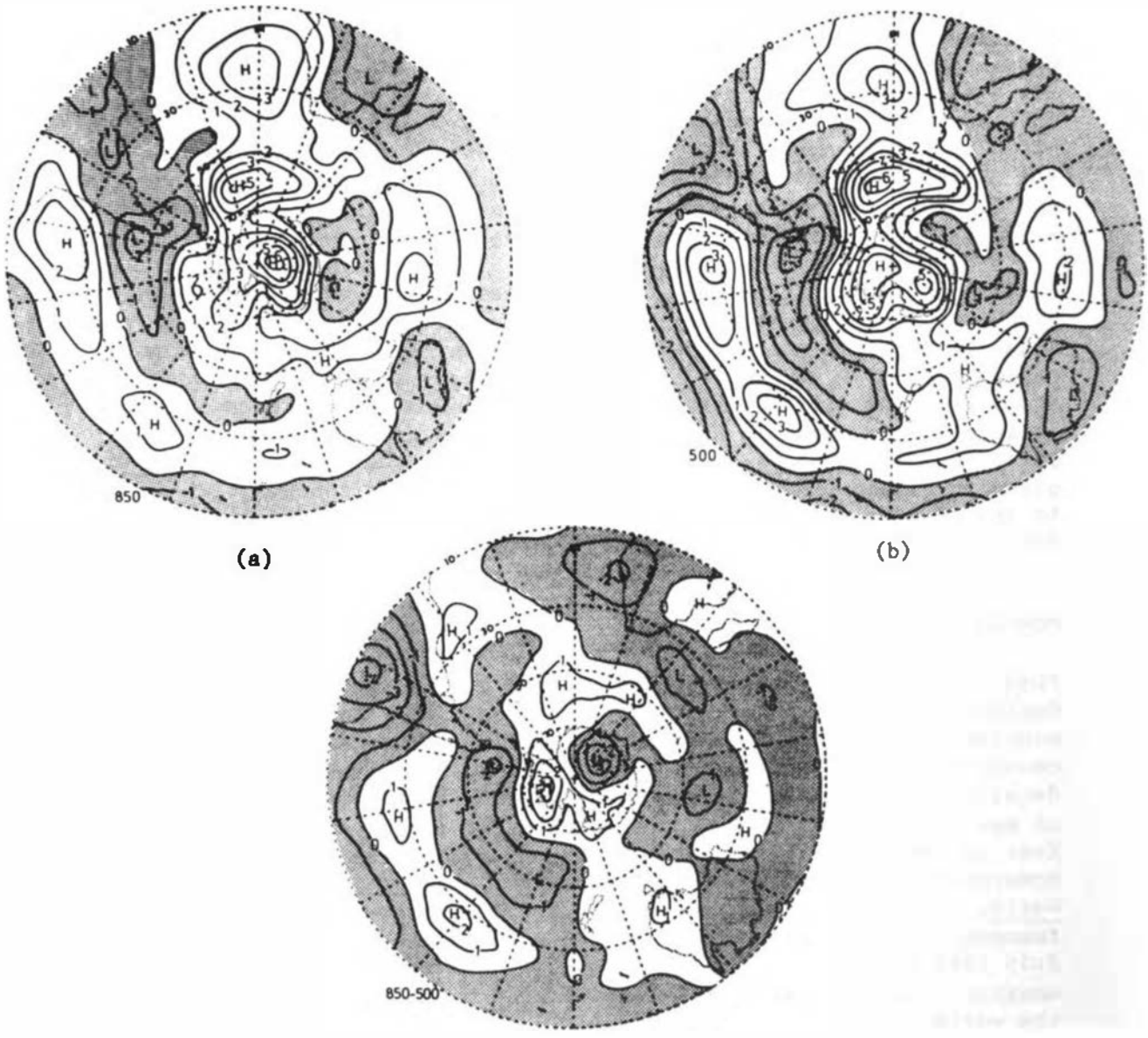


**Figure 16. Differences from the atlas (Taljaard et al. 1969) of the Australian mean annual fields. Negative values have been shaded. (a) 850 mb, (b) 500 mb, (c) 850- to 500-mb thickness (dam). (From Swanson and Trenberth 1981.)**

temperatures. It is clear that major changes in the jet stream and major storm tracks do occur from year to year, apparently with substantial consequences for outbreaks of warm air advection well into the Antarctic continent. The impact on the local heat budget of any increase in such events could be profound. Only with increased understanding of the way that the entire circulation, including the mean flow, transient baroclinic storms, and blocking anticyclones, varies with increasing $CO_2$ in the atmosphere, can we adequately address the fundamental questions.

## REFERENCES

Schwerdtfeger, W., 1981. Elevation of Amundsen-Scott South Pole Station: 2,835 meters. Antarctic Journal of the United States, 16, 10-11.

Sinclair, M. R., 1981. Record-high temperatures in the Antarctic--a synoptic case study. Monthly Weather Review, 109, 2234-2242.

Swanson, G. S. and K. E. Trenberth, 1981. Trends in the Southern Hemisphere tropospheric circulation. Monthly Weather Review, 109, 1879-1889.

Taljaard, J. J., H. van Loon, H. L. Crutcher, and R. L. Jenne, 1969. Climate of the Upper Air: Southern Hemisphere, Volume 1, Temperatures, Dew Points and Heights at Selected Pressure Levels. NAVAIR 50-1C-55. Naval Weather Service Command, Washington, D.C.

Trenberth, K. E., 1979. Interannual variability of the 500 mb zonal mean flow in the Southern Hemisphere. Monthly Weather Review, 107, 1515-1524.

Trenberth, K. E., 1980. Planetary waves at 500 mb in the Southern Hemisphere. Monthly Weather Review, 108, 1378-1389.

Trenberth, K. E., 1981a. Observed Southern Hemisphere eddy statistics at 500 mb: frequency and spatial dependence. Journal of Atmospheric Science, 38, 2585-2605.

Trenberth, K. E., 1981b. Interannual variability of the Southern Hemisphere 500 mb flow: regional characteristics. Monthly Weather Review, 109, 127-136.

Trenberth, K. E., 1982. Seasonality in Southern Hemisphere: eddy statistics at 500 mb. Journal of Atmospheric Science, 39, 2507-2520.

Trenberth, K. E., in press. Interannual variability of the Southern Hemisphere circulation: representativeness of the year of the Global Weather Experiment. Montly Weather Review.

Trenberth, K. E. and G. S. Swanson, 1983. Blocking and persistent anomalies in the Southern Hemisphere. In First International Conference on Southern Hemisphere Meteorology, July 31-August 6, 1983, San Jose dos Campos, Brazil (pp. 73-76) Preprint volume.

White, G. H., 1982. The Global Circulation of the Atmosphere December 1980-November 1981 Based upon ECMWF Analyses. University of Reading, Reading, United Kingdom.

## ATTACHMENT 4

# WEST ANTARCTIC SEA ICE

S. F. Ackley
U.S. Army Cold Regions Research and
Engineering Laboratory, Hanover, New Hampshire

## INTRODUCTION

As with the other snow and ice forms, Antarctic sea ice possibly has a nonlinear or feedback effect on climate. In addition to the well-known albedo-radiation feedback attributed to snow cover, the large ice sheets, and sea ice, several other mechanisms have been postulated. These include a number of pycnocline stability effects (Kellogg 1975; Gordon 1981) that can produce climatic feedbacks of either sign. For example, sea-ice formation can be self-limiting (a negative feedback), because the freezing of the ice induces an overturning in the water column by thermohaline rejection, bringing up ocean heat from intermediate-depth waters and either preventing more ice from forming or melting the existing ice. Formation of sea ice can also reduce vertical mixing (positive feedback), for ice growth rates slow as the ice thickens, leading to higher stability in the upper layers, a reduction in upwelled heat, and a potential increase in rates of ice growth. Another mechanism is hypothesized in the deep-ocean-temperature/sea-ice-extent oscillator model of Saltzman (1978) and Saltzman and Moritz (1980). Here, a coupled response of the ice extent and ocean temperature is suggested, leading to oscillations of the two parameters, with characteristic periods of from hundreds to thousands of years.

Although these mechanisms have been suggested and many others can be postulated, a consideration of the present formation and decay of Antarctic sea ice may help us determine (a) if sea ice will respond to a $CO_2$-induced climatic warming, and (b) how this sea-ice change will affect the West Antarctic environment. Some unique aspects of Antarctic sea ice are readily apparent in its interaction with climatic change. For example:

1. The location of the ice is on the southern boundary of the westerly wind system of the Southern Hemisphere, which in midlatitudes is a major repository of kinetic energy of the general circulation of the atmosphere. Schwerdtfeger (1979), for example, has shown how ice transport from the Weddell Sea strongly affects midlatitude temperature and presumably circulation in the South Atlantic region at the present time.

2. The free boundary of the southern sea ice with the world ocean, as opposed to the Mediterranean nature of the Arctic Ocean, suggests, qualitatively at least, a more interactive role than that of the Arctic with global-scale processes.

3. The region south of the Polar Front, at least half involving the sea-ice cover, is a "heat exchanger," where heat taken up by the ocean elsewhere is dissipated, thus affecting the total heat transport by the oceans and the ocean-atmosphere interaction in polar regions (Gordon 1979, 1981).

4. As part of the heat-exchange process, the formation of Antarctic sea ice leads to thermohaline processes producing Antarctic bottom water (Foster and Carmack 1976) and thereby affects the meridional heat and salt transport by oceanic waters, as well as the global cycling of sea waters for nutrient and gas exchange.

## CHARACTERISTICS OF WEST ANTARCTIC SEA ICE

West Antarctic sea ice consists of the ice covers in the Weddell Sea (extending past the Greenwich Meridian), in the Amundsen-Bellingshausen Seas, and in the Ross Sea. These three units have some distinctive characteristics in their sea-ice covers, basically in the seasonal cycle, which we review here. The premise is that some understanding of the processes involved will improve projections of the effects of $CO_2$ warming. Figure 1 shows the advance-retreat characteristics for the total area around Antarctica and for tne individual sectors, including the three mentioned. These are for the three years 1973-1975, as obtained from satellite imagery (Zwally et al. 1979). As indicated here, the Amundsen-Bellingshausen sector shows the least seasonal swing of the regions and only accounts for about 20 percent of the total West Antarctic pack, compared with over half for the Weddell pack and about 30 percent for the Ross Sea pack ice at maximum extent. The Ross and Weddell seas are similar in that they both show sharp increases in ice area during the early season, building to a maximum in June, followed by a relatively constant ice-covered area during the height of the winter season (July-September). The decay phase is characterized by a relatively precipitous decline in ice-covered area during the November-January period.

This decay behavior, or "seasonality" has been modeled for the Weddell region (Hibler and Ackley 1983) as a phenomenon associated with ice transport and dynamics. In the early season, the onset of cold conditions in the high-latitude embayments of the Weddell and Ross seas leads to high production of ice. The ice and accompanying cold air are rapidly advected, leading to freeze-over in the embayments until warm oceanic conditions are encountered at the southern edge of the Polar Front. The ice cover then stops advancing througn a balance between ice transport to the edge and ice melting occurring there. Figure 2 shows data-buoy drift tracks from 2 years in the Weddell Sea, illustrating the broad and relatively constant flow of ice to the ice edge throughout the year. This "conveyor-belt transport" accounts for continuation of the maximum extents until well past the time of retreat

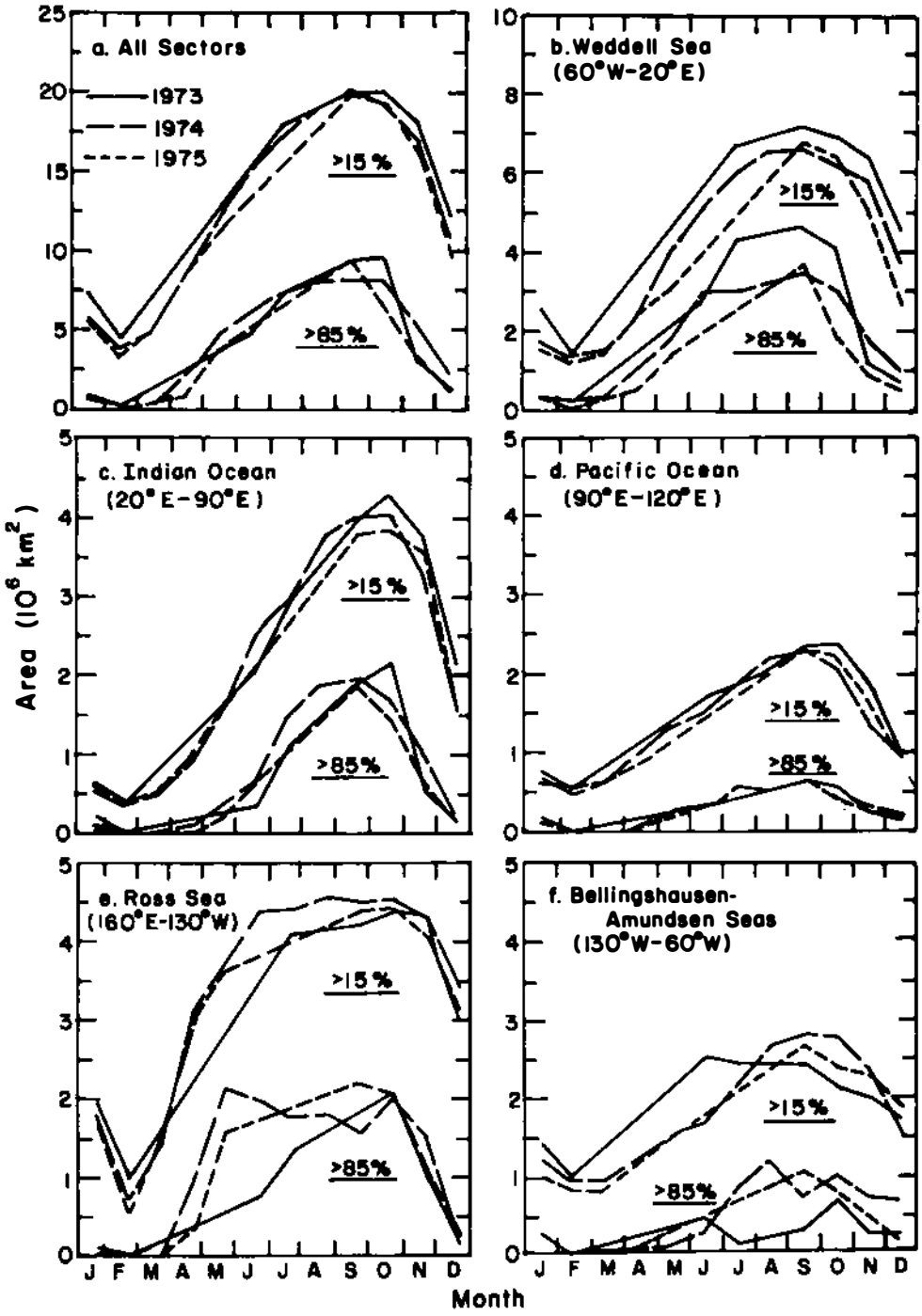


**Figure 1. Total ice and ice area by sectors around Antarctica (1972, 1974, 1975). The areas of more than 15 percent ice concentration and more than 85 percent ice concentration are indicated. (After Zwally et al. 1979.)**

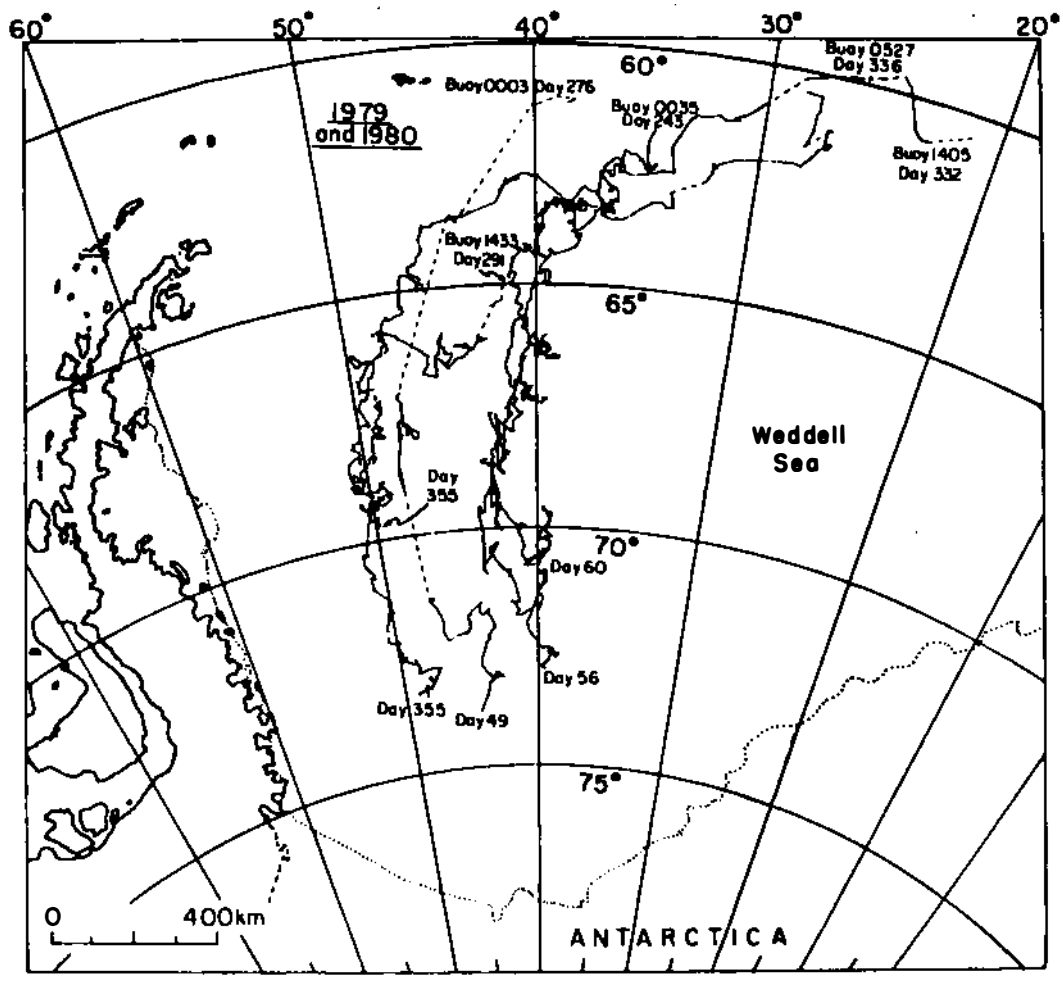


**Figure 2. Drift tracks of buoys 0003, 0035, 0527, 1405, and 1433.**

in other, more thermodynamically controlled regions, such as East Antarctica and the Amundsen-Bellingshausen Seas. As Hibler and Ackley (1983) have shown, feedback between the presence of ice and air temperature prevents ice retreat until summer insolation effects are high. Intense heating in open water created by ice dynamics, together with continuous transport of ice to the outer regions of the pack, eventually leads to the rapid late-season decline in ice extent characteristic of the Weddell Sea. Figure 3 shows the effect of including the first-order air temperature feedback, extending the season of the maximum extent of the pack and creating a major sink for ice melting in the outer regions of the pack ice. Figure 4 indicates the mass-balance characteristics modeled for the Weddell region, showing the high ice production in the south. This ice is advected and decays in a relatively narrow region in the north and east parts of the Weddell Sea. The major features of the ice modeling have been verified by buoy-drift comparisons (Figure 2), by measurements of field-ice thickness, and by satellite estimates of ice extents and variations in

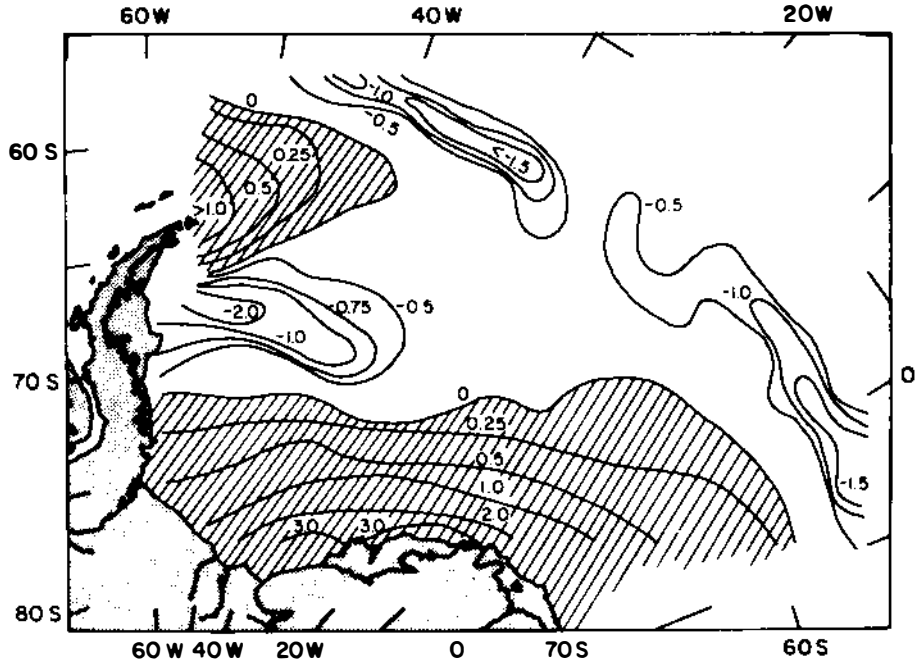


Figure 3. Contours (in meters) of the net annual ice growth over an annual cycle for the fully coupled dynamic-thermodynamic model. The contours were compiled from the third year of the feedback simulation.

ice concentration (Ackley 1979; Gow et al. 1982; Clarke and Ackley 1982).

Information on the Ross Sea pack is considerably more limited. However, as mentioned before, it has several features in common with the Weddell Sea pack. A single drift track of the ship Aurora in 1915-1916 shows similar velocities to present buoy drifts in the Weddell Sea (~5 km/day) and a generally northern track out of the Ross Sea, paralleling the movement of ice in the Weddell Sea from the southern low-temperature embayment out into the warmer ocean regions. It appears that the Ross Sea reaches an equilibrium maximum sooner in the winter season (May-June) and further south than does the Weddell. This feature perhaps reflects the enhanced ocean heat flux in the vicinity of the Polar Frontal Zone, which is at a more southern location in the Pacific than in the Atlantic. Preliminary analysis of ice ridging on data obtained from airborne laser profilometry over the Ross Sea (Govoni et al. in press) indicates less ridging in the Ross than in the Weddell Sea (Ackley 1979). Therefore, ice-deformation contributions to the mass balance in the Ross Sea may be somewhat reduced compared with the Weddell Sea pack ice, as indicated in Figure 4.

Knowledge of the ice characteristics in the Amundsen-Bellingshausen seas is similarly limited. The only drift track, that of the Belgica in 1897-1899, does indicate considerably less ice motion (~1 km/day) than in either the Ross or Weddell seas. The motion is also west to east rather than south to north. The annual cycle, as shown in

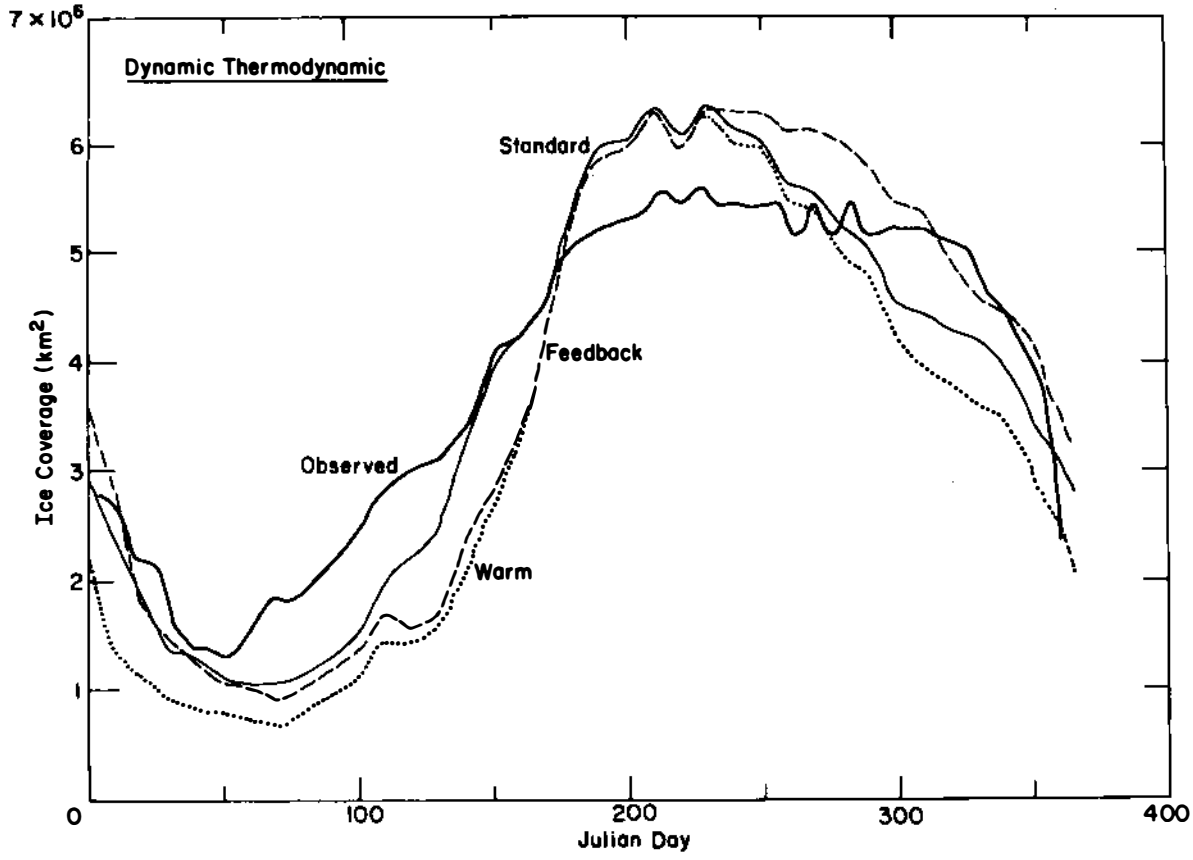


**Figure 4. Time series of total area covered by ice within the simulation region for dynamic-thermodynamic simulation.**

**Figure 1, is also of considerably less amplitude and gradient than in these other two seas. The relative sluggishness of the pack and its stability over the annual cycle suggest more thermodynamic than dynamic controls on the pack ice of this section than on that of either the Ross or Weddell seas.**

## CONCLUSIONS

**To develop a full understanding of climatic influences on the behavior of the majority of the pack ice influencing the West Antarctic environment, it is necessary to deal with the dynamic influences affecting the majority of the ice cover mainly concentrated in the Ross and Weddell seas. Major questions also remain about the influences of the oceanic heat flux, especially in controlling the position of the maximum extent of the pack ice. Modeling results for the Weddell Sea pack ice have shown that major effects in the seasonal cycle can be accounted for by assuming a thermodynamic control on the maximum ice extent and basically dynamic controls on the ice retreat to its minimum. The pack ice in these highly dynamic areas appears to prolong**

its maximum extent by local feedback effects between the ice presence and surface air temperatures. This behavior gives a delayed response to the buildup of summer insolation until ice dynamics creates sufficient open water to absorb radiation and, at that point, leads to the decay of the pack ice. Wind-forcing effects, therefore, have a strong influence on the advance-decay characteristics of the pack ice. Simplified $CO_2$ scenarios that predict temperature rises may be difficult to relate to sea-ice changes, since wind-field changes associated with the $CO_2$ temperature increases are not known at present. Hibler (1984) has shown, for example, that raising the temperature by 4 K in a full dynamic-thermodynamic simulation of the Weddell pack ice has a relatively modest effect on the extent of the pack ice. The wind behavior may be difficult to predict, as it probably interacts with the pack ice as well as the temperature field. The pack ice is responding in a highly coupled manner to both temperature and wind fields. Given the "robustness" of the ice dynamics in these locations, it is suggested that $CO_2$-induced temperature rises would be severely modulated by the ice dynamics in these regions. We know, for example, that the presence of pack ice restrains temperature rises to no more than the freezing point, at least until all the ice has disappeared at that location. An "across the board" temperature rise in all polar locations, as modelers suggest, may not, therefore, be physically realistic in ice-covered areas. Predicted $CO_2$-induced changes in the environment of West Antarctica may have to be treated in a complex manner because of the considerable interaction with atmospheric circulation, with ice freezing and melting, with ice transport, and with other indirect but strong influences on the ice pack such as the ocean heat flux. Our experience in the Weddell Sea indicates that an integrated modeling and field-measurement program offers the best potential for complete understanding of the various influences on pack-ice behavior.

## REFERENCES

Ackley, S. F., 1979. Mass balance aspects of Weddell Sea pack ice. Journal of Glaciology, 24 (90), 391-406.

Clarke, D. B. and S. F. Ackley, 1982. Physical, chemical, and biological properties of winter sea ice in the Weddell Sea. Antarctic Journal of the United States, 17 (5), 107-109.

Foster, T. and E. Carmack, 1976. Frontal Zone mixing and Antarctic Bottom Water formation in the Southern Weddell Sea. Deep-Sea Research, 12, 301-317.

Gordon, A., 1979. Meridional heat flux in the Southern Ocean. In M. Sterm and F. K. Mellor (eds.), Notes on Polar Oceanography. AD A082511.

Gordon, A., 1981. Seasonality of Southern Ocean sea ice. Journal of Geophysical Research, 86 (5), 4193-4197.

Govoni, J., S. F. Ackley, and E. Holt (in press). Sea ice roughnesses in the Ross Sea. Antarctic Journal of the United States, 18.

Gow, A., S. F. Ackley, W. Weeks, and J. Govoni, 1982. Physical and structural characteristics of Antarctic sea ice. Annals of Glaciology, 3, 113-117.

Hibler, W., 1984. On the role of sea ice dynamics in the $CO_2$ problem. In Climate Processes and Climatic Sensitivity. Maurice Ewing Volume 5. Geophysical Monograph 29. American Geophysical Union, Washington, D.C.

Hibler, W. and S. F. Ackley, 1983. Numerical simulation of the Weddell Sea pack ice. Journal of Geophysical Research, 88 (C5), 2873-2887.

Kellogg, W., 1975. Climatic feedback mechanisms involving the polar regions. In G. Weller and S. Bowling (eds.), Climate of the Arctic. University of Alaska, Fairbanks.

Saltzman, B., 1978. A simple sea ice-ocean temperature oscillator model. Advances in Geophysics, 20, 281-290.

Saltzman, B. and R. Moritz, 1980. A time-dependent climatic feedback system involving sea ice extent, ocean temperature, and $CO_2$. Tellus, 32, 93-118.

Schwerdtfeger, W., 1979. Meteorological aspects of the drift of ice from the Weddell Sea. Journal of Geophysical Research, 84, 6321-6328.

Zwally, J., C. Parkinson, F. Carsey, P. Gloersen, W. Campbell, and R. Ramseier, 1979. Antarctic sea ice variations, 1973-75. NASA Weather-Climate Review, 56, 335-340.

## ATTACHMENT 5

# ASSOCIATED CHANGES IN WEST ANTARCTIC CYCLONIC ACTIVITY AND SEA ICE

Andrew M. Carleton
Arizona State University, Tempe

Growth and decay of sea ice in the West Antarctic display high seasonal variability in the embayments, notably in the Ross, Bellingshausen, and Weddell Seas (Figure 1). About one half of the interannual variability is centered on the Weddell sector (Figures 2 and 3). Antiphase relationships are often observed between the embayments in terms of ice extent. These variations are most pronounced in midsummer and midwinter, but in terms of possible $CO_2$-induced warming effects on the ice extent, summer variations would probably be the more noticeable in that even less ice might be expected to survive the melt period. The substantial seasonal change in extent of the Antarctic sea ice is manifest in a variety of meteorological elements, such as temperature, pressure, and wind speed.

Attempts to find direct relationships between the extent of Antarctic sea ice and cyclonic activity over the southern oceans are frustrated by the strongly regional character of ice-atmosphere interactions. Although it has been shown that zonally averaged variations in cyclone frequency between autumn and spring are apparently related to the seasonal increase in ice extent, this relationship is not the case during the winter when the circumpolar trough migrates poleward during the period of ice advance, a manifestation of the semiannual pressure oscillation. However, in terms of cyclogenesis alone, the latitude of peak frequency moves generally in phase with the seasonal extent of sea ice and temperature changes at the sea surface (Figure 4). This finding reinforces the idea that although only a general relationship can be demonstrated between cyclone tracks, most of which originate at lower latitudes, and the sea-ice margin, the patterns of cyclogenesis indicate some "control" by the ice edge in certain regions, as shown in Figure 5, on a seasonally averaged basis, and in Figure 6, for individual years.

The presence of a high-latitude cyclogenetic zone in the South Pacific (Figure 5), as detected using satellite imagery, verifies Taljaard's tentative location for a winter Antarctic front lying just equatorward of the mean winter ice-edge location and near the oceanic Polar Front (Figure 7). This strongly defined feature is absent in the summer, partly as the result of fewer polar low (comma cloud) developments. Most summer cyclogenesis is middle latitude (frontal wave) in origin and associated with the dominant hemispheric three-wave

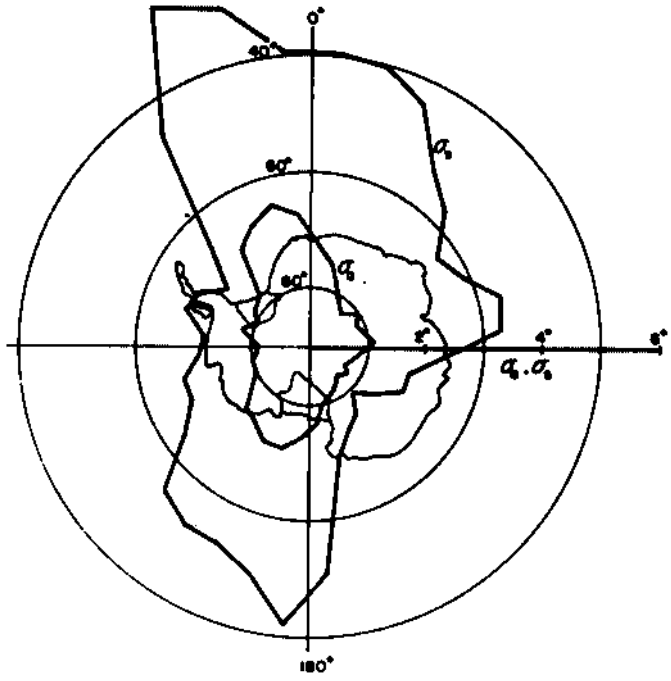


**Figure 1. Annual cycle (σs) and sea-ice anomaly (σa) standard deviation as a function of region around Antarctica. (From Lemke et al. 1980.)**

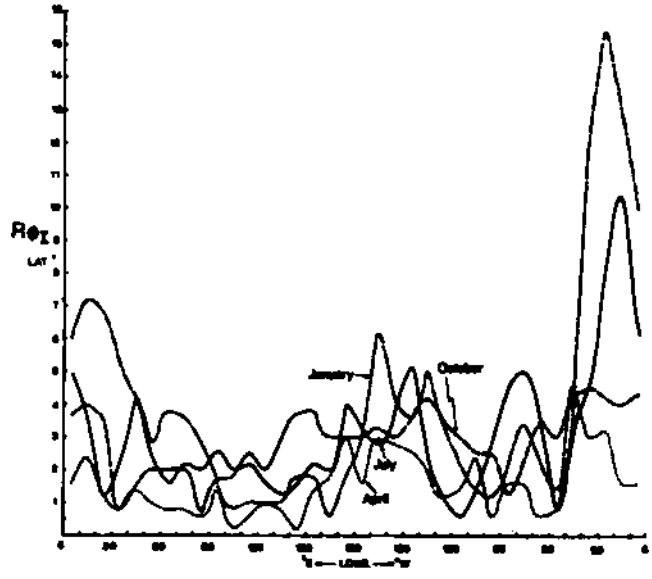


**Figure 2. Range of the Antarctic sea-ice extent $R_{\phi I}$, for 5 years (1972-1977), for selected months. (From Streten and Pike 1980.)**

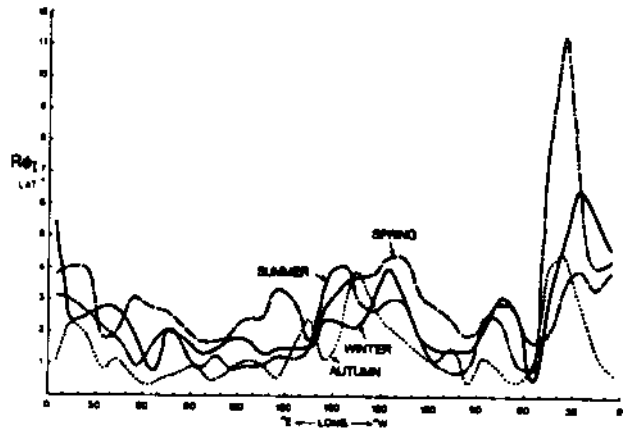


Figure 3. Range of the seasonal Antarctic sea-ice extent $R_{\phi I}$ for 5 years (1972-1977). (From Streten and Pike 1980.)

pattern (Figure 8), although there is some correspondence between the 100- to 500-mb thickness gradient maximum at high latitudes and the summer pack-ice margin (Figure 9). This relationship implies a certain amount of frontal activity in this season.

Cyclones tend to track southeast and dissipate generally in the major Antarctic embayments in all seasons (Figure 10). The cyclolysis patterns coincide, both in summer and winter, with the longitudes of maximum seasonal and interannual variability of the sea-ice extent (Figure 11). Thus, changes in the longitudinal frequency of depression centers may influence seasonal ice distribution via wind and vorticity fields, even on short (few day) time scales (Figure 12). The pattern is generally one of equatorward advection of the ice to the west of longitudes having a maximum number of cyclones and is particularly

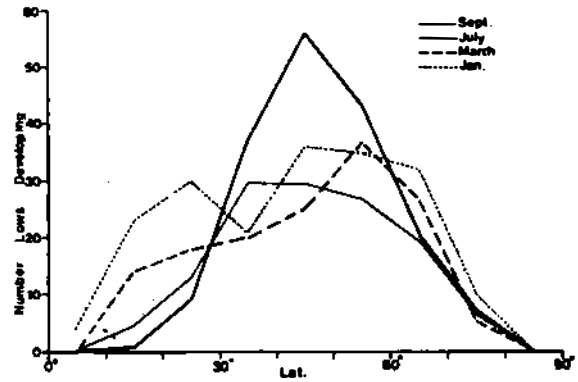


Figure 4. Mean number of new cyclones formed for each 10° latitude band in the Southern Hemisphere and shown for months of January, March, July, and September. The data are averaged over the period 1975-1979. (From Budd 1982.)

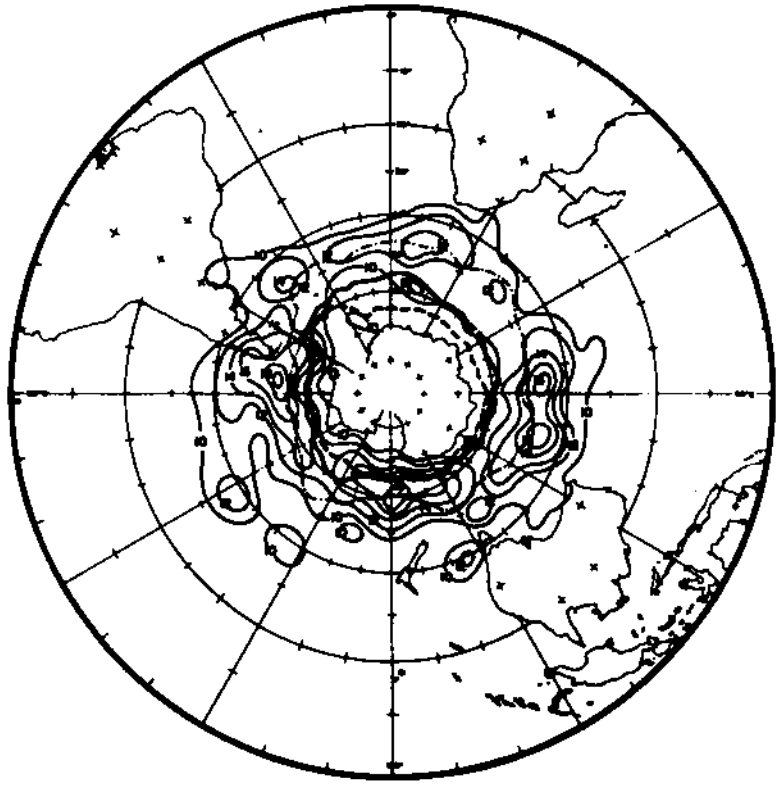

Figure 5. Mean monthly distribution of cyclogenetic cloud vortices for winters 1973-1977, showing the relationship to the ocean Polar Front (the dot-dashed line) and to the mean positions of the sea-ice margin for June (heavy dashed line) and September (heavy solid line). Isopleth values are area-normalized to 45°S. (From Carleton 1981.)

important for interannual ice variations in the Ross and Bellingshausen seas (for example, Figure 13). There is evidence that decreased ice concentration in the Bellingshausen Sea, induced by poleward advection of warm air, may intensify regional cyclonic activity via synoptic feedback. Similar effects have been noted in association with the winter and spring polynya in the Weddell Sea. Minimal changes in ice extent are associated with sub-Antarctic high-pressure ridges. As Figure 14 indicates, more extensive ice in the Ross sector in winter 1973 is associated with a strengthened "mean" low in the embayment, with less extensive ice in winter 1976 corresponding to a much weaker cyclonic pattern. There is a less clear relationship between interannual variations in ice extent in the the Weddell Sea and regional cyclonic activity, at least for the winter, owing to the overriding importance of the oceanic gyre. For winters of extreme Weddell ice extent, however, there is some evidence of a synoptic-scale feedback involving cyclonic activity near the ice edge (Figure 15). Additional research is clearly required on Antarctic ice-cyclone interactions for the summer season.

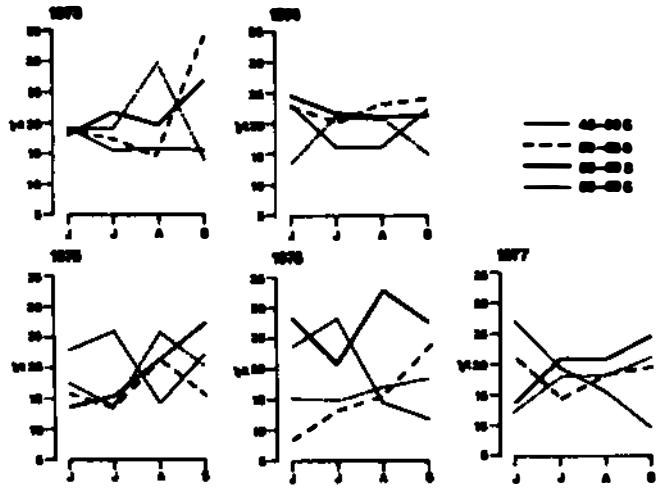

Figure 6. Monthly variations in the frequencies of satellite-observed "polar low" cyclogenesis (comma clouds) in four latitude zones for winters 1973-1977. Frequencies are expressed as the percent of the total number of polar lows over all latitudes in that month. Cyclogenesis generally increases over ocean latitudes adjacent to the ice margin through this season. (From Carleton 1983.)

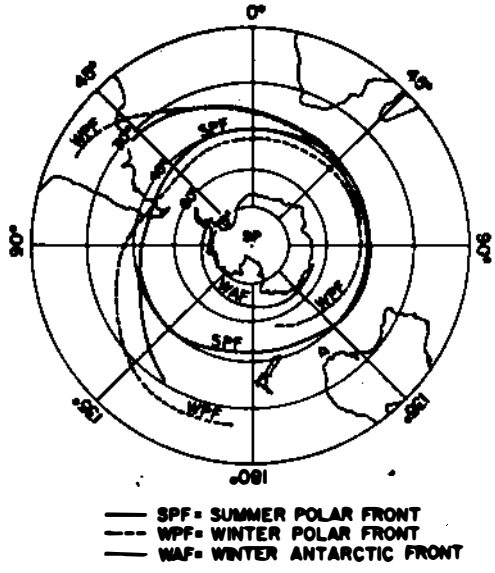


Figure 7. Climatological positions of the Polar Front in summer (SPF) and winter (WPF) and of the Antarctic Front in winter (WAF). (From Taljaard 1972.)

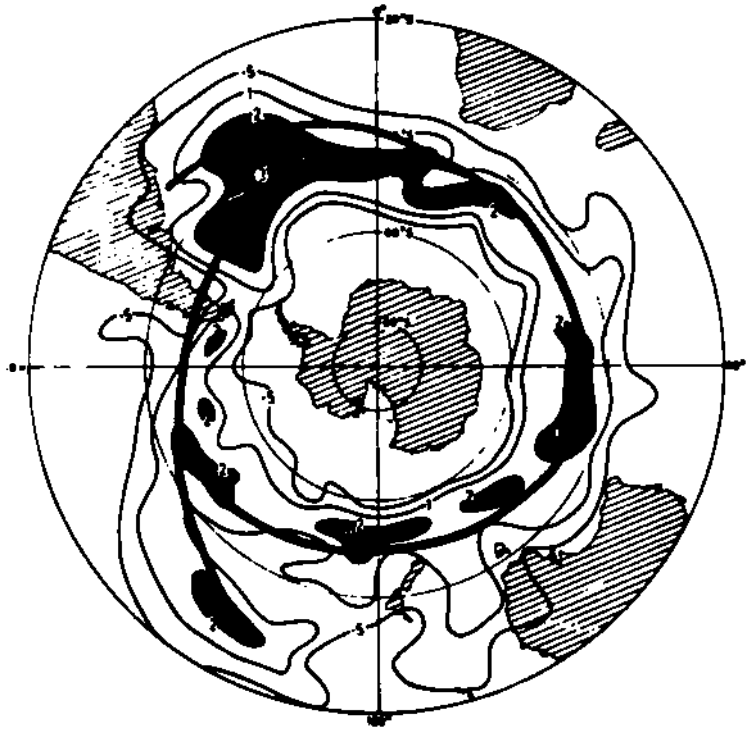

**Figure 8. Frequency of developing cloud vortices (cyclogenesis) in summer. Full line is the position of Taljaard's Polar Front in summer. (From Streten and Troup 1979.)**

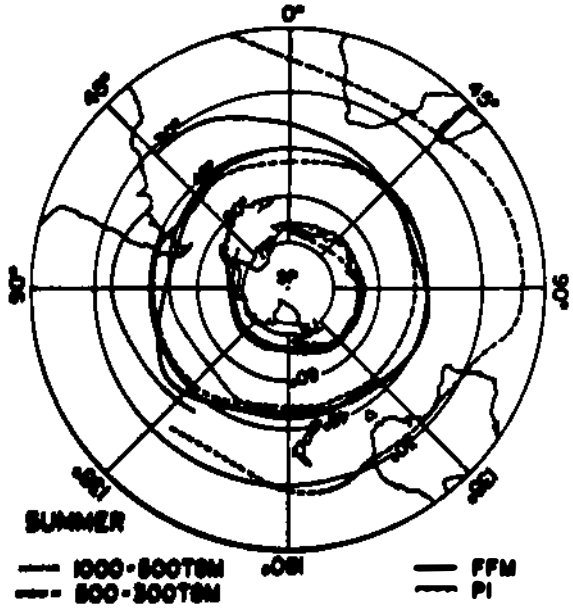


**Figure 9. Surface frontal frequency maxima (FFM), 1,000- to 500-mb and 500- to 300-mb thickness gradient maxima (TGM), and pack-ice limits (PI) for summer. (From Taljaard 1972.)**

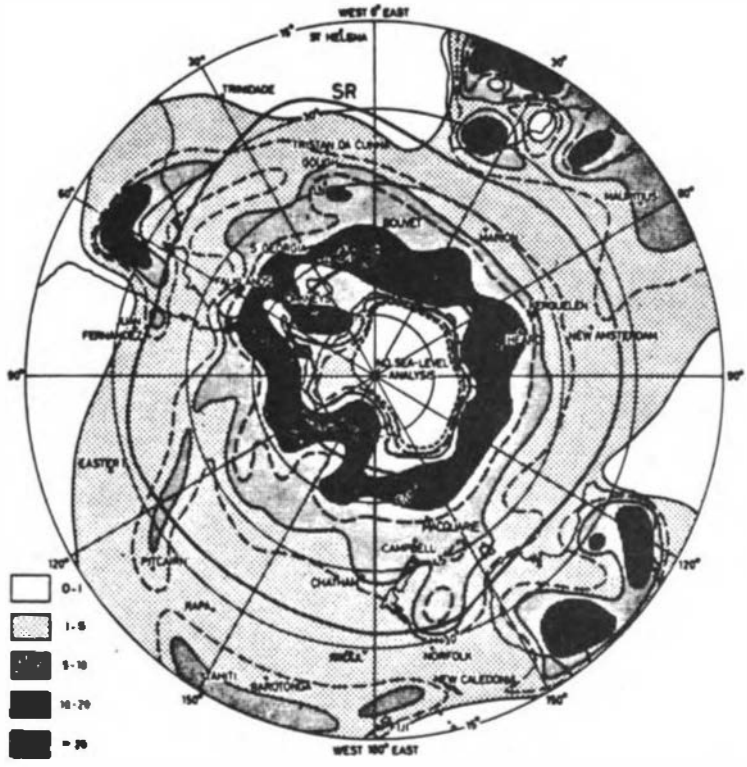


**Figure 10. Distribution of cyclone centers per unit area (438,000 $km^2$) per summer season (December-March) of the IGY. (From Taljaard 1972.)**

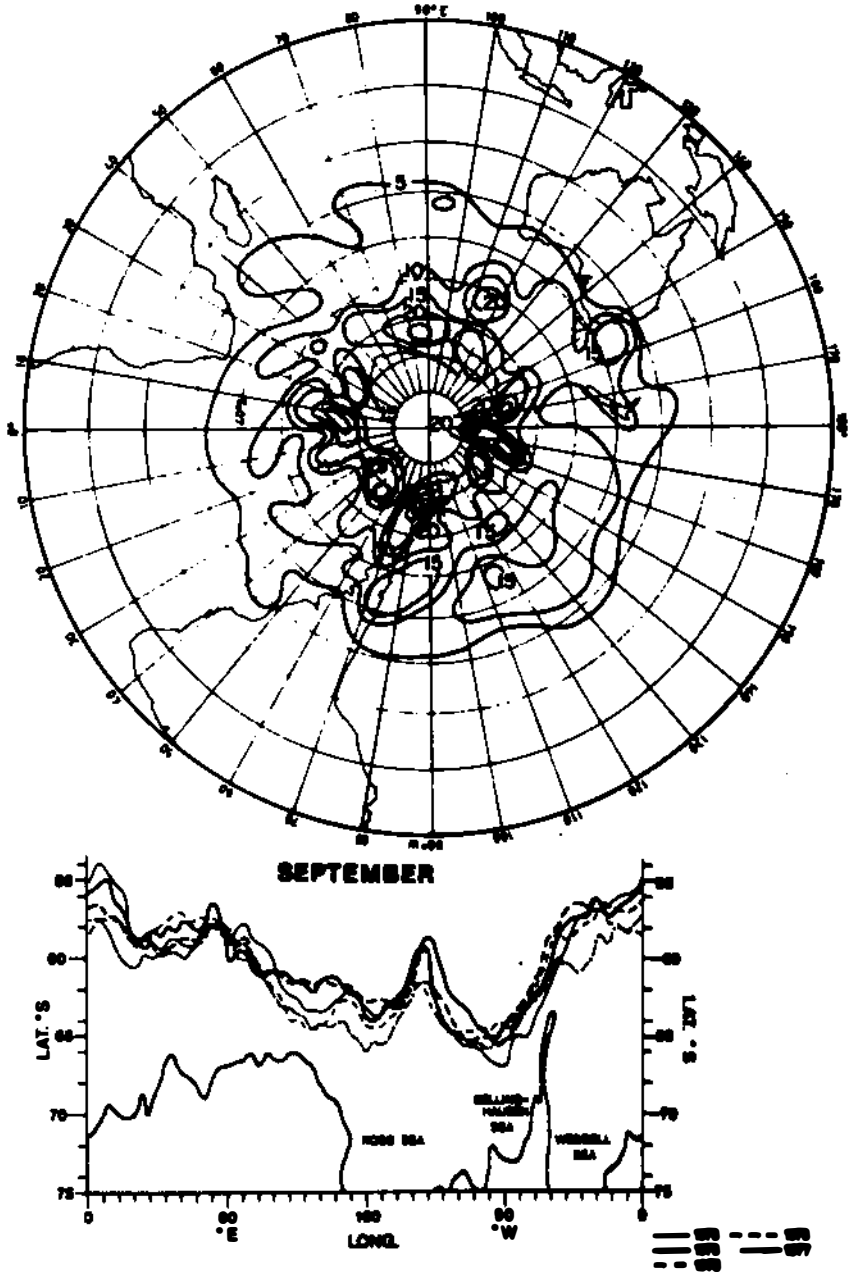


**Figure 11. The range of dissipating cloud vortices (cyclolysis) for the five winters 1973-1977. Isopleths represent the difference between the lowest and highest normalized values in each 5° latitude/10° longitude unit. Also shown are the monthly mean ice-edge locations in September for each of the five winters, showing the high variability in the embayments. (From Carleton 1979, 1983.)**

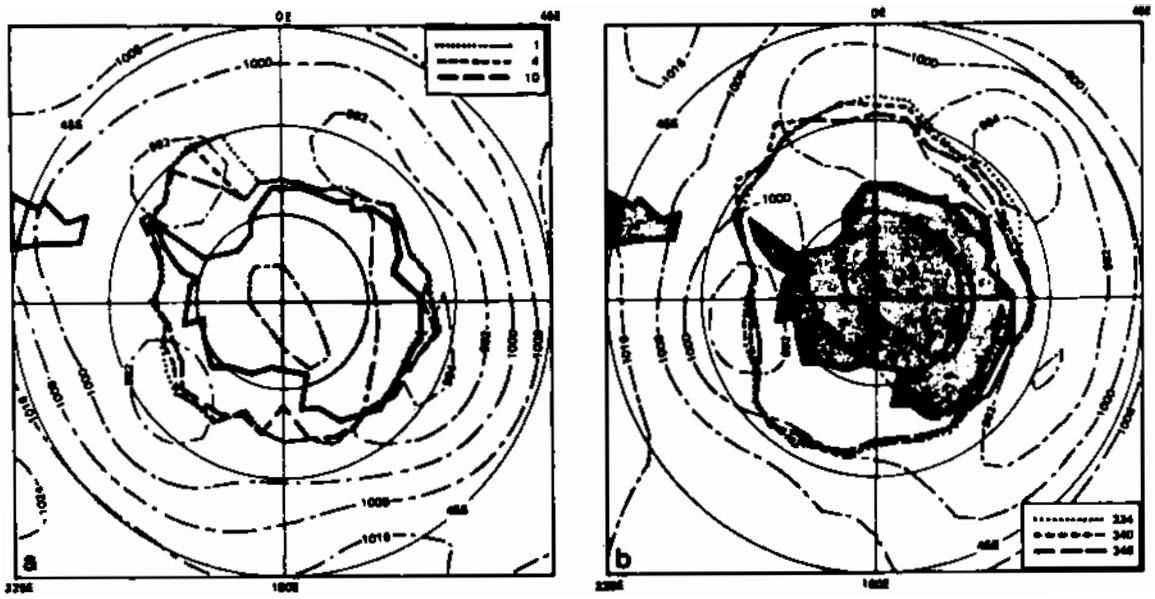

Figure 12. Changes in extent of Antarctic sea ice and corresponding mean sea-level pressure fields for (a) 1-12 January 1974 (Julian days 1-12), and (b) 30 November to 14 December 1974 (Julian days 334-348). (From Cavalieri and Parkinson 1981.)

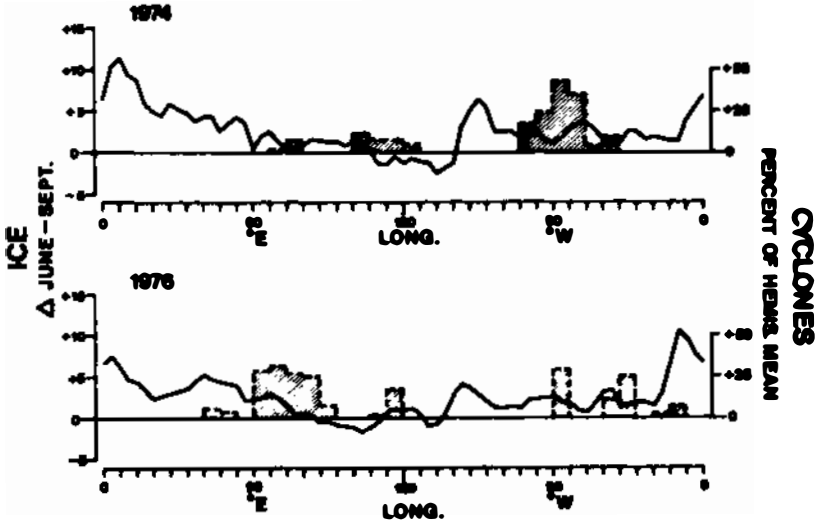


Figure 13. Change (in degrees of latitude) of mean monthly position of ice edge between June and September, winters 1973 and 1976, together with the major cyclonic frequency maxima for the 50-70°s zone. (From Carleton 1981.)

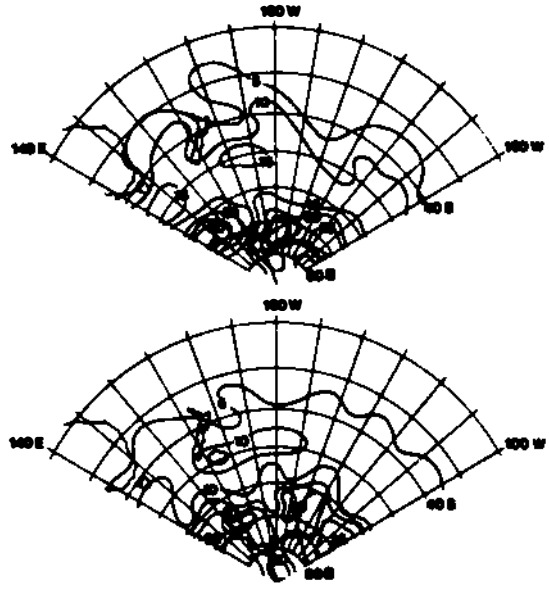


**Figure 14. Distribution of dissipating frontal depressions in the Ross Sea sector for winters (top) 1973 and (bottom) 1976. Isopleth values are area-normalized to 45°S. (From Carleton 1983.)**

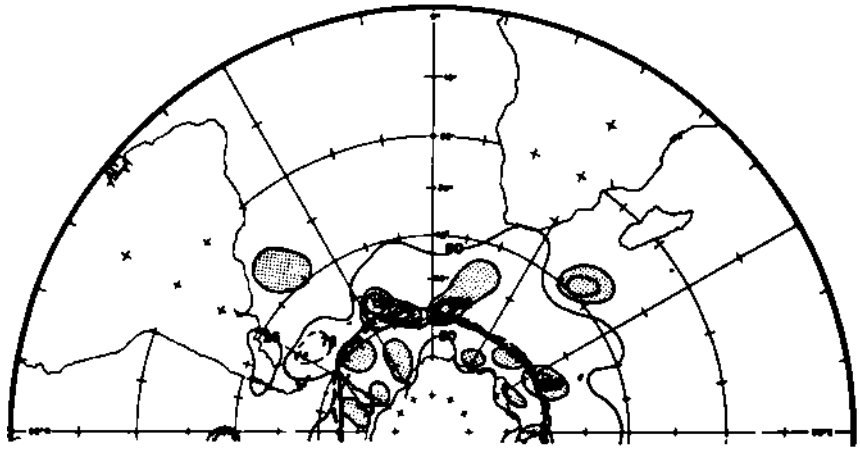

**Figure 15. Cyclones (cloud vortex frequencies) for the winter of 1976 expressed as a percentage of those for winter 1974. Stippled areas highlight greater 1976 cyclonic activity. Mean location of the winter sea-ice margin for 1974 is given by solid heavy line; for winter 1976, by heavy dashed line. Note the ice margin-cyclone relationships in the Weddell Sea between the 2 years. (From Carleton 1981.)**

## REFERENCES

Budd, W. F., 1982. The role of Antarctica in Southern Hemisphere weather and climate. Australian Meteorological Magazine, 30, 265-272.

Carleton, A. M., 1979. A synoptic climatology of satellite-observed extratropical cyclone activity for the southern hemisphere winter. Archives for Meteorology, Geophysics and Bioclimatology Series B, 27, 265-279.

Carleton, A. M., 1981. Ice-ocean-atmosphere interactions at high southern latitudes in winter from satellite observation. Australian Meteorological Magazine, 19, 183-195.

Carleton, A. M., 1983. Variations in Antarctic sea ice conditions and relationships with southern hemisphere cyclonic activity, winters 1972-77. Archives for Meteorology, Geophysics and Bioclimatology Series B, 32, 1-22.

Cavalieri, D. J. and C. L. Parkinson, 1981. Large-scale variations in observed Antarctic sea ice extent and associated atmospheric circulation. Monthly Weather Review, 109, 2323-2336.

Lemke, P., E. W. Trinkl, and K. Hasselmann, 1980. Stochastic dynamic analysis of polar sea ice variability. Journal of Physical Oceanography, 10, 2100-2120.

Streten, N. A. and D. J. Pike, 1980. Characteristics of the broadscale Antarctic sea ice extent and the associated atmospheric circulation 1972-77. Archiv fuer Meteorologie, Geophysiks und Bioklimatologie Series A, 29, 279-299.

Streten, N. A. and A. J. Troup, 1979. A synoptic climatology of satellite-observed cloud vortices over the Southern Hemisphere. Quarterly Journal of the Royal Meteorological Society, 99, 56-72.

Taljaard, J. J., 1972. Synoptic meteorology of the Southern Hemisphere. In C. W. Newton (ed.), Meteorology of the Southern Hemisphere, Meteorological Monograph 13 (35). American Meterological Society, Boston, Massachusetts.

ATTACHMENT 6

# PRECIPITATION REGIME OF THE WEST ANTARCTIC ICE SHEET

David H. Bromwich
Institute of Polar Studies, Ohio State University

## INTRODUCTION

The West Antarctic Ice Sheet (Figure 1), located in the Western Hemisphere and lying on the Pacific side of the Transantarctic Mountains, is much smaller in areal extent and lower in elevation than the ice mass of East Antarctica: $2.3 \times 10^6$ km$^2$ compared with $10.2 \times 10^6$ km$^2$, and 1290 m compared with 2500 m, respectively, when the ice shelves are excluded (Bardin and Suyetova 1967). The meteorological station networks during the International Geophysical Year (IGY), 1957-1958, and during the winter of 1982 are given in Figure 1. In contrast to East Antarctica, no upper-air observations are taken at present along the West Antarctic coast. Notice also that the free atmsophere over the interior of the ice sheet is unmonitored.

Direct precipitation measurement in Antarctica is difficult due to the frequent conjunction of strong winds and snowfall in coastal areas and the predominant occurrence of trace amounts in the interior (Schwerdtfeger 1970). An approximate idea of the multiannual precipitation distribution is obtained from the surface net balance. This net snow buildup at the ice-sheet surface is the end result of precipitation (from both cloudy and cloud-free skies; Schwerdtfeger 1970), evaporation, deposition (i.e., rime and hoarfrost formation), drift-snow transport divergence, and (for low elevations) runoff due to melting (Bromwich 1979). To a first order, precipitation equals net balance in the interior of the ice sheet. The isopleths in Figure 2 show that, in general, annual snowfall in West Antarctica decreases from east to west and from north to south.

Most of West Antarctica is dominated by the "circumpolar" vortex in the low to middle troposphere (Figure 3). This statistical feature tilts with height toward the South Pole and determines the mean moisture flux into West Antarctica, especially during winter. As a result of the comparatively low elevations, sea level cyclones and midtropospheric vortices do penetrate inland (Figure 4). These circulation characteristics combined with the ice-sheet topography (Figure 1) qualitatively explain the observed annual precipitation distribution (Rubin and Giovinetto 1962).

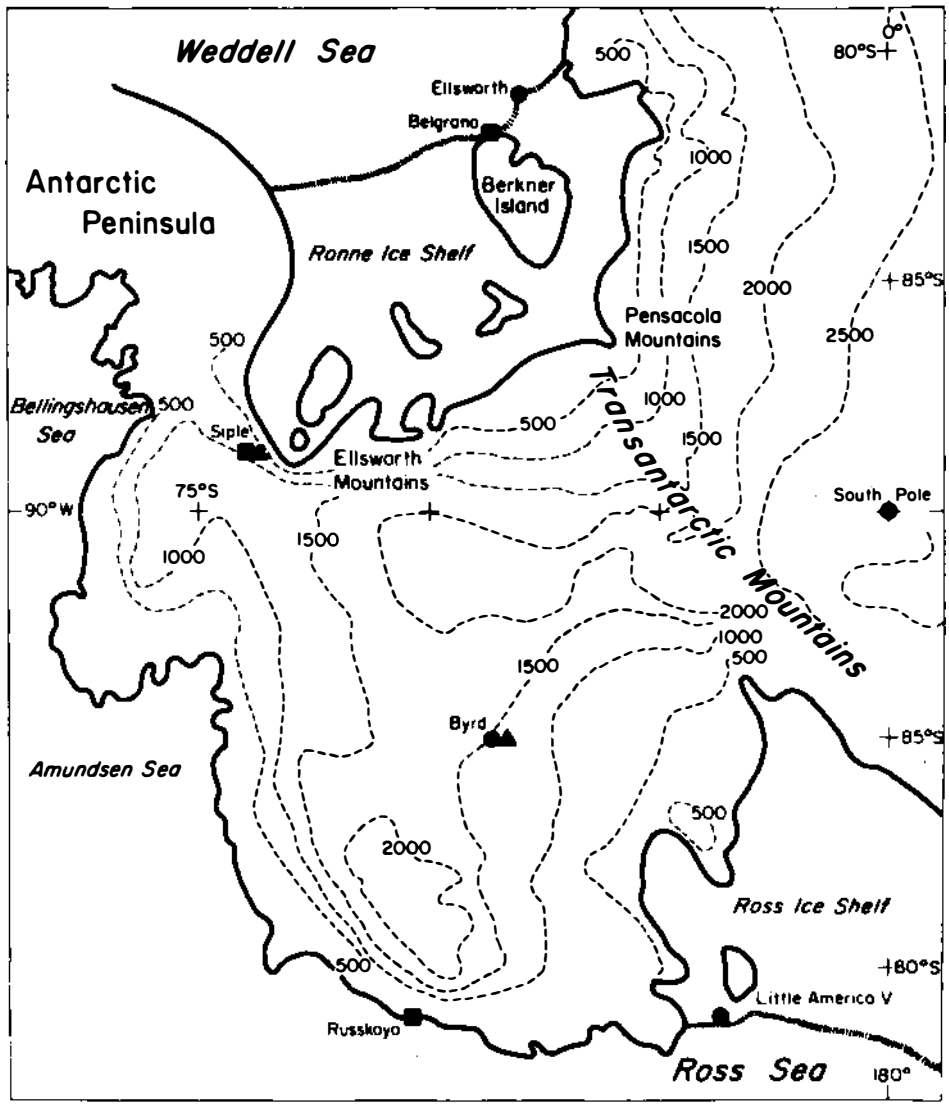


**Figure 1. Map of West Antarctica, giving smoothed elevations of the ice-sheet surface (dashed lines) in meters and the locations of meteorological stations during the IGY and the winter of 1982. The base map was adapted from the American Geographical Society of New York's 1970 map of Antarctica.**

**Station key: Solid circles are manned sites where surface and upper-air observations were collected during 1958 (Schwerdtfeger 1970). All stations have been closed apart from South Pole, where a full meteorological program has been maintained without interruption since the IGY. Solid squares are manned meteorological stations collecting only surface data during the winter of 1982 (Scientific Committee on Antarctic Research 1982). Solid triangles are automatic weather stations (monitoring surface values of wind speed, wind direction, air temperature, and atmospheric pressure) operating during the 1982 winter season. (From Stearns 1982.)**

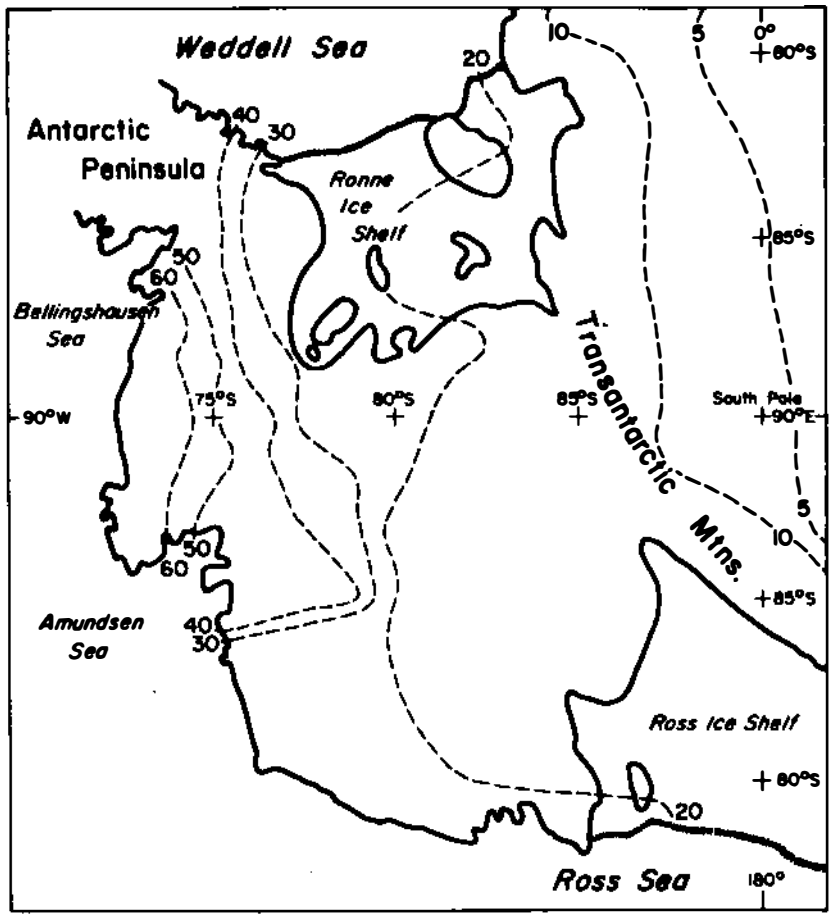


**Figure 2. Annual net balance (dashed lines) in West Antarctica, modified from Bull (1971), in g $cm^{-2}$.**

## STUDIES OF WEST ANTARCTIC PRECIPITATION

The author is aware of only two additional papers that focus on the atmospheric hydrologic cycle over West Antarctica. These semiquantitative analyses of data collected around the time of the IGY are the following.

1. Lettau (1969) examined the annual atmospheric water balance for the Antarctic continent: the net cross-coastal flow of water vapor approximately equals the precipitation (Bromwich 1979). He compared mean moisture transports, calculated from observed mass transports and very approximate water-vapor estimates, with net balance values for Antarctica. By assuming that the annual mass and water-vapor transports are proportional, Lettau demonstrated that:

- A substantial fraction of the atmospheric moisture flow into Antarctica occurs over West Antarctica.

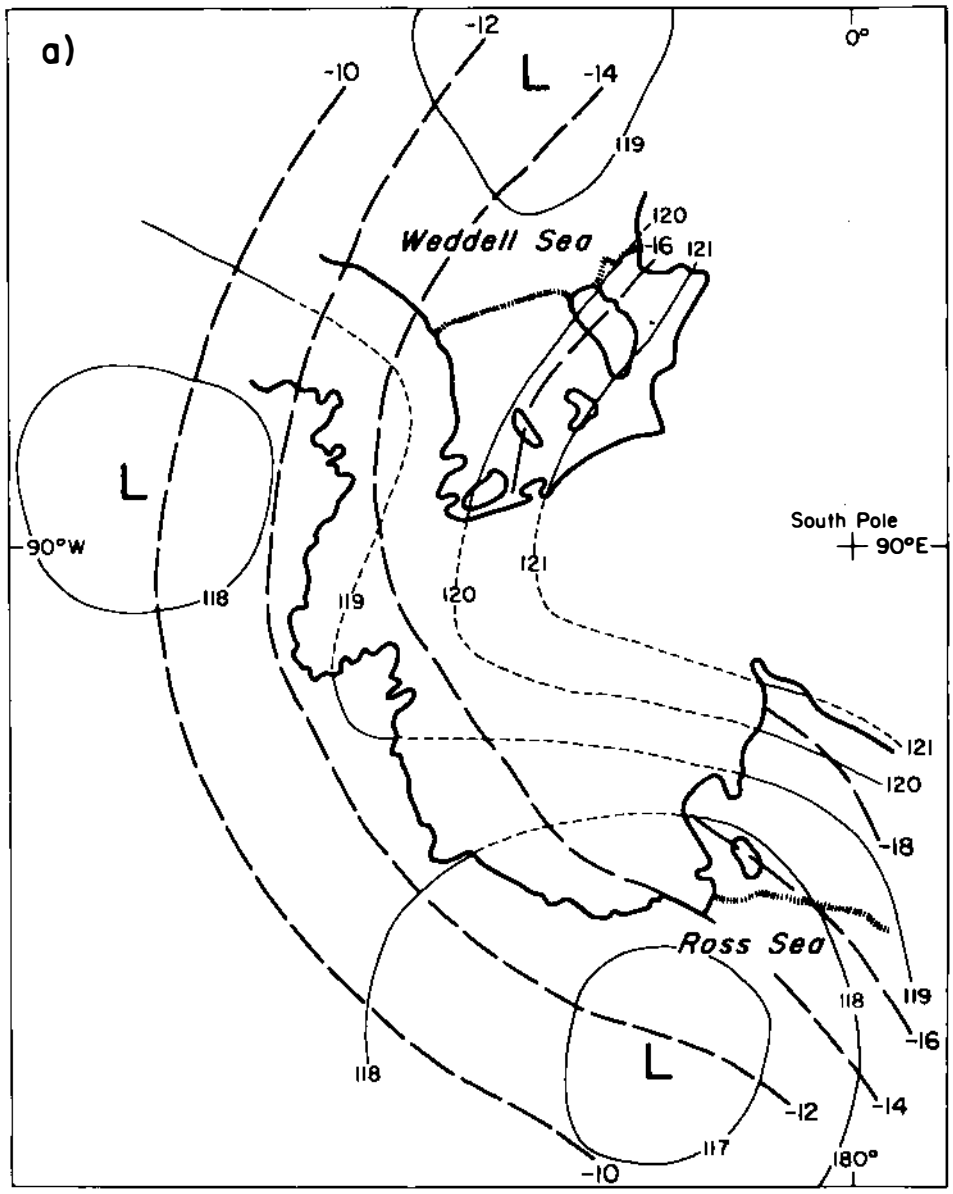


**Figure 3. Climatological fields of geopotential height (solid lines, in dkm) and dew-point temperature (long-dashed lines, in °C) on the 850-mb surface in the vicinity of West Antarctica in (a) January and (b) July. In Figure 3b, the time-averaged, clockwise, geostrophic flow around the east side of the Ross Sea low suggests a marked moisture flow into West Antarctica. Short-dashed height contours indicate that the 850-mb level is located mostly below the ice-sheet surface. Data are tabulated by Taljaard et al. (1969).**

- **The mean and eddy moisture fluxes (the latter resulting from covariance between wind speed and atmospheric water-vapor content) probably contribute equally to the total West Antarctic transport.**

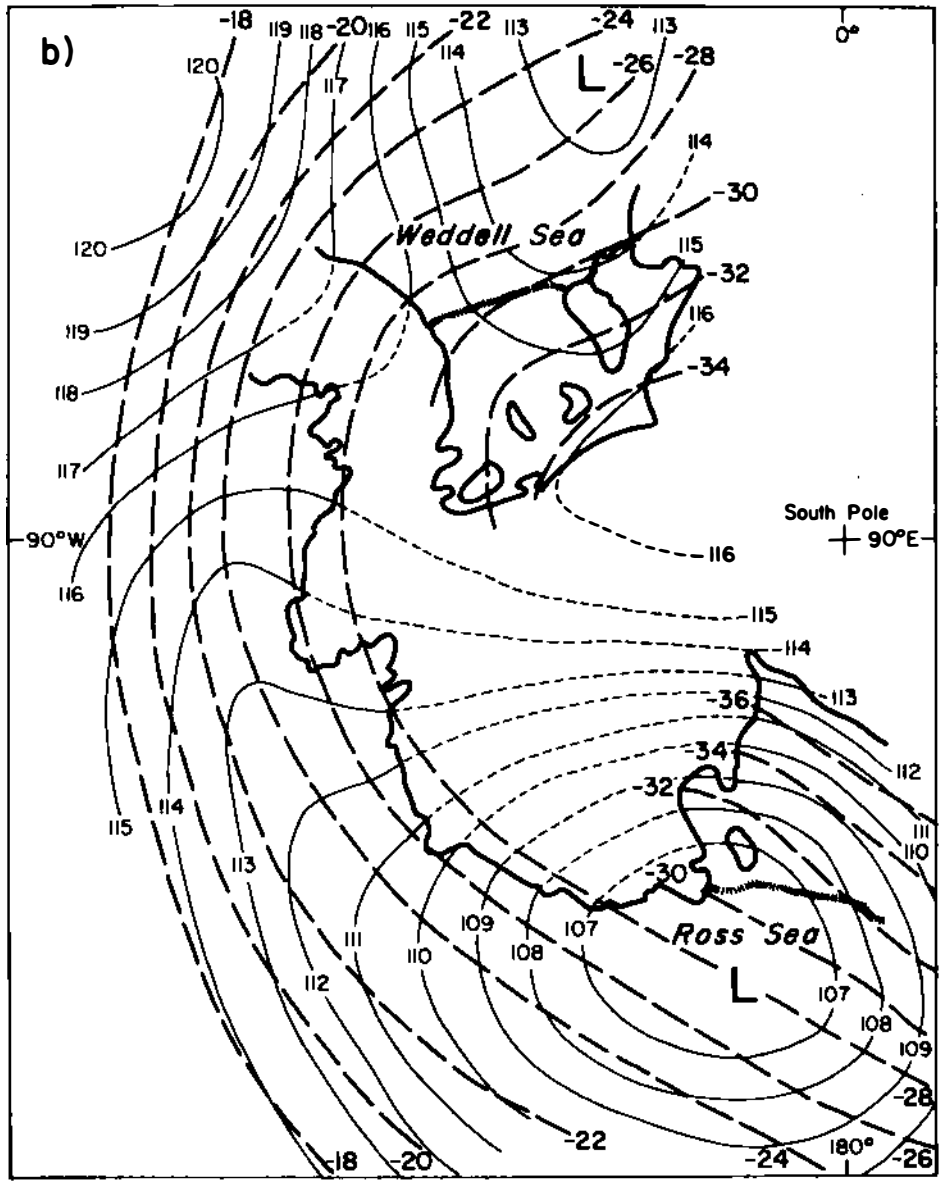


**Figure 3b.**

- **Meteorological processes can exert a strong control over West Antarctic moisture transport; perhaps one-fifth of the total annual transport at Byrd Station took place during three consecutive days in February 1958 (Figure 5).**
- **The interannual variability of precipitation inland of Byrd Station, and perhaps over West Antarctica as a whole, may be large; the annual frequency of synoptic events like that of February 1958 could be highly variable.**

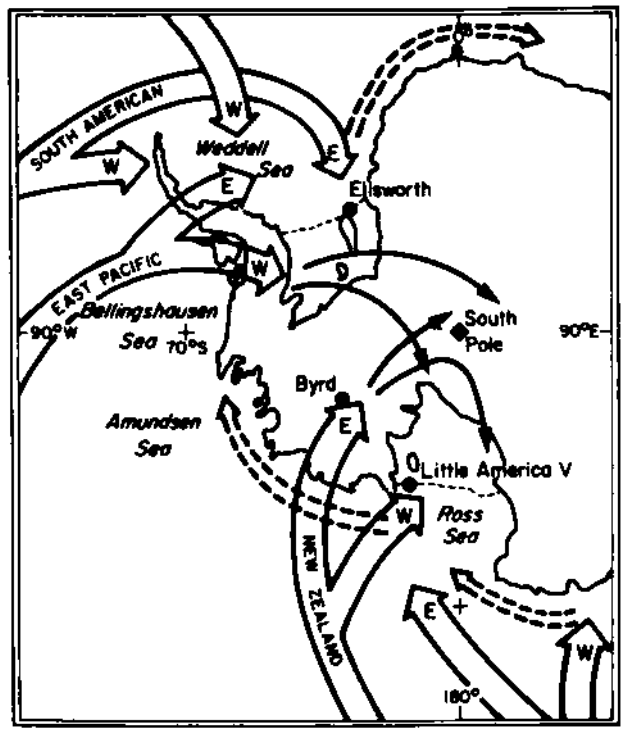


Figure 4. Tracks of sea level (wide arrows) and 700 mb vortices during 1958, as deduced from synoptic maps (after Rubin and Giovinetto 1962). E and W in the broad arrows identify the east and west parts of the main storm track.

2. Vickers (1966) compared surface synoptic pressure maps with net balance records from Little America, Ellsworth, Byrd, and South Pole (Figure 1). The strong synoptic control of West Antarctic snowfall was highlighted. In particular, he demonstrated that:

- The maximum precipitation rate in fall coincides with the influx of maritime cyclones.
- Most large storms affect wide areas of West Antarctica within a 2-day period (Figure 6).
- Snowfall for 1958 was significantly less than for 1957, primarily following from the absence of the heavy snow events of June and October 1957.

## CONCLUSIONS AND RECOMMENDATIONS

The main conclusion of this review is that the precipitation regime in West Antarctica is dominated by synoptic events. The high interannual variability of the Southern Hemisphere circulation suggests that the variability of annual precipitation may be correspondingly high. Lettau's (1969) finding that the time-averaged airflow over West Antarctica transports large quantities of moisture into Antarctica is

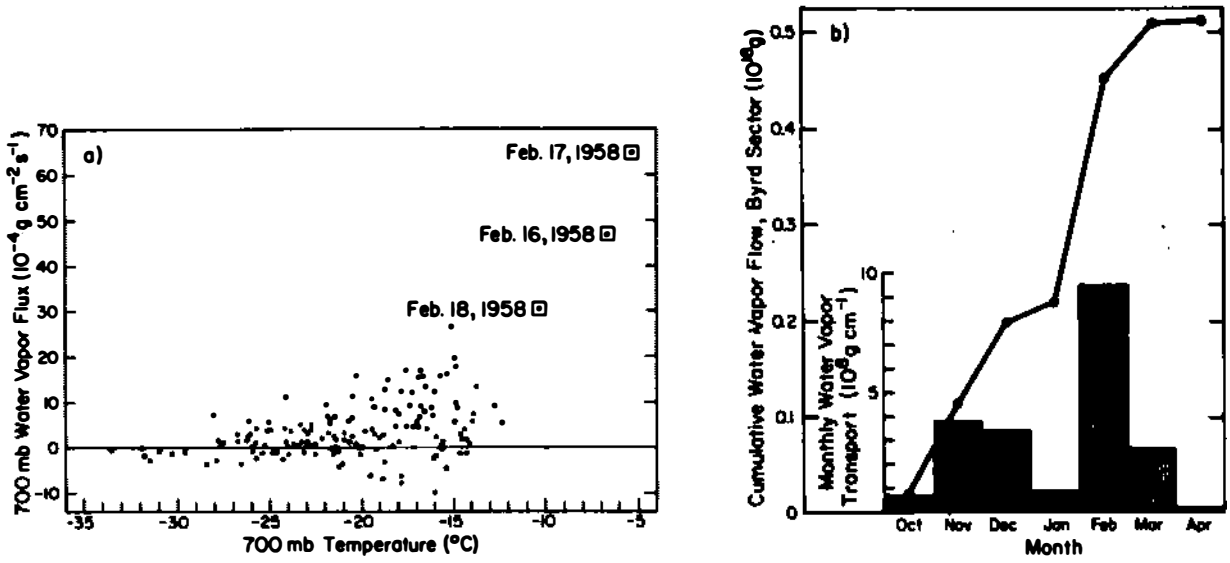


**Figure 5. (a) Daily 700-mb moisture flux plotted against 700-mb temperature at Byrd Station between October 1957 and March 1958. (b) Net monthly moisture transport through the Byrd sector during the austral summer 1957-1958. (Modified from Lettau 1969.)**

relevant to the comprehensive simulations for a $CO_2$-enriched atmosphere presented by Manabe and Stouffer (1980). It suggests that their atmospheric general circulation model (AGCM) in part may calculate Antarctic precipitation amounts 4 times larger than observed because the modeled low-tropospheric temperatures are some 10°C too warm and because the moisture-holding capacity of air is an exponentially increasing function of temperature. This suggestion is consistent with the findings of Manabe and Stouffer (1980) and Manabe and Wetherald (1980), who noted that the increased poleward water-vapor transport (comparison of 4 x $CO_2$ and 1 x $CO_2$ experiments) arose because of the increased moisture content of the air.

Research is needed to substantially extend Lettau's (1969) atmospheric water-balance analysis. This extension can be done by using upper-air moisture measurements; as demonstrated by Bromwich (1979), these data are fairly reliable, at least on an average basis. The contribution of the eddy moisture fluxes should be quantitatively established. Atmospheric water-vapor fluxes, which are linked to precipitation via the atmospheric water balance, can be used to constrain AGCM calculations of snowfall.

Research is also needed to link synoptic events quantitatively to observed net balances; valuable new results can be extracted from available information, especially the IGY data set. Such findings could provide another way to estimate the precipitation that would accompany the simulated circulation of a $CO_2$-enriched atmosphere. Experience with numerical weather prediction models indicates that the large-scale atmospheric behavior is easier to predict than the precipitaton rate (e.g., Shuman 1978; Ramage 1982).

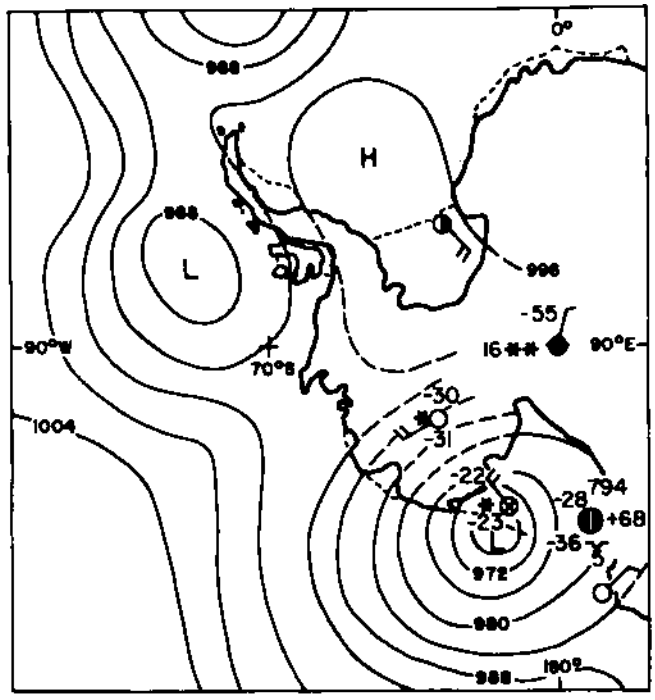


Figure 6. A large-scale snowfall event in West Antarctica on 14 July 1957. (Adapted from Vickers 1966.)

ACKNOWLEDGMENTS

This contribution to the workshop was supported by NSF grant DPP 8100142. The figures were drafted by R. Tope.

REFERENCES

Bardin, V. I. and I. A. Suyetova, 1967. Basic morphometric characteristics for Antarctica and budget of the Antarctic ice cover. In T. Nagata (ed.), Proceedings of the Symposium on Pacific-Antarctic Science (pp. 92-100). National Science Museum, Tokyo.

Bromwich, D. H., 1979. Precipitation and accumulation estimates for East Antarctica, derived from Rawinsonde information. Ph.D. dissertation, Department of Meteorology, University of Wisconsin, Madison.

Bull, C., 1971. Snow accumulation in Antarctica. In Research in the Antarctic Publication 93 (pp. 367-421). American Association for the Advancement of Sciences, Washington, D.C.

Lettau, B., 1969. The transport of moisture into the Antarctic interior. Tellus, 21, 331-340.

Manabe, S. and R. J. Stouffer, 1980. Sensitivity of a global climate model to an increase of $CO_2$ concentration in the atmosphere. Journal of Geophysical Research, 85, 5529-5554.

Manabe, S. and R. T. Wetherald, 1980. On the distribution of climate change resulting from an increase in $CO_2$ content of the atmosphere. Journal of Atmospheric Science, 37, 99-118.

Ramage, C. S., 1982. Have precipitation forecasts improved? Bulletin of the American Meteorological Society, 63, 739-743.

Rubin, M. J. and M. B. Giovinetto, 1962. Snow accumulation in central West Antarctica as related to atmospheric and topographic factors. Journal of Geophysical Research, 67, 5163-5170.

Schwerdtfeger, W., 1970. The climate of the Antarctic. In H. E. Landsberg (ed.), World Survey of Climatology. Volume 14 (pp. 253-355). Elsevier, New York.

Scientific Committee on Antarctic Research, 1982. SCAR Bulletin 72. Polar Record, 21, 309-322.

Shuman, F. G., 1978. Numerical weather prediction. Bulletin of the American Meteorological Society, 59, 5-17.

Stearns, C. R., 1982. Antarctic automatic weather stations. Antarctic Journal of the United States, 17 (5), 217-219.

Taljaard, J. J., H. van Loon, H. L. Crutcher, and R. L. Jenne, 1969. Climate of the Upper Air: Southern Hemisphere. Volume 1. Temperatures, Dew Points and Heights at Selected Pressure Levels. NAVAIR 50-1C-55. Naval Weather Service Command, Washington, D.C.

Vickers, W. W., 1966. A study of ice accumulation and tropospheric circulation in West Antarctica. In M. J. Rubin (ed.), Studies in Antarctic Meteorology. Antarctic Research Series 9 (pp. 135-176). American Geophysical Union, Washington, D.C.

ATTACHMENT 7

# WEST ANTARCTIC TEMPERATURES, REGIONAL DIFFERENCES, AND THE NOMINAL LENGTH OF SUMMER AND WINTER SEASONS

D. W. S. Limbert
British Antarctic Survey
Natural Environment Research Council
Cambridge, England

## INTRODUCTION

The temperature records for stations in Antarctica dating from the International Geophysical Year (IGY) are now sufficiently long to illustrate the full range of Antarctic climates. The interannual variability of the coastal Antarctic stations in relation to sea-ice extent (Budd 1975) emphasizes location differences. Regional differences have also been briefly described in the annual reports of the British Antarctic Survey (1980, 1981).

This paper discusses the available West Antarctic temperature records and relates them to other Antarctic regions and, where possible, to the atmospheric and oceanic circulations. Because of the sparseness of long temperature records, some proxy data based on snow accumulation rates are used.

## WEST ANTARCTIC TEMPERATURES

Meteorologically, West Antarctica can be defined as the sector extending from longitude 60°W to 160°E between latitudes 70° and 85°S. The Antarctic Peninsula projects northward from the continent between longitudes 60° and 80°W; the polar plateau south of 85°S is not included because, as will be shown, its temperatures and, by inference, its weather are virtually decoupled from the temperatures of West Antarctica. Raper et al. (1983a,b) confirm the decoupling of the polar plateau in a principal component analysis of Antarctic temperatures.

The interannual variability of temperature relative to that observed at Faraday Station is given in Figure 1. Byrd and McMurdo have about half the variability of Faraday, while ocean islands show much less variability. Table 1 gives the correlations between Antarctic stations. The most significant connection in Table 1 is the close correlation between McMurdo and Byrd Station, the most continental West Antarctic station. Byrd closed early in 1970; since 1980 an automatic weather station has been operating at Byrd and appears to be giving reliable data (Stearns and Savage 1981), but the record is as yet too short for comparisons with the earlier data series. Table 1 shows further that McMurdo and Faraday (Argentine

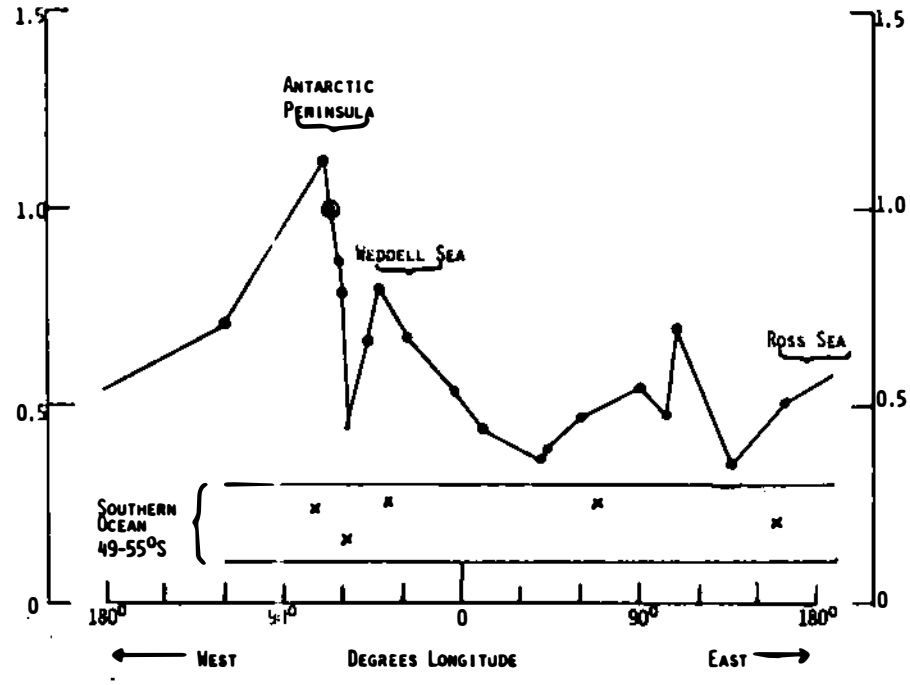


**Figure 1. Annual temperature variability in Antarctica related to that at Faraday.**

**TABLE 1. Interstation Temperature Correlations**

| Station | Date | Summer | Autumn | Winter | Spring | Annual |
|---|---|---|---|---|---|---|
| Byrd-Amundson-Scott | 1957-1969 | - | - | - | - | -.01 |
| Byrd-Frarady | 1957-1969 | -.10 | - | .30 | - | -.01 |
| Byrd-McMurdo | 1957-1969 | .86 | - | .79 | - | .83 |
| McMurdo-Fraday | 1957-1969 | .09 | .01 | .18 | .42 | .43 |
| McMurdo-MacQuarie Is. | 1957-1978 | .09 | .15* | .03 | -.268* | -.10 |
| MacQuarie Is.-Faraday | 1949-1978 | .30 | .21* | .37 | .33 | .51 |
| McMurdo-Amundsen-Scott | 1957-1978 | - | - | - | - | .10 |

Summer data from December, January, and February; autumn data from March, April, and May; winter data from June, July, and August; spring data from September, October, and November.

*Gap of 3 years, 1969-1971.

Islands) temperatures are correlated in spring and on an annual basis at a low significance level and that Faraday temperatues are also correlated with those at Macquarie Island, principally annually.

The poor correlation between Macquarie and McMurdo reflects the separation of the midlatitudes and the Antarctic by the circumpolar trough (CPT). The Faraday-Macquarie correlation is similar to an atmospheric circulation coupling and a feature already noted by Pittock (1980a,b), who represented it by the "Trans-polar index," defined as the mean sea level pressure anomaly difference between Tasmania and the Falkland Islands.

The role of the different seasons in the annual temperature is indicated by the correlations in Table 2.

The winter temperatures play the dominant roles at both stations; the generally higher values in the Antarctic Peninsula reflect its larger interannual variability, which raises or lowers all temperatures during a year.

## SEA ICE AND OCEAN INFLUENCES AND LOCAL CLIMATE PERSISTENCE

The question arises: Does a neighboring region's previous season affect West Antarctica in any way? Budd (1975) suggested that temperatures of a coastal strip are directly related to the regional extent of sea ice. He plotted annual temperature anomalies of stations around the Antarctic periphery and suggested that there was a west-to-eastward movement of the temperature anomalies. The evidence is not completely convincing, and an analysis of the positions of the main peaks and troughs of the annual temperature cycles for each of the coastal regions in a smoothed (running 3-year mean) temperature record seems to provide evidence for a contrary movement from east to west around the coast of Antarctica (Figure 2). Both effects may be real if the controlling factor is the ocean current system (Figure 3), with the Antarctic coastal current and the Southern Ocean current interacting in a semiperiodic fashion. For example, late development of sea ice in one particular coastal region could modify the local climate and maintain a positive temperature anomaly as that particular band of sea ice and water moves westward in the coastal current. Thus, a seasonal temperature anomaly may be recognizable further west in the following season.

Table 2. Seasonal Influence on Annual Variability

| Season/Year | Faraday (n=40) | McMurdo (n=26) |
|---|---|---|
| Summer correlated with year | .67 | .43 |
| Autumn correlated with year | .78 | .36 |
| Winter correlated with year | .92 | .61 |
| Spring correlated with year | .66 | .63 |

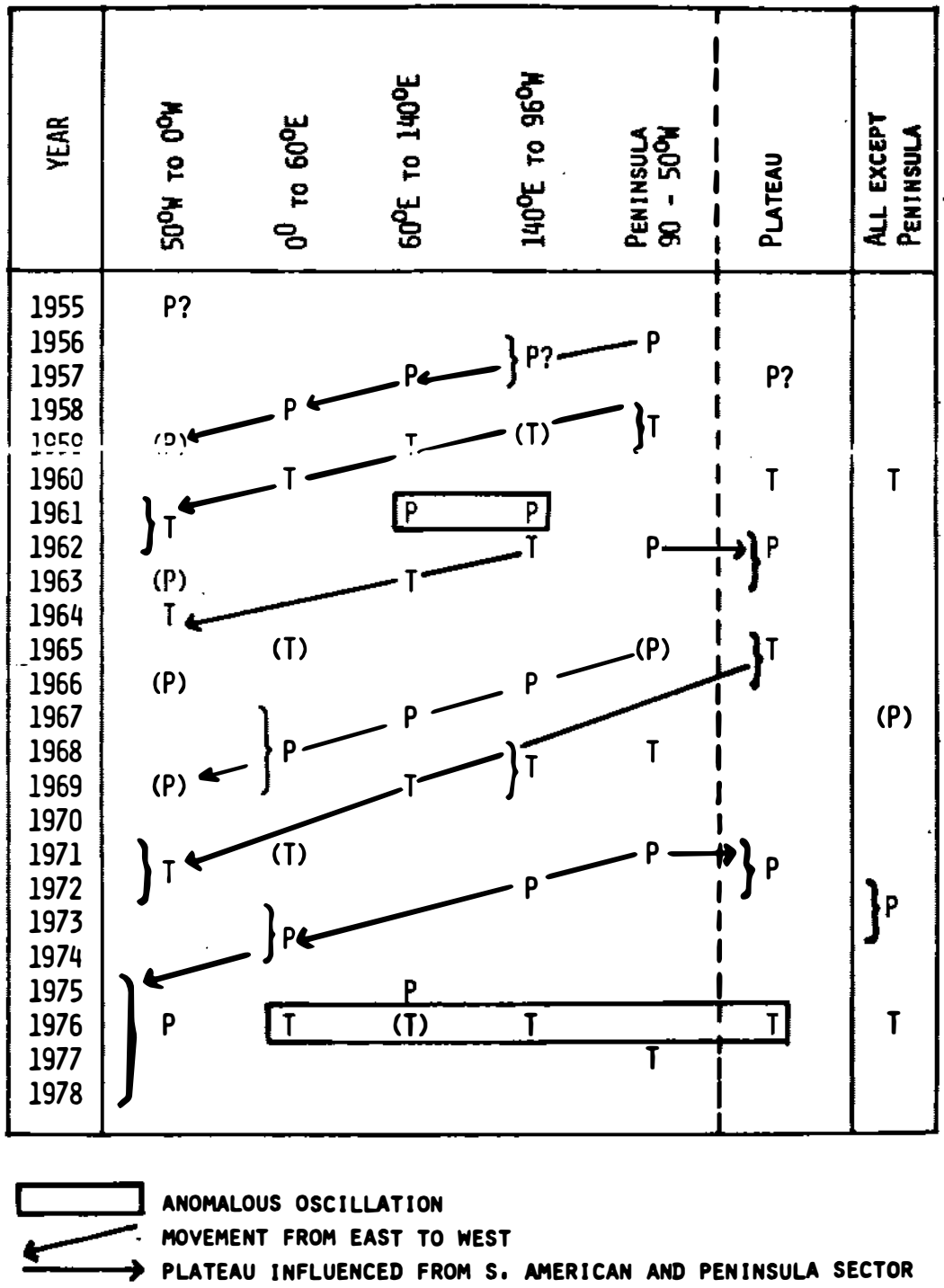


Figure 2. Peaks (P) and troughs (T) in the trend of smoothed 3-year moving averages of regional mean annual temperatures in Antarctica.

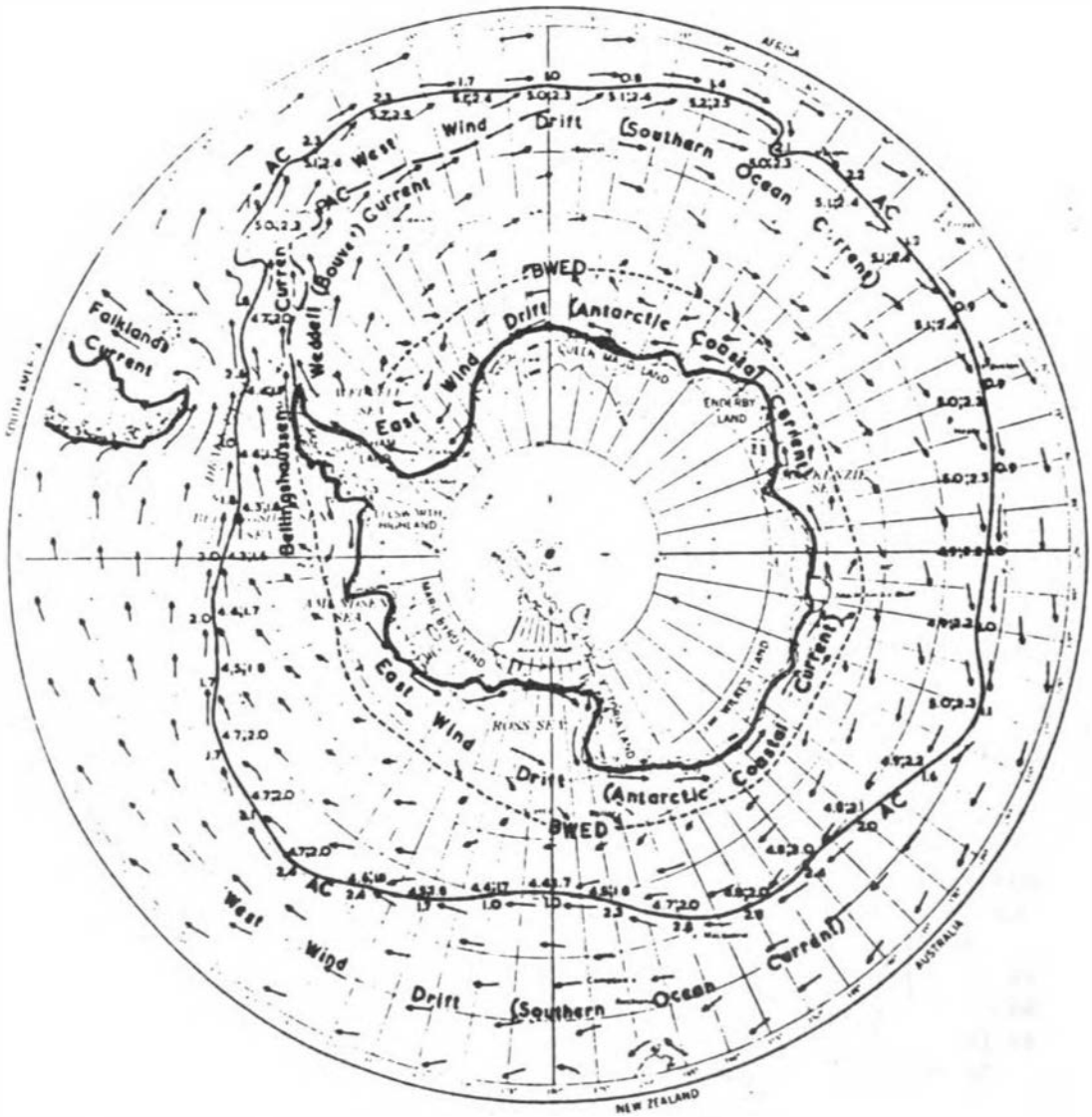


**Figure 3. The Antarctic Convergence (AC) and surface ocean currents south of 45°S. The values entered on the equatorward side of the AC represent temperature discontinuities (in °C) at 10° intervals, and the pairs of numbers on its poleward side are the middle temperatures in the warmest month (February) and coldest month (October), respectively. PAC is Pacific-Atlantic Convergence. BWED is boundary between west and east wind drifts. The arrows represent direction and approximate speed (1 cm = 1 knot) of the surface currents.**

To test this idea, some lag correlations between Faraday and McMurdo are given in Table 3.

Two correlations stand out. Faraday spring temperature anomalies appear to be followed by similar anomalies in the McMurdo summer, and this may be evidence of the hypothesized effect of the Antarctic coastal current. Although the remaining positive correlations from Faraday to McMurdo are not significant, they do not contradict the hypothesis of westward movement. The McMurdo-to-Faraday seasonal lag correlations are contradictory and not significant. Surprisingly, the annual lag correlation from McMurdo to Faraday is significant; this may be an example of west-to-east influence and evidence of the importance of gross changes in hemispheric circulation and total distribution of sea ice, as distinct from local effects. The regional averages discussed in a subsequent section on temperature trends support the east-to-west coastal movement.

## STORM TRACKS AND TEMPERATURE

The relation of storm tracks to the edge of the sea ice can be seen in Figures 4a and 4b. The storms move predominantly along the ice edge in West Antarctica but with a movement across the ice edge in the lee of the Antarctic Peninsula. A preferred storm track leads from the Ross Sea into West Antarctica near Byrd Station. Similar storm tracks were identified by Astapenko (1960). It is axiomatic that in polar regions, storms bring warmer weather in all seasons other than summer. The increased wind velocity destroys the surface inversion, and the increased cloudiness prevents radiative cooling. More important, warmer Southern Ocean air is introduced into the continent. Thus, the position of storm tracks influences the annual temperature cycle. Mayes (1981) has analyzed 22 years of depression tracks for the Antarctic Peninsula based on working synoptic charts produced in the Falkland Islands between 1947 and 1968. Figure 5 shows the total number of cyclones identified between latitudes 50° and 70°S between longitudes 40° and 65°W. As pointed out by van Loon (see Attachment 2), the analyses for the summers 1955-1956 and 1957-1958 deserve more credence than the rest. In this context, the low frequency during the

Table 3. Interseason Correlations and Persistence, 1957-1982

| Season | McMurdo | Faraday | McMurdo-Faraday | Faraday-McMurdo |
|---|---|---|---|---|
| Summer-autumn | .17 | .62 | <.01 | .33 |
| Autumn-winter | -.08 | .58 | .27 | .28 |
| Winter-spring | .16 | .26 | -.15 | .26 |
| Spring-summer | .39 | .29 | .27 | .56 |
| Year 1 to year 2 | - | - | .61 | .38 |

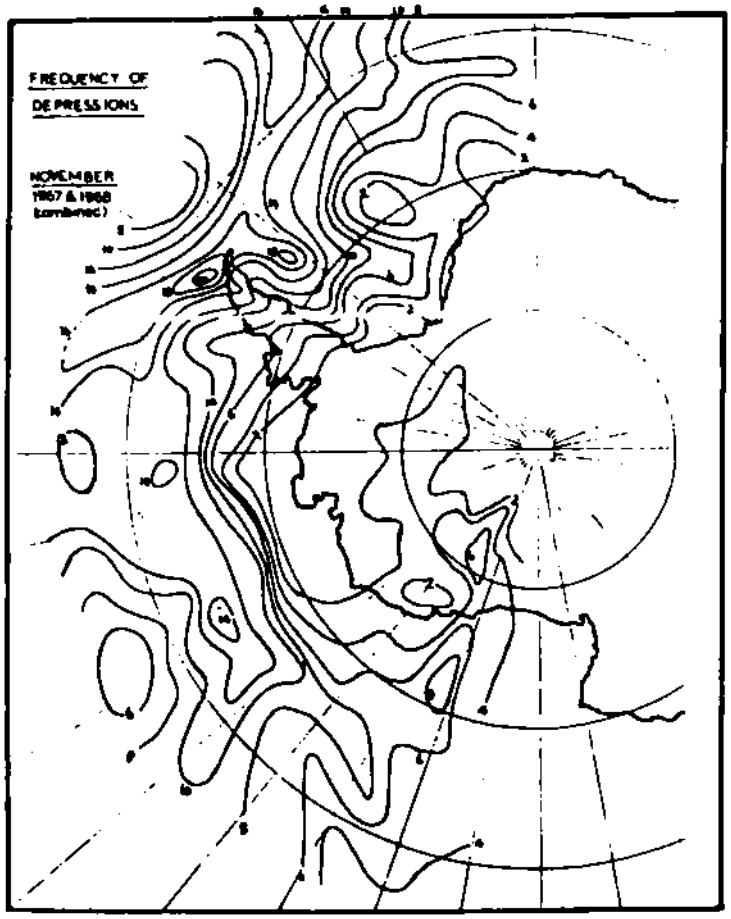


**Figure 4a. Numbers of depressions observed during November 1967 and 1968.**

1957-1958 IGY summer should be noted, and also the systematically greater storminess of the seven following summers. Winter cyclone tracks are concentrated in a narrower latitude band, and the latitude of the main cyclone tracks is not the same from year to year.

A recent analysis I have made shows that four main weather patterns (Figure 6) can be identified as those governing the overall climate of the Peninsula. By comparison of seasonal temperature anomalies, precipitation frequency, pressure variations, and the principal wind direction at Faraday, it has been possible to infer the probable locations of the circumpolar trough between 1947 and 1982. These findings are summarized in Tables 4 and 5. The easterly type (low pressure north of 65°S) can give warm or cold winters. The westerly type (trough south of 65°S) tends to give cold winters. The change in the 1960s from westerly/trough domination to a dominant easterly pattern was marked by the cessation of the 4- through 5-year temperature oscillation of Peninsula temperatures (Figure 7). The effect of the different air masses on Faraday can be seen in the latest temperature analysis for that station, which has been extended back to 1944 by reference to earlier stations now closed.

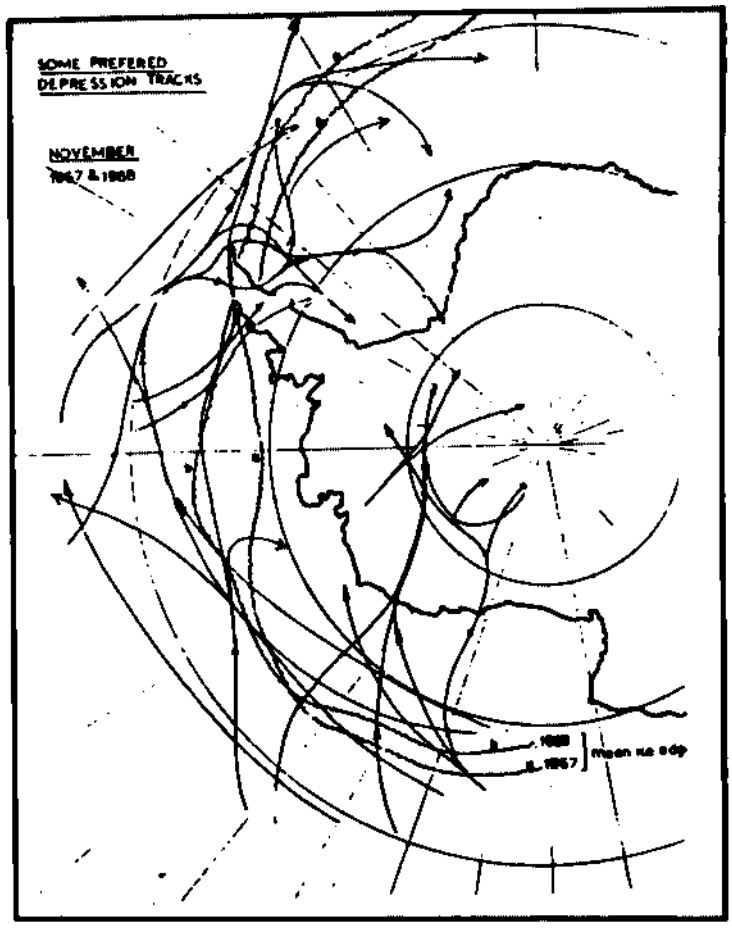


Figure 4b. Preferred cyclone tracks during November 1967 and 1968.

The main features can be summarized as follows:

1. Autumn and winter temperature values show very large variations from year to year. Spring and summer values show much less variation.
2. The very large winter variations have the greatest effect on the annual average temperature.
3. Before 1960 there were large 4- or 5-year cyclic variations. Since then, the cyclic behavior has become irregular.
4. In the early 1970s each season was, in general, warmer than the average, giving higher than average annual temperatures.

No similar analysis has been possible for the McMurdo-Ross Sea region of West Antarctica.

## LENGTH OF WINTER AND SUMMER SEASONS

As a more physical alternative to the standard definition of the winter or summer seasons as 3-month periods, a season can be defined by using a criterion based on actual temperatures. The summer season would best

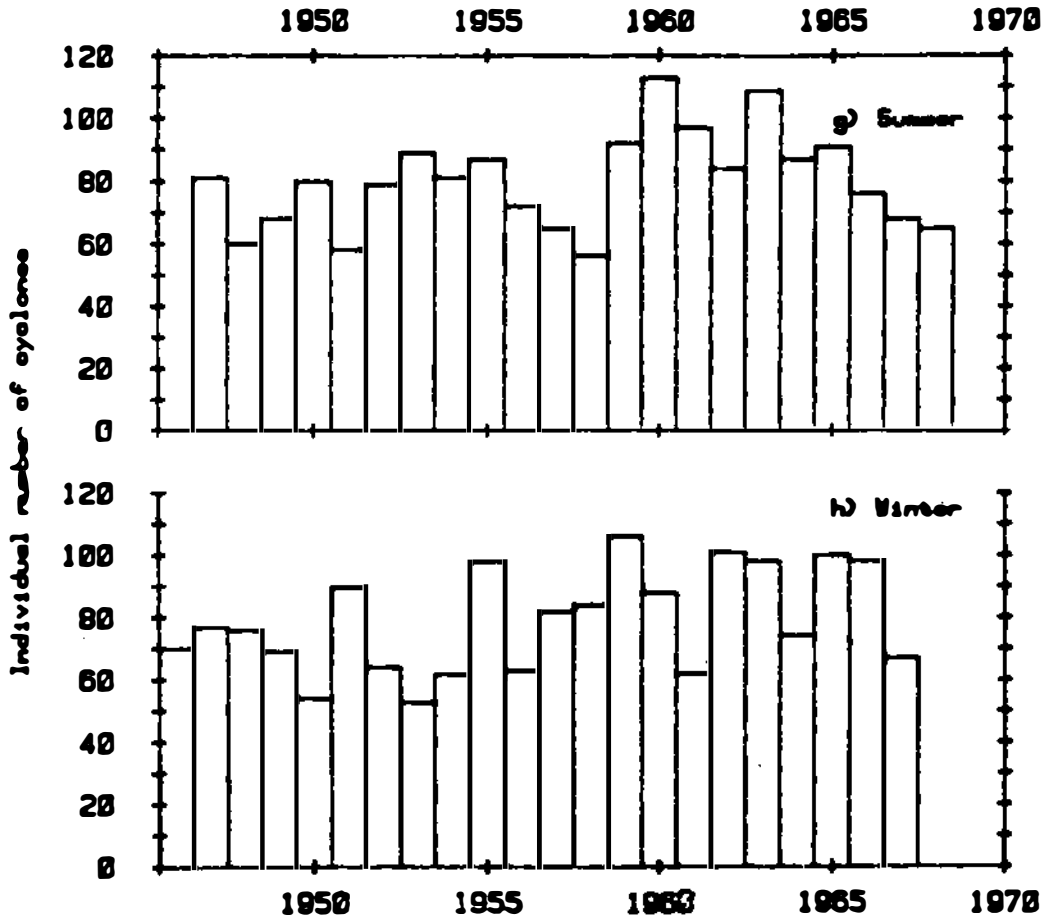


Figure 5. Seasonal numbers of cyclones observed between longitudes 40° and 65°W and latitudes 50° and 70°S during 1947-1968 (Mayes 1981).

be defined as the period when daytime upper-air temperatures show, on the average, a decrease upward from the surface; that is, the winter surface inversion has not developed. Unfortunately, there are few published continuous upper-air temperature records, so this approach cannot be used for a time series study. To give an idea of the differences across West Antarctica, upper-air data for 1958 show the following approximate "summer" lengths:

| | |
|---|---|
| Amundsen-Scott | December |
| Byrd | November-February |
| Little America V | November-January |
| Halley | October-April |
| Faraday | October-April |

To use the more readily available surface data, different criteria are needed. At Faraday the "winter" can be taken to begin when the maximum temperature falls below 0°C. The monthly mean temperature is at least 2°-3°C lower, and new snowfall accumulates. This gives a guide to changes in the length of winter, which in part determines the amount of sea ice in the Peninsula area. The variations in the date of

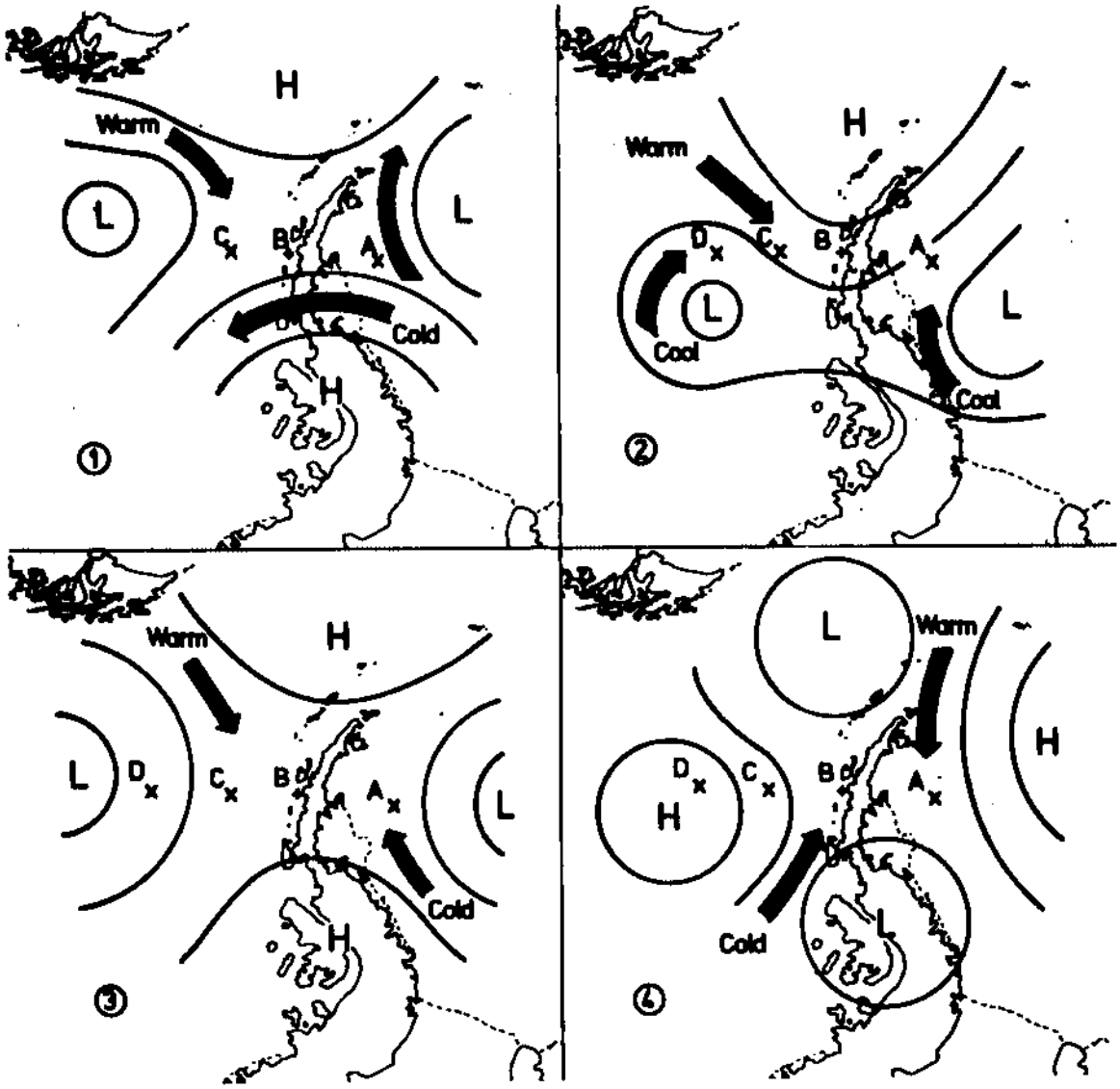


**Figure 6. Weather patterns governing the climate of the Antarctic Peninsula.**

start of winter as defined above are generally larger than those for the end of winter (Figure 8). In the 1970s the late start and early end of winter resulted in a relatively lengthy period of warm winters and easier ice conditions. Since the early 1950s the overall change has been toward shorter winters, that is, a warming. Short winters mean longer summers and greater potential for ice melt.

A similar analysis of season length has also been made using McMurdo data. McMurdo is close to the Ross Ice Shelf, and its temperatures are lower than those at Faraday, an island station. Sea ice can form at any time in the year. But for the initial formation of sea ice (melting point -1.8°C), persistent temperatures below -5° to -8°C are needed after the summer warming of Antarctic Ocean water

Table 4. Occurrence of Dominant Weather Systems in Winter for the Antarctic Peninsula, 1947-1982

| | Temperature Compared to Winter Average | | |
|---|---|---|---|
| Weather system | Cold | Average | Warm |
| Type 1 (easterly) | 2 | 7 | 9 |
| Type 2 (westerly) | 3 | 3 | 0 |
| Type 3 (trough) | 5 | 1 | 3 |
| Type 4 (col) | 1 | 2 | 0 |

(Limbert 1970). Therefore, a mean monthly temperature of -5°C has been used as the criterion for the summer/winter divide. The results are shown in Figure 9.

A comparison of the lengths of summer seasons at Faraday and McMurdo further confirms the lack of direct seasonal linkage between the Antarctic Peninsula and the Ross Sea sector of West Antarctica. The reason is simple: McMurdo is well inside the circumpolar trough (CPT) and mainly influenced by continental air flow; Faraday is on a low island at a latitude close to the CPT and is frequently visited by predominantly oceanic air masses. But both stations show that, in general, the areas they represent are returning to shorter summer periods after warm spells in the late 1960s and early 1970s. The ice extent in the Atlantic sector also shows an increase from 1975, but no such increase is to be found in the Pacific sector (Chiu 1983). The difference is difficult to explain. The general conclusion is that over a period of years the dates of start and end of summer and winter seasons must respond to gross circulation patterns that have been described by Rogers and van Loon (1982) and Swanson and Trenberth (1981).

Table 5. Occurrence of Dominant Weather Systems in Winter for the Antarctic Peninsula, 1947-1982

| Date | Type 1 Easterly | Type 2 Westerly | Type 3 Trough | Type 4 Col |
|---|---|---|---|---|
| 1947-1960 | 2 | 5 | 5 | 2 |
| 1961-1970 | 6 | 1 | 2 | 1 |
| 1971-1982 | 10 | 0 | 2 | 0 |

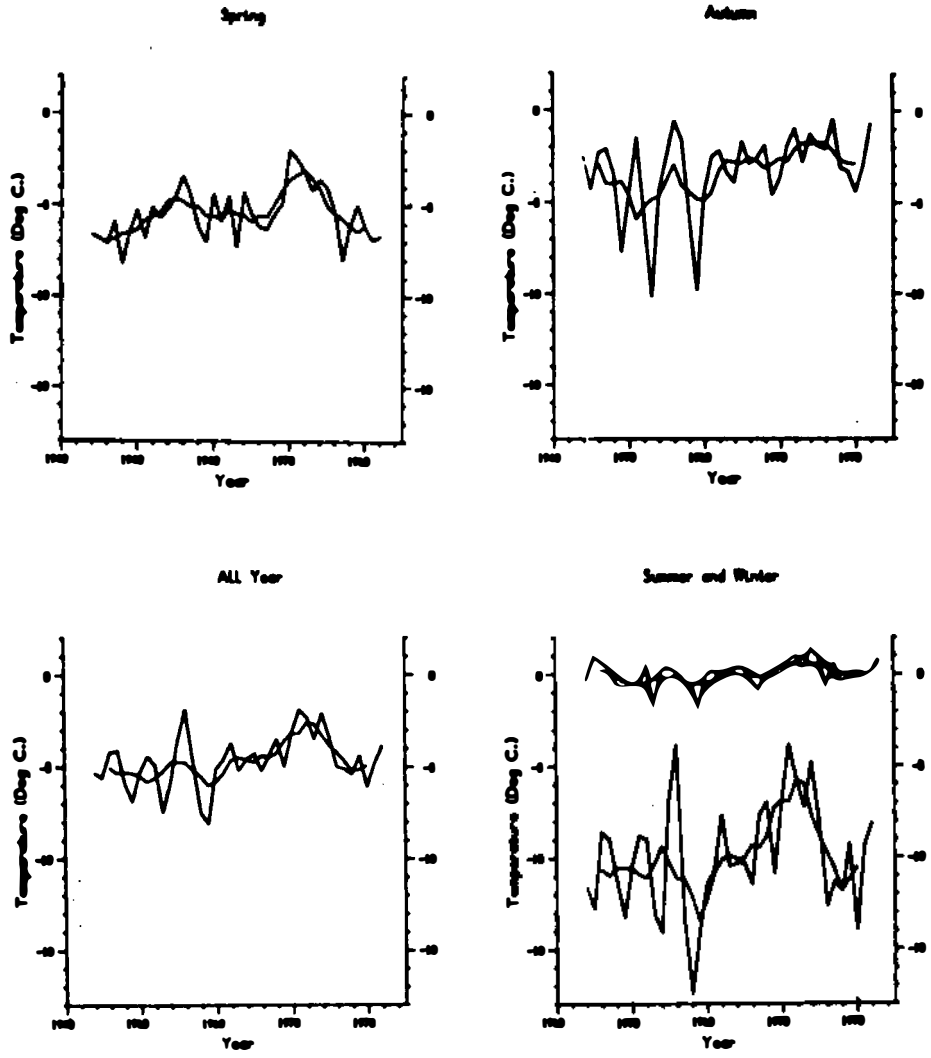


Figure 7. Seasonal and annual temperatures at Faraday.

## PROXY TEMPERATURES

Snow accumulation in the Antarctic depends on the water-vapor transport to the continent (Loewe 1962). Thus, accumulation should be related to the local mean saturated vapor pressure. To a first approximation, the saturation vapor pressure ($e_i$) is related to temperature ($T_C$) by the relation

$$\ln e_i \sim BT_C + C.$$

Hence, if the hypothesis is valid, we should expect that for snow accumulation (A),

$$\ln A \sim B'T_C + C'.$$

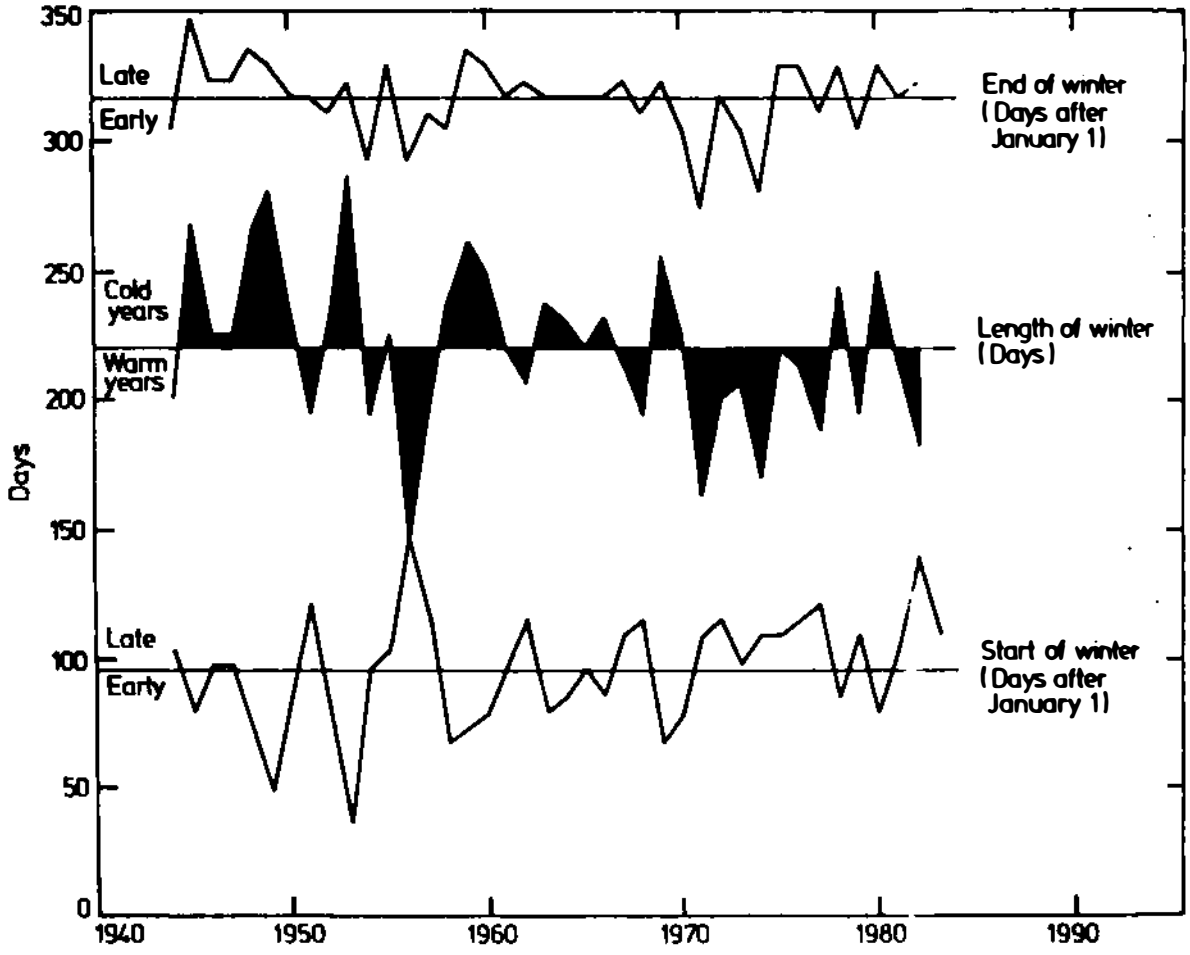


**Figure 8. Date of start and end of winter and length of winter. Faraday 65°S, 64°W, 1944-1983.**

The relation can only hold for a limited temperature range, say 10°C, around the mean temperature for each location. Mellor (1963) compared 256 pairs of data and obtained $\log_{10} A = 0.0235T + 1.95$, with a correlation coefficient $r = .72$. Robin (1977) and C. Lorius (private communication, 1983) have confirmed the validity of the log-linear relation. Morgan (1982) points out that the method is incapable of distinguishing seasonal changes. However, if we are only dealing with annual amounts, we may not have an exact equivalence, but there should be a variation related to the variation in annual temperature.

Mean temperature and annual accumulation data collected at Halley since 1956 give the relation

$$\bar{T} = 6.135 \ln A - 40.8$$

($r = .69$, $n = 22$). Mellor's equation would be

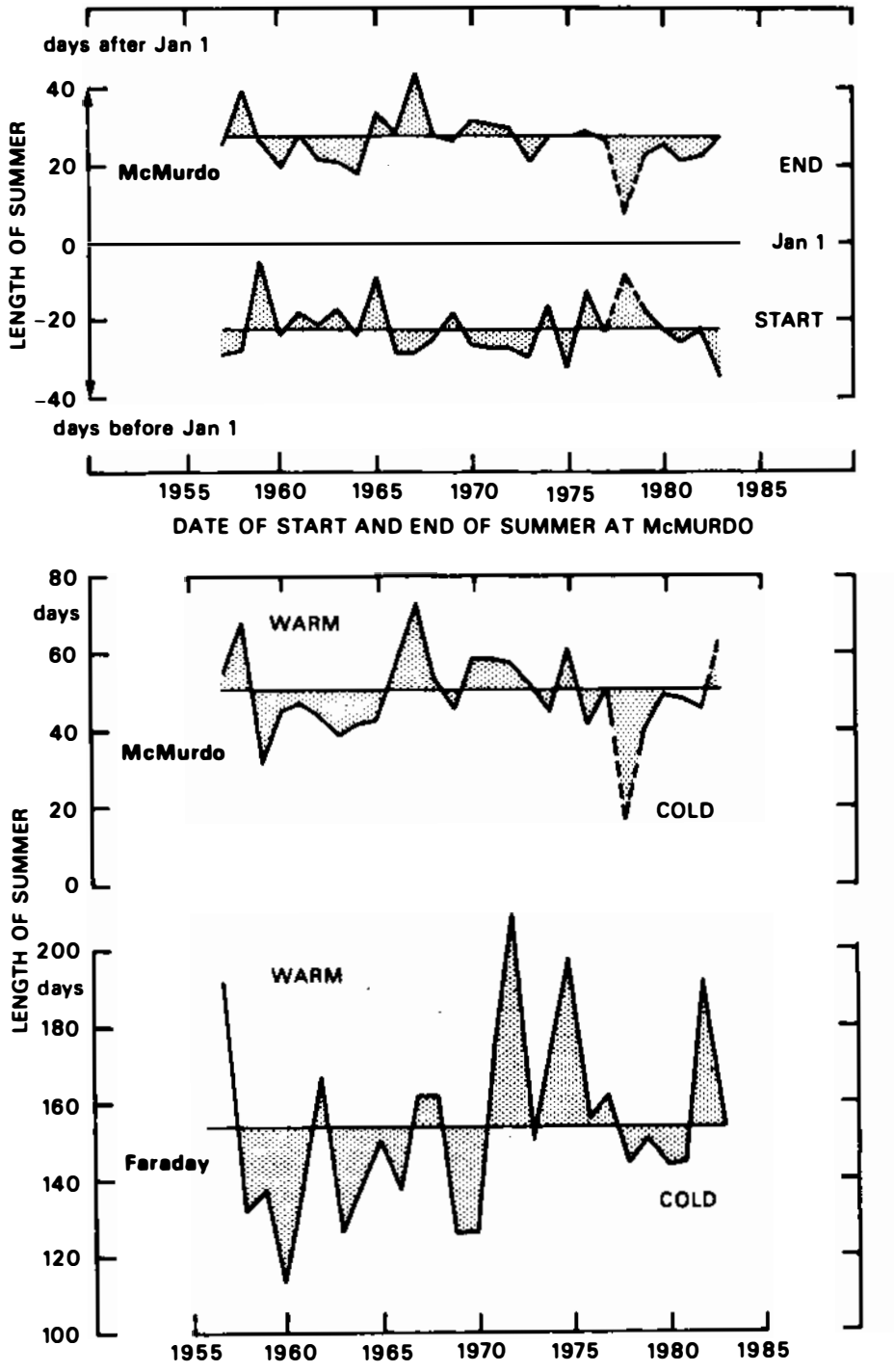


**Figure 9. Start and end of summer at McMurdo and Faraday.**

$$\overline{T} = 18.48 \ln A - 82.98.$$

The different constants illustrate site differences of temperature regime, evaporation, and the like.

Thus the accumulation rate provides a way of determining past temperature variations without reference to isotopic analysis, and we can use deep-pit stratigraphy records to estimate the approximate sign and magnitude of past climate/temperature changes. I have examined five such records for the Antarctic, including one for Byrd (Gow 1961). They show (Figure 10) that:

- The inferred temperature range is between 2 and 3°C;
- Periods of maximum accumulation do not occur at the same time;
- Wilkes (Goldthwaite 1959) and Byrd show similar broad-scale features;
- South Ice (Lister 1960) and South Pole are similar.

Wilkes and Byrd are both influenced by weather systems approaching the Ross Sea. South Ice is directly influenced by events in the Weddell Sea; the parallelism with Pole Station then points to climate effects from the South Atlantic/South American sector. SANAE Station (Neethling 1970), at the northeast entrance to the Weddell Sea, is completely out of phase with South Ice. The inference is that in the 1920s, frequent blocking anticyclones occurred close to 0° longitude in 60° or 65°S, which forced depressions to go deep into the Weddell Sea to bring extra snowfall and higher temperatures. That same cyclonic

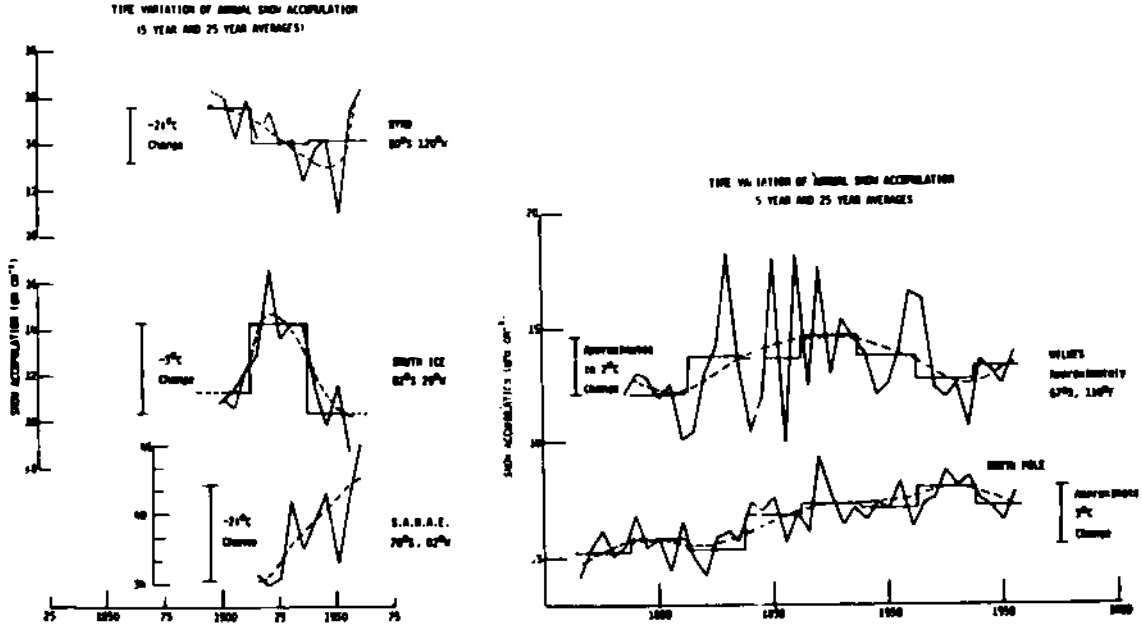

Figure 10. Accumulation rates at Antarctic stations (from pit stratigraphy) and inferred temperatures.

circulation in the Weddell Sea forces export of ice to the South Orkneys, together with a flow of cold air northward between 40° and 60°W. The 1920s were very cold in the South Orkneys, with hard sea-ice conditions (Heap 1964). Available expedition records suggest the same was true for the Peninsula at 65°S. More recent temperature trends are discussed in the next section.

## TEMPERATURE TRENDS

Figures 11 and 12 show Antarctic regional temperature trends based on my analysis of the principal stations of Antarctica, reported by the British Antarctic Survey (1980, 1981). The sectors are based on the natural divisions of Antarctica defined by the surface wind flow (Mather and Miller 1967). Least-squares regression lines for (a) 1956-1978 and, where possible, for (b) longer periods, show most of the trends to be nonsignificant. Only after 1960 is there any significant coherent upward change in temperatures. That change ceased between 1970 and 1975, and the movement has been downward ever since. Taken together, all regions give positive evidence of a general temperature rise, which averaged over the continent (excluding the Antarctic Peninsula), was +0.35°C between 1957 and 1978 (+0.0169 $\pm$ 0.0129°C $yr^{-1}$); about the same change occurred in West Antarctica, but 4 times as large a change was recorded in the Peninsula.

The continental temperature rise has a parallel in the record from islands in the Southern Ocean (Figure 13). Here, the interannual variability is smaller, and the air temperature is controlled by the surrounding ocean, which is conservative in temperature response. The combined ocean-island increase from 1957-1978 was +0.42°C (0.0189 $\pm$ 0.0072°C $yr^{-1}$), which agrees with the change over Antarctica and statistically is more significant. The combined ocean-island change since 1949 is, however, smaller (+0.36°C).

A recent study by Raper et al. (1983a), based on principal component analysis of fewer stations than are considered here, gave a much greater increase in the Antarctic temperatures. This finding is open to doubt because it implies an extra increase of 0.4°C between 1978 and 1981, conflicting with the actual observed downward trend. To complete the present analysis for West Antarctica, all expedition records have been used and adjusted to apply to three broad sectors, taking into account the temperature differences caused by geographic location and interannual change. The results are shown in Figure 14. The trend claimed for Little America by Wexler, when adjusted in this way, is no longer significant. In both the Ross Sea and the Antarctic Peninsula sectors of West Antarctica, it was probably warmer around 1910, cooler in the 1930s, and again warmer in the late 1960s and early 1970s. The year 1981 was unusually warm as a consequence of a very warm winter in the Antarctic sector south of Australia and New Zealand, and this temporarily interrupted the downard temperature trend (Raper et al. 1983b). The causes of the particular anomaly merit a full case study.

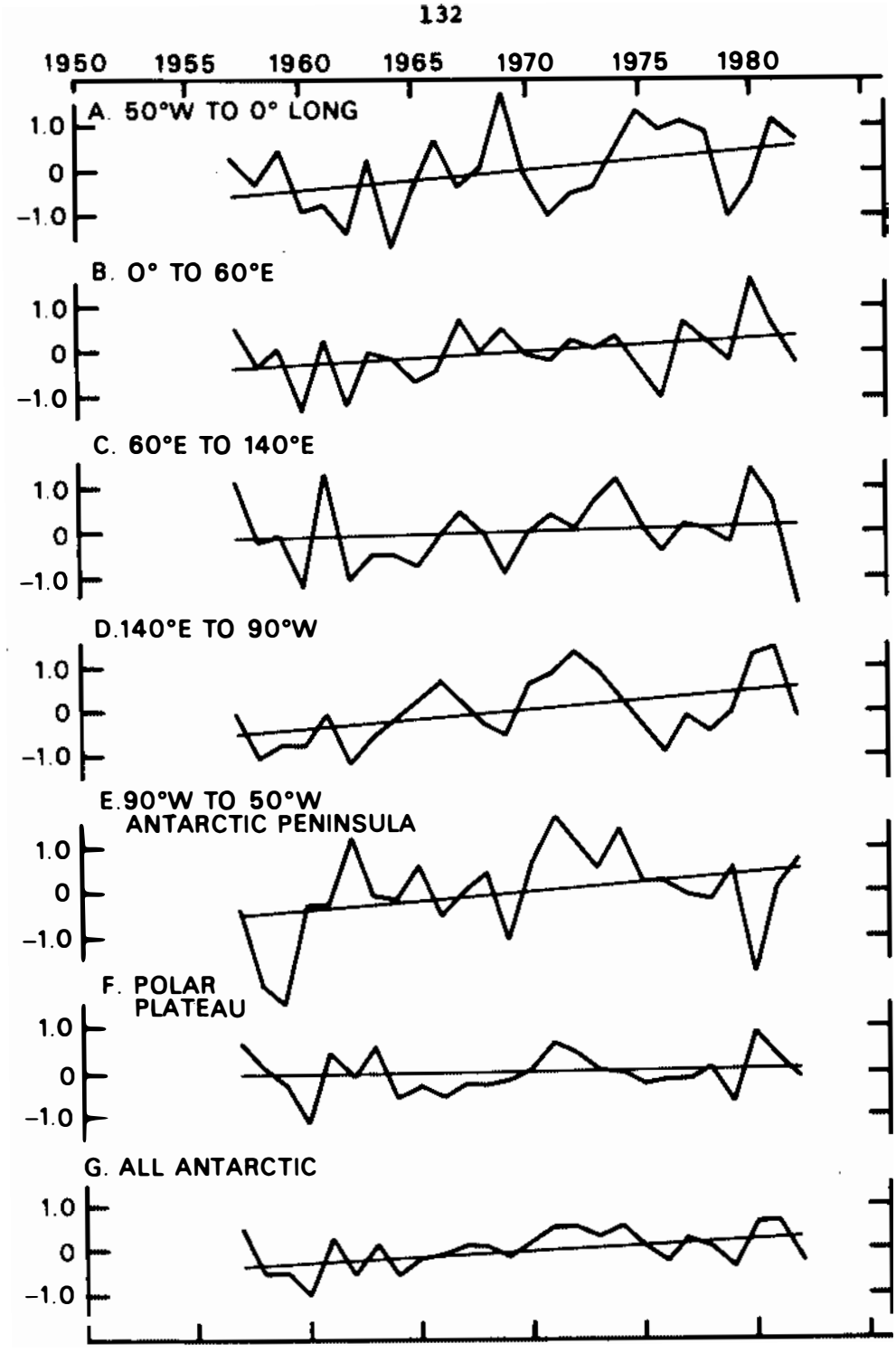


REGIONAL ANTARCTIC ANNUAL TEMPERATURE ANOMALIES 1957–1982

**Figure 11. The apparent trends indicated by the least-squares regression lines are not significant for regions A, B, C, E, and F. The trends in regions D and G are barely significant at the 5 percent level (r=.44 in both cases).**

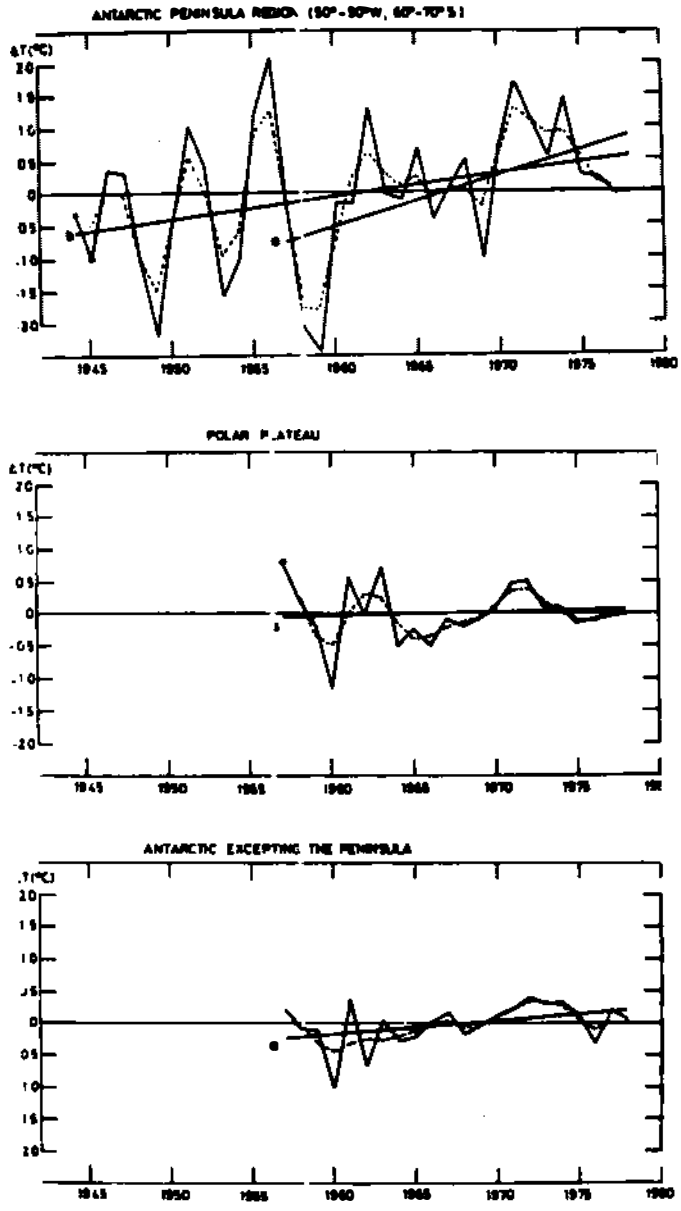


**Figure 12. Antarctic temperature trends. Symbol "a" marks regression lines for 1956-1978; "b" marks regression line for entire record.**

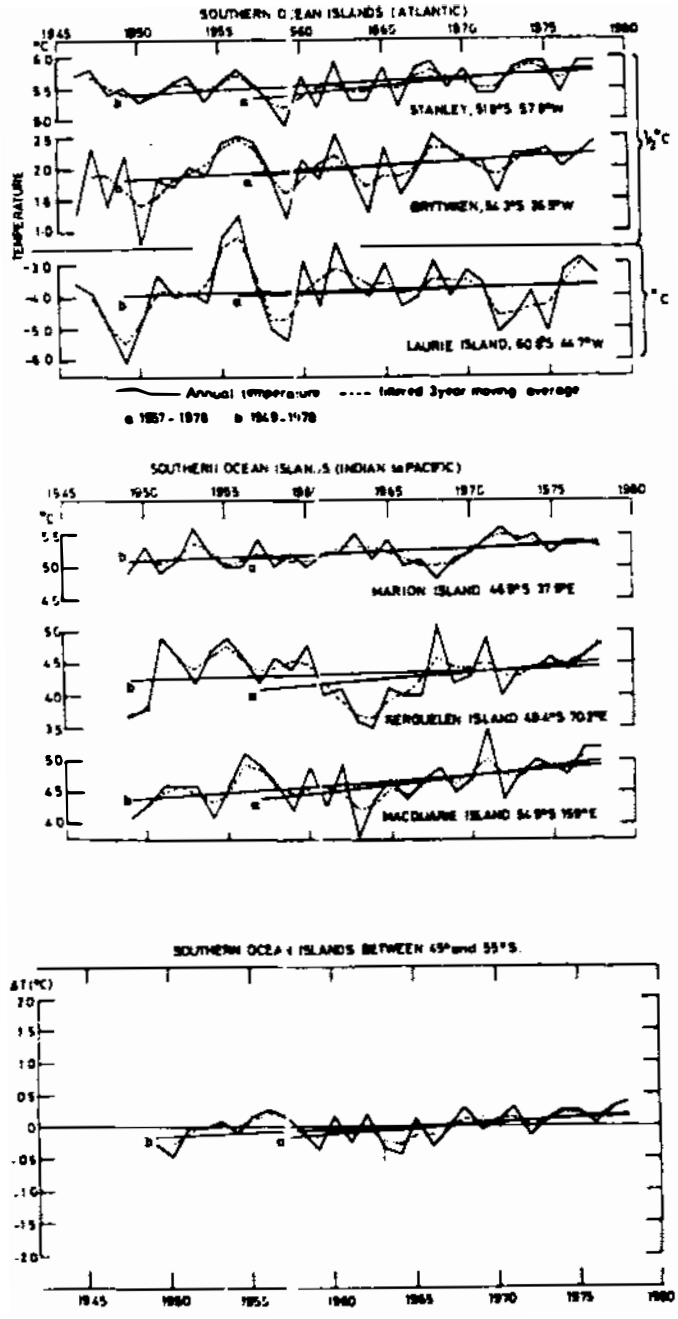


**Figure 13. Temperature trends at sub-Antarctic islands. Symbol "a" marks regression lines for 1956-1978; "b" marks regression lines for the entire record.**

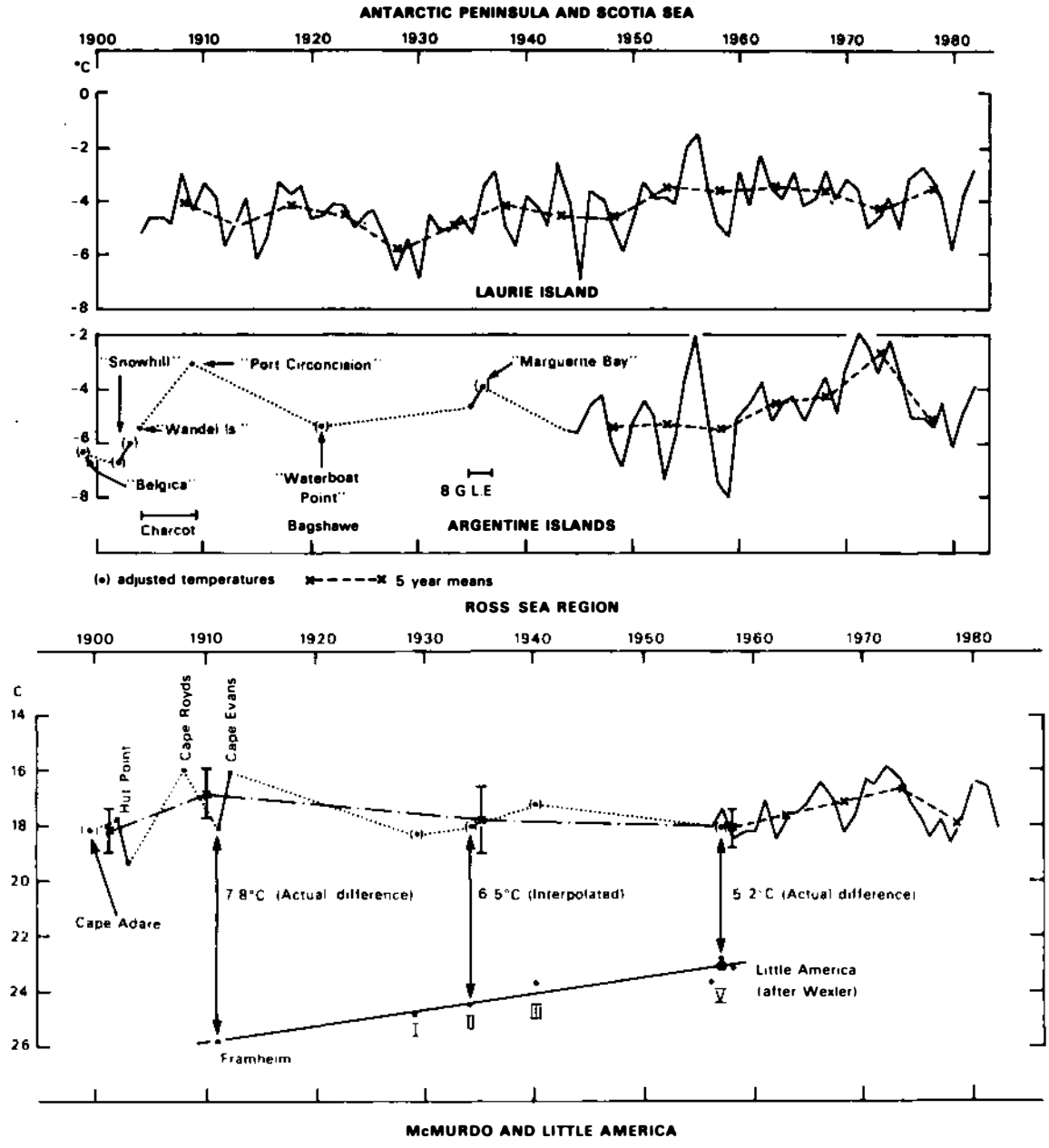


**Figure 14. Long temperature records for West Antarctica.**

## CONCLUSIONS

**Temperature trends constructed for West Antarctica and the Antarctic as a whole are inconclusive. They do not show any significant warming outside the normal range of temperature variability. Proxy temperature data suggest that temperature variations within a 2°-3°C temperature range have occurred over the last 100-200 years. This finding emphasizes the natural climate variability over a time span of only a few generations.**

There is some evidence of the influence on Antarctic temperatures of the Antarctic coastal current, and a better understanding is needed of how the Antarctic circumpolar current and the Antarctic coastal current interact, as well as of their effects on the annual temperature cycle and interannual climate variability. However, by far the most important factor in Antarctic temperature changes seems to be the position of the circumpolar trough and the storm tracks penetrating the Ross and Weddell seas. These are dominated by large-scale changes in hemispheric circulation caused by slow changes in the average position of the main midlatitude blocking anticyclones.

The lack of observational data from West Antarctica is to be deplored; every effort should be made to maintain the newly established automatic weather station at Byrd and to extend the deployment of other such stations to the coast of West Antarctica. The lack of upper-air data hampers research and analysis. It is significant that the long time series of upper-air data for Faraday has less interannual variability and shows that many of the surface trends are biased by the local environment (Figure 15).

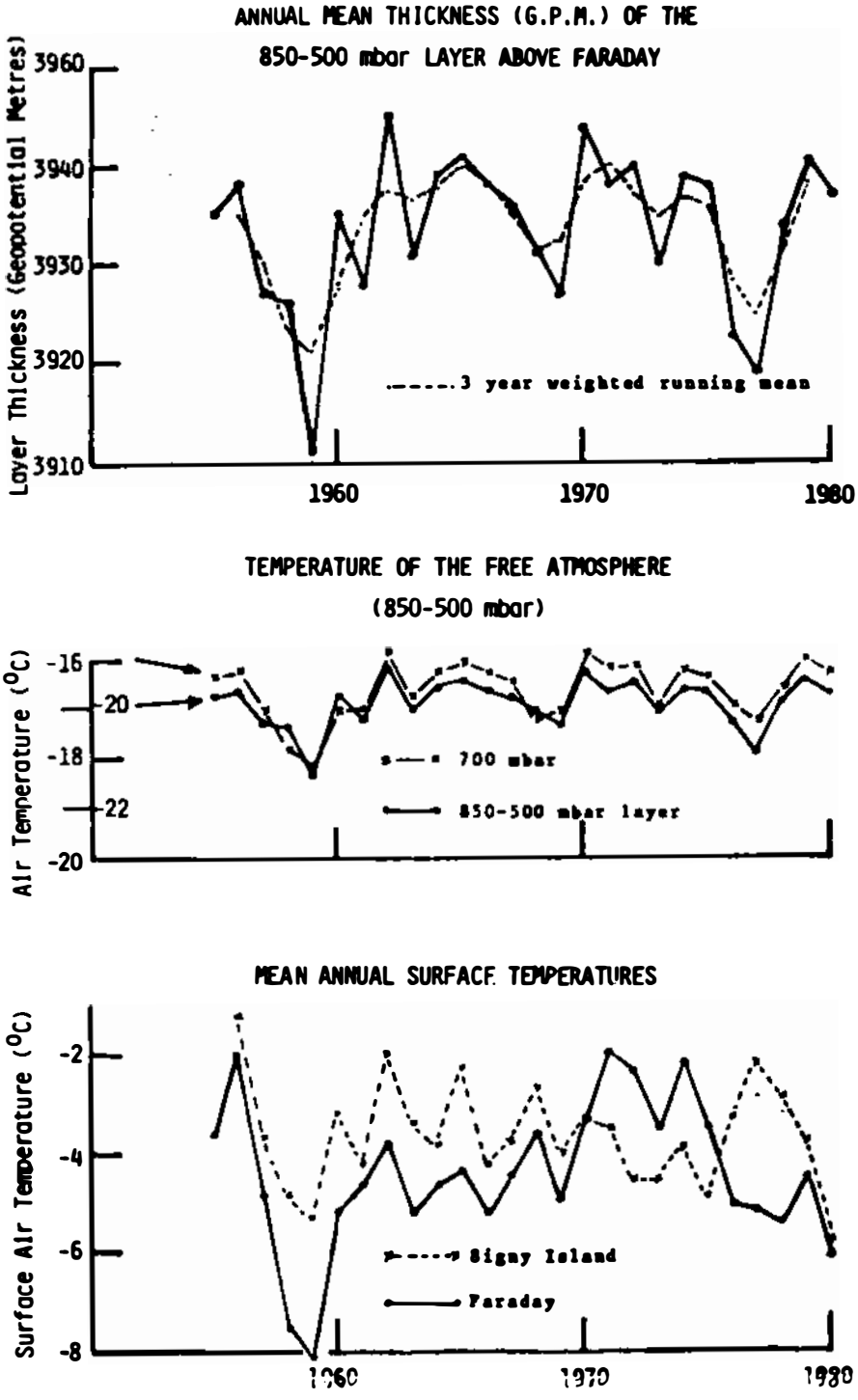


**Figure 15. Surface and upper-air temperatures over the Antarctic Peninsula.**

## REFERENCES

Astapenko, P.D., 1960. Atmospheric Processes in the High Latitudes of the Southern Hemisphere. Israel Program for Scientific Translations, Jerusalem.

British Antarctic Survey, 1980. Physics of the atmosphere--meteorology and climatology. BAS Annual Report for 1979-80 (pp. 24-29). Natural Environment Research Council, Cambridge, United Kingdom.

British Antarctic Survey, 1981. Meteorology and climatology. BAS Annual Report for 1980-81 (pp. 21-24). Natural Environment Research Council, Cambridge, United Kingdom.

Budd, W. F., 1975. Antarctic sea-ice variations from satellite sensing in relation to climate. Journal of Glaciology, 15, 417-427.

Chiu, L. S., 1983. Variation of Antarctic sea ice: an update. Monthly Weather Review, 3, 578-580.

Goldthwaite, R. P., 1959. USNC-IGY Antarctic Glaciological Data Field Work 1957 and 1958. Research Foundation Report 825-1, Part III. Ohio State University, Columbus.

Gow, A. J., 1961. Drill Hole Measurements and Snow Studies at Byrd Station, Antarctica. CRREL Technical Report 78. U.S. Army Cold Regions Research and Engineering Laboratory, Hanover, New Hampshire.

Heap, J. A., 1964. Pack ice. In R. E. Priestley, R. J. Adie, and G. Robin (eds.), Antarctic Research. Butterworth, London.

Limbert, D. W. S., 1970. The thermal balance of sea ice at Halley Bay. In A. J. Gow, C. Keeler, C. C. Langway, and W. F. Weeks (eds.), International Symposium on Antarctic Glaciological Exploration (ISAGE), Hanover, New Hampshire, 1968. IAHS Publication 86 (pp. 520-541). International Association of Hydrological Sciences, Geneva.

Lister, H., 1960. Glaciology. 1. Solid precipitation and drift snow. Scientific Reports. Transantarctic Expedition 1955-1958, 5.

Loewe, F., 1962. On the mass economy of the Antarctic ice cap. Journal of Geophysical Research, 67, 5171-5177.

Mather, K. R. and G. S. Miller, 1967. Notes on Topographic Factors Affecting the Surface Wind in Antarctica, with Special Reference to Katabatic Winds. Technical report. Geophysical Institute, University of Alaska, Fairbanks.

Mayes, P. R., 1981. Atmospheric circulation trends in southern South America and the Antarctic Peninsula area. Ph.D. thesis, University of East Anglia, Norwich, United Kingdom.

Mellor, M., 1963. Remarks concerning the Antarctic mass balance. Polarforschung, 5, 179-180.

Morgan, V. I., 1982. Oxygen isotope ratios, accumulation and Antarctic temperatures. In N. Young (ed.), Antarctica: Weather and Climate, 11-13 May 1981. Royal Meteorological Society, Australian Branch, University of Melbourne, Melbourne, Australia.

Neethling, D. C., 1970. Snow accumulation on the Fimbul ice shelf, western Dronning Maud Land, Antarctic. In A. J. Gow, C. Keeler, C. C. Langway, and W. F. Weeks (eds.), International Symposium on Antarctic Glaciological Exploration (ISAGE), Hanover, New

Hampshire, 1968. IAHS Publication 86 (pp. 390-404). International Association of Hydrological Sciences, Geneva.

Pittock, A. B., 1980a. Patterns of climatic variation in Argentina and Chile. I. Precipitation 1931-60. Monthly Weather Review, 108, 1347-1361.

Pittock, A. B., 1980b. Patterns of climatic variation in Argentina and Chile. II. Temperature 1931-60. Monthly Weather Review, 108, 1362-1369.

Raper, S. C. B., T. M. L. Wigley, P. R. Mayes, P. D. Jones, and M. J. Salinger, 1983a. Variations in surface air temperatures: Part 3. The Antarctic, 1956-1981. Submitted to Monthly Weather Review.

Raper, S. C. B., T. M. L. Wigley, P. D. Jones, P. M. Kelly, P. R. Mayes, and D. W. S. Limbert, 1983b. Recent temperature changes in the Arctic and Antarctic. Submitted to Nature.

Robin, G. de Q., 1977. Ice cores and climate change. Philosophical Transactions of the Royal Society, London, Series B, 280, 143-168.

Rogers, J. C. and H. van Loon, 1982. Spatial variability of sea level pressure and 500 mb height anomalies over the Southern Hemisphere. Monthly Weather Review, 110, 1375-1392.

Stearns, C. R. and M. L. Savage, 1981. Automatic weather stations 1980-81. Antarctic Journal of the United States, 16, 190-192.

Swanson, G. S. and K. E. Trenberth, 1981. Trends in the Southern Hemisphere troposphere. Monthly Weather Review, 109, 1890-1897.

ATTACHMENT 8

# PRESENT AND FUTURE MELTING ON ANTARCTIC ICE SHELVES

W. S. B. Paterson
Paterson Geophysics Inc., British Columbia, Canada

## INTRODUCTION

As the concentration of $CO_2$ in the atmosphere continues to rise, efforts to predict the extent and consequences of the expected climatic warming are being intensified. Most studies predict that warming will be greatest in the polar regions (Gates 1980). The floating ice shelves that surround much of Antarctica may be particularly vulnerable to warming; their surfaces are only a few hundred meters above sea level, and the air temperature reaches 0°C around the coast in summer. Increased melting and runoff at the surface, or increased melting at the base, would thin the ice shelf. Moreover, in time, surface warming would increase the ice temperature and, therefore, the spreading rate, which would reduce the ice thickness irrespective of any melting.

The ice shelves are important because the base of the ice sheet in West Antarctica, unlike those in East Antarctica and Greenland, lies well below sea level. Many believe that such an ice sheet is buttressed by its surrounding ice shelves, in this case, mainly by the Ross and Filchner-Ronne ice shelves, and that removal of these would cause the whole ice sheet to disintegrate (Thomas 1979). This disintegration would raise world sea level by about 5 m. An extreme view is that doubling the atmospheric concentration of $CO_2$, which will happen in about 50 years if present trends in fossil fuel consumption continue, will be enough to bring this about (Mercer 1978).

In this paper I review the data on surface melt rates on ice shelves, try to predict how much these will be increased by $CO_2$-induced warming, and assess the seriousness of the threat to the ice shelves. By restricting this review to the ice-shelf surface, I do not imply that melting at the base is unimportant. Atmospheric warming will increase the temperature of the ocean and thus the amount of heat available for basal melting, which may well be more important than changes at the surface.

Table 1 gives information about four of the best-studied ice shelves: George VI (Bishop and Walton 1981; Lennon et al. 1982), Maudheim (Schytt 1958a,b; Swithinbank 1960), Ross (Clary and Chapman 1963; Bentley et al. 1979; Zotikov et al. 1980; Thomas et al. in press), and Amery (Budd 1966; Budd et al. 1982). Figure 1 shows the locations for the major ice shelves.

Table 1. Ice-Shelf Data

| | George VI | Maudheim | Ross | Amery |
|---|---|---|---|---|
| Latitude, °S | 70 to 73 | 71 | 78 to 83 | 69 to 71 |
| 10-m temp., °C | -1 to -10 | -17 | -22 to -27 | -19 to -24 |
| Thickness, m | 100 to 500 | 180 | 220 to 800 | 300 to 800 |
| Surface balance, m/a (ice) | 0.01 to 0.8 | 0.4 | 0.1 to 0.3 | 0.04 to 0.5 |
| Basal balance, m/a (ice) | -0.5 to -10 | -0.9 | +0.02 to -1.0 | 0 to +0.5 |

## MELTING ON ICE SHELVES

When the surface snow starts to melt in summer, the water percolates into the underlying layers. When it reaches a depth where the temperature is still below 0°C, it refreezes. When there is enough refrozen meltwater to form a continuous layer, further water collects on top of it until, when all the snow has been melted, a pool is formed. Water in the pools may eventually drain into crevasses, or off the front or sides of the ice shelf; or it may remain in place and refreeze at the end of the summer. The small surface slope of ice shelves favors accumulation rather than drainage. Melting does not change the mass balance of the ice shelf if the meltwater refreezes at the surface, in the snowpack, or in a crevasse. If, however, the water runs off into the sea, the mass of the ice shelf is reduced.

On George VI Ice Shelf, much of the surface is covered with melt pools in summer. Some of the water drains off the western side of the ice shelf. The net mass balance at the surface remains positive everywhere, however, although in places it is only 0.01 m/a (Bishop and Walton 1981). Although the ice front has retreated in the past 30 years, parts of the shelf may be thickening (Doake 1982). Geological evidence indicates that the ice shelf disappeared during the postglacial Hypsithermal interval and reformed when temperature decreased (Clapperton and Sugden 1982). Because most estimates suggest that a doubling of atmospheric $CO_2$ would result in temperatures at least as high as in the Hypsithermal, the George VI Ice Shelf would probably disappear.

At Maudheim, there is much less melting than on George VI Ice Shelf, and all the water refreezes in the firn. Schytt (1958a) made a detailed study in a 12-m pit. Each summer's surface could be distinguished, and accumulation rate was calculated from the thickness and density of each annual layer. Schytt's values are given in Table 2. Each "year" starts at the end of the melt season. Thus, 1950 extends from middle or late January 1950 to middle or late January 1951. From the area of each melt feature in the stratigraphic section, I calculated the total thickness of refrozen meltwater in each annual layer on the assumption that all melt features had a density of 900 $kg/m^3$. I assumed that each summer's meltwater refroze in the same

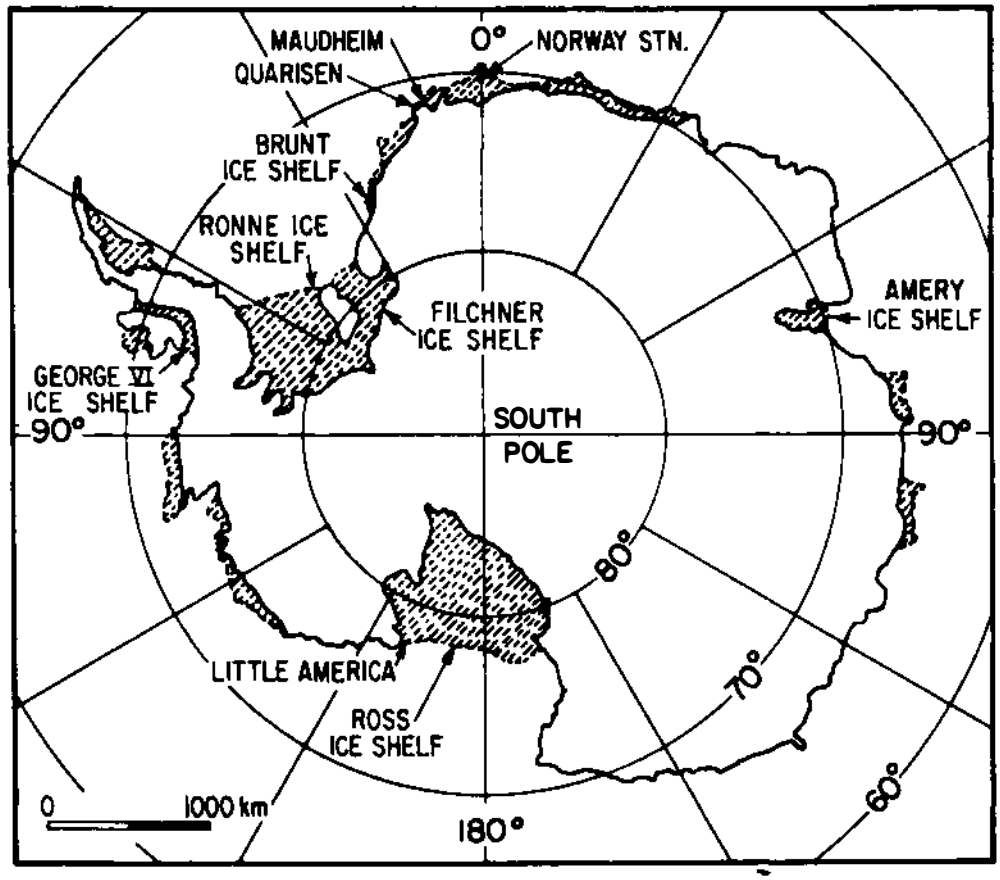


**Figure 1. Map of Antarctica showing the major ice shelves (shaded). From Thomas et al (in press).**

annual layer; this is true, except in 1949. Results are given in Table 2. The thickness of refrozen meltwater is a minimum figure because some meltwater merely increases the size of the firn grains. Because maximum percolation depth is highly correlated with the total thickness of melt features, it could be used as a rough measure of the amount of melting and, thus, of summer warmth.

The results illustrate the large year-to-year variations in the Antarctic climate. Accumulation varied by a factor of 2.5 over the 17 years of record. The thickness of refrozen meltwater also varied widely, but in no case did it exceed 15 percent of the annual layer. This finding contrasts with conditions over most of George VI Ice Shelf, where the whole of each annual layer is melted.

A stratigraphic record for the period 1913-1967 has been obtained at SANAE on the Fimbul Ice Shelf some 400 km east of Maudheim, although details have not been published (Neethling 1970). Because meteorological observations were made from 1960 to 1968, these data could be used to relate meltwater to summer temperature.

On Amery Ice Shelf, the percentage of refrozen meltwater in an annual layer increases with distance from the ice front and reaches 50 percent at the grounding line. The lower part of Lambert Glacier,

Table 2. Maudheim Melt Data

| Year | Annual Accumulation, mm of water equivalent | Total Melt, mm of water equivalent | Percolation depth, m |
|---|---|---|---|
| 1951 | 355 | 5 | ? |
| 1950 | 244 | 3 | ? |
| 1949 | 368 | 30 | >0.90 |
| 1948 | 243 | 32 | 0.36 |
| 1947 | 391 | 42 | 0.77 |
| 1946 | 448 | 15 | 0.83 |
| 1945 | 342 | 1 | 0.03 |
| 1944 | 298 | 45 | 0.69 |
| 1943 | 430 | 8 | 0.40 |
| 1942 | 356 | 27 | 0.39 |
| 1941 | 325 | 10 | 0.37 |
| 1940 | 469 | 8 | 0.35 |
| 1939 | 585 | 12 | 0.16 |
| 1938 | 221 | 4 | 0.02 |
| 1937 | 407 | 4 | 0.39 |
| 1936 | 267 | 12 | 0.53 |
| 1935 | 450 | 9 | 0.21 |
| Mean | 365 | 16 | 0.43 |

which feeds the ice shelf, is a "blue ice" area and is covered with melt pools in summer (Budd et al. 1967). Blue ice areas are found in regions of strong katabatic winds. These prevent snow accumulation so that the surface consists of ice that is ablated by evaporation and wind erosion throughout the year (Schytt 1961). Moreover, because ice has a much lower albedo than snow, melting can occur when the air temperature is a few degrees below 0°C. Lambert Glacier is heavily crevassed upstream of the blue ice area. There is some melting here also, but whether any of the meltwater is lost, rather than merely refreezing in the crevasses, is unclear (Budd et al. 1967).

Stratigraphic studies at Camp Michigan, near the front of the Ross Ice Shelf, showed one melt layer in 6 years (Zumberge 1958).

## THERMAL EFFECTS OF MELTWATER

In regions where the surface never reaches the melting point, the 10-m firn temperature is approximately equal to the mean annual air temperature. Where there is melting, however, the 10-m firn

temperature exceeds the mean annual air temperature, because each gram of meltwater that refreezes releases enough latent heat to raise the temperature of 160 g of snow or firn by 1 K. (This is a maximum figure because some of the heat may escape to the air.) Mercer (1978) suggested that this process will eventaully raise the temperature throughout an ice shelf to the melting point when $CO_2$ warming increases the melt rate. However, meltwater can penetrate a few meters of firn at most before refreezing. Moreover, the process is self-limiting; when enough water has refrozen to form a continuous ice layer, there will be no more percolation below that depth.

Data on warming by refreezing of meltwater are summarized in Table 3 and Figure 2. On White Glacier, the 10-m temperature varied by several degrees in the same borehole in different years and between different boreholes at the same elevation, so I took mean values. Warming is relatively slight on George VI Ice Shelf, because the surface below the winter snowpack consists of impermeable ice. On the Greenland Ice Sheet at latitude 77°N, the lapse rate is constant (1 K per 100 m) above 1500 m but appears to decrease steadily below. This finding suggests that there is no melting above 1500 m and that, below this limit, the amount of melting increases with decrease of elevation. Stratigraphic studies (Benson 1962) confirm this assumption. The maximum warming is 4.5 K. That there is melting at Maudheim and SANAE (10-m temperature of -18°C) but not at Little America (-22°C) supports the idea that a mean annual air temperature of about -20°C may be the critical value for the onset of melting. Melting, however, depends on maximum summer rather than mean annual temperature, and the data from Devon Island show that the critical value is sometimes below -20°C. In summary, refreezing of percolating meltwater raises 10-m temperatures by from 2 to 5 K above mean annual air temperatures. The values of 7 and 8 K observed on two glaciers in the European Alps (Paterson 1981, p. 190) should be an upper limit.

Meltwater that drains into crevasses reaches much greater depths than water that percolates through firn. Many of the ice streams that feed the ice shelves have heavily crevassed areas, with summer melting, immediately upstream of the grounding line. Stuiver et al. (1981, p. 403) suggested that latent heat released by water refreezing in these crevasses will produce anomalously high temperatures in the upper layers of the ice shelf near the grounding line. However, the heavily crevassed melting area on Lambert Glacier appears to have no effect on the temperature of the Amery Ice Shelf; the 10-m temperature near the grounding line (-23.5°C) is lower than elsewhere on the ice shelf (Budd 1966). Moreover, the temperature-depth profile some 200 km downstream has no anomalously warm bulge (Budd et al. 1982), even though a water pocket, which presumably originated as a water-filled crevasse, was encountered when drilling at a depth of 50 m (W. F. Budd, personal communication, 1983). Jarvis and Clarke (1974) found anomalously warm temperatues at depths between 20 and 80 m in Steele Glacier (Yukon). They ascribed it to freezing of water in crevasses opened during a surge 6 years before and verified the interpretation by a numerical model that provided an excellent fit to the observed temperature profile. The greatest temperature anomaly was about 7 K. The amount

Table 3. Ten-Meter Versus Mean Annual Air Temperature

| Name | $T_{10}$, °C | ΔT, K | Method | Reference |
|---|---|---|---|---|
| George VI Ice Shelf* | -8 to -10 | 0 to 2 | measurement | Bishop and Walton (1981) |
| Barnes Ice Cap | ~-10 | 2 to 5 | modeling | Hooke (1976) |
| Devon Island Ice Cap | -23 | 2.8 | modeling | Paterson and Clarke (1978) |
| White Glacier | -11 to -15 | 3 to 7 | measurement | Müller (1976) |

*Near Fossil Bluff.

of meltwater on Steele Glacier is much greater than on any Antarctic ice stream. Moreover the crevasses are deeper: 80 m compared with 20 m on Byrd Glacier, which feeds the Ross Ice Shelf (Pfeffer 1982). Thus, I think it unlikely that, in Antarctica, water refreezing in crevasses could raise the temperature of the surrounding ice by more than a few degrees. Present 10-m temperatures in the Ross Ice Shelf range from -22 to -28°C. I do not believe that, even with the $CO_2$ warming, this process will be sufficient to raise the ice temperature near the grounding line to the melting point and, thus, to trigger the disintegration of the ice shelf, as Stuiver et al. (1981, p. 403) suggested.

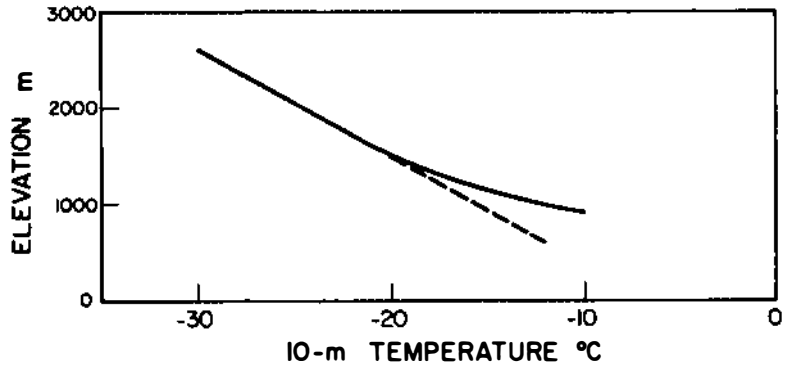


Figure 2. Ten-meter temperature (solid line) versus elevation at latitude 77°N in West Greenland (adapted from Robin et al. 1969). The broken line shows what the relation would be for temperatures below -20°C if there were no surface melting.

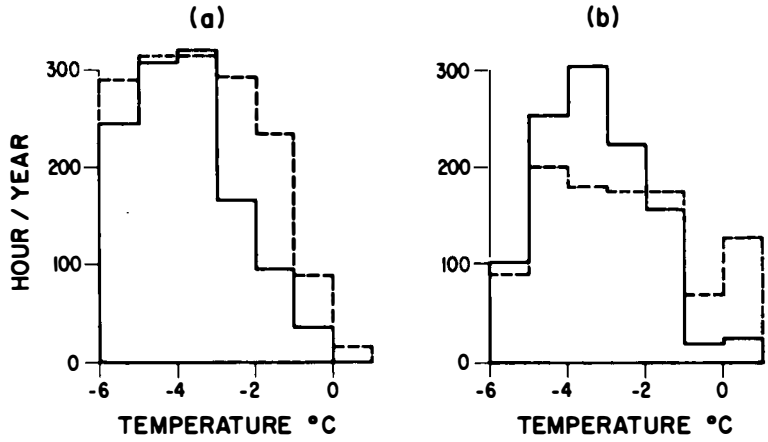


Figure 3. Frequency distributions of air temperatures about -6°C at (a) Maudheim for 1950-1951 (broken line) and 1951-1952 (solid line) and (b) Little America for 1956-1957 (broken line) and 1958-1958 (solid line).

## PREDICTION OF MELT FROM METEOROLOGICAL AND ENERGY-BUDGET DATA

Because meteorological and energy-budget data are basic requirements for any prediction of melt, I now review some data from ice shelves. Year-round meteorological observations were made at Maudheim for 2 years, at SANAE and Norway Station (about 25 km from SANAE) for several years, and at Little America for 4 years. In addition, there are summer observations from about 10 stations on the Ross Ice Shelf.

Figure 3 shows frequency distributions of air temperatures above -6°C for 2 years at Maudheim and Little America (not the same years for each). It should be noted that:

1. Variations from year to year are large. At Little America, air temperature was above freezing for 0, 4, 22, and 137 hours in the 4 years of record.
2. Temperatures at Maudheim exceeded 0°C for only 18 hours in the 2 years. There was very little melting, as the stratigraphic record (see Table 2) shows.
3. Temperatures exceed -4°C much more often than they exceed 0°C. For example, temperatures were -4°C or above for 1564 hours in the 2 years at Maudheim. At Little America, temperatures were -4°C or above for 1448 hours but were above 0°C for only 149 hours. These data suggest that if the mean summer temperatures were to rise by 4 K, as Manabe and Stouffer (1980) have predicted will happen at latitude 80°S with an atmospheric concentration of $CO_2$, that is, 4 times greater than at present, the amount of surface melting on the ice shelves would increase substantially. This argument rests on the questionable assumption that the frequency distribution of temperature would be unchanged.

**Table 4. Times When Air Temperature at Little America was ≥0°C**

| Date | Hours |
|---|---|
| 17 December 1934 | 1100-1600 |
| 22 December | 1100-1900 |
| 29 December | 1500 |
| 2 January 1935 | 1200 |
| 27 January | 0700-1200 |
| 28 January | 0700-1300 |
| | 2200-2400 |
| 20 January | 0100-0600 |
| | 0800-1400 |
| 31 January | 1100-1400 |

Table 4 shows a most important feature of the melt season. It is discontinuous; the air temperature never stays above 0°C for more than a few hours at a time. Thus, the surface is melted and frozen repeatedly.

The most detailed surface energy budget measurements on an ice shelf are those of Liljequist (1957) at Maudheim. Table 5 shows the mean energy balance for the whole of December, except for periods when the air temperature was ≥0°C. The energy budget did not vary much with temperature below 0°C, nor was there a great difference between clear-calm and cloudy-windy conditions. However, 0°C is an important threshold, not only because melting starts, but also because the surface energy budget changes. There are two reasons for this change: (a) the albedo of melting snow is 0.6 compared with 0.82 for fresh snow, so the amount of solar radiation absorbed is doubled when the surface starts to melt; and (b) the turbulent heat transfer to the surface depends on the temperature gradient above it, which increases with air temperature because the surface temperature cannot rise above 0°C. There was hardly any melting in either of the years when Maudheim was occupied, so there are no measurements of the energy budget under melting conditions. Instead, Liljequist calculated it by assuming that (a) the incoming solar radiation was as measured, but the surface albedo was 0.6; (b) the net long-wave radiation was unchanged; and (c) the turbulent transfer term had a value measured under similar conditions in Svalbard. Table 5 shows the result. When the air temperature rises to 4°C, the surface receives 8 times as much energy as it does under freezing conditions. Liljequist concluded, "In order to get a noticeable thinning out of the Antarctic inland ice and ice shelves, the air temperature in the summer must exceed 0°C, i.e., there must be a radical change in the atmospheric circulation, at least in the summer."

Table 5. Maudheim: December Energy Balance

| | $W/m^2$ |
|---|---|
| **Measured: Actual Weather Conditions with $T_{air}$ <0°C** | |
| Absorbed shortwave | +62 |
| Net longwave | -49 |
| Turbulent | +7 |
| Energy to surface | +20 |
| **Estimated for $T_{air}$ = +4°C** | |
| Absorbed shortwave | +140 |
| Net longwave | -49 |
| Turbulent | +73 |
| Energy to surface | +163 |

From Liljequist (1957).

I do not believe that the amount of melting on Antarctic ice shelves can be predicted by any simple method such as a correlation with mean summer temperature or degree-hours above freezing. The melt season consists of a number of short periods spread over 2 or 3 months. Therefore, the surface has to be melted repeatedly, and summer snowfalls, by increasing the surface albedo, reduce the amount of heat available for melting when the air temperature rises above freezing again. Thus a given amount of heat supplied in a series of short periods produces much less melting than would the same amount supplied in one period of the same total length. For this reason I think that Young's (1981) estimate of a surface melt rate of 0.18 m/a for a 5°C warming is much too high. The minimum information for predicting surface melt is the following:

1. Number and duration of periods when air temperature is above freezing;
2. Air temperature and wind speed during these periods;
3. Amount of snowfall between melting periods.

In other words, meteorological data are needed. The amount of melting can then be estimated by two methods:

a. Using field data to relate the amount of summer melting to the relative frequency of different synoptic weather situations, and
b. Using a numerical model to calculate heat budgets throughout the summer from standard meteorologial observations (Vowinckel and Orvig 1969).

Both methods have been used successfully for predicting the mass balance of ice caps in Arctic Canada (Holmgren 1971; Alt 1978, 1979; Paterson 1981, pp. 314-319).

I suggest the following approach to the problem of predicting future amounts of melting on Antarctic ice shelves:

1. Find out what synoptic situations produce air temperatures above freezing at coastal stations.
2. Try to relate the amount of melting in a given year, as determined by stratigraphic studies on the ice shelf, to frequency and duration of favorable synoptic situations. Existing data from Fimbul Ice Shelf (SANAE and Norway Stations) or Brunt Ice Shelf (Halley Bay) may be adequate. If not, new stratigraphic studies will be necessary.
3. Use an atmospheric general circulation model to predict how increased concentrations of atmospheric $CO_2$ will change the frequency of synoptic situations that favor melting.
4. Use the relation established in item 2 to predict the resulting amount of melting.

In the following section, I use existing data to give a rough estimate of the effects of $CO_2$-induced warming on the Ross Ice Shelf.

## POSSIBLE EFFECTS OF $CO_2$-INDUCED WARMING ON ROSS ICE SHELF

Gates (1980) has reviewed predictions of $CO_2$-induced warming. Predicted increases in globally averaged annual surface air temperature, resulting from a doubling of the present atmospheric $CO_2$ concentration, range from 0.75 to 4 K, with a mean of about 2 K, which Gates regards as the best estimate. Most models predict greatest warming at the poles and least at the equator. However, the warming at the poles is greater in the north than in the south and greater in winter than summer. One of the most detailed studies predicts that with four times the present $CO_2$ concentration, the mean annual temperature would increase by 5 K, and the mean summer temperature by 4 K, at the latitude and longtitude of the Ross Ice Shelf (see Manabe and Stouffer 1980, Figure 23). I use these estimates in the following discussion.

Present 10-m temperatures over about 75 percent of the Ross Ice Shelf are between -26° and -28°C, with maximum values of -23°C near the ice front and along the base of the Transantarctic Mountains (Thomas et al. in press). These should be approximately equal to the mean annual air temperature because melting is negligible. A $CO_2$-induced increase of 5 K will increase the 10-m temperatures by the same amount, or more if there is significant melting. Because there is some melting in most years at Maudheim (10-m temperature of -18°C), I believe that $CO_2$-induced warming will cause melting on the warmer parts of the Ross Ice Shelf. The data reviewed here suggest that the 10-m temperature may then be between 2 and 5 K warmer than the mean annual air temperature, which suggests that, after a quadrupling of the

atmospheric $CO_2$ concentration, the maximum 10-m temperature in the Ross Ice Shelf would be between -13° and -16°C, and the minimum would be about -23°C. I, therefore, disagree with the suggestion of Mercer (1978) that, with increased $CO_2$, refreezing meltwater in firn would raise the temperature to the melting point and cause the ice shelf to disintegrate.

If $CO_2$-induced melting on the Ross Ice Shelf were sufficient to melt the whole of each annual layer, the surface would consist of ice, meltwater pools could form, and some of the water might drain off the shelf, reducing its mass balance. However, from comparison with the present situation at Maudheim, where an average of only 5 percent of each annual layer is melted (Table 2), I think that this is unlikely. Thus, $CO_2$-induced warming will not cause any ablation from the surface; indeed, the surface mass balance will probably increase because of increased snowfall. Manabe and Stouffer (1980, Figure 24), for example, predicted that, with 4 times the present concentration of $CO_2$, precipitation at latitude 80°S will be about 10 percent greater than at present. (Note, however, that their model predicts a present precipitation rate of 0.55 m/a, which is about double the actual value.) On the other hand, $CO_2$-induced warming will probably result in increased melting at the base of the ice shelf. Basal melting depends on water circulation under the ice shelf and is difficult to predict. It is outside the scope of this review.

Surface warming will eventually increase the temperature of the bulk of the ice and, thus, increase its spreading rate. Heat transfer by conduction and downward advection of ice is slow, however; Young (1981) calculated that a new steady state strain rate was not established until 1,000 years after the temperature change. Moreover, basal melting would reduce the mean temperature of the ice shelf, which would decrease the spreading rate (Thomas and MacAyeal 1982).

To summarize, I believe that a concentration of atmospheric $CO_2$ of 4 times the present value will have the following effects on the Ross Ice Shelf:

1. The surface mass balance will increase slightly because of increased precipitation.
2. Although there will be significant surface melting near the edges, it will not result in any ablation.
3. The basal mass balance will decrease because of increased basal melting.
4. Surface warming will tend, in time, to increase the mean temperature of the ice shelf and, thus, the spreading rate. This spreading would thin the shelf.
5. Increased basal melting will remove more of the warmest ice, which will decrease the mean temperature and the spreading rate and tend to thicken the shelf, thus counteracting the effect of surface warming.

To estimate the relative importance of these effects and whether the ice shelf will grow thicker or thinner requires a numerical model that treats ice flow and heat transfer simultaneously. Assumptions

will have to be made about basal melt rates. Paterson (in press) has proposed such a model.

Although, on the basis of the meager data available at present, I disagree with the opinions of Mercer (1978) and Stuiver et al. (1981) that the predicted amount of $CO_2$-induced warming will be enough to cause the West Antarctic Ice Sheet to disintegrate, I am convinced by Mercer's argument (Mercer 1968a, 1981) that it did so at the height of the last interglacial (marine substage 5e). World sea level at that time was 5 m above the present level, the only time it has been so in the past 700,000 years. Of the possible sources of this water, West Antarctica, Greenland, or part of East Antarctica, I believe that West Antarctica is by far the most likely. This theory suggests that temperatures in the south polar region at that time were higher than those predicted for a concentration of atmospheric $CO_2$ 4 times the present one. Lake sediments and inactive solifluction flows beside Reedy Glacier, which drains into the Ross Ice Shelf, suggest interglacial temperatures of from 6 to 10 K above those at present (Mercer 1968b). Oxygen-isotope analysis of the ice core from Vostok, East Antarctica, should provide another estimate.

I have outlined here one possible way of estimating future melting and its effect on the West Antarctic Ice Sheet. The problem needs a great deal of further study, using a wide range of approaches. Bentley (1982) has recently produced an excellent summary of what needs to be done.

## ACKNOWLEDGMENT

This paper is a contribution to the Cooperative Institute for Research in Environmental Sciences/Environmental Research Laboratory Ice Sheet Modeling Program, University of Colorado.

## REFERENCES

Alt, B. T., 1978. Synoptic climate controls of mass-balance variations on Devon Island ice cap. Arctic and Alpine Research, 10, 61-80.

Alt, B. T., 1979. Investigation of summer synoptic climate controls on the mass balance of Meighen Ice Cap. Atmosphere-Ocean, 17, 181-199.

Benson, C. S., 1962. Stratigraphic studies in the snow and firn of the Greenland Ice Sheet. SIPRE Research Report 70.

Bentley, C. R., 1982. Carbon Dioxide Effects Research and Assessment Program. Environmental and Societal Consequences of a Possible $CO_2$-Induced Climatic Change. Volume II, Part I. DOE/EV/10019-02. U.S. Department of Energy, Washington, D.C.

Bentley, C. R., J. W. Clough, K. C. Jezek, and S. Shabtaie, 1979. Ice-thickness patterns and the dynamics of the Ross Ice Shelf, Antarctica. Journal of Glaciology, 24, 287-294.

Bishop, J. F. and J. L. W. Walton, 1981. Bottom melting under George VI Ice Shelf, Antarctica. Journal of Glaciology, 27, 429-447.

Budd, W. F., 1966. The dynamics of the Amery Ice Shelf. Journal of Glaciology, 6, 335-358.

Budd, W. F., I. L. Smith, and E. Wishart, 1967. The Amery Ice Shelf. In H. Oura (ed.), Physics of Snow and Ice. Volume I (pp. 447-467). Institute of Low Temperature Science, Hokkaido University, Sapporo, Japan.

Budd, W. F., M. J. Corry, and T. H. Jacka, 1982. Results from the Amery Ice Shelf Project. Annals of Glaciology, 3, 36-41.

Clapperton, C. M. and D. E. Sugden, 1982. Glacier fluctuations in George VI Sound area, West Antarctica (abstract). Annals of Glaciology, 3, 345.

Clary, A. P. and W. H. Chapman, 1963. Additional glaciological measurements at the abandoned Little America Station, Antarctica. Journal of Geophysical Research, 68, 6064-6065.

Doake, C. S. M., 1982. State of balance of the ice sheet in the Antarctic Peninsula. Annals of Glaciology, 3, 77-82.

Gates, W. L., 1980. A Review of Modeled Surface Temperature Changes Due to Increased Atmospheric $CO_2$. Report 17. Oregon State University, Climate Research Unit, Corvallis, Oregon.

Holmgren, B., 1971. Climate and energy exchange on a sub-polar ice cap in summer. Parts A to F (pp. 107-112). Uppsala Universitet, Meteorologiska Institutionen, Meddelande, Uppsala, Sweden.

Hooke, R. L., 1976. Near-surface temperatures in the superimposed ice zone and lower part of the soaked zone of polar ice sheets (abstract). Journal of Glaciology, 16, 302-304.

Jarvis, G. T. and G. K. C. Clarke, 1974. Thermal effects of crevassing on Steele Glacier, Yukon, Canada. Journal of Glaciology, 13, 243-254.

Lennon, P. W., J. Loyness, J. G. Paren, and J. R. Potter, 1982. Oceanographic observations from George VI Ice Shelf, Antarctic Peninsula. Annals of Glaciology, 3, 178-183.

Liljequist, G. H., 1957. Energy exchange of the snow surface. In Norwegian-British-Swedish Antarctic Expedition, 1949-52. Scientific Results. Volume 2 (pp. 291-298). Norsk Polarinstitutt, Oslo, Norway.

Manabe, S. and R. J. Stouffer, 1980. Sensitivity of a global climate model to increase of $CO_2$ concentration in the atmosphere. Journal of Geophysical Research, 85, 5529-5554.

Mercer, J. H. 1968a. Antarctic ice and Sangamon sea level. IAHS Publication 79 (pp. 217-225). International Association of Hydrological Sciences, Geneva.

Mercer, J. H., 1968b. Glacial geology of the Reedy Glacier area, Antarctica. Geological Society of America Bulletin, 79, 471-486.

Mercer, J. H., 1978. West Antarctic ice sheet and $CO_2$ greenhouse effect: a threat of disaster. Nature, 271, 321-325.

Mercer, J. H., 1981. West Antarctic ice volume: the interplay of sea level and temperature, and a strandline test for absence of the ice sheet during the last interglacial. IAHS Publication 131 (pp. 323-330). International Association of Hydrological Sciences, Geneva.

Müller, F., 1976. On the thermal regime of a high-arctic valley glacier. Journal of Glaciology, 16, 119-133.

Neethling, D. C., 1970. Snow accumulation on the Fimbul Ice Shelf, western Dronning Maud Land, Antarctica. In A. J. Gow, C. Keeler, C. C. Langway, and W. F. Weeks, International Symposium on Antarctic Glaciological Exploration (ISAGE), Hanover, New Hampshire, 1968. IAHS Publication 86 (pp. 390-404). International Association of Hydrological Sciences, Geneva.

Paterson, W. S. B., 1981. The Physics of Glaciers: Second Edition. Pergamon, London.

Paterson, W. S. B., in press. A Numerical Model for Estimating the Response of an Ice Shelf to $CO_2$-Induced Climatic Warming. CIRES/ERL Report. University of Colorado, Boulder.

Paterson, W. S. B. and G. K. C. Clarke, 1978. Comparison of theoretical and observed temperature distributions in Devon Island ice cap, Canada. Geophysical Journal of the Royal Astronomical Society, 55, 615-632.

Pfeffer, T., 1982. The effect of crevassing on the radiative absorptance of a glacier surface (abstract). Annals of Glaciology, 3, 353.

Robin, G. de Q., S. Evans, and J. T. Bailey, 1969. Interpretation of radio echo sounding in polar ice sheets. Philosophical Transactions of the Royal Society, London, Series A, 265, 437-505.

Schytt, V., 1958a. Snow studies at Maudheim. Norwegian-British-Swedish Antarctic Expedition, 1949-52, Scientific Results. Volume 4 (pp. 20-61). Norsk Polarinstitutt, Oslo, Norway.

Schytt, V., 1958b. The inner structure of the ice shelf at Maudheim as shown by core drilling. Norwegian-British-Swedish Antarctic Expedition, 1949-52, Scientific Results. Volume 2 (pp. 115-151). Norsk Polarinstitutt, Oslo, Norway.

Schytt, V., 1961. Blue-ice fields, moraine features and glacier fluctuations. Norwegian-British-Swedish Antarctic Expedition, 1949-52, Scientific Results. Volume 2 (pp. 181-204). Norsk Polarinstitutt, Oslo, Norway.

Stuiver, M., G. H. Denton, T. J. Hughes, and J. L. Fastook, 1981. History of the marine ice sheet in West Antarctica during the last glaciation: a working hypothesis. In G. H. Denton and T. J. Hughes (eds.), The Last Great Ice Sheets (pp. 319-436). Wiley-Interscience, New York.

Swithinbank, C. W. M., 1960. Maudheim revisited: the morphology and regime of the ice shelf, 1950-60. Norsk Polarinstitutt Årbok, 1960, 28-31.

Thomas, R. H., 1979. The dynamics of marine ice sheets. Journal of Glaciology, 24, 167-177.

Thomas, R. H. and D. R. MacAyeal, 1982. Derived physical characteristics of the Ross Ice Shelf, Antarctica. Journal of Glaciology, 28, 397-412.

Thomas, R. H., D. R. MacAyeal, D. H. Eilers, and D. R. Gaylord, in press. Glaciologial studies on the Ross Ice Shelf, Antarctica, 1973-1978. Antarctic Research Series. American Geophysical Union, Washington, D.C.

Vowinkel, E. and S. Orvig, 1969. Climatic change over the polar ocean. A method for calculating synoptic energy budgets. Archives for Meteorology, Geophysics and Bioclimatology Series B, 17, 121-146.

Young, N. W. 1981. Responses of Ice Sheets to Environmental Changes. IAHS Publication 131 (pp. 331-360). International Association of Hydrological Sciences, Geneva.

Zotikov, I. A., V. S. Zagorodnov, and J. V. Raikovsky, 1980. Core drilling through the Ross Ice Shelf (Antarctica): Confirmed basal freezing. Science, 207, 1463-1465.

Zumberge, J. H., 1958. Preliminary Report on the Ross Ice Shelf Deformation Project. IAHS Publication 47 (pp. 56-63). International Association of Hydrological Sciences, Geneva.

ATTACHMENT 9

# ATMOSPHERIC GENERAL CIRCULATION MODEL SIMULATIONS OF THE MODERN ANTARCTIC CLIMATE

Michael E. Schlesinger

Department of Atmospheric Sciences and
Climate Research Institute
Oregon State University, Corvallis

## INTRODUCTION

General circulation models of the atmosphere (atmospheric GCMs or AGCMs) determine the surface pressure and the vertical distributions of velocity, temperature, density, and water vapor as a function of time and geographical location from the mass conservation law and hydrostatic approximation, Newton's second law of motion, the first law of thermodynamics, the equation of state, and the conservation law for water vapor. AGCMs also predict the temperature of the earth's nonwater surfaces, the water in soil, the mass of snow on the surface, and the cloudiness.

The governing equations of AGCMs are nonlinear, partial differential equations whose solution cannot be obtained except by numerical mathematical methods on the most rapid computers. These numerical methods subdivide the atmosphere vertically into discrete layers, wherein the variables are "carried" and computed. For each layer the horizontal variations of the predicted quantities are determined either at discrete grid points over the earth, as in the grid point (finite difference) models, or by a finite number of prescribed mathematical functions, as in the spectral models. The values of the predicted variables for each layer (including the surface) and grid point (or mathematical function) are determined from the governing equations by "marching" (integrating) forward in time in discrete steps starting from some given initial conditions.

The spatial resolution of AGCMs is constrained for practical reasons by the speed and memory capacity of the computer used to perform the numerical integrations. Increasing the resolution not only increases the memory required (linearly for vertical resolution and quadratically for horizontal resolution) but also frequently requires a reduction in the integration time step. Consequently, the computer time required increases rapidly (nonlinearly) with increasing resolution. Contemporary GCMs have from 2 to about 15 vertical layers, a horizontal resolution of a few hundred kilometers, and a time step ranging from 5 to 40 minutes. These models require from one-half minute to several minutes to simulate one day on a fifth-generation computer such as the CRAY 1 and CYBER 205.

Because of their limited spatial resolution, AGCMs do not resolve several physical processes important in predicting climate. However, the effects of these subgrid-scale processes on the scales resolved by the AGCM are incorporated in the model by relating them to the resolved-scale variables themselves. Such a relation is called a parameterization and is based on both observational and theoretical studies.

To validate an atmospheric GCM, it is possible to treat the sea surface temperature (SST) and sea-ice thickness as given boundary conditions rather than as predicted variables of the climate system. Then, since it is the ability of the AGCMs to simulate climatic change that is of interest, and since the seasons are the best-documented climatic changes, the seasonal performance of the models can be evaluated from a simulation in which the SST and sea-ice distributions are taken equal to their observed values. This has been done most frequently by simulating single winter and summer months, usually July and January (with reference to the Southern Hemisphere), and comparing the simulated atmospheric variables with their observed counterparts. The seasonal performance of several models has also been determined from extended integrations over more than one annual cycle, wherein the SST and sea-ice distributions are prescribed to repeat their observed annual cycles.

This paper presents the modern summer and winter climates in and around Antarctica simulated by six contemporary global AGCMs shown in Table 1. This table also shows for each model the number of vertical layers, pressure at the top of the model atmosphere, representation (grid point or spectral) of the horizontal variation of the dependent variables, horizontal resolution, the source for the prescribed SST and sea ice, and the number and identity of the months that were used to form the summer and winter average climates shown in the figures that follow. An example of the prescribed surface boundary conditions is shown in Figure 1 in terms of the surface elevation of the OSU model (Ghan et al. 1982) and that model's prescribed January and July SST and sea-ice extent. In Figure 1 the lowest latitude is 30°S, and the geography is that shown by Taljaard et al. (1969). The spatial resolution of this geography is much finer than that of the models (Table 1).

## SIMULATED CLIMATE

The climate simulated by the AGCMs listed in Table 1 is presented here in terms of the surface air temperature, sea-level pressure, and precipitation rate. The geographical distributions of these quantities are presented on the polar projection of Figure 1 for both the simulations and the observations. Results are also presented from the predecessors of the models listed in Table 1 for the zonal mean precipitation rate and sea-level pressure and for the geographical locations of cyclogenesis and the tracks of cyclones.

Table 1. General Circulation Models, Characteristics, and Simulations

| | Number of Vertical Layers | Top Pressure, mbar | Horizontal Representation | Resolution | Prescribed SST and Sea-Ice Source | Simulations: Identity of Summer/Winter Months | Simulations: Number Averaged |
|---|---|---|---|---|---|---|---|
| GFDL[a] (Manabe and Hahn 1981; Mechoso 1981; D.G. Hahn, personal communication) | 9 | 0 | Spectral | 15 waves in both lat. and long. | U.S. Naval Oceanographic Office (1944, 1957, 1958, 1967a,b, 1969) | Jan./July | 15 |
| GISS[b] (Hansen et al. 1983) | 9 | 10 | Grid point | 8° lat. 10° long. | Robinson and Bauer (1981) | Jan./July[g] | 5 |
| GLAS[c] (Shukla et al. 1981) | 9 | 10 | Grid point | 4° lat. 5° long. | SST: Same as GFDL Sea Ice: British Met. Office (1977) | Feb./July | 1 |
| NCAR[d] (Pitcher et al. 1982) | 9 | 0 | Spectral | 15 waves in both lat. and long. | Alexander and Mobley (1976) | Jan./July | Perpetual[h] |
| OSU[e] (Schlesinger and Gates 1981) | 2 | 200 | Grid point | 4° lat. 5° long. | Alexander and Mobley (1976) | Jan./July | 10 |
| UCLA[f] (Mechoso et al. 1979) | 15 | 1 | Grid point | 2.4° lat. 3.0° long. | SST: Wigle and Mendenhall (1974); Antarctic sea ice: Bakayev (1966); Arctic sea ice: Defant (1961) | Jan./July | 1 |

[a]Geophysical Fluid Dynamics Laboratory/NOAA, Princeton University, New Jersey.
[b]NASA Goddard Space Flight Center, Institute for Space Studies, New York.
[c]NASA Goddard Space Flight Center, Laboratory for Atmospheric Sciences Modeling and Simulation Facility, Greenbelt, Maryland.
[d]National Center for Atmospheric Research, Boulder, Colorado.
[e]Oregon State University, Climatic Research Institute, Corvallis.
[f]Department of Atmospheric Sciences, University of California, Los Angeles.
[g]For precipitation the seasonal averages for December-January-February and June-July-August are shown.
[h]Each simulation was for 200 days with fixed (perpetual) insolation, SST, and sea ice.

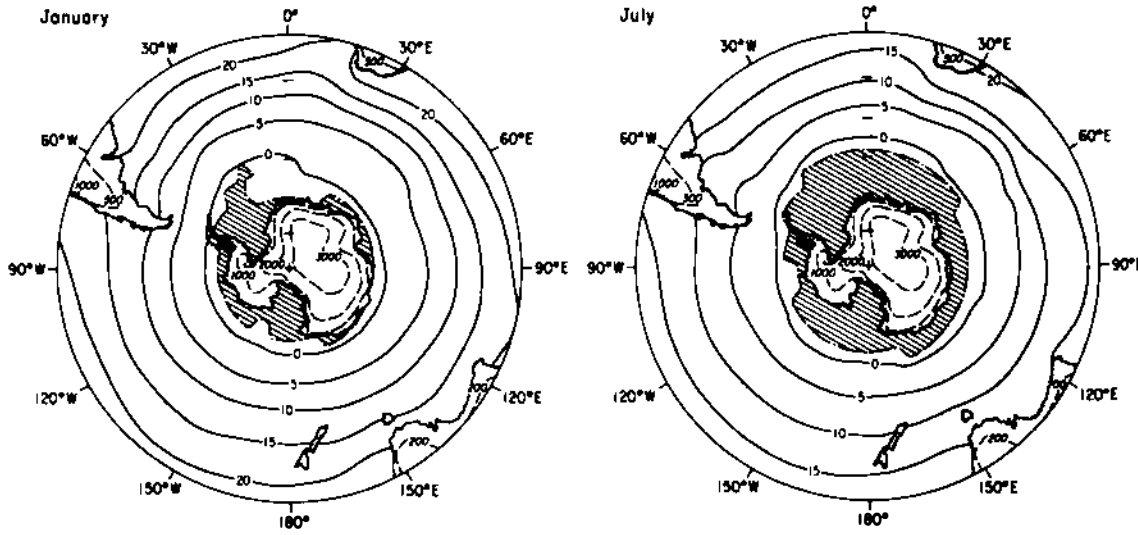


**Figure 1. The observed January and July sea surface temperatures and sea-ice extent (hatched area) based on data of Alexander and Mobley (1976), and the surface elevation (in meters) for the OSU model. (From Ghan et al. 1982.)**

## Surface Air Temperature

The summer and winter surface air temperatures simulated by the AGCMs are shown in Figures 2 and 3, respectively, together with the corresponding observed surface air temperatures. The latter are based on the data of Taljaard et al. (1969), as available from the National Center for Atmospheric Research (NCAR) archive (Jenne 1975) and interpolated onto the 4° x 5° latitude-longitude grid of the OSU model (Ghan et al. 1982).

Summer: The summer surface air temperatures presented in Figure 2 are the observed January temperatures and the January temperatures simulated by the GFDL, GISS, NCAR, and OSU models. For the GLAS model the simulated February temperature is shown. (The surface air temperature for the UCLA model was not available.)

In the subtropics, near 30°S, the observed air temperatures over the oceans, as the SSTs themselves (Figure 1), are warmer than 20°C everywhere except in the eastern regions of the South Pacific, South Atlantic, and Indian oceans. Each of the models simulates this reasonably well.

The observed air temperatures over South America and Australia are warmer than those over the ocean at the same latitude, with temperatures greater than 25°C near 30°S. This land-sea temperature contrast is simulated well by the GFDL and GLAS models and reasonably well by the OSU model. The GFDL, GLAS, and OSU models simulate air temperatures warmer than those observed, and the GISS and NCAR models simulate temperatures colder than those observed, over South America, Africa, and Australia.

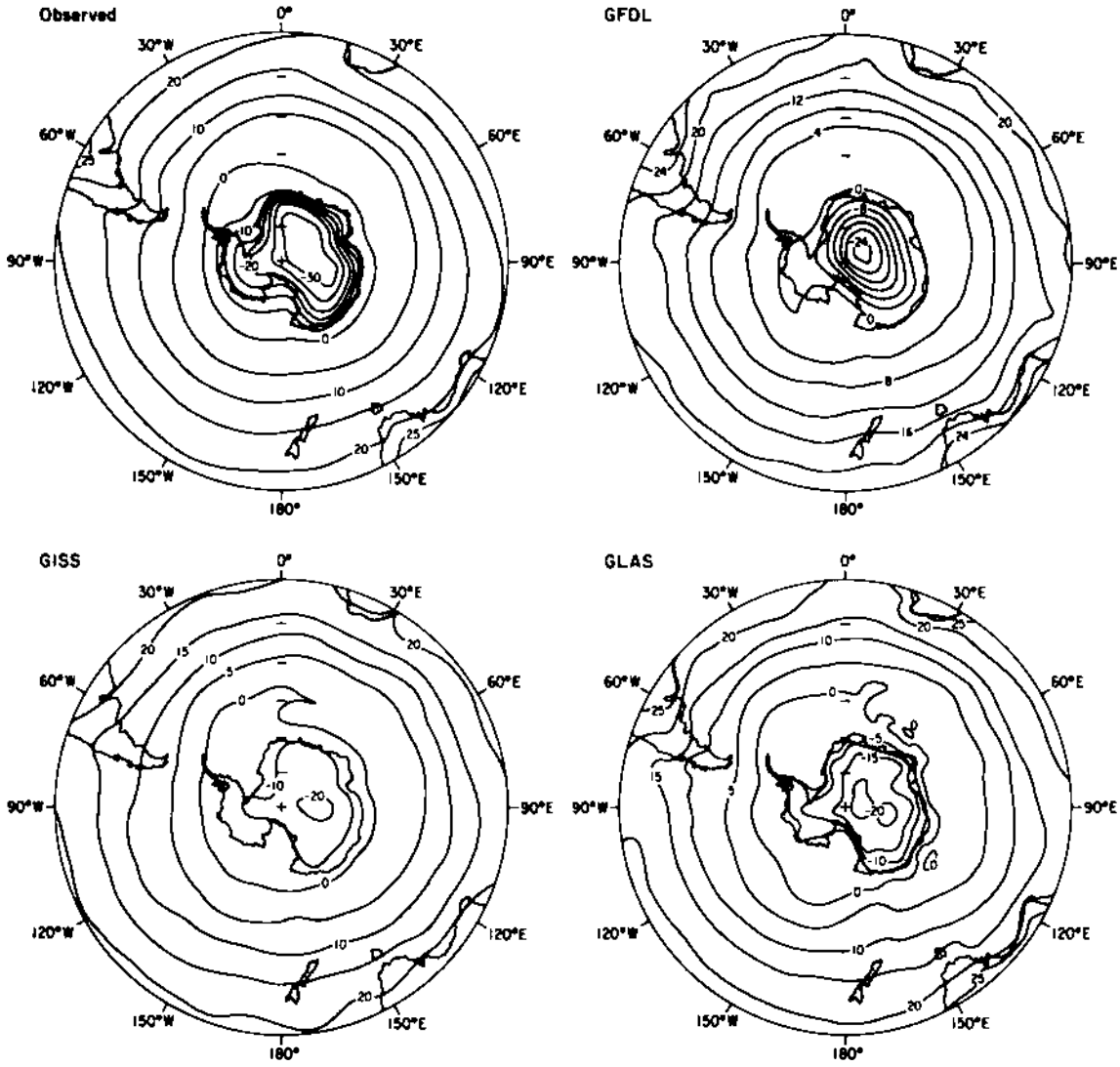


**Figure 2. The observed and simulated Southern Hemisphere surface air temperatures (°C) for summer. The mean January observed temperature and the mean January temperatures simulated by the GFDL, GISS, NCAR, and OSU models are presented. The simulated mean February temperature is shown for the GLAS model. The observed data are based on Taljaard et al. (1969) as available from the NCAR archive (Jenne 1975).**

The observed temperatures decrease with increasing southern latitude, with the air temperatures over the ocean closely following the SSTs (Figure 1). Each of the models simulates this reasonably well. In the region from 30°S latitude to the position of the 0°C isotherm, the maritime air temperatures simulated by the GISS, GLAS, and OSU models are colder than those observed. The temperatures simulated by the GFDL model are colder than those observed in the eastern South Pacific and Indian oceans and warmer than those observed

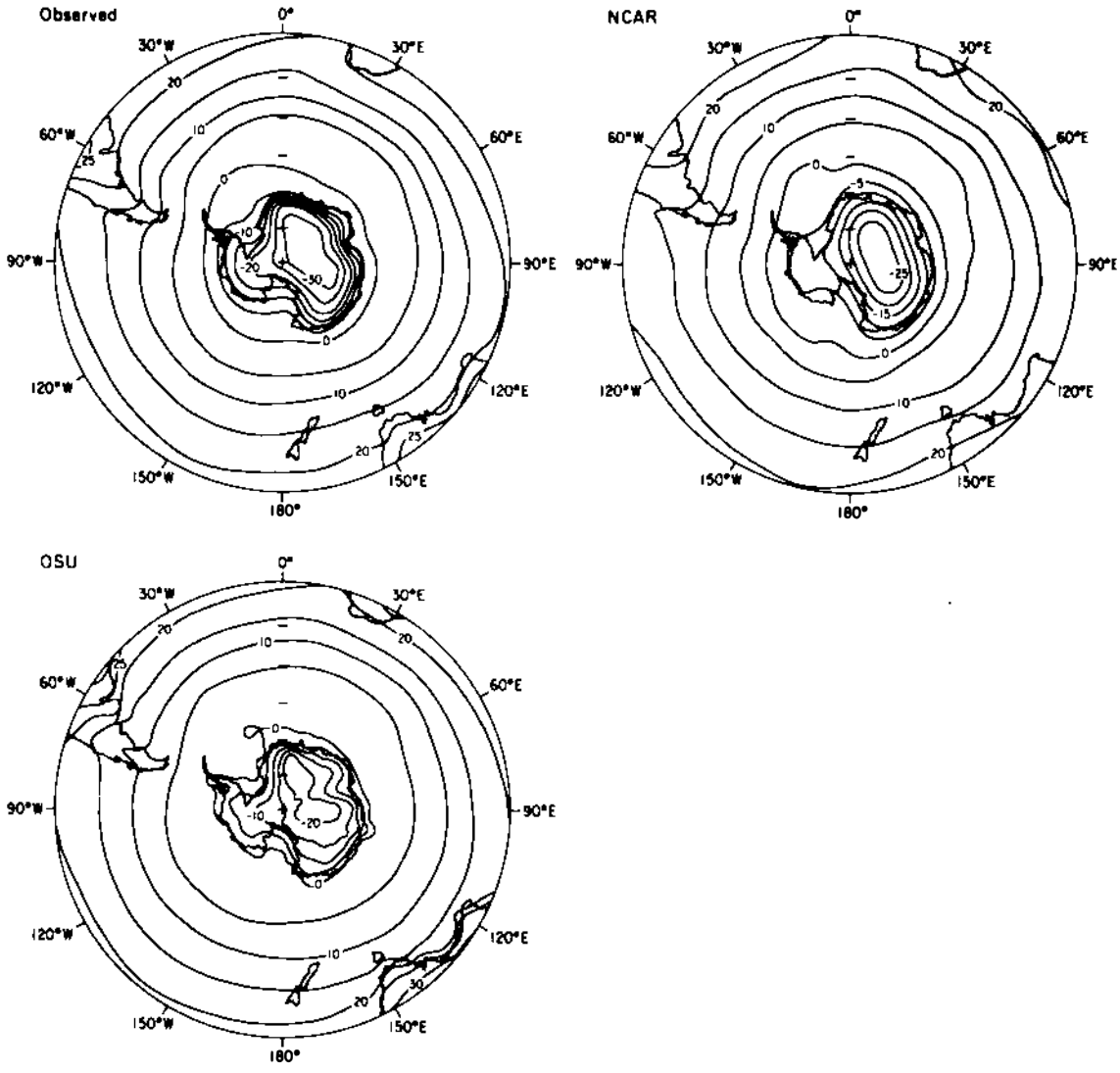


**Figure 2. (continued)**

in the central South Atlantic and western South Pacific oceans. The temperatures simulated by the NCAR model are colder than those observed in the eastern and western South Pacific and central Indian oceans and warmer than those observed in the eastern Indian and South Atlantic Oceans.

The observed 0°C surface air temperature isotherm is located over the ocean generally on or poleward of the 0°C SST isotherm and equatorward of the observed sea-ice margin (Figure 1). The GISS and NCAR models simulate the position of the 0°C air temperature isotherm reasonably well, although the GISS model simulates the 0°C isotherm equatorward of its observed position near 0° longitude, and the NCAR model, near 180°. The GLAS model simulates the 0°C air temperature isotherm equatorward of its observed position. (The 0°C SST isotherm

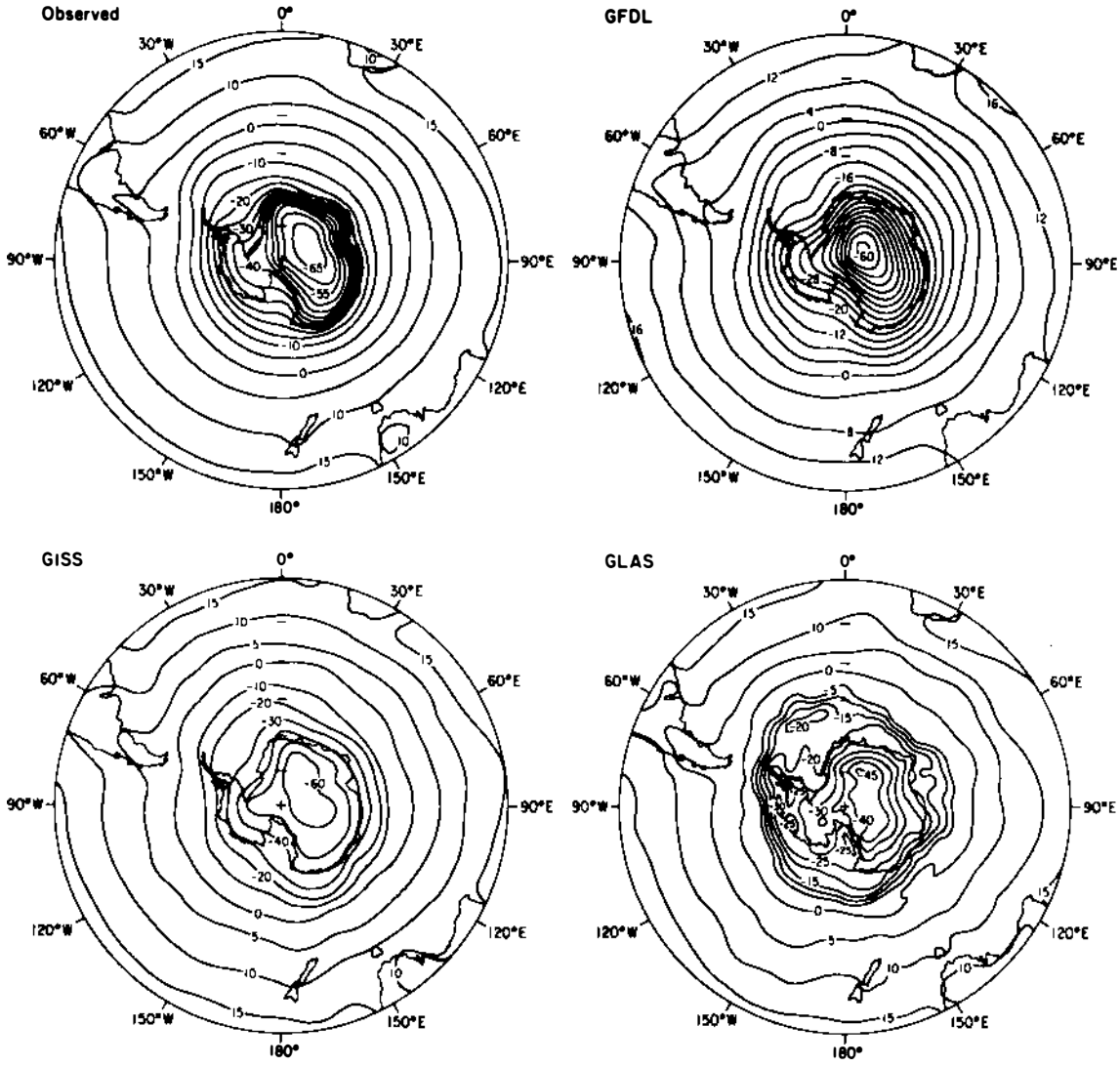


**Figure 3. The observed and simulated Southern Hemisphere surface air temperatures (°C) for winter. The mean July observed temperature and the mean July temperatures simulated by each model are presented. The observed data are based on Taljaard et al. (1969) as available from the NCAR archive (Jenne 1975).**

for February, the month simulated by the GLAS model, is located on or slightly poleward of the observed January SST 0°C isotherm.) The GFDL and OSU models simulate the 0°C isotherm considerably poleward of its observed position, particularly in the Weddell and Ross seas. All of the models simulate the air temperatures over the sea ice adjoining West Antarctica warmer than the observed temperatures. The GFDL, GISS, and OSU models also simulate the air temperatures over the ocean adjoining East Antarctica warmer than the observed temperatures.

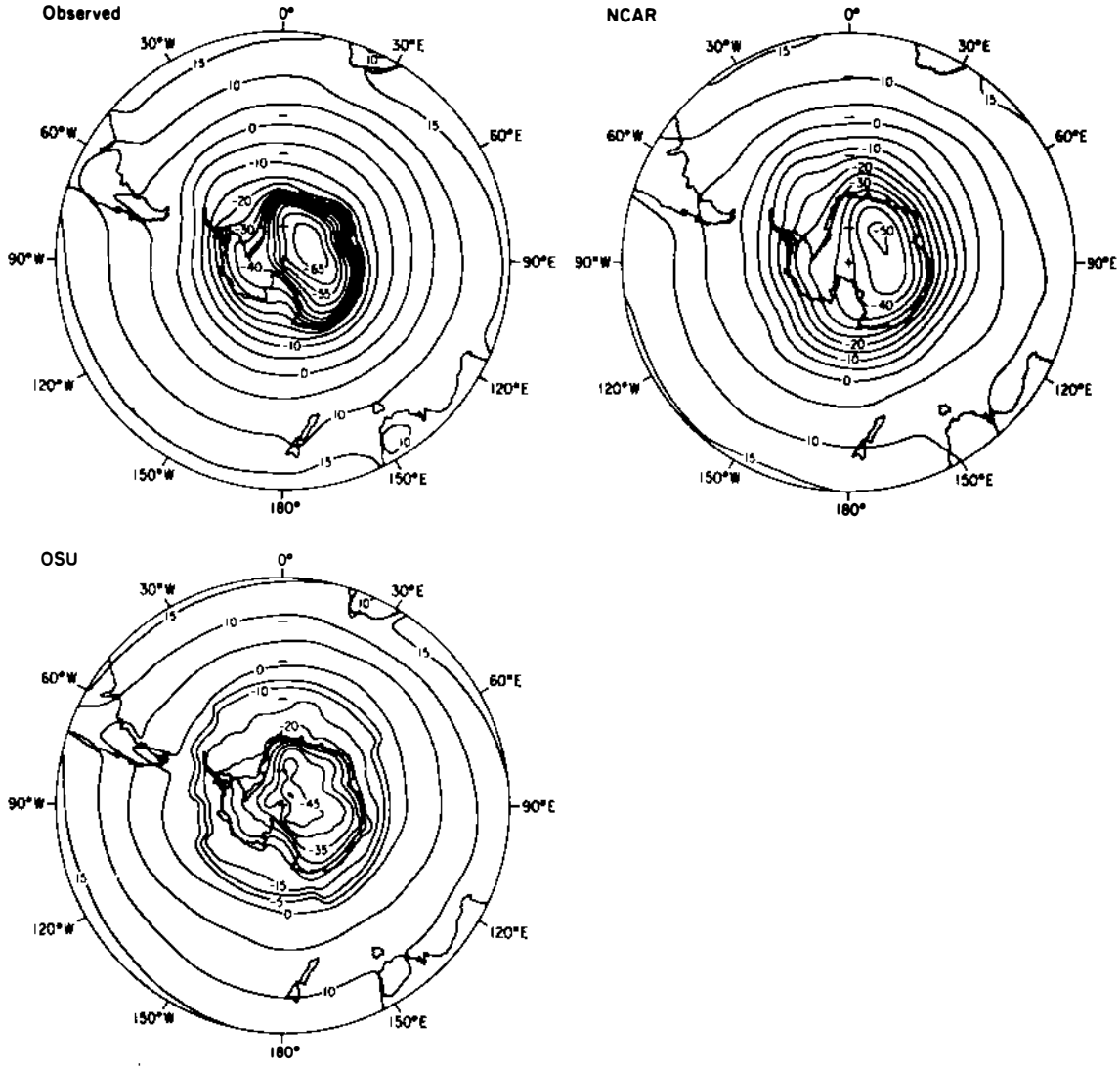


**Figure 3. (continued)**

The observed air temperatures have a minimum value of less than -30°C over the high-elevation interior of East Antarctica, with cold air following the topographic contours (Figure 1) toward the coasts near 0° and 150°E and into West Antarctica. Each of the models simulates the coldest air over East Antarctica; however, the coldest temperatures are simulated 5°C (GFDL, NCAR) and 10°C (GISS, GLAS, OSU) warmer and less extensive than those observed. The warm air ridge near 70°E is simulated by the GISS, GLAS, and OSU (grid point) models but not by the GFDL and NCAR (spectral) models.

The observed air temperatures over West Antarctica decrease from -5°C and -10°C on the coast to -25°C near the South Pole. Each of the models simulates this poleward temperature decrease; however, the temperatures are warmer than those observed by up to 5°C (GISS, GLAS,

NCAR) and 10°C (GFDL, OSU) on the coast and by 10°C at the South Pole (all models).

These results show that the errors in the surface air temperatures simulated by the models for Southern Hemisphere summer are both positive and negative over the southern oceans and low-latitude continents, positive over the Antarctic sea ice, particularly around West Antarctica, and positive over both East and West Antarctica. The magnitude of the errors is generally less than about 3°C over the southern oceans, less than about 5°C over the low-latitude continents, from 5°C to 10°C over sea ice, and 10°C over Antarctica.

Winter: The winter surface air temperatures presented in Figure 3 are the observed July temperatures and the July temperatures simulated by each model. (The surface air temperature for the UCLA model was not available.)

In the subtropics, near 30°S, the observed air temperatures over the oceans are warmer than 15°C everywhere except in the eastern regions of the South Pacific and South Atlantic oceans. This is similar to the observed SST distribution (Figure 1) near 30°S everywhere except off the west coast of Africa, where SSTs warmer than 15°C are found. All of the models simulate the observed colder air temperatures off the west coasts of South America and Africa reasonably well; however, the simulated maritime air temperatures are generally colder than those observed.

The observed air temperatures over South America, Africa, and Australia are colder than those over the ocean at the same latitude, with temperatures less than 15°C near 30°S. This land-sea temperature contrast is simulated reasonably well by all the models. Each of the models simulates temperatures colder than those observed in South America, and the GFDL and OSU models also simulate colder than observed temperatures in Africa. The GISS, GLAS, and NCAR models simulate warmer than observed temperatures in Africa and colder than observed temperatures in Australia.

The observed air temperatures decrease with increasing southern latitude and closely follow the SSTs (Figure 1) over the ocean. This is simulated well by each of the models. However, in the region from 30°S latitude to the position of the 0°C isotherm, the air temperatures simulated by all the models are colder than those observed.

The observed 0°C temperature isotherm is located over the ocean equatorward of the observed 0°C SST isotherm, which itself is located equatorward of the observed sea-ice margin (Figure 1). Each of the models simulates the position of the 0°C air temperature isotherm reasonably well. The GLAS, NCAR, and OSU models simulate the 0°C isotherm somewhat poleward of its observed position between 120°E and 150°E. The GFDL model simulates the 0°C isotherm generally equatorward of its observed position, as does the GLAS model from 30°W to 30°E, and the OSU model over Patagonia and extending southwest from South America. The GLAS and OSU models simulate a large temperature gradient near the sea-ice margin. Such an intensified gradient is not as evident in the GFDL, GISS, and NCAR simulations or in the observations. Each of the models except the GLAS simulates the air temperatures over

the sea ice bordering East Antarctica colder than the observed temperatures. The GISS and GLAS models simulate temperatures colder than those observed over the sea ice around West Antarctica; the GFDL and OSU models simulate temperatures there warmer than those observed.

The observed air temperatures have a minimum value of less than -65°C over the high-elevation interior of East Antarctica, with cold air following the topographic contours (Figure 1) toward the coasts near 0° and 150°E, and into West Antarctica. Each of the models simulates the coldest air over East Antarctica; nowever, the coldest temperatures are simulated from 5°C (GFDL, GISS) to 15°-20°C (NCAR, GLAS, OSU) warmer than the observed temperatures. The warm air ridge near 70°E is simulated by the GISS, GLAS, and OSU (grid point) models but not by the GFDL and NCAR (spectral) models.

The observed air temperatures over West Antarctica decrease from -20°C and -25°C on the coast to -55°C near the South Pole. Each of the models simulates the coastal temperatures and poleward temperature decrease reasonably well. The NCAR and OSU models give results about 15°C warmer than the observed temperatures near the South Pole, and the GLAS model, about 20°C warmer.

The results presented above show that the errors in the surface air temperatures simulated by the models for Southern Hemisphere winter are negative over the southern oceans, both positive and negative over the low-latitude continents and Antarctic sea ice, and positive over both East and West Antarctica. The magnitude of the errors is generally less than about 3°C over the southern oceans and low-latitude continents, from 5°C to 10°C over sea ice, and 15°C over Antarctica.

## Sea-Level Pressure

By definition, the sea-level pressure over the ocean and land at sea level is simply the measured surface barometric pressure for the observations and the analogous quantity for the simulations. Because of the hydrostatic balance between the changes in the vertical of pressure and the weight of atmosphere per unit horizontal area, the sea-level pressure over the ocean and land at sea level equals the weight per unit horizontal area of the entire atmosphere above. However, over land above sea level, the sea-level pressure is a fictitious quantity obtained as the sum of the observed or simulated surface barometric pressure and the weight per unit horizontal area of an imaginary atmosphere between sea level and the altitude of the surface. This "reduction" of the surface pressure to sea level is done to compensate for the differing elevations of land and thereby to facilitate comparison of the pressure data. However, such a reduction requires an assumption about the temperature profile in the imaginary atmosphere between the surface and sea level. Although there are standard procedures for reducing the observed surface pressure to sea level (World Meteorological Organization 1968), somewhat different procedures are used to obtain the simulated sea-level pressures. In view of the high elevation of most of Antarctica (Figure 1), differences between the simulated and observed sea-level pressures there should be interpreted with caution.

Because of the near geostrophic balance between the horizontal variation of pressure and turning (Coriolis) force on air in motion, which results from the earth's rotation, the sea-level pressure distribution can be used to infer the surface wind direction and speed, at least over the ocean and low-elevation land. In the Southern Hemisphere this geostrophic wind flows along the isobars in a clockwise direction around a center of low pressure and in a counterclockwise direction around a high-pressure center. (Because of friction, the actual wind near the surface would flow somewhat across the isobars from high to low pressure.) The speed of the geostrophic wind is inversely proportional to the spacing of the isobars. These relations will be used in the following sections to describe the surface geostrophic wind. For convenience, this will simply be called the surface wind. The summer and winter sea-level pressures simulated by the AGCMs are presented in Figures 4 and 5, respectively, together with the corresponding observed sea-level pressures. The observed fields are based on the data of Taljaard et al. (1969) as tabulated by Schutz and Gates (1971) on the 4° x 5° latitude-longitude grid of the OSU model.

Summer: The summer sea-level pressures presented in Figure 4 are the observed January pressures and the January pressures simulated by the GFDL, GISS, NCAR, OSU, and UCLA models. For the GLAS model, the simulated Feburary sea-level pressure is shown.

1. Observed. At 30°S latitude the sea-level pressure is maximum in the subtropical highs that are located over the eastern South Pacific Ocean, the eastern South Atlantic Ocean, and the central Indian Ocean. The pressures over South America, Africa, and Australia are less than the pressures over the neighboring oceans. As a result of this sea-level pressure distribution, the surface winds have a westerly (from the west) component everywhere to the south of the maximum subtropical pressure or subtropical ridge (STR) and an easterly component to the north. The surface winds have a southerly component along the west coasts of South America, Africa, and Australia and a northerly component along the east coasts of these continents.

The sea-level pressure decreases with increasing southern latitude to about 62°S around East Antarctica and to 70°S around West Antarctica. Between this minimum subpolar pressure or subpolar trough (SPT) and the STR, the surface winds are westerly. The maximum westerly winds occur near 50°S, where the sea-level pressure gradient is largest. Sea-level pressure minima of 988 mb are located around West Antarctica near the Bellingshausen and Ross seas; minima of 984 mb are found around East Antarctica near 20°E and 100°E.

The sea-level pressure increases poleward of the SPT. A sea-level pressure high is situated over East Antarctica with a pattern that generally follows the topographic contours (Figure 1). The reversal in the pressure gradient at the SPT results in a reversal in the direction of the surface geostrophic wind. Winds with an easterly component are found everywhere along the coast of Antarctica.

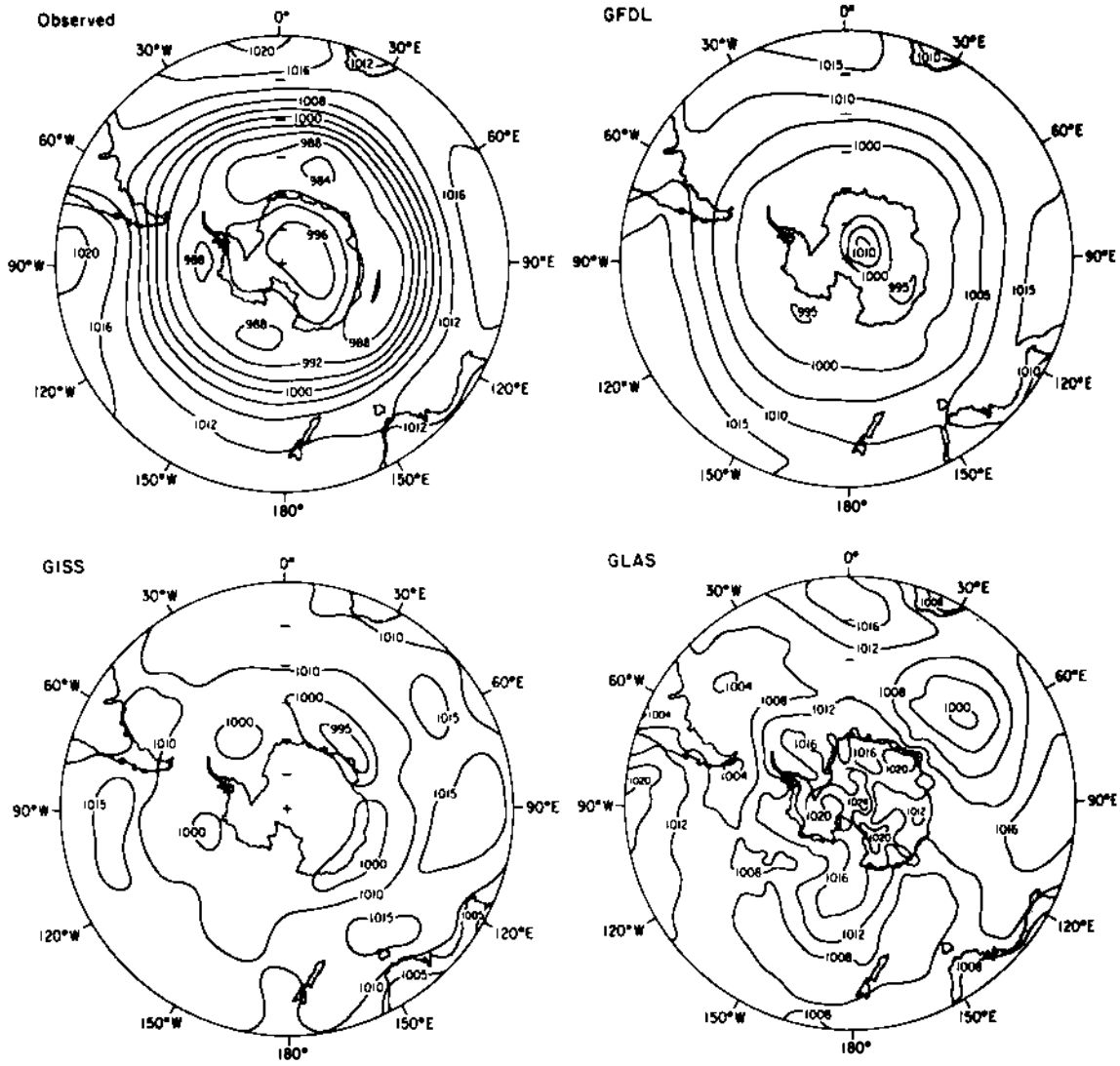


**Figure 4. The observed and simulated Southern Hemisphere sea-level pressures (mb) for summer. The mean January observed sea-level pressure and the mean January sea-level pressures simulated by the GFDL, GISS, NCAR, OSU, and UCLA models are presented. The simulated mean February pressure is shown for the GLAS model. The observed data are based on Taljaard et al. (1969) as tabulated by Schutz and Gates (1971).**

**2. GFDL Model. The maritime positions of the subtropical highs are simulated reasonably well, but the intensities of the highs are underestimated by about 5 mb over the South Pacific and South Atlantic oceans. The minimum pressures observed over South America, Africa, and Australia are also simulated reasonably well, as are the location of the STR where the winds change from easterlies to westerlies; the southerlies along the west coasts of South America, Africa, and**

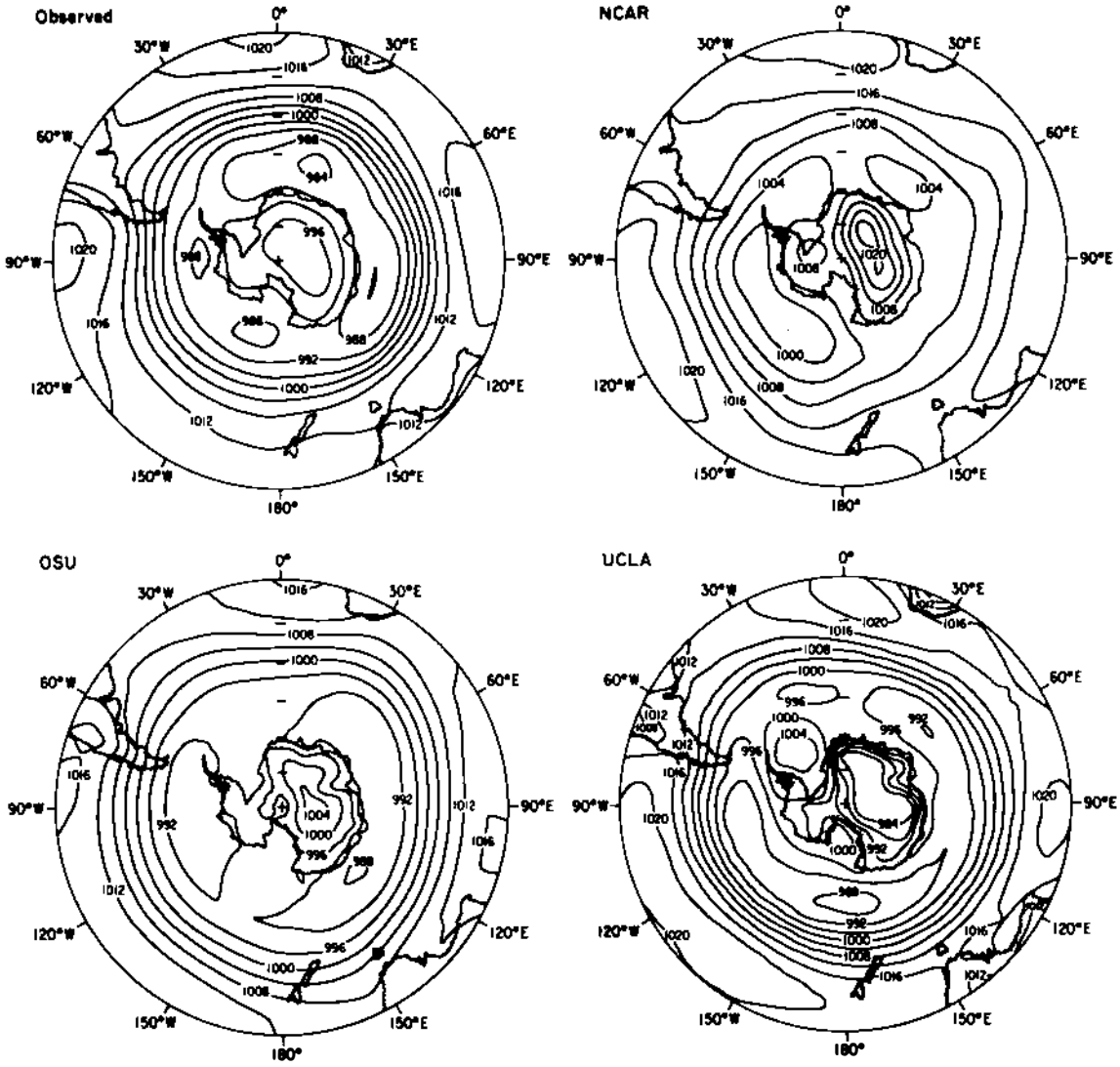


**Figure 4. (continued)**

Australia; and the northerlies along the east coasts of these continents.

The simulated sea-level pressures decrease from the STR to an SPT located at about 70°S around West Antarctica and over East Antarctica, the latter in contrast to the observed maritime position. The simulated SPT pressure is about 10 mb higher than the observed pressure. As a result of the poleward displacement and underestimate of the SPT intensity, the speeds of the simulated midlatitude westerly winds are only about one-third to one-half the observed values.

The simulated pressure increases from the SPT to a maximum value over East Antarctica, as observed. However, the pressure maximum is less extensive and 10 mb higher than the observed pressure. Easterly winds are located over West Antarctica and in the interior of East

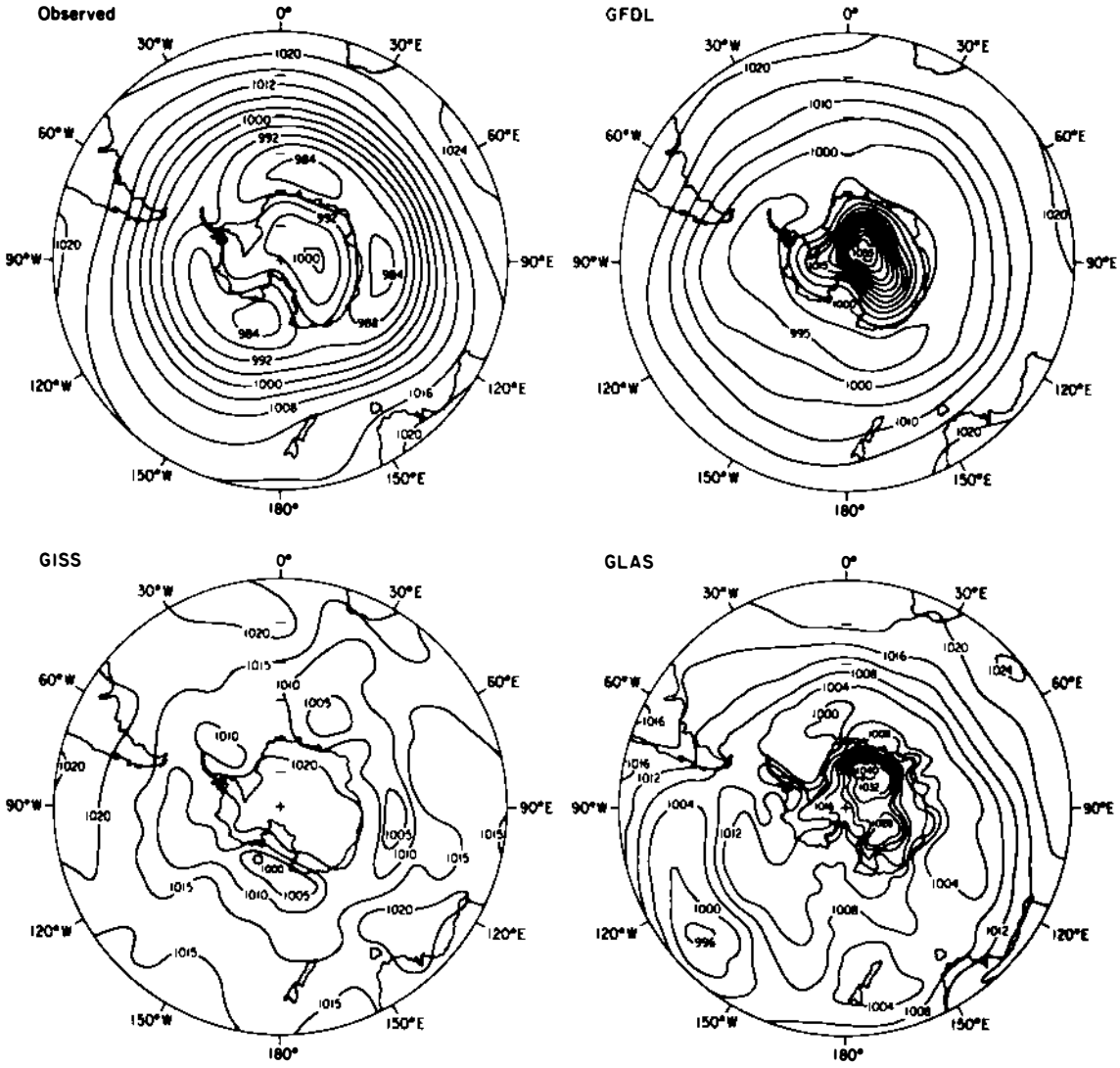


**Figure 5. The observed and simulated Southern Hemisphere sea-level pressures (mb) for winter. The mean July observed sea-level pressure and the mean July sea-level pressures simulated by each model are presented. The observed data are based on Taljaard et al. (1969) as tablulated by Schutz and Gates (1972).**

**Antarctica as observed. Yet, unlike the observations, westerly winds are found along the coast of East Antarctica as a result of the poleward displacement of the SPT there.**

**3. GISS Model. The simulated subtropical highs are located about 10 degrees poleward of the observed positions and are from 5 to 10 mb weaker than the observed highs. As a result, the simulated tropical easterly winds extend poleward about 10 degrees of latitude more than the observed easterlies. The simulated pressures over South America, Africa, and Australia are lower than those over the neighboring oceans**

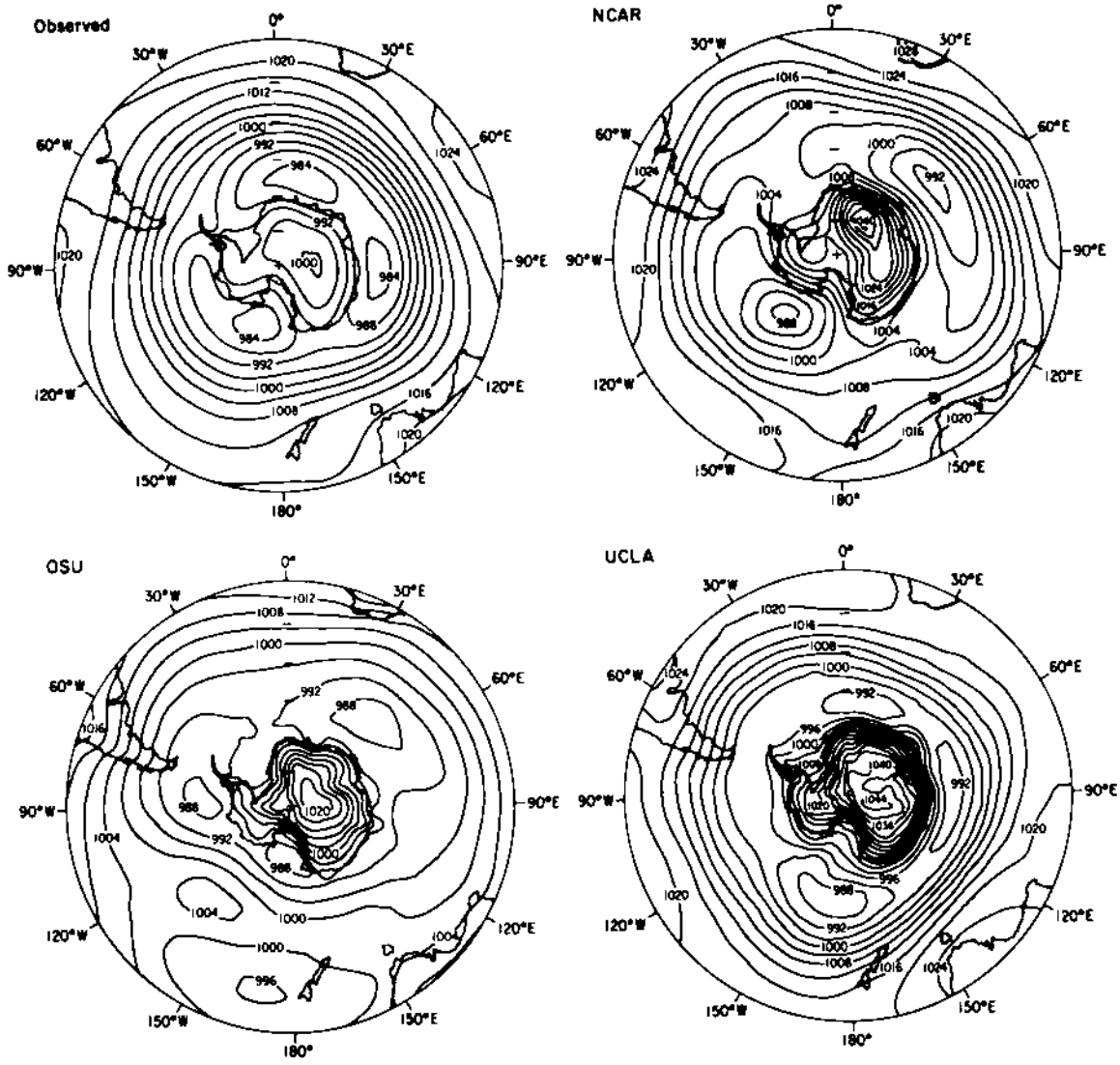


**Figure 5. (continued)**

as observed; however, the simulated pressures there are about 5 mb lower than the observed pressures. The observed southerly and northerly winds along the west and east coasts of the continents, respectively, are simulated reasonably well.

The simulated pressure decreases from the STR to an SPT located near 65°S around Antarctica. The simulated SPT pressure is about 10 mb higher than the observed pressure. The westerlies simulated between the STR and the SPT are weaker than the observed westerlies, particularly around West Antarctica, where they have only one-third to one-half the observed speeds.

Poleward of the SPT the simulated sea-level pressure increases by less than 10 mb (as evidenced by the absence of a 1010-mb isobar). The pressure over Antarctica is somewhat greater than the observed

pressure, but in contrast to the observations, there is no pressure maximum over East Antarctica. The simulated winds around the coasts of West and East Antarctica are easterly as observed.

4. GLAS Model. The positions of the subtropical highs are simulated reasonably well, as are the lower pressures over South America, Africa, and Australia. The intensity of the simulated highs is about 4 mb weaker than that observed over the South Pacific and South Atlantic oceans, and the continental lows are from 4 to 8 mb deeper than those observed. The simulated winds are southerly and northerly along the west and east coasts of the continents, respectively, as are the observed winds.

The simulated pressures decrease from the STR to an "SPT," which is located equatorward of the observed position by as much as 25 degrees of latitude. Also, the pressure of the SPT is as much as 20 mb higher than has been observed. As a result of the equatorward displacement and weakened SPT, the latitudinal extent and strength of the simulated westerlies are much less than those observed.

Poleward of the SPT the pressure increases toward Antarctica. Highs are simulated over both East and West Antarctica, and the simulated pressures are about 20 mb higher than the observed pressures. Easterly winds are found along the coasts of Antarctica as observed.

5. NCAR Model. The positions of the subtropical highs are simulated reasonably well, but their intensity is overestimated by about 4 mb. The lower pressures over South America, Africa, and Australia are simulated with values from 4 to 8 mb higher than the observed pressures. The simulated winds are southerly and northerly along the west and east coasts of these continents, respectively, in agreement with the observed winds.

The simulated sea-level pressures decrease from the STR to an SPT, which is located between 60°S and 65°S, that is, slightly equatorward of the observed SPT position. However, the simulated SPT pressures are from 10 to 20 mb higher than the simulated pressures. As a result, the simulated surface westerlies located between the STR and the SPT are weaker than the observed westerlies, particularly in the eastern hemisphere near 50°S, where the simulated wind speeds are only about 25 percent of the observed speeds.

The simulated pressures increase poleward of the SPT to a maximum value over East Antarctica as observed. However, the maximum pressure is 20 mb higher than the observed pressure. Easterly winds are simulated around the coasts of Antarctica as observed.

6. OSU Model. The simulated subtropical highs are weaker than the observed highs by about 4 mb, and the high over the eastern South Pacific Ocean extends into South America in contrast to the observations. A minimum pressure is simulated over Australia as observed, with southerly and northerly winds off the west and east coasts, respectively. However, minimum pressures are simulated east of South America and Africa, rather than over these continents as observed, with the result that southerly winds are located along their east coasts in contrast to the observed northerly winds.

The simulated pressures decrease with increasing southern latitude to the SPT located between about 60°S and 70°S, with SPT pressures about 4 mb higher than those observed. The simulated westerly winds are also somewhat weaker than the observed winds.

The simulated sea-level pressure increases as observed from the SPT to a maximum value over East Antarctica, with a pressure that is about 4 mb higher than the observed pressure. Easterly winds are located around Antarctica as observed.

6. UCLA Model. The maritime positions of the subtropical highs are simulated reasonably well; however, the intensity of the simulated subtropical highs is larger than observed by from 4 to 8 mb. Low pressures are simulated over South America, Africa, and Australia as observed, with values that are about 4 mb lower than those observed. Southerly winds are simulated along the west coasts, and northerly winds along the east coasts of South America, Africa, and Australia as observed.

The simulated sea-level pressure decreases from the STR to an SPT that is located between 55°S and 62°S, that is, about 5 degrees of latitude equatorward of the observed SPT position. The simulated SPT pressure is from 4 to 8 mb higher than the observed pressure. Westerly surface winds are simulated between the STR and SPT, with maximum speeds near 50°S latitude as observed. The simulated wind speeds are somewhat larger than those observed over the South Pacific Ocean as a result of the higher than observed pressure simulated there.

In contrast to the observations, the simulated pressure increases poleward of the APT only as far as the coasts of East and West Antarctica, and to the sea-ice margin in the Weddell and Ross seas (Figure 1), where subpolar highs are simulated. An extensive low-pressure center is simulated over East Antarctica in contrast to the observed high pressure there. As a result of the simulated pressure distribution in and around Antarctica, the coastal winds are westerly rather than easterly as observed.

To summarize, the results show that each model's simulation of the summer sea-level pressures poleward of 30°S latitude exhibits errors in comparison with the observed sea-level pressures. All the models simulate the pressures of the subtropical highs within about 5 mb of their observed pressures, and most of the models simulate the observed positions of the subtropical highs reasonably well. The models are generally less successful in simulating the position and intensity of the SPT and, therefore, underestimate the speed of the midlatitude surface westerly winds. The SPT errors are also shown in Figure 6, which presents the zonal mean sea-level pressures simulated by the predecessors of the six models considered here, the pressures simulated by four models not considered here (BMO, MGO, AES, and ANMRC), and the observed zonal mean sea-level pressures. Figure 6 also shows another error that is common to most of the models' simulations discussed here, namely, the overestimate of the sea-level pressure in the interior of Antarctica.

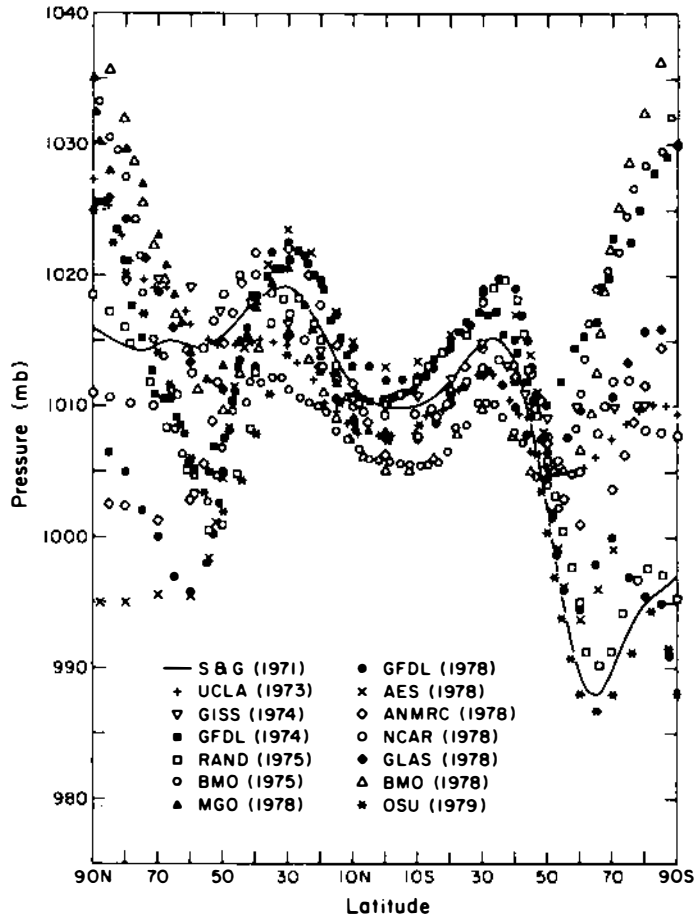


**Figure 6. The mean January sea-level pressure as simulated by various atmospheric general circulation models and as observed. Here (and in Figure 9), NCAR (1971) is from Kasahara and Washington (1971), UCLA (1973) is from unpublished results, GISS (1974) is from Somerville et al. (1974), BMO (1975) is from Gilchrist (1975), RAND (1975) is from Gates and Schlesinger (1977), GFDL (1978) is from Manabe et al. (1979), NCAR (1978) is from Washington et al. (1979), GLAS (1978) is from Halem et al. (1979), BMO (1978) is from Gilchrist (1979), ANMRC (1978) is from McAvaney et al. (1979), MGO (1978) is from Meleshko et al. (1979), AES (1978) is from Boer and McFarlane (1979), and OSU (1979) is from Schlesinger and Gates (1979). The observed data (S & G) are from Schutz and Gates (1971). (From Gates and Bach 1981.)**

**Winter: The winter sea-level pressures presented in Figure 5 are the observed July pressures and the July pressures simulated by each model.**

**1. Observed. At 30°S latitude the sea-level pressure is maximum in the subtropical highs, which are located over the eastern South Pacific Ocean, the region extending from the South Atlantic Ocean to the Indian Ocean, and over Australia. The pressure over South America**

is less than the pressure over the neighboring oceans. As a result of this sea-level pressure distribution, the surface winds have a westerly component everywhere at 30°S, a southerly component along the west coast of South America and the east coast of Australia, and a northerly component along the east coasts of South America and Africa.

The sea-level pressure decreases with increasing southern latitude to about 62°S around East Antarctica and to 70°S around West Antarctica. Between this SPT and the STR located slightly equatorward of 30°S, the surface winds are westerly. The maximum westerly winds occur near 50°S, where the sea-level pressure gradient is largest. Sea-level pressure minima of 984 mb are located near the Ross Sea and around East Antarctica near 20°E and 90°E.

The sea-level pressure increases poleward of the SPT. A relative sea-level pressure maximum is situated over East Antarctica with a pattern that generally follows the topographic contours (Figure 1). The reversal in the pressure gradient at the SPT results in a reversal in the direction of the surface geostrophic wind. Winds with an easterly component are found along the coast of Antarctica.

2. GFDL Model. The observed position of the STR equatorward of 30°S is correctly simulated by the model as are the positions of the subtropical highs over Australia, the Indian Ocean, and the South Atlantic Ocean. However, the pressure simulated over South America is higher than the observed pressure, and the pressures simulated over Africa and the South Pacific Ocean are lower than those observed. The surface winds have a westerly component at 30°S and poleward as observed. Along the west coasts of South America and Africa the simulated winds have a northerly and southerly component, respectively, unlike the observed winds.

The simulated sea-level pressure decreases with increasing southern latitude to about 60°S around East Antarctica and to 70°S around West Antarctica as observed. However, the simulated SPT is about 10 mb higher than the observed pressure. The maximum westerly winds are located near 50°S as observed, but have about half the observed speeds.

The simulated pressure increases from the SPT to a maximum value over East Antarctica as observed; however, the simulated maximum pressure is 50 mb higher than the observed pressure. Winds with an easterly component are simulated along the coast of Antarctica as observed.

3. GISS Model. In contrast to the observations, the simulated STR is located poleward of 30°S over most of the hemisphere, with a maximum poleward position of 50°S over the South Pacific Ocean. Consequently, easterly winds are simulated poleward of 30°S, unlike the observed winds. Subtropical highs are simulated over the eastern South Pacific Ocean, the central South Atlantic Ocean, and south of Australia. High pressure is simulated over South America where low pressure is observed, and low pressure is simulated over Africa where high pressure is observed.

The simulated sea-level pressures decrease from the STR to an SPT located about 5° equatorward of its observed position around East Antarctica and the Bellingshausen Sea. The simulated SPT pressures are about 20 mb higher than the observed pressure; however, the

longitudinal positions of the simulated low-pressure centers are in good agreement with the observations. The maximum westerly winds are located near 55°S and are weaker than the observed winds by about a factor of 2.

Poleward of the SPT the simulated sea-level pressure increases to 1020 mb virtually everywhere over Antarctica and is, therefore, about 20-30 mb higher than the observed pressure. The simulated surface winds around the coast of Antarctica have an easterly component as observed.

4. GLAS Model. The position of the simulated STR is located poleward of 30°S except over South America, Australia, and near 50°E, in reasonable agreement with the observations. The simulated subtropical highs over the eastern South Atlantic and Indian oceans are located near the observed positions and have the observed intensities; the high-pressure centers over the eastern South Pacific Ocean and Australia are weaker than their observed counterparts.

The simulated pressures decrease with increasing southern latitude to an SPT that is located near the observed SPT around East Antarctica but is located more than 30° equatorward of the observed SPT from 90°W to the Dateline. In this quadrant the simulated westerly winds extend poleward only to 40°S, in marked contrast to the observed winds. Elsewhere the simulated westerly winds are weaker than the observed winds by at least a factor of 2. The SPT pressure is about 15 mb higher than the observed pressure.

Poleward of the SPT the pressure increases toward Antarctica. The maximum sea-level pressure is simulated over East Antarctica as observed, but the maximum pressure is 40 mb greater than the observed. Easterly winds are simulated around the Antarctic coast as observed. Easterly winds are also simulated as far equatorward as 40°S over the South Pacific Ocean, in marked contrast with the observations.

5. NCAR Model. The position of the simulated STR is located equatorward of 30°S everywhere except near 165°W, in good agreement with the observations. A subtropical high is located over Australia as observed, but a high is also found over South America, which is not observed. The simulated surface winds near 30°S are westerly in accord with the observations, as is the southerly flow along the east coast of Australia. However, flow with a northerly component is simulated along the west coast of South America, in contrast to the southerly wind observed there.

The simulated sea-level pressure decreases with increasing southern latitude to an SPT that is located about 5° equatorward of its observed position around most of Antarctica. The simulated SPT pressure is about 10 mb hgiher than the observed pressure. The maximum westerly winds are located about 5° equatorward of their observed position. The speed of the westerlies is simulated reasonably well on the equatorward flanks of the low-pressure centers near 60°E and 140°W. Elsewhere the westerly wind speeds are underestimated by the model.

The simulated pressures increase poleward of the SPT to a maximum value over East Antarctica as observed. However, the maximum pressure is about 40 mb higher than that observed. Easterly winds are simulated around the Antarctic coasts as observed.

6. OSU Model. The position of the simulated STR is located equatorward of 30°S everywhere as observed. A subtropical high is located over Australia as observed, but with an intensity that is underestimated by about 12 mb. A subtropical high is also simulated over South America instead of over the eastern South Pacific Ocean as observed, and the sea-level pressure there and over the Indian Ocean is underestimated by 10-20 mb. The surface winds have a westerly component everywhere at 30°S as observed. Flow with a southerly component is simulated along the east coast of Australia in agreement with the observed wind, while the simulated northerly component along the west coast of South America is opposite to the observed southerly component there.

The sea-level pressure decreases with increasing southern latitude everywhere except over the South Pacific Ocean. A weak low-pressure center is simulated east of New Zealand and, farther east and poleward, a weak high-pressure center. This simulated doublet-like feature is not found in the observations, and the weak easterly wind simulated between the high and the low is in contrast to the observed westerly wind.

The simulated SPT is located about 5° equatorward of its observed position around East Antarctica between 30°E and 60°E, 10° too far toward the equator near 60°W, and somewhat poleward of the observed position over the Ross Sea. The simulated SPT pressure is about 4 mb higher than the observed pressure. The maximum westerly winds are located about 10° equatorward of the observed position from 90°W eastward to 120°E, and about 10° poleward of the observed position near 150°W. The speed of the maximum surface westerly winds is underestimated by a factor of 2 over much of the hemisphere.

The pressure increases poleward of the SPT to a maximum value over East Antarctica as observed, but with a pressure that is 20 mb higher than the observed pressure. Along the Antarctic coast the wind has an easterly component as observed.

7. UCLA Model. Subtropical highs are simulated over Australia, the eastern South Pacific Ocean, and the South Atlantic Ocean as observed, with an intensity about 4 mb higher than that observed. The subtropical high observed over the Indian Ocean at 30°S is not shown in the simulation, and the simulated high pressure over South America is not found in the observations. Winds with a westerly component are simulated almost everywhere near 30°S in agreement with the observations.

The simulated sea-level pressure decreases with increasing southern latitude to the SPT, which is located about 5° equatorward of its observed position near 30°E, and 10° too far equatorward near 60°W and 180°. The simulated SPT pressure is about 4 mb higher than the observed pressure, and the longitudinal positions of the simulated low-pressure centers are in good agreement with the observations. The maximum westerly winds are located close to the observed latitudes everywhere except near 180° where they are displaced toward the equator by about 10°. The speed of the westerlies is simulated reasonably well.

The sea-level pressure increases poleward of the SPT to a maximum pressure over East Antarctica as observed, but with a pressure that is

40 mb higher than observed. Along the Antarctic coast the surface geostrophic winds have an easterly component in agreement with observations.

These results indicate that the subtropical sea-level pressures simulated by most of the models are in reasonable agreement with the observations. However, no model reproduces the observed high pressure over Australia and low pressure over South America. The models generally simulate the SPT equatorward of its observed position with an intensity that is weaker than that observed. As a result, the surface westerly winds simulated by most of the models are considerably weaker than the observed winds. Finally, the models overestimate the high pressure over East Antarctica by from 20 to 50 mb.

## Precipitation Rate

The summer and winter precipitation rates simulated by the AGCMs are shown in Figures 7 and 8, respectively, together with the corresponding observed precipitation rates. The latter are based on the data of Jaeger (1976) as represented on the 4° x 5° latitude-longitude grid of the OSU model. The contour levels shown in Figures 7 and 8 for the simulated precipitation rates are not all the same as those shown for the observed precipitation rates. This tends to exaggerate the differences between the simulated and observed fields. Although this was also true for the surface air temperatures and sea-level pressures previously shown for two of the models, the perception errors are much larger for the precipitation rate. Accordingly, each model's simulated precipitation rate has been compared with a separate figure of the observed rate having the same contour levels as shown for the simulated rate, as well as with the observed precipitation rates shown in Figures 7 and 8.

Summer: The summer precipitation rates presented in Figure 7 are the observed January rates and the January rates simulated by the GFDL, NCAR, OSU, and UCLA models. For the GLAS model the simulated February precipitation rate is shown; the December-January-February mean rate is presented for the GISS model.

1. Observed. At 30°S the precipitation rate is less than 0.5 mm $day^{-1}$ off the west coasts of South America, Africa, and Australia in the regions of the subtropical highs (Figure 4). Precipitation maxima are located over the east coasts of South America, Africa, and Australia, and a precipitation minimum in central Australia.

The precipitation rate exceeds 2 mm $day^{-1}$ virtually everywhere between 40°S and 60°S except off the east coast of South America and near 55°S, 30°E, where the Jaeger data show a precipitation minimum. In this latitude belt, precipitation rates in excess of 5 mm $day^{-1}$ are located northwest of New Zealand, off the west coast of South America, and near 60°S from 70°E to 155°W on the equatorward flank of the SPT (Figure 4). Less extensive precipitation maxima are also

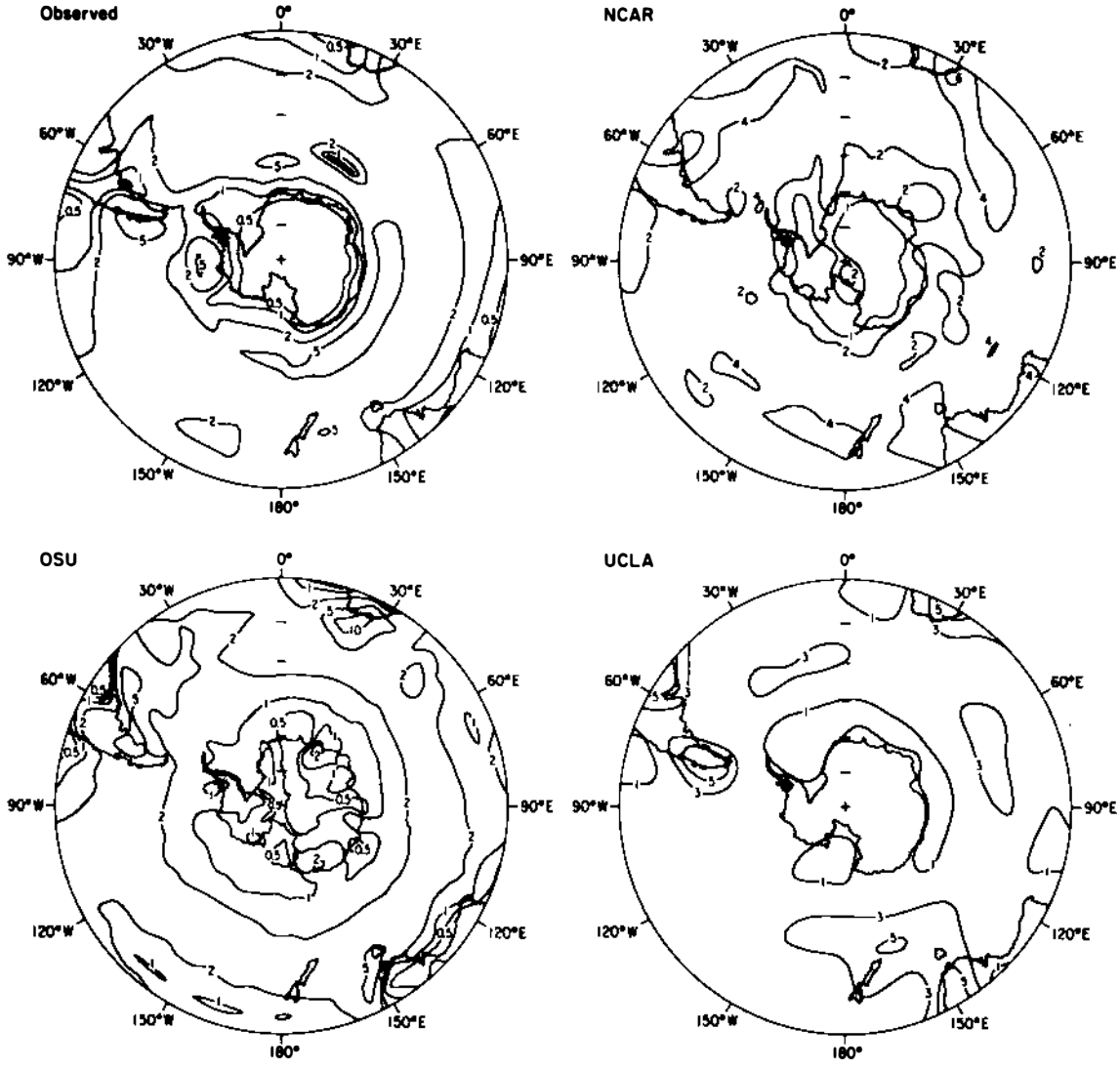


**Figure 7. The observed and simulated Southern Hemisphere precipitation rates (mm day$^{-1}$) for summer. The mean January observed precipitation rate and the mean January precipitation rates simulated by the GFDL, NCAR, OSU, and UCLA models are presented. The mean December-January-February rate is shown for the GISS model, and the mean February rate for the GLAS model. The observations are based on the data of Jaeger (1976).**

located near the SPT at somewhat higher southern latitudes over the Bellingshausen Sea and at the Greenwich Meridian.

The precipitation rate decreases from about 65°S toward Antarctica. Rates less than 1 mm day$^{-1}$ are observed over most of the Antarctic coast and over the sea ice in the Weddell Sea (Figure 1). The precipitation rate over the interior of East Antarctica and much of West Antarctica is less than 0.5 mm day$^{-1}$. Rates of this size are also found over the sea ice in the Weddell and Ross seas (Figure 1).

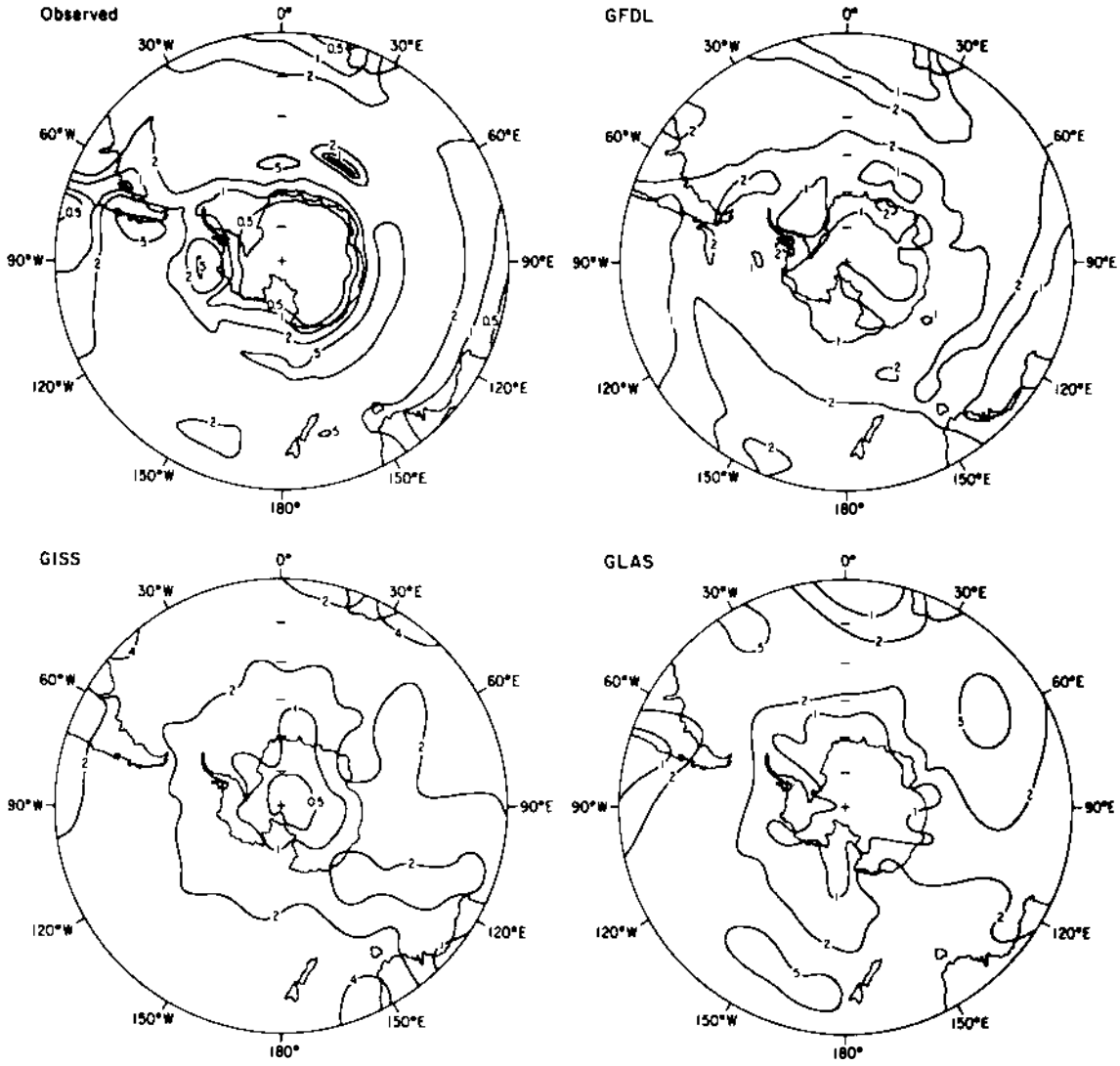


**Figure 7. (continued)**

**2. GFDL Model. Precipitation rate minima are simulated at 30°S off the west coasts of South America, Africa, and Australia in correspondence with the position of the model's subtropical highs (Figure 4) and the observed precipitation rate. The simulated rates over the oceans are in reasonable agreement with the observed rates everywhere except over the eastern South Pacific Ocean, where they are somewhat less than the observed rates. The simulated precipitation is maximum over the east coast of South America and increases from west to east across Africa and Australia in accord with the observations. The precipitation minimum observed over central Australia is not reproduced by the model. In the latitude band from 40°S to 60°S the simulated precipitation rates do not exceed 2 mm day$^{-1}$ everywhere as observed but only in a precipitation maximum centered near 50°S around much of**

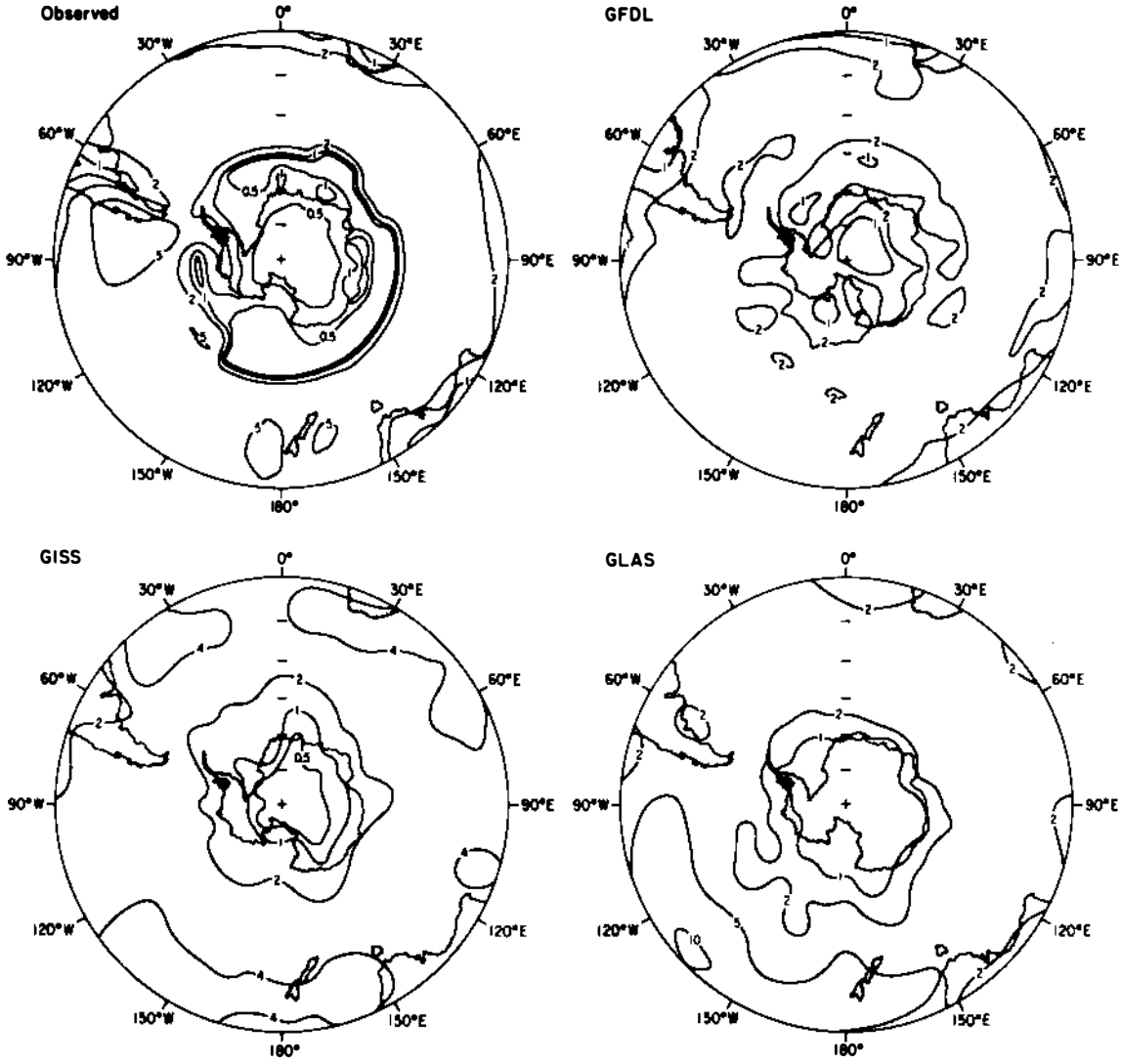


**Figure 8. The observed and simulated Southern Hemisphere precipitation rates (mm day$^{-1}$) for winter. The mean July observed precipitation rate and the mean July rates simulated by the GFDL, GLAS, NCAR, OSU, and UCLA models are presented. The mean June-July-August rate is shown for the GISS model. The observations are based on the data of Jaeger (1976).**

the hemisphere. The precipitation maximum off the west coast of South America is simulated by the model, but it is less than half the observed intensity. The observed precipitation maxima located near 60°S are not simulated by the model, and the simulated precipitation rates there are about half the observed values. However, the model does simulate a precipitation minimum at 30°E, albeit somewhat equatorward of the observed position.

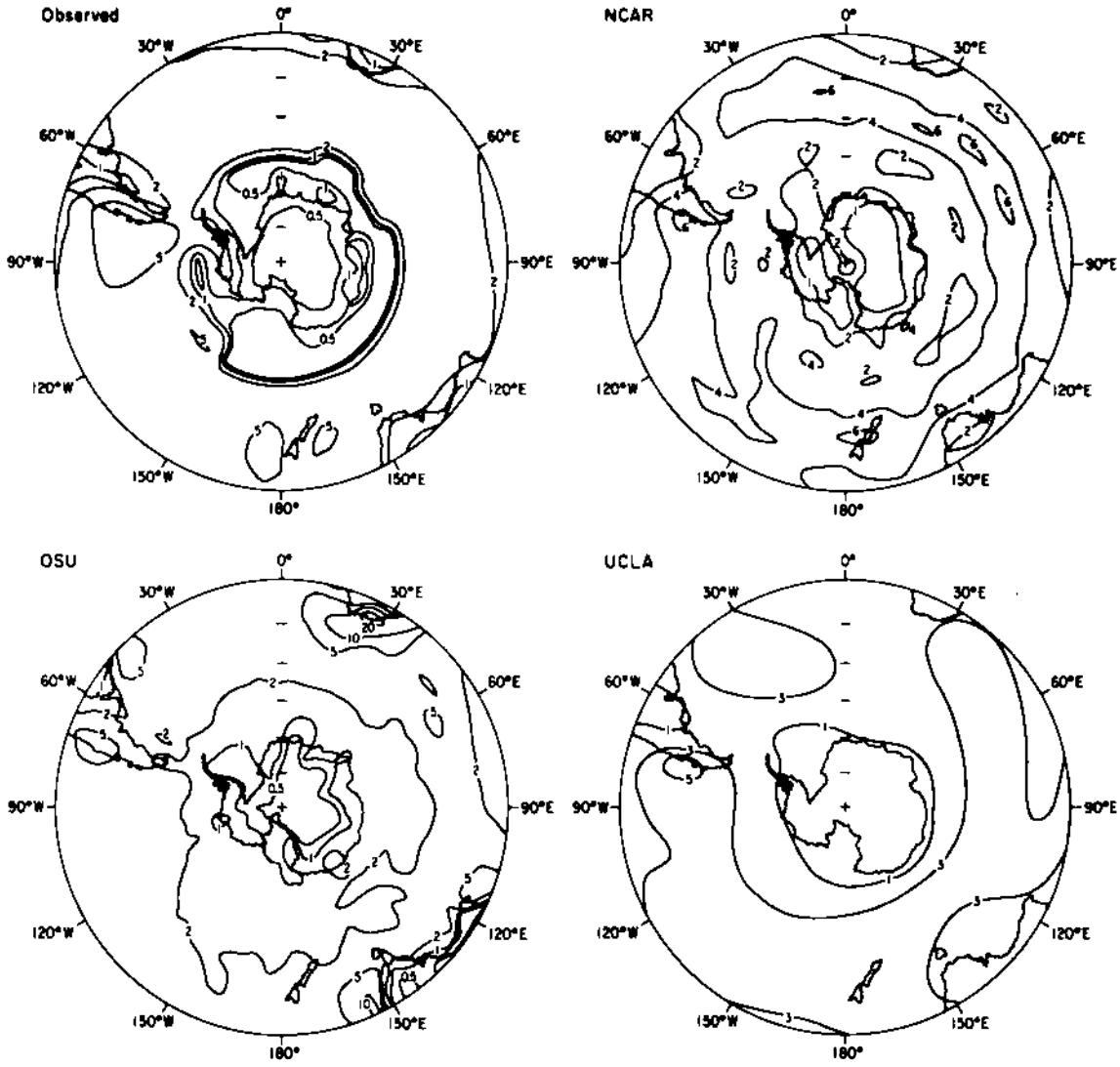


**Figure 8. (continued)**

The simulated precipitation rates generally decrease with increasing southern latitude toward Antarctica. Rates less than 1 mm $day^{-1}$ are simulated over much of Antarctica and over the sea ice in the Weddell and Ross seas (Figure 1) as observed. However, the precipitation rates simulated over the coast of East Antarctica are larger than the observed rates by as much as a factor of 2. It appears that the precipitation rate simulated over the Antarctic interior is larger than the observed rate; however, the absence of the 0.5 mm $day^{-1}$ contour prevents a precise comparison.

3. GISS Model. Precipitation rate minima are simulated at 30°S over the eastern regions of the South Pacific, South Atlantic, and Indian oceans as observed, even though the simulated subtropical highs are not located in these regions as observed (Figure 4); however, the

simulated rates are twice the observed rates. Precipitation rate maxima are simulated over or near the east coasts of South America, Africa, and Australia as observed, but the simulated rates are about twice the observed rates. The model simulates a precipitation minimum over Australia as observed, albeit with an intensity somewhat larger than that observed.

The model is reasonably successful in simulating the observed precipitation rates larger than 2 mm $day^{-1}$ in the 40°S to 60°S latitude band. However, the observed precipitation maxima off the west coast of South America and around much of Antarctica near 60°S are not simulated by the model.

The simulated precipitation rates decrease toward and into Antarctica as observed, and the precipitation rates simulated over the sea ice in the Weddell and Ross seas are in reasonable agreement with the observations. However, over much of Antarctica the simulated precipitation rates are twice the observed values.

4. GLAS Model. At 30°S the model simulates precipitation rates less than 1 mm $day^{-1}$ off the west coasts of South America and Africa as observed. A precipitation minimum is also simulated off the west coast of Australia as observed, but with a value about twice the observed one. The simulated precipitation increases from west to east across South America, Africa, and Australia as observed, but the minimum observed over Australia is not shown by the model. A precipitation maximum in excess of 5 mm $day^{-1}$ is simulated over the central South Atlantic Ocean, which is not shown by the observations.

Precipitation rates in excess of 2 mm $day^{-1}$ are simulated between 40°S and 60°S virtually everywhere in agreement with the observations. Precipitation maxima in excess of 5 mm $day^{-1}$ are simulated over the central Indian Ocean and over the South Pacific Ocean east of New Zealand, which are not found in the observations. On the other hand, the precipitation maxima in excess of 5 mm $day^{-1}$ observed off the west coast of South American and around Antarctica near 60°S are not simulated by the model.

The simulated precipitation rate decreases toward and into Antarctica as observed. Rates less than 1 mm $day^{-1}$ are simulated over most of the sea ice in the Weddell and Ross seas (Figure 1) as observed. The simulated precipitation rates over much of the Antarctic coast are larger than the observed precipitation rates. It appears that the simulated precipitation rate over the interior of Antarctica is larger than the observed rate; however, the absence of the 0.5 mm $day^{-1}$ contour does not permit a precise comparison.

5. NCAR Model. Precipitation rate minima are simulated at 30°S off the west coasts of South America and Africa as observed, but with values that are about twice those observed. In contrast to the observations, a precipitation minimum is not simulated off the west coast of Australia. Precipitation rate maxima are simulated over the east coasts of South America, Africa, and Australia in agreement with the observations, but the simulated values are about twice the observed values, and the simulated southeastward extensions over the oceans are not shown by observations.

Precipitation rates in excess of 2 mm $day^{-1}$ are simulated almost everywhere between 40°S and 60°S in agreement with the observations. A precipitation maximum larger than 4 mm $day^{-1}$ is simulated near New Zealand as observed, as is the precipitation minimum less than 2 mm $day^{-1}$ near 130°W, but the observed maximum off the west coast of South America is not simulated by the model. Also, the precipitation maxima observed near 60°S around much of Antarctica are not simulated by the model.

The simulated precipitation rates decrease toward and into Antarctica. Precipitation rates less than 1 mm $day^{-1}$ are simulated over the sea ice in the Weddell and Ross seas (Figure 1) in reasonable agreement with the observations. However, the simulated precipitation rates around the Antarctic coast and over the Antarctic interior are about twice the observed values.

6. OSU Model. At 30°S the model simulates precipitation minima off the west coasts of South America, Africa, and Australia that are in reasonable agreement with the observations in regard to intensity but that are less extensive in longitude than indicated by observations. The model simulates a precipitation minimum on the east coast of South America, where a precipitation maximum is observed and simulates less precipitation over Australia than is observed. A weak precipitation minimum is simulated over the western South Pacific Ocean, which is not shown in the observations.

In the latitude band from 40°S to 55°S the simulated precipitation rates exceed 2 mm $day^{-1}$ everywhere as observed. Precipitation rate maxima in excess of 5 mm $day^{-1}$ are simulated off the east coasts of Australia and South America, and greater than 10 mm $day^{-1}$ off South Africa, with no correspondence to the observations. Furthermore, the observed precipitation maxima off the west coast of South America at 50°S and around much of Antarctica at 60°S are not simulated by the model.

The simulated precipitation rate generally decreases toward Antarctica. Precipitation rates less than 1 mm $day^{-1}$ are simulated over the sea ice and ocean bordering most of Antarctica, and the simulated rates are less than the observed rates in the quadrants from 0° to 90°E and 180° to 90°W. Precipitation rates larger than observed are simulated along much of the Antarctic coastline, and the precipitation rates simulated over tha Antarctic interior are generally larger than those observed.

7. UCLA Model. At 30°S the model simulates the precipitation rate minima off the west coasts of South America, Africa, and Australia and the maxima along the east coasts of these continents. However, the simulated minima are less extensive over the adjoining oceans than the observed minima, and the simulated maxima are nearly twice as intense as the observed maxima. A precipitation minimum is simulated over Australia as observed, but the precipitation over Australia is everywhere larger than that observed.

Precipitation maxima greater than 3 mm $day^{-1}$ are simulated at 50°S in reasonable agreement with the observations; in particular, the precipitation maximum over the west coast of South America is represented quite well. The observed precipitation maxima at 60°S around much of Antarctica are not simulated by the model.

Precipitation less than 1 mm $day^{-1}$ is simulated over the sea ice in the Weddell and Ross seas in agreement with the observations. However, the simulated precipitation rates are less than the observed rates over the sea ice around East Antarctica (Figure 1). Over both East and West Antarctica the simulated precipitation rates are at least twice the observed values.

The results presented for the various models show that they are reasonably successful in simulating the precipitation rate minima and maxima, respectively, off the west and east coasts of South America, Africa, and Australia; however, only some of the models simulate the precipitation minimum observed in central Australia. The models are less successful in simulating the precipitation maximum observed off the west coast of South America at 50°S, and only the UCLA model reproduces the observed intensity there.

None of the models simulates the precipitation rate maxima shown by the Jaeger (1976) data at 60°S. This is also evident from Figure 9, which presents the zonal mean precipitation rates simulated by the predecessors of the six models considered here, as well as by four other models, the Jaeger observations, and those of Möller (1951) as reported by Schutz and Gates (1972). Both the Jaeger and Möller observations show maximum, zonal mean precipitation rates in the Southern Hemisphere midlatitudes; however, Jaeger shows the maximum to be 4 mm $day^{-1}$ at 60°S, while Möller shows 3 mm $day^{-1}$ at 50°S. Clearly, the maximum midlatitude precipitation simulated by the models agrees more with the Möller observations than with those of Jaeger.

Figure 9 also shows another error that is common to the simulations of the models presented here, namely, the overestimate of the precipitation rates over Antarctica.

Winter: The winter precipitation rates presented in Figure 8 are the observed July rates and the July rates simulated by the GFDL, GLAS, NCAR, OSU, and UCLA models. For the GISS model the simulated mean precipitation rate for June-July-August is shown.

1. Observed. At 30°S the precipitation rate has minima of less than 1 mm $day^{-1}$ located over the continents and off the west coast of Africa. Precipitation rates less than 2 mm $day^{-1}$ are located to the west of the continents over the oceans and eastward from Africa over the Indian Ocean.

Over the central South Pacific Ocean the maximum precipitation occurs equatorward of 30°S, and the precipitation rate is relatively uniform to about 55°S. Elsewhere, the precipitation rate increases with increasing southern latitude to a maximum near 45°S. Precipitation maxima in excess of 5 mm $day^{-1}$ are located to the west and east of New Zealand and off the west coast of South America.

The precipitation rate decreases poleward of 45°S to a minimum value less than 0.5 mm $day^{-1}$ near 61°S from 30°W eastward to 150°W. Precipitation rates larger than 0.5 mm $day^{-1}$ are found along the coast of Antarctica, with values larger than 1 mm $day^{-1}$ near 0°, 30°E, and 90°E. The precipitation rate is larger than 1 mm $day^{-1}$

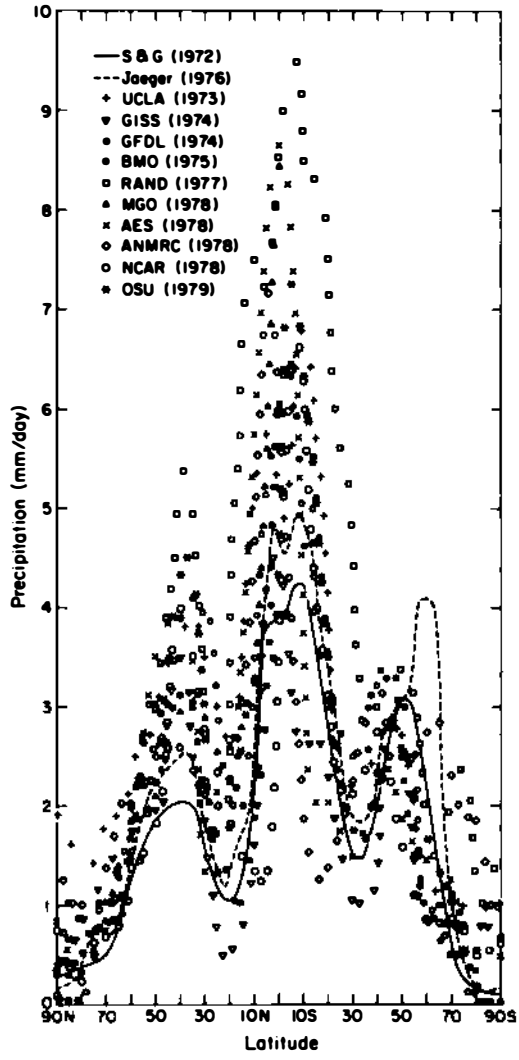


**Figure 9. The mean January precipitation rate as simulated by various atmospheric general circulation models and as observed. (See Figure 6 for identification of the models.) The observed data are from Schutz and Gates (1972) and Jaeger (1976). (From Gates and Bach 1981.)**

along much of the coast of West Antarctica, and rates larger than 2 mm day$^{-1}$ are observed over the Palmer Peninsula, extending westward over the coast of Ellsworth Land.

The precipitation rate decreases inland from the Antarctic coast, and rates less than 0.5 mm day$^{-1}$ are shown over a region that corresponds roughly to that encompassed by the 2000-m topographic contour (Figure 1).

2. GFDL Model. At 30°S the simulated precipitation rate shows minimum values of less than 1 mm day$^{-1}$ over South America and over the west coast of Africa, extending westward over the oceans, in reasonable agreement with the observations. The simulated

precipitation rate over Australia is larger than the observed rate, as is the simulated precipitation rate along the east coast of Africa. However, the model underestimates the precipitation rate observed off the east coasts of South America and Australia.

The simulated precipitation rate is relatively uniform over the central South Pacific Ocean, and elsewhere it increases with increasing southern latitude to about 45°S, in agreement with the observations. However, the precipitation maxima observed off the west coast of South America and east and west of New Zealand are not simulated by the model.

Poleward of 45°S the simulated precipitation rate decreases to a minimum value somewhat larger than 1 mm $day^{-1}$ around most of Antarctica near 60°S, in qualitative agreement with the observations. The simulated precipitation rate has a maximum value along the coast of Antarctica as observed, but the simulated intensities are about twice the observed intensities.

The precipitation rate decreases inland from the Antarctic coast, and rates less than 1 mm $day^{-1}$ are simulated over a region corresponding roughly to that encompassed by the 3000-m orographic contour. The precipitation rates simulated over much of the Antarctic interior are about twice the observed rates.

3. GISS Model. A precipitation rate minimum is simulated at 30°S over South America that extends westward over the South Pacific Ocean as observed; however, the simulated South American minimum is larger than the observed minimum. The precipitation rates simulated over Africa and Australia exceed the observed rates by about a factor of 2. Precipitation rates in excess of 4 mm $day^{-1}$ are simulated over the central South Pacific Ocean, the western regions of the South Atlantic, Indian, and South Pacific oceans, and the eastern regions of the South Atlantic and Indian oceans. Observations show precipitation rates this large only over the central South Pacific Ocean.

The maximum simulated precipitation rates are near 35°S latitude over much of the hemisphere; that is, about 10° equatorward of the observed position. The precipitation rate maxima observed east and west of New Zealand are simulated by the model but not that observed off the west coast of South America.

The simulated precipitation rates decrease with increasing southern latitude toward and into Antarctica. The precipitation rate minimum observed over the ocean and sea ice around most of Antarctica is not simulated by the model, and the simulated rates there are larger than the observed rates by as much as a factor of 4. The precipitation rates simulated around much of the Antarctic coast are also somewhat larger than those observed; however, the model underestimates the observed rates somewhat over the Palmer Peninsula. Over the interior of Antarctica the precipitation rates simulated by the model are in reasonably good agreement with the observations.

4. GLAS Model. Precipitation rates less than 2 mm $day^{-1}$ are simulated at 30°S off the east coasts of South America, Africa, and Australia in agreement with the observations. A precipitation minimum is simulated over Australia as observed, but the simulated rate is about twice the observed rate. The precipitation minima observed over South America and Africa are not simulated by the model, and the

simulated precipitation rates there are about twice the observed values. Precipitation rates in excess of 5 mm $day^{-1}$ are simulated over the central and western South Pacific Ocean, with a rate larger than 10 mm $day^{-1}$ near 135°W. These simulated rates are larger than the observed rates in this region.

The simulated precipitation rates are larger than 2 mm $day^{-1}$ equatorward of about 60°S, in agreement with the observations. A precipitation rate less than 2 mm $day^{-1}$ is simulated along the east coast of South America in accord with the observations; however, the precipitation maximum observed off the South American west coast is not found in the simulation.

The simulated precipitation rate decreases toward and into Antarctica. The precipitation rate minimum over the ocean and sea ice bounding Antarctica is not simulated by the model, and the observed rate there is overestimated by a factor of 4. The precipitation rate simulated over the Antarctic coast is in reasonable agreement with the observed rate, although the latter is underestimated by the model over the Palmer Peninsula. A precise comparison of the simulated and observed precipitation rates over the Antarctic interior cannot be made due to the absence of the 0.5-mm $day^{-1}$ contour for the simulation.

5. NCAR Model. At 30°S, precipitation rates less than 2 mm $day^{-1}$ are simulated off the west coasts of South America and Africa as observed; however, the precipitation rate simulated off the east coast of Australia is larger than the observed rate. Precipitation rates less than 2 mm $day^{-1}$ are simulated over South America, western Africa, and western Australia as observed, but the simulated rates exceed the observed rates over most of Australia, eastern Africa, and central South America. Precipitation rates less than 2 mm $day^{-1}$ are simulated over the western Indian Ocean, and rates greater than 4 mm $day^{-1}$ over the central South Pacific Ocean, in agreement with the observations.

The precipitation rate maxima observed off the west coast of South America and east and west of New Zealand are simulated by the model. A precipitation rate maximum is simulated near 45°S everywhere except over the central South Pacific Ocean in agreement with the observations; however, the simulated intensity is larger than that observed by about 2 mm $day^{-1}$. Precipitation rate minima less than 2 mm $day^{-1}$ are simulated at 55°S at several longitudes. These simulated minima are similar to the observed minimum around Antarctica but are larger in intensity, located farther equatorward, and less longitudinally continuous.

The precipitation rates simulated along the coast and interior of much of Antarctica are larger than those observed.

6. OSU Model. Precipitation minima are simulated at 30°S over South America and Australia; however, the former are located east of the observed position, and the latter have rates that are somewhat smaller than those observed. The precipitation rate minima observed off the west coast of the continents are not simulated by the model at 30°S, and the maxima in excess of 5 mm $day^{-1}$ simulated off the east coasts of the continents are not found in the observations.

The precipitation rate maximum observed off the west coast of South America is simulated by the model, but at a location about 10° equatorward of the observed position. The precipitation rate maxima east and west of New Zealand are not simulated by the model. The simulated precipitation rate exceeds 2 mm $day^{-1}$ equatorward of about 55°S everywhere except near 150°W, in reasonable agreement with the observations. The model does not reproduce the observed precipitation rate minimum observed over the ocean and sea ice surrounding Antarctica.

The precipitation rates simulated over the East Antarctic are somewhat larger than those observed and are smaller than observed over the Palmer Peninsula. The minimum observed over the interior of Antarctica is reproduced reasonably well.

7. UCLA Model. Precipitation rates greater than 3 mm $day^{-1}$ are simulated at 30°S over the central and western South Pacific Ocean and the western South Atlantic Ocean in accord with the observations. However, the simulated rates larger than 3 mm $day^{-1}$ over the Indian Ocean at 30°S are not found in the observations. A precipitation minimum less than 1 mm $day^{-1}$ is simulated over South America as observed. The observed minima less than 1 mm $day^{-1}$ over Africa and Australia are not simulated by the model.

Precipitation rates larger than 3 mm $day^{-1}$ are simulated to about 55°S, with a maximum near 45°S over much of the hemisphere as observed. The precipitation maximum observed off the west coast of South America is simulated, although it is less extensive than that observed. The observed maxima east and west of New Zealand are not simulated by the model.

The precipitation rate minimum observed over the ocean and sea ice surrounding Antarctica is not found in the simulation, and the simulated precipitation rates there are from 2 to 4 times the observed rates. The precipitation rates simulated around the Antarctic coast are in agreement with the observed rates everywhere except near the Palmer Peninsula and 105°E, where the model somewhat underestimates the observed precipitation rates. Due to the absence of the 0.5-mm $day^{-1}$ contour, it is not possible to compare the simulated precipitation rate over the Antarctic interior with the observed precipitation rate.

In summary, the results show that the models are successful in simulating the observed precipitation rates larger than 2 mm $day^{-1}$ in the latitudes between 40°S and 60°S. The models are less successful in simulating the precipitation minima over South America, Africa, and Australia and, generally, overestimate the observed rates there and westward over the oceans. Some of the models simulate either the precipitation maxima observed near 50°S off the west coast of South America or that surrounding New Zealand, but none of the models simulates both of these features reasonably well. The models also either do not simulate the precipitation minimum observed around much of Antarctica near 60°S, or they simulate a weak minimum equatorward of the observed location. Most of the models overestimate the precipitation over East Antarctica and underestimate the observed precipitation over the Palmer Peninsula and Ellsworth Land. Finally, two of the models (GISS, OSU) simulate the precipitation over the

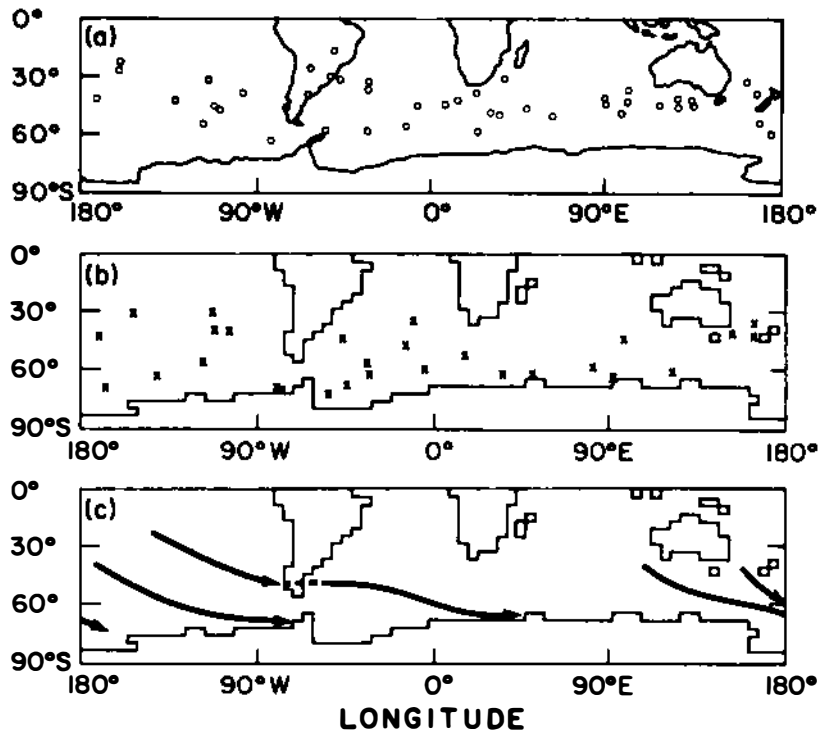


Figure 10. Position of cyclogenesis (a) as observed (Taljaard 1972) for July, and (b) as obtained by an earlier version of the UCLA model. (c) Simulated major cyclone tracks. (From Mechoso et al. 1979.)

Antarctic interior reasonably well, two of the models (GFDL, NCAR) overestimate the precipitation, and the simulated precipitation of two of the models (GLAS, UCLA) cannot be compared precisely with the observations because of the difference in plotted contour levels.

## Cyclogenesis and Cyclone Tracks

Figure 10 shows the geographical distribution of cyclogenesis simulated for July by an earlier verson of the UCLA model, with six vertical layers, top at 50 mb, and 4° x 5° latitude-longitude resolution (Mechoso et al. 1979), together with the observed locations for winter during the International Geophysical Year (IGY). Here, cyclogenesis is defined as the initial location of those cyclonic vortices for which a closed sea-level pressure contour could subsequently be followed for at least two consecutive days. Figure 11 shows similar results from an earlier version of the GFDL model, with the same vertical structure as the model of Table 1, but with 30 spectral waves in both latitude and longitude (Manabe et al. 1979), both with and without mountains.

Figure 10 shows that the earlier UCLA model simulated only about 60 percent of the observed number of cyclones formed (28 cf. 45), with no cyclogenesis over the eastern coast of South America, southeast of

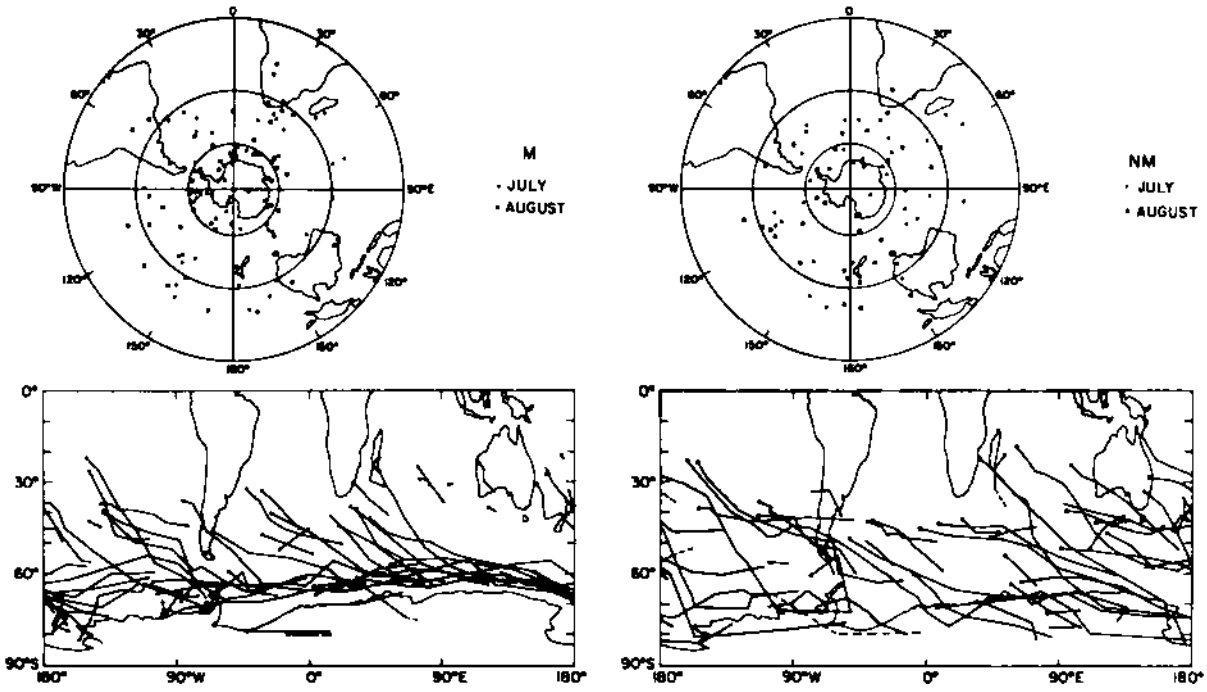


**Figure 11. Location of cyclogenesis and cyclone tracks simulated by an earlier version of the GFDL model, with mountains (M) and without mountains (NM). (From Mechoso 1981.)**

Africa, and south of Australia, unlike the observations. Furthermore, the locations of cyclogenesis simulated by the model occur closer to the Antarctic coast than has been observed. Figure 11 shows that the earlier GFDL model simulates the number of cyclones formed in July (47 cf. 45) reasonably well but failed to simulate the July cyclogenesis over the east coast of South America and south of Australia. It simulates more cyclogenesis near the coast of Antarctica than is observed. The earlier GFDL model simulates fewer July cyclones when the mountains are removed (34 cf. 47), with fewer cyclones forming near the Antarctic coast.

## DISCUSSION AND RECOMMENDATIONS

The surface air temperatures simulated by the models over Antarctica are 10°C warmer than the observed temperatures in summer and 15° warmer in winter. These errors may be a consequence of the models' prescribed topographies, which have been smoothed in accord with their horizontal resolution and are, therefore, of lower elevation than in reality. Alternatively, the surface air temperature observations of Taljaard et al. (1969) may be colder than reality. In fact, the most recently published global atmospheric circulation statistics (Oort 1983) show observed temperatures over Antarctica that are 20°C warmer than the Taljaard et al. (1969) observations for summer and 30°C warmer for

winter. Clearly, if these most recently published observations are correct, the models' results are from 10° to 15°C colder than reality rather than vice versa!

The surface air temperatures simulated by the models over the Antarctic sea ice are generally warmer than the observed temperatures in summer, and both warmer and colder in winter. These errors are not due to the models' prescribed topographies, and there appears to be less difference between the Taljaard et al. (1969) and Oort (1983) observations around the Antarctic coast. It may be that too much solar radiation is absorbed by the sea ice as a result of its prescribed surface albedo being to small or that too much longwave radiation is incident on the sea ice as a result of an overestimate in the simulated cloudiness and/or a cloud emissivity that is too large. In any event, the most recent (satellite) observations of the extent of sea ice (Zwally et al. 1983) show that the Antarctic sea ice prescribed for some of the AGCMs, at least those based on the data of Alexander and Mobley (1976), is more estensive than in reality. (However, this would probably cause those models to underestimate the surface air temperature over the sea ice.)

The surface air temperature simulated by the models over the Southern Hemisphere oceans is in reasonable agreement with the observed surface air temperatures. This, of course, is not surprising, for the underlying sea surface temperatures are prescribed and, therefore, strongly constrain the surface air temperatures. In fact, the surface air temperature errors that are displayed by the models over the oceans may reflect, to a large extent, the differences among the observed sea surface temperature data sets shown in Table 1. Consequently, to validate the AGCMs over the ocean, it is necessary to compare their simulated surface fluxes of heat (and moisture and momentum), in addition to their surface air temperatures, with the observations insofar as possible.

The sea-level pressures simulated by the models are in reasonable agreement with the observed sea-level pressures in the Southern Hemisphere subtropics in both summer and winter. The models are less successful in simulating the SPT around Antarctica, generally placing it equatorward of its observed position, with an intensity that is too weak. The OSU model simulates the summer SPT with some fidelity, while the NCAR model simulates the winter SPT reasonably well. Only the UCLA model reproduces both the summer and winter SPT with some accuracy. As this model has the highest horizontal resolution of all the grid point models (Table 1), its comparatively superior performance suggests that horizontal resolution may be an important factor in simulating the SPT reasonably well. This conjecture is given some support by the weak SPT simulated by the grid point model with the lowest horizontal resolution, namely, the GISS model. In any case, the models' relatively poor simulation of the SPT is tantamount to the simulated surface geostrophic westerly winds being generally much weaker than the observed geostrophic westerly winds. This surface-wind error is likely to cause serious errors in the simulated sea surface temperatures and oceanic circulation around Antarctica when the AGCMs are coupled with dynamic models of the ocean.

The sea-level pressures simulated over Antarctica by all the models are higher than the observed sea-level pressures by from 20 to 50 mb in winter. It is likely that these errors are due in part to the methods used to reduce the surface pressure to sea level over the great elevation of most of Antarctica. However, the facts that the simulated surface air temperatures are warmer than the observed temperatures and the prescribed surface elevation less than in reality suggest that the sea-level pressures should be underestimated by the models. Also, not all the models overestimate the Antarctic sea-level pressure in summer; the GISS and OSU models give a reasonably accurate representation, and the UCLA model considerably underestimates the observed sea-level pressure. This finding suggests that at least part of the winter sea-level pressure errors represents an actual error in the distribution of mass over Antarctica. This conjecture is given some support by the models' underestimate of the SPT, an error that occurs over the ocean and, therefore, clearly is not due to any reduction in sea-level error.

The Jaeger (1976) precipitation observations show a precipitation maximum greater than 5 mm $day^{-1}$ at 60°S around much of Antarctica in summer (January), and a precipitation minimum less than 0.5 mm $day^{-1}$ at 60°S, also around much of Antarctica in winter (July). None of the models simulates the observed summer maximum, and only two of the models display precipitation rate features that bear some resemblance to a minimum, albeit weaker and more equatorward than that observed. However, the absence of these summer and winter precipitation extremes in the model simulations may not be errors, because the Möller (1951) seasonal precipitation observations (December-January-February and June-July-August) show neither the summer maximum nor the winter minimum.

On the other hand, both the Jaeger (1976) and Möller (1951) observations show a precipitation maximum in excess of 5 mm $day^{-1}$ located off the west coast of South America near 50°S in summer and 45°S in winter. Most of the models are not successful in simulating this precipitation maximum. The GFDL model simulates a summer maximum, but with half the observed intensity and no winter maximum; the NCAR model simulates the winter maximum, with about the observed intensity but no summer maximum; and the GISS, GLAS, and OSU models simulate neither maximum. Only the UCLA model reproduces the precipitation maximum in both summer and winter.

The precipitation simulated by the models is generally larger than the observed precipitation over East Antarctica and less than that observed over the Palmer Peninsula and the coast of Ellsworth Land. However, the latter may not be a simulation error because the Möller (1951) precipitation observations are about half the Jaeger (1976) precipitation observations in this region. Although a precise comparison between the simulated and observed precipitation rates over the Antarctic interior cannot be made for all the models because of the lack of sufficiently small contour levels, the models generally appear to overestimate the observed rate by a factor of about 2.

Finally, the results from the predecessors of two of the models considered here show an absence of cyclogenesis over the east coast of

South America and southeast of Africa. As suggested by Mechoso et al. (1979), this may be a consequence of the models' smoothed representations of the Andes Mountains and the African Highlands. On the other hand, the results of Mechoso (1981) shown in Figure 11 suggest that if the elevation of Antarctica were raised, more cyclones would form off the coast of Antarctica in apparent further disagreement with the observations.

The following recommendations are based on the discussion presented here and the author's review of the simulations of $CO_2$-induced climatic change.

Model validation: How well do AGCMs simulate the present Antarctic climate?

1. Observations should be critically appraised and their standard errors quantified.
2. Comparison should be made of the models' simulated variables in the free atmosphere, such as temperature, winds, mositure, and clouds, with observational data.
3. The models' simulations of cyclogenesis and cyclone tracks should be compared with observations, for example, by the method proposed by Trenberth (see Attachment 3).
4. The components of the surface energy budget (solar radiation, upward and downward longwave radiation, sensible and latent heat fluxes) simulated by the models should be compared with observations.
5. These recommended comparisons should be extended to as many AGCMs as possible.

Model sensitivity studies: How are the AGCM simulation errors produced and how can they be corrected?

1. The reasons that most models underestimate the intensity of the Antarctic subpolar trough should be determined, as well as the reasons that most improvements in this feature result in the generation of an "Arctic subpolar trough."
2. An effort should be made to determine whether the errors in the simulated surface air temperatures, precipitation rates, and cyclogenesis result from the prescribed orography being too low in elevation and too smooth.
3. Whether sea-level pressure errors over Antarctica are due to an erroneous method of reduction to sea level or represent an error in the distribution of mass should be determined.

AGCM-ocean model simulations of $CO_2$-induced climatic change: How do models simulate $CO_2$-induced climatic change?

1. The models' simulations of the present climate, which are used as the controls for the enhanced $CO_2$ climates, should be comprehensively documented, with particular attention to the cryospheric variables, namely, sea ice and snow.

2. Studies should be performed to ascertain the statistical significance of the models' simulated climatic changes.

3. The models' statistically significant climatic changes should be analyzed to determine the role of the predicted cryospheric components in the warming and the acceleration of the hydrological cycle and the effects of the climatic change on the unpredicted cryospheric components such as the West Antarctic Ice Sheet and shelves.

## ACKNOWLEDGMENTS

The author expresses his appreciation to Douglas G. Hahn, Jim Hansen, Jagadish Shukla, Eric J. Pitcher, and Carlos R. Mechoso for making available the results from the GFDL, GISS, GLAS, NCAR, and UCLA models, respectively, and to W. Lawrence Gates, Wilfrid Bach, and Carlos R. Mechoso for permission to reproduce their figures. He is also grateful to R. L. Mobley for preparing the graphics for the OSU model, L. Riley for typing the manuscript, M. B. Schlesinger and M. L. Schlesinger for assistance with the figures, and J. Stark for drafting the figures.

Support for this study was provided by the Polar Research Board of the National Research Council and the National Science Foundation under grant ATM-8205992.

## REFERENCES

Alexander, R. C. and R. L. Mobley, 1976. Monthly average sea-surface temperatures and ice pack limits on a 1° global grid. Monthly Weather Review, 104, 143-148.

Bakayev, V. G. (ed.), 1966. Atlas Antarktiki Moscow (225 pp.). Glavnoe Upravlenie Geodezii i Kargografii MG, SSSR.

Boer, G. J. and N. A. McFarlane, 1979. The AES atmospheric general circulation model. In W. L. Gates (ed.), Report of the JOC Study Conference on Climate Models: Performance, Intercomparison and Sensitivity Studies. GARP Publication Series 22, Volume I (pp. 409-460). World Meteorological Organization, Geneva.

British Meteorological Office, 1977. Monthly Ice Charts. Bracknell, Berkshire, England.

Defant, A., 1961. Physical Oceanography. Volume I (729 pp.). Pergamon, New York.

Gates, W. L. and W. Bach, 1981. Analysis of a Model-Simulated Climate Change as a Scenario for Impact Studies. R&D 104 02 513 (163 pp). German Federal Environmental Agency, Bonn.

Gates, W. L. and M. E. Schlesinger, 1977. Numerical simulation of the January and July global climate with a two-level atmospheric model. Journal of Atmospheric Science, 23, 36-37.

Ghan, S. J., J. W. Lingaas, M. E. Schlesinger, R. L. Mobley, and W. L. Gates, 1982. A Documentation of the OSU Two-level Atmospheric General Circulation Model. Report 35 (395 pp.). Climate Research Institute, Oregon State University, Corvallis.

Gilchrist, A., 1975. A general circulation model of the atmosphere incorporating an explicit boundary layer top. Unpublished manuscript. Technical Note II/29, Volume 20 (35 pp.). Meteorological Organization.

Gilchrist, A., 1979. The Meteorological Office 5-layer general circulation model. In W. L. Gates (ed.), Report of the JOC Study Conference on Climate Models: Performance, Intercomparison and Sensitivity Studies. GARP Publication Series 22, Volume I (pp. 254-295). World Meteorological Organization, Geneva.

Halem, M., J. Shukla, Y. Mintz, M. L. Wu, R. Godbole, G. Herman, and Y. Sud, 1979. Comparisons of observed seasonal climate features with a winter and summer numerical simulation produced with the GLAS general circulation model. In W. L. Gates (ed.), Report of the JOC Study Conference on Climate Models: Performance, Intercomparison and Sensitivity Studies. GARP Publication Series 22, Volume I (pp. 207-253). World Meteorological Organization, Geneva.

Jaeger, L., 1976. Monatskarten des Niederschlags fur die ganze Erde. Berlin Deutscher Wetterdienstes, 139, 38 pp.

Jenne, R. L., 1975. Data Sets for Meteorological Research. NCAR Technical Note NCAR-TN/IA-111 (194 pp.). National Center for Atmospheric Research, Boulder, Colorado.

Kasahara, A. and W. M. Washington, 1971. General circulation experiments with a six-layer NCAR model, including orography, cloudiness and surface temperature calculation. Journal of Atmospheric Science, 28, 657-701.

Manabe, S. and D. G. Hahn, 1981. Simulation of atmospheric variability. Monthly Weather Review, 109, 2260-2286.

Manabe, S., D. G. Hahn, and J. L. Holloway, Jr., 1979. Climate simulations with GFDL spectral models of the atmosphere: effect of spectral truncation. In W. L. Gates (ed.), Report of the JOC Study Conference on Climate Models: Performance, Intercomparison and Sensitivity Studies. GARP Publication Series 22, Volume I (pp. 41-94). World Meteorological Organization, Geneva.

McAvaney, G., W. Bourke, and K. Puri, 1979. A simulation of the January global circulation using a spectral model. In W. L. Gates (ed.), Report of the JOC Study Conference on Climate Models: Perfomance, Intercomparison and Sensitivity Studies. GARP Publication Series 22, Volume I (pp. 296-317). World Meteorological Organization, Geneva.

Mechoso, C. R., 1981. Topographic influences on the general circulation of the Southern Hemisphere. A numerical experiment. Monthly Weather Review, 109, 2131-2139.

Mechoso, C. R., M. J. Suarez, and A. Arakawa, 1979. July simulation by the UCLA general circulation model. In Fourth Conference on Numerical Weather Prediction (pp. 282-289). American Meteorological Society, Boston, Massachusetts.

Meleshko, V. R., B. E. Shneerov, M. E. Shvets, L. R. Dmitrieva, G. V. Parshina, C. V. Bogachenko, V. A. Pnomarev, E. P. Yushina, L. H. Magazenkov, and D. A. Sheinin, 1979. Simulation of January climate with a MGO general circulation model. In W. L. Gates (ed.), Report of the JOC Study Conference on Climate Models:

Performance, Intercomparison and Sensitivity Studies. GARP Publication Series 22, Volume I (pp. 371-408). World Meteorological Organization, Geneva.

Möller, F., 1951. Vierteljahrskarten des Niederschlags fur die ganze Erde. Petermanns Geographische Mitteilungen, 95, 1-7.

Oort, A. H., 1983. Global Atmospheric Circulation Statistics, 1958-1973. NOAA Professional Paper 14 (180 pp.). U.S. Government Printing Office, Washington, D.C.

Pitcher, E. J., R. C. Malone, V. Ramanathan, M. L. Blackmon, K. Puri, and W. Bourke, 1982. January and July simulations with a spectral general circulation model. Journal of Atmospheric Science, 40, 580-604.

Robinson, M. and R. Bauer, 1981. Oceanographic Monthly Summary, 1. Report 2 (pp. 2-3). NOAA National Weather Service, Washington, D.C.

Schlesinger, M. E. and W. L. Gates, 1979. Numerical Simulation of the January and July Global Climate with the OSU Two-Level Atmospheric General Circulation Model. Report 9 (102 pp.). Climatic Research Institute, Oregon State University, Corvallis.

Schlesinger, M. E. and W. L. Gates, 1981. Preliminary Analysis of the Mean Annual Cycle and Interannual Variability Simulated by the OSU Two-Level Atmospheric General Circulation Model. Report 23 (47 pp.). Climatic Research Institute, Oregon State University, Corvallis.

Schutz, C. and W. L. Gates, 1971. Global Climatic Data for Surface, 800 mb, 400 mb: January. R-915-ARPA (173 pp.). The Rand Corporation, Santa Monica, California.

Schutz, C. and W. L. Gates, 1972. Global Climatic Data for Surface, 800 mb, 400 mb: July. R-1029-ARPA (180 pp.). The Rand Corporation, Santa Monica, California.

Shukla, J., D. Straus, D. Randall, Y. Sud, and L. Marx, 1981. Winter and Summer Simulations with the GLAS Climate Model. Technical Memorandum 83866 (282 pp.). Laboratory for Atmospheric Sciences, Modeling and Simulation Facility, NASA Goddard Space Flight Center, Greenbelt, Maryland.

Somerville, R. C. J., P. H. Stone, M. Halem, J. E. Hansen, J. S. Hogan, L. M. Druyan, G. Russell, A. A. Lacis, W. J. Quirk, and J. Tenenbau, 1974. The GISS model of the global atmosphere. Journal of Atmospheric Science, 31, 84-117.

Taljaard, J. J., 1972. Synoptic meteorology of the Southern Hemisphere. In C. W. Newton (ed.), Meteorology of the Southern Hemisphere. Meteorological Monograph 13(35) (Chapter 8). American Meteorological Society, Boston, Massachusetts.

Taljaard, J. J., H. van Loon, H. L. Crutcher, and R. L. Jenne, 1969. Climate of the Upper Air: Southern Hemisphere. Volume 1. Temperatures, Dew Points and Heights at Selected Pressure Levels. NAVAIR 50-1C-55. Naval Weather Service Command, Washington, D.C.

U.S. Naval Oceanographic Office, 1944. World Atlas of Sea Surface Temperatures. 2nd edition. H. O. Publication 225. U.S. Navy Hydrographic Office, Washington, D.C.

U.S. Naval Oceanographic Office, 1957. Oceanographic Atlas of the Polar Seas. Part I. Antarctic. H. O. Publication 705. Washington, D.C.

U.S. Naval Oceanographic Office, 1958. Oceanographic Atlas of the Polar Seas. Part II. Arctic. H. O. Publication 705. Washington, D.C.

U.S. Naval Oceanographic Office, 1967a. Monthly Charts of Mean, Minimum, and Maximum Sea Surface Temperature of the Indian Ocean. Report SP-99. Washington, D.C.

U.S. Naval Oceanographic Office, 1967b. Oceanographic Atlas of the North Atlantic Ocean. Section II: Physical Properties. Publication 700, Washington, D.C.

U.S. Naval Oceanographic Office, 1969. Monthly Charts of Mean, Minimum, and Maximum Sea Surface Temperature of the North Pacific Ocean. Report SP-123. Washington, D.C.

Washington, W. M., R. Dickinson, V. Ramanathan, T. Moyer, D. Williamson, G. Williamson, and R. Wolski, 1979. Preliminary atmospheric simulation with the third-generation NCAR general circulation model: January and July. In W. L. Gates (ed.), Report of the JOC Study Conference on Climate Models: Performance, Intercomparison and Sensitivity Studies. GARP Publication Series 22, Volume I (pp. 95-138). World Meteorological Organization, Geneva.

Wigle, W. F. and B. R. Mendenhall, 1974. Climatology of Upper Thermal Structure of the Seas. Technical Report M-106 (79 pp.). Meteorology International Incorporated, Monterey, California.

World Meteorological Organization, 1968. Methods in Use for the Reduction of Atmospheric Pressure. Technical Note 91, 226.TP.120 (21 pp.). World Meteorological Organization, Geneva.

Zwally, H. J., J. C. Comiso, C. L. Parkinson, W. J. Campbell, F. D. Carsey, and P. Gloersen, 1983. Antarctic Sea Ice, 1973-1976: Satellite Passive Microwave Observations. NASA Special Publication SP-459 (206 pp.). National Aeronautics and Space Administration, Washington, D.C.

## ATTACHMENT 10

# ON MODELING THE OCEANIC ENVIRONMENT OF WEST ANTARCTICA, INCLUDING $CO_2$-INDUCED CHANGES

Albert J. Semtner, Jr.
National Center for Atmospheric Research, Boulder

One way in which the ocean can influence the marine ice sheet of West Antarctica is through the atmospheric response to changes in sea surface temperature (SST) and in sea ice. The fields of SST and sea ice are determined by processes of oceanic heat transport and heat storage and by exchanges at the sea surface. In many parts of the world ocean, there is an approximate balance between local heat storage in the mixed layer and surface exchanges, so that the treatment of the upper ocean as a slab of constant heat capacity gives a fairly good seasonal cycle of SST as well as an estimate of the annual mean value. Manabe and Stouffer (1980) assumed that the entire world ocean could be treated in such a way; they were able to predict, at least approximately, the climatic changes near Antarctica that would result from quadrupling the concentration of $CO_2$ in the atmosphere (cf. Figure 1). The changes in the vicinity of West Antarctica included disappearance of sea ice, increases in SST and air temperature by several degrees, and precipitation increases on the order of 0.1 m $year^{-1}$. The atmospheric changes are not large enough to influence the marine ice sheet from above on time scales of a few hundred years (Bentley 1983). On the surface, therefore, it seems that oceanic changes will have little effect on glacial ice.

To see that the ocean might have a large influence on the West Antarctic, one must consider the subsurface oceanic processes in this region. Jacobs et al. (1979) have documented intrusions of relatively warm water at 250-m depth along the Ross Ice Shelf Barrier (see Figure 2). Their measurements poleward of 82°S beneath the ice shelf indicate that basal melting of 0.25 m $year^{-1}$ may be occurring as a result of the warm inflow. Gordon (1983) indicates that changes in pycnocline stability alone, due to surface $CO_2$ effects, could increase the temperature of the warm intrusions by 0.5°C. This rise in temperature might increase basal melting to 0.5 m $year^{-1}$. Bentley (1983) speculates that if basal melting were to increase to 1 m $year^{-1}$ due to additional circulation changes, then unpinning of the ice shelf might occur in 100 years, followed by destabilization of the grounded portion of the ice sheet on a time scale of several hundred years. Thus, a proper treatment of $CO_2$ influence on West Antarctica must deal with the three-dimensional ocean circulation in that region.

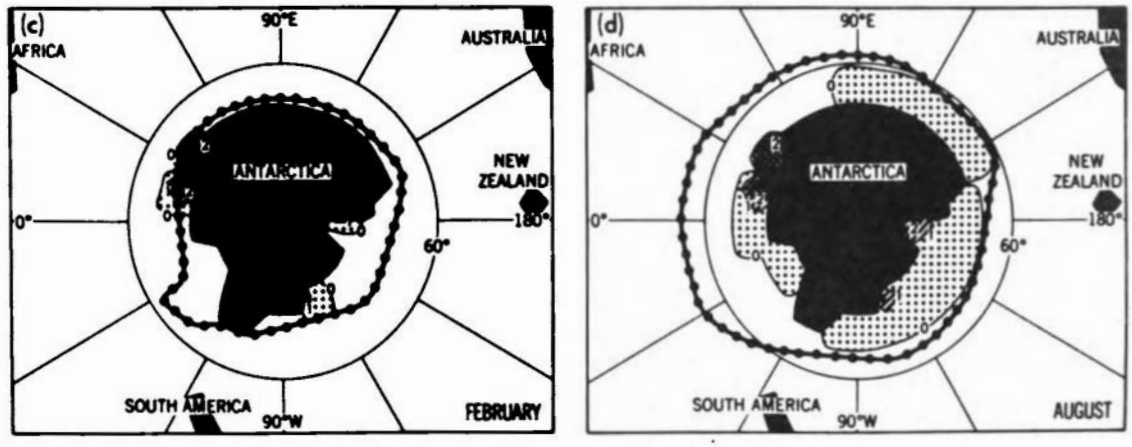


Geographical distributions of sea ice thickness (meters) from the 1 × $CO_2$ experiment. (*a*) Northern hemisphere—February. (*b*) Northern hemisphere—August. (*c*) Southern hemisphere—February. (*d*) Southern hemisphere—August. Dashed-dotted lines indicate the observed mean sea ice boundaries from the compilation by *U.S. Naval Oceanographic Office* [1957, 1958].

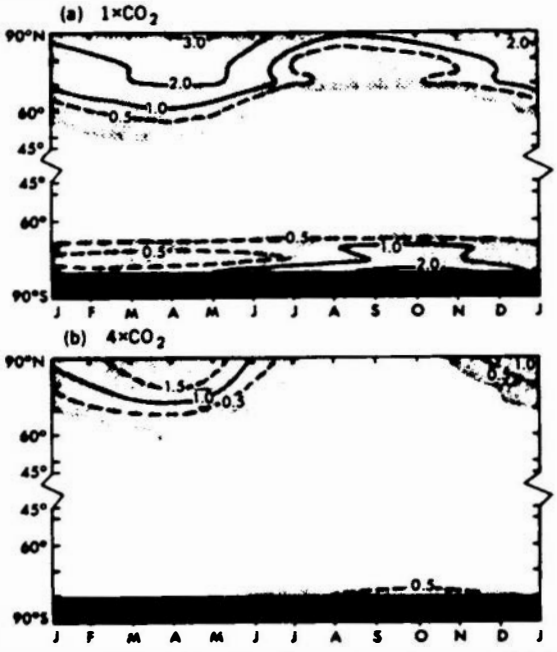


Latitude-time distributions of sea ice thickness (centimeters). Top: 1 × $CO_2$ experiment. Bottom: 4 × $CO_2$ experiment. Shading indicates the regions where sea ice thickness exceeds 0.1 m.

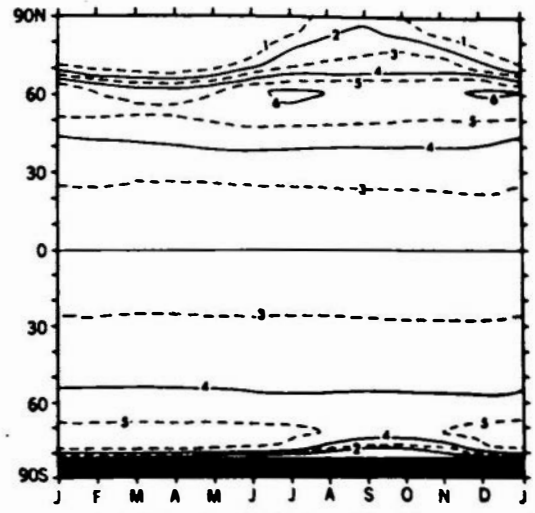


The latitude-time distribution of the difference in zonal mean surface water temperature (degree Celsius) of the mixed layer model ocean between the 4 × $CO_2$ and 1 × $CO_2$ experiments.

**Figure 1. Some results from the $CO_2$ quadrupling study of Manabe and Stouffer (1980).**

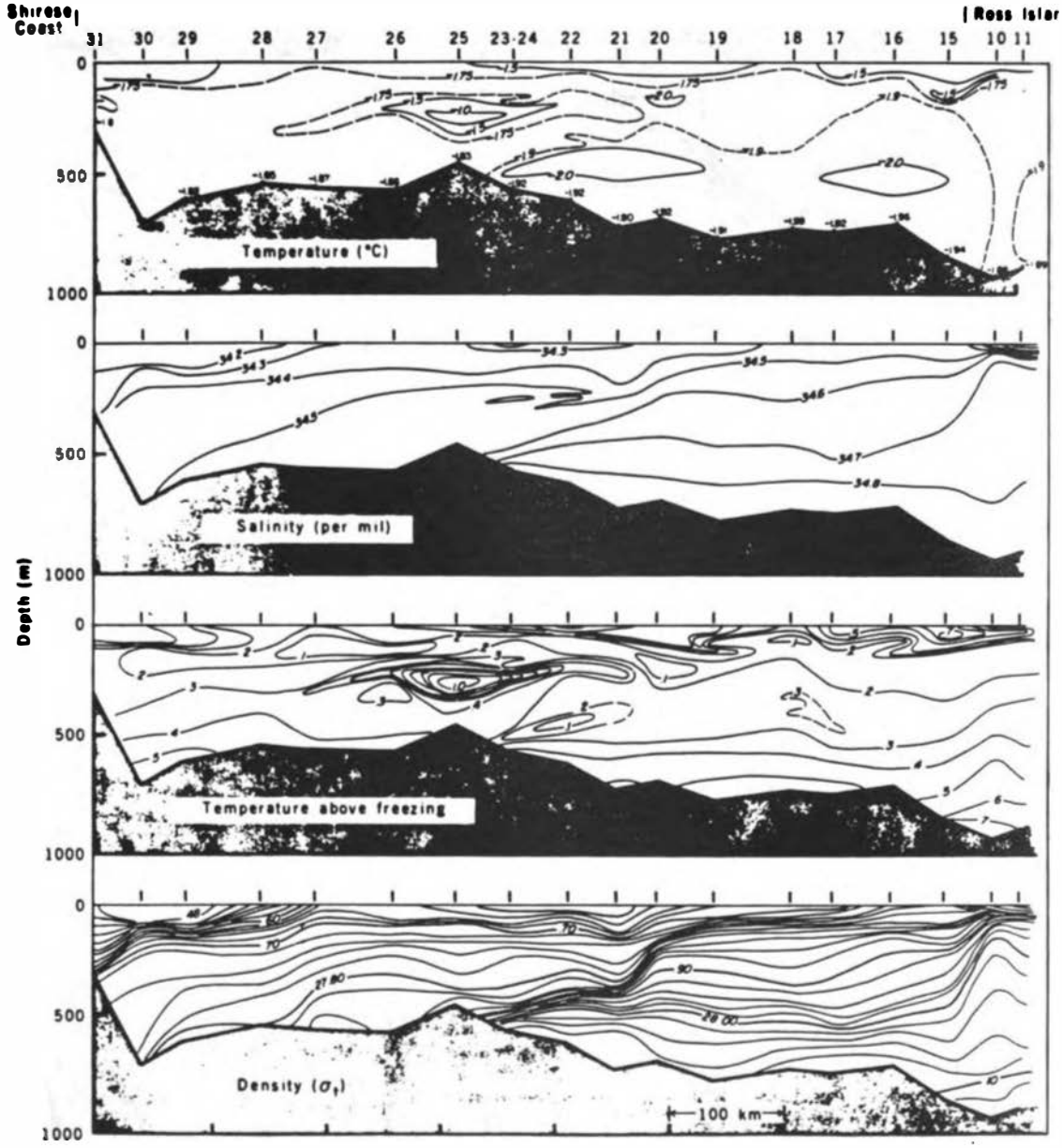


**Figure 2. Ross Sea observations of Jacobs et al. (1979).**

**Figure 3 (from Foster and Carmack 1976) clearly illustrates that warm intrusions of circumpolar deep water (CDW) also occur over the Weddell Shelf, where local mixing processes, both along and across isopycnals, lead to the formation of Antarctic bottom water (AABW). As indicated in Figure 4a, meridional circulations on a global scale are involved in bringing warm water onto the Antarctic continental shelf to**

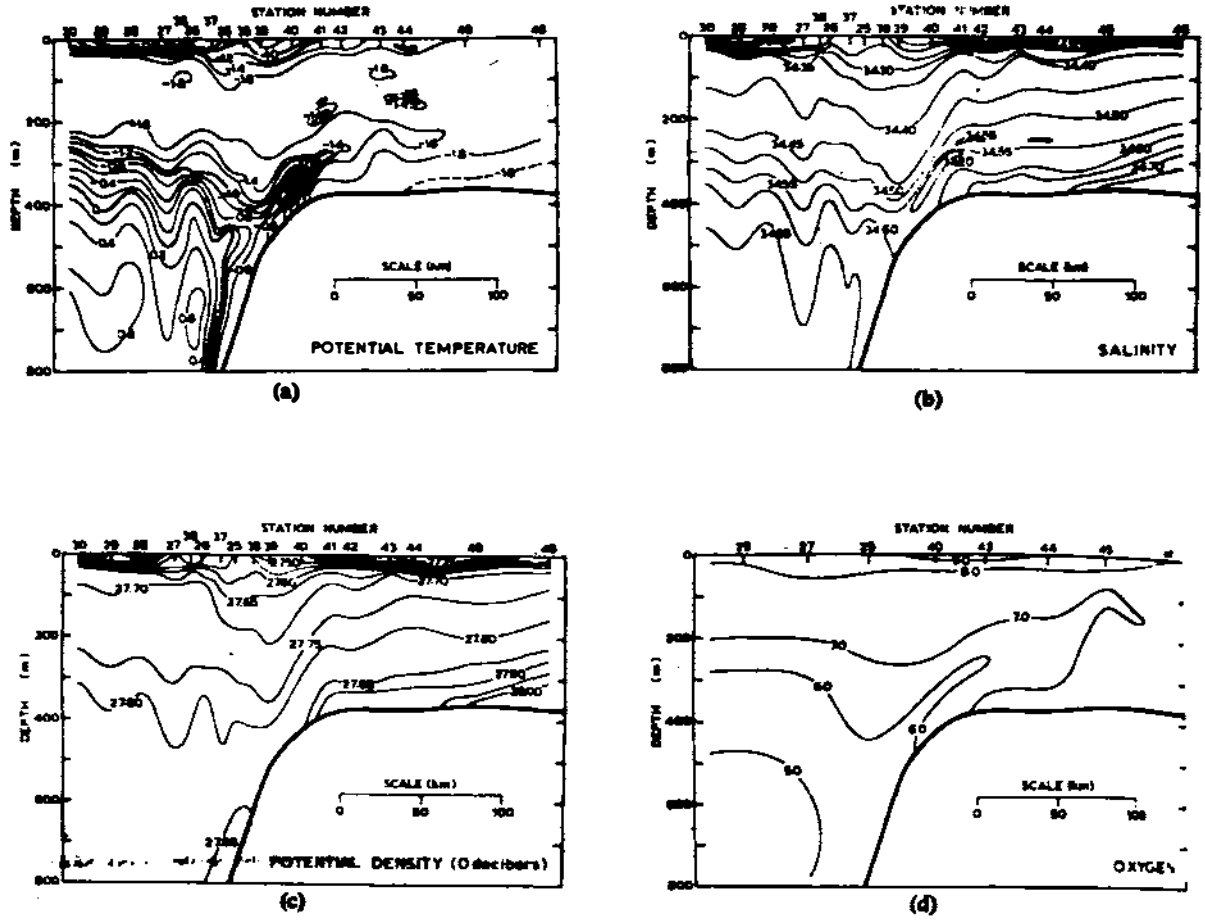


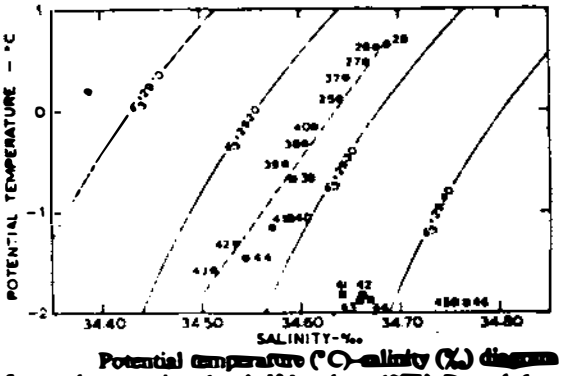


Potential temperature (°C)–salinity (‰) diagram for section crossing the shelf break at 40°W. Round dots indicate θ–*S* at the subsurface temperature maximum. Squares indicate θ–*S* at bottom. From offshore to onshore the order of stations is 35, 34, 33, 32, 31, 30, 29, 28, 27, 36, 26, 37, 25, 38, 39, 40, 41, 42, 43, 44, 45, and 46.

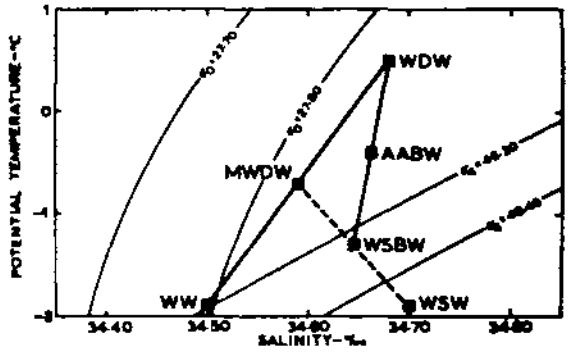


Idealized mixing scheme shown on a potential temperature–salinity diagram.

Figure 3. Weddell Sea observations of Foster and Carmack (1976).

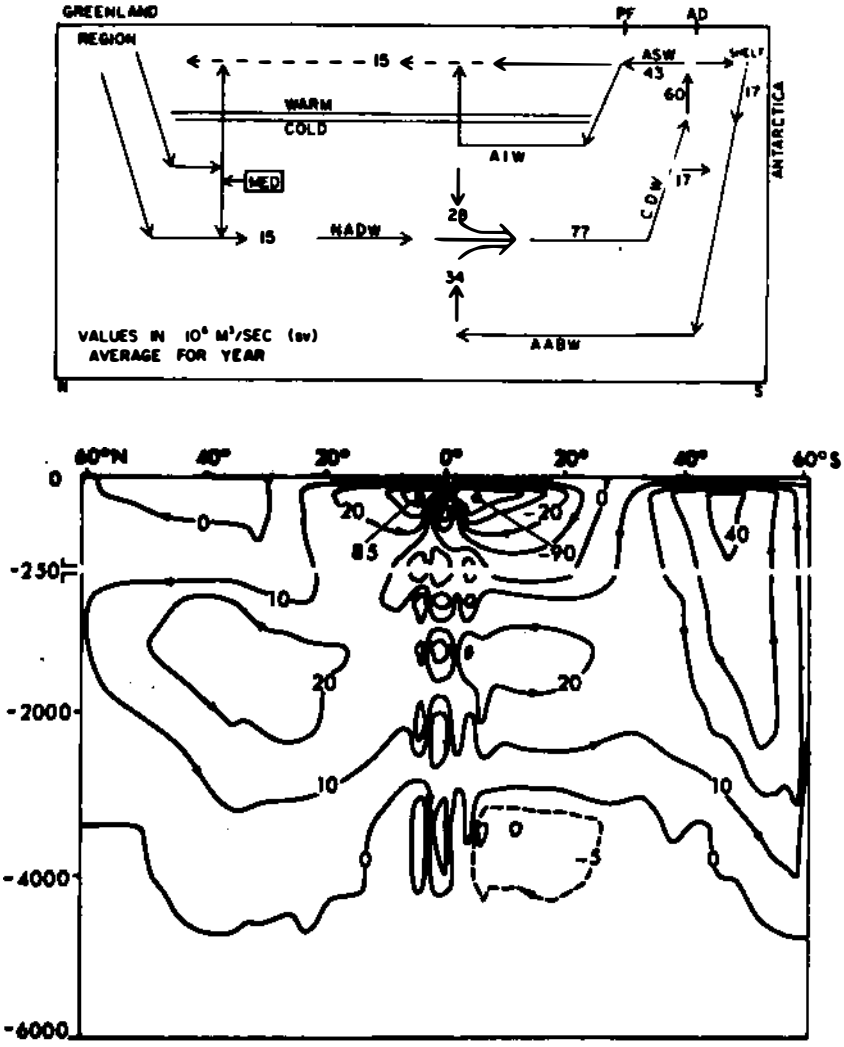


**Figure 4. Meridional circulation of the world ocean, (a) as inferred from observations (Gordon 1971) and (b) as computed by an ocean circulation model (Cox 1975).**

promote melting of ice shelves. An important component in the whole system is North Atlantic deep water (NADW), whose rate of production may significantly affect interhemispheric transports of heat (Rooth 1982).

The circulations inferred from water mass analysis in Figure 5a have been reproduced in a numerical ocean model having 200-km grid spacing, which is initialized with observed temperature and salinity and integrated for 2 years with observed wind forcing (Figure 4b). That same model of Cox (1975) also shows horizontal transport patterns (Figure 5a) comparable to those inferred from data (Figure 5b), although the steady model currents lack the mesoscale variability that is observed (cf. Cheney et al. 1983). The mesoscale variability of the

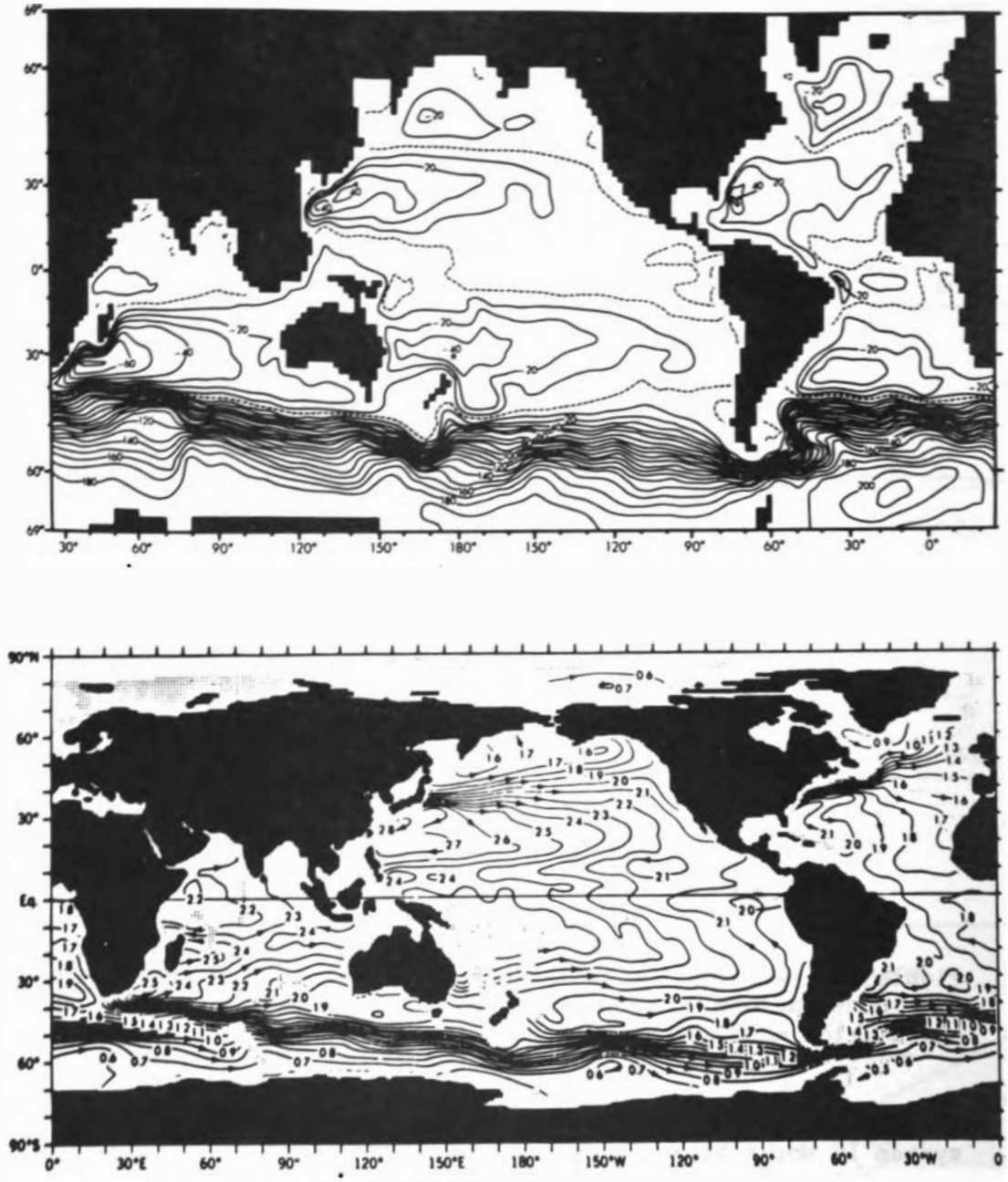


**Figure 5. (a) Streamlines of mass transport from the model of Cox (1975). (b) Streamlines of surface currents inferred from the observed density field (Levitus 1982).**

Antarctic circumpolar current (ACC) is implicitly included in Cox's model by the prescriptions of eddy diffusion coefficients; that is, $A_M = 8 \times 10^4$ m$^2$ s$^{-1}$ and $A_H = 10^3$ m$^2$ s$^{-1}$ for horizontal diffusions of momentum and heat, respectively, with $K_M = 10^{-4}$ m$^2$ s$^{-1}$ and $K_H = 10^{-4}$ m$^2$ s$^{-1}$ for the corresponding vertical processes. The value of $A_H$ is reasonable on the basis of observations in the Drake Passage (Bryden 1979) and idealized model studies with resolved eddies (See Figure 6, from McWilliams et al. 1978). However, the latter study suggests the values $A_M = -3 \times 10^3$ m$^2$ s$^{-1}$ and $K_M = 1.0$ m$^2$ s$^{-1}$, as a result of baroclinic instability. Momentum converges horizontally into the core of the current and is transferred downward by eddy processes (e.g., form drag) and lost to the bottom by friction. Cox's model misrepresents these frictional processes with a dominance of horizontal diffusion.

Since Cox's (1975) study, the Antarctic Ocean has been included in a number of studies employing a coarser horizontal grid than his (typically with 500-km spacing) and (of necessity) larger values of $A_H$ and $A_M$ by factors of 2 or more and 10, respectively. The large mixing coefficients led to underestimates of transport by the ACC (see Table 1 and Figure 7a) and unrealistically warm SST in the Antarctic (see Figure 8). However, much of the unrealistic SST pattern in the GFDL model of Bryan et al. (1975) is caused by unrealistic model wind forcing (see their Figure 4); in the NCAR simulation of Washington et al. (1980), a large value of $A_H = 2 \times 10^4$ m$^2$ s$^1$ distorted the SST pattern. When $A_H = 2 \times 10^3$ was used by Meehl et al. (1982), the NCAR model showed better ability to simulate observed ocean heat transport, including transports by individual oceans (see Figure 9). The simulation of Han and Gates (1984) gives a good representation of Southern Ocean heat transport using 500-km horizontal grid spacing, but horizontal mass transports are still too low in relation to observations.

Improved modeling of the horizontal motion field in the Antarctic region will require a grid size that allows the coefficient of momentum diffusion to be of the order of $10^3$ m$^2$ s$^{-1}$. A 100-km or less grid size is needed in this case, on the basis of numerical considerations (Bryan et al. 1975). It is suggested that regional simulations of the Antarctic be attempted at this resolution and that some consideration be given as well to incorporating the effects of negative viscosity and eddy form drag in the vicinity of strong currents. A dependence of vertical heat diffusion on stability should also be included (cf. Gordon 1983).

To the author's knowledge, there are no simulations to date of the three-dimensional circulations near the continental shelves shown in Figures 2 and 3. Proper modeling of features like these is essential to a valid assessment of the $CO_2$ effects in West Antarctica. A recent simulation of the Arctic Ocean shows some promise in being able to model analogous phenomena in that region with 100-km grid spacing and 13 vertical levels. Figure 10a shows the intermediate-level circulation at 560-m depth in the Arctic Ocean and Greenland Sea, as predicted by a model (Semtner in press). Convergent flow toward the shallow continental shelf allows the warm Atlantic water to rise and

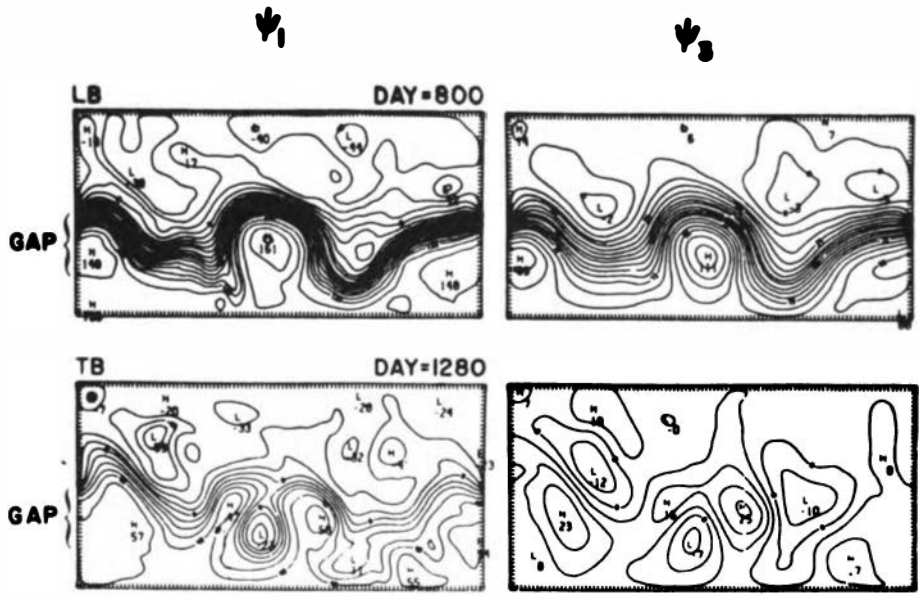


Instantaneous streamfunction patterns on selected days during the equilibrium

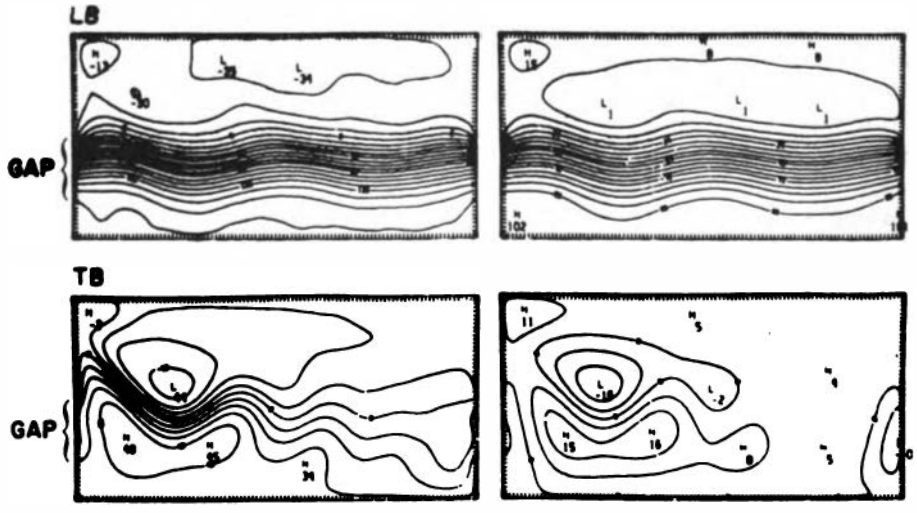


Time averaged streamfunction patterns

**Figure 6. Some results from eddy resolving simulations of the Antarctic by McWilliams et al. (1978), both for a flat bottom (LB) and for a topographic bump (TB).**

**Table 1. Diffusion Coefficients and Drake Passage Transports from Various World Ocean Simulations**

| | Cox (1975) | Washington et al. (1980) | Bryan et al. (1975) | Meehl et al. (1982) | Han and Gates (Unpublished Manuscript) |
|---|---|---|---|---|---|
| $A_H$ | $10^3$ m$^2$ s$^{-1}$ | $2 \times 10^4$ | $2.5 \times 10^3$ | $2 \times 10^3$ | $2 \times 10^3$ |
| $A_M$ | $0.8 \times 10^5$ m$^2$ s$^{-1}$ | $10^6$ | $0.8 \times 10^6$ | $10^6$ | $0.8 \times 10^6$ |
| $\Delta\psi$ | 186 m$^3$ s$^{-1}$ | 50 | 22 | 105 | 85 |

flow onto the shelf. Figure 10b shows a local maximum predicted by the model in the temperature field at 175 m at the mouth of the Kara Sea. This behavior is consistent with observations (Hanzlick and Aagaard 1980). Thus, the intrusion of an intermediate-water mass onto the continental shelf appears to be properly modeled. Cyclonic wind forcing in this area is similar to that near the Antarctic continental shelves.

Table 2 outlines a plan for modeling the response of the Antarctic Ocean to $CO_2$ increase, based on some of the previous considerations. The plan is computationally feasible at the present time, and it should lead to meaningful qualitative insights into the West Antarctic response. More quantitative model simulations could be designed on the basis of the results obtained, using improved parameterizations and more realistic forcing and geometry.

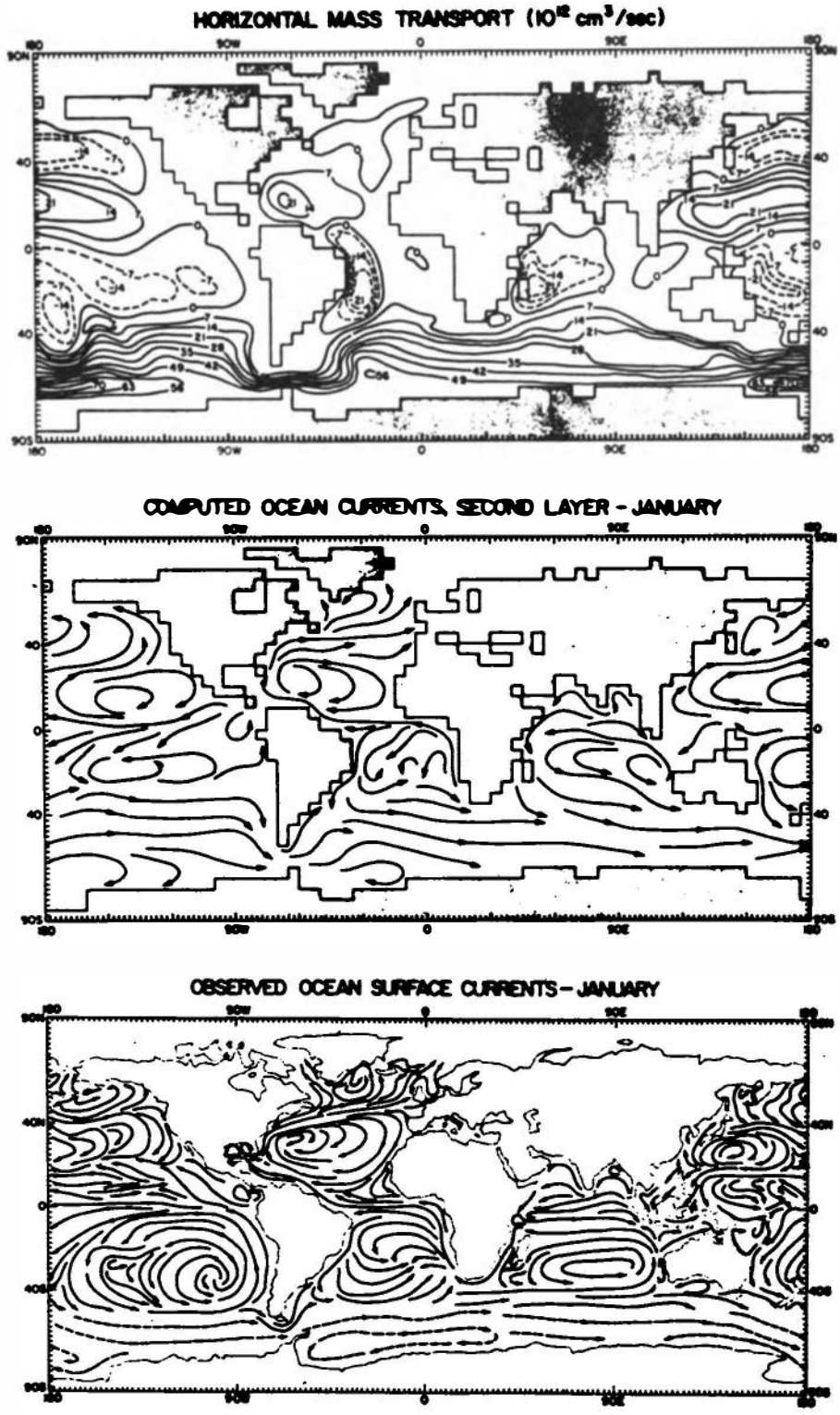


**Figure 7. Some results from coarse grid simulation of Washington et al. (1980).**

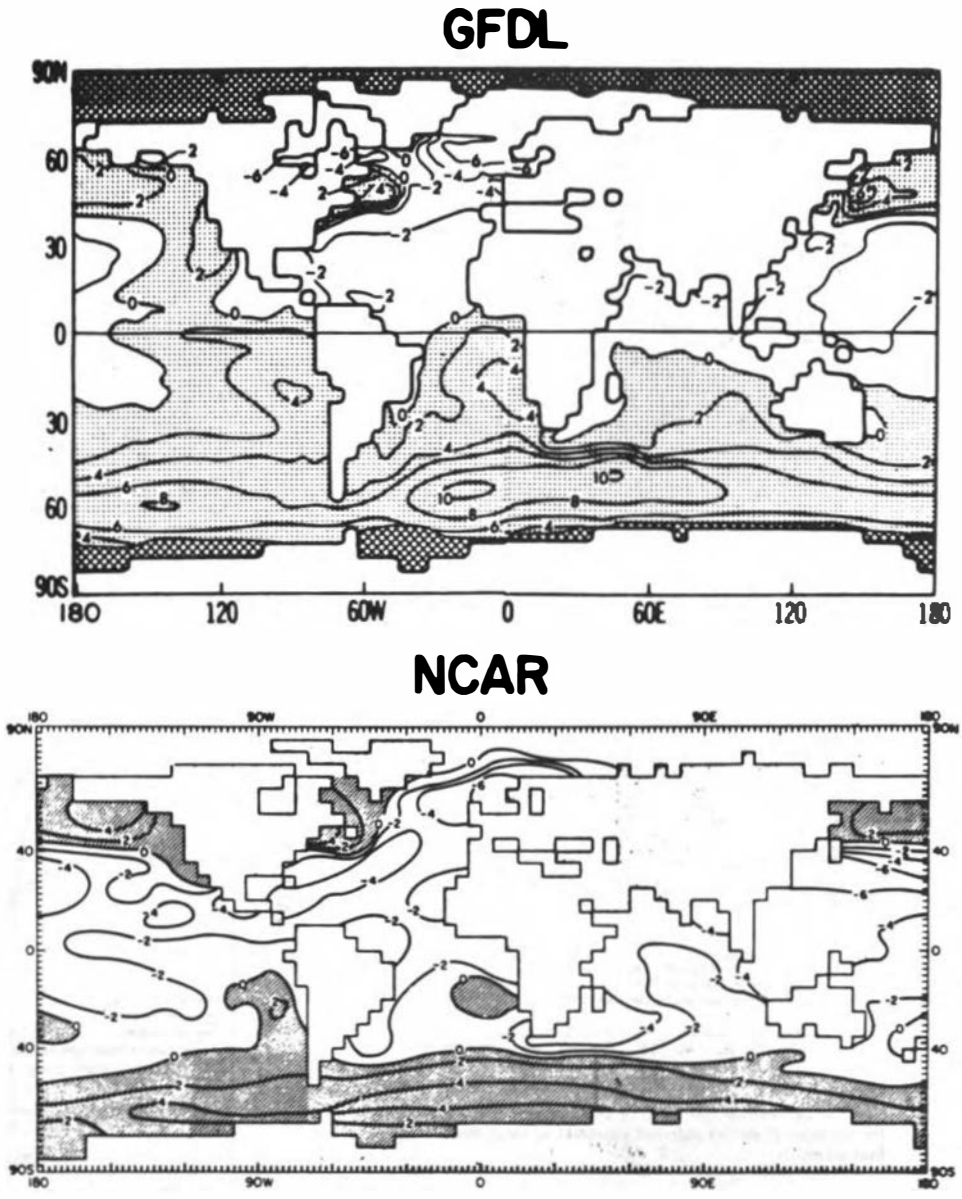


**Figure 8. Annual average SST differences (computed minus observed from coupled model studies at GFDL and at NCAR. (From Washington et al. 1980.)**

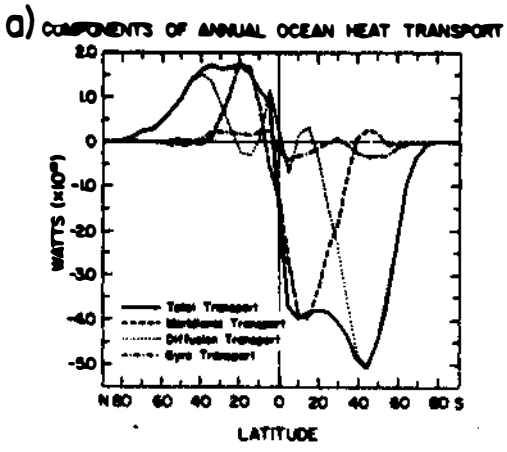


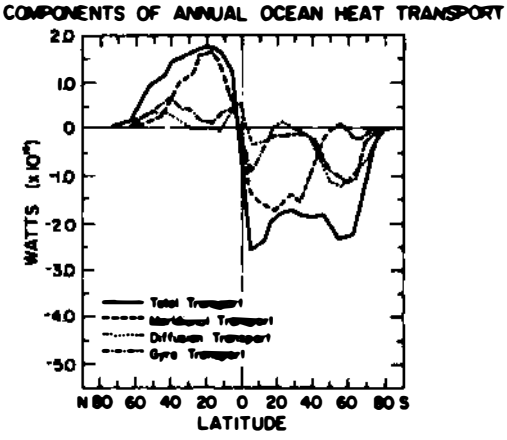


Annual mean zonally averaged ocean model heat transport for the decreased heat diffusion experiment.

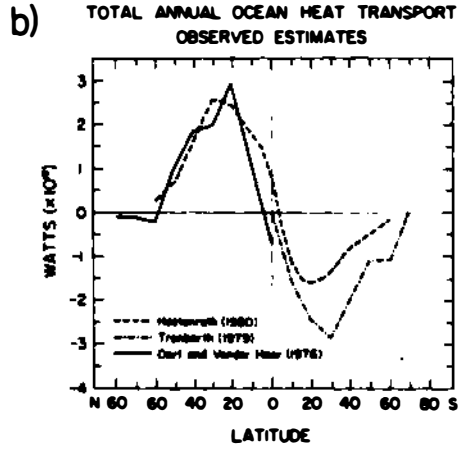


(a) Annual mean zonally averaged ocean heat transport for the basic case; (b) observed estimates of total annual ocean heat transport.

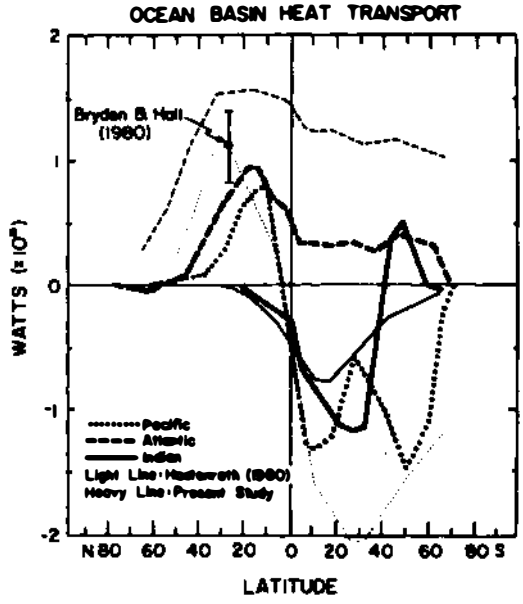


Meridional circulation component of heat transport from ocean model (decreased heat diffusion experiment) for each ocean basin, and observed estimates of net ocean basin heat transport from Hastenrath (1980).

**Figure 9. Aspects of oceanic heat transport from studies with models and observations. (From Meehl et al. 1982).**

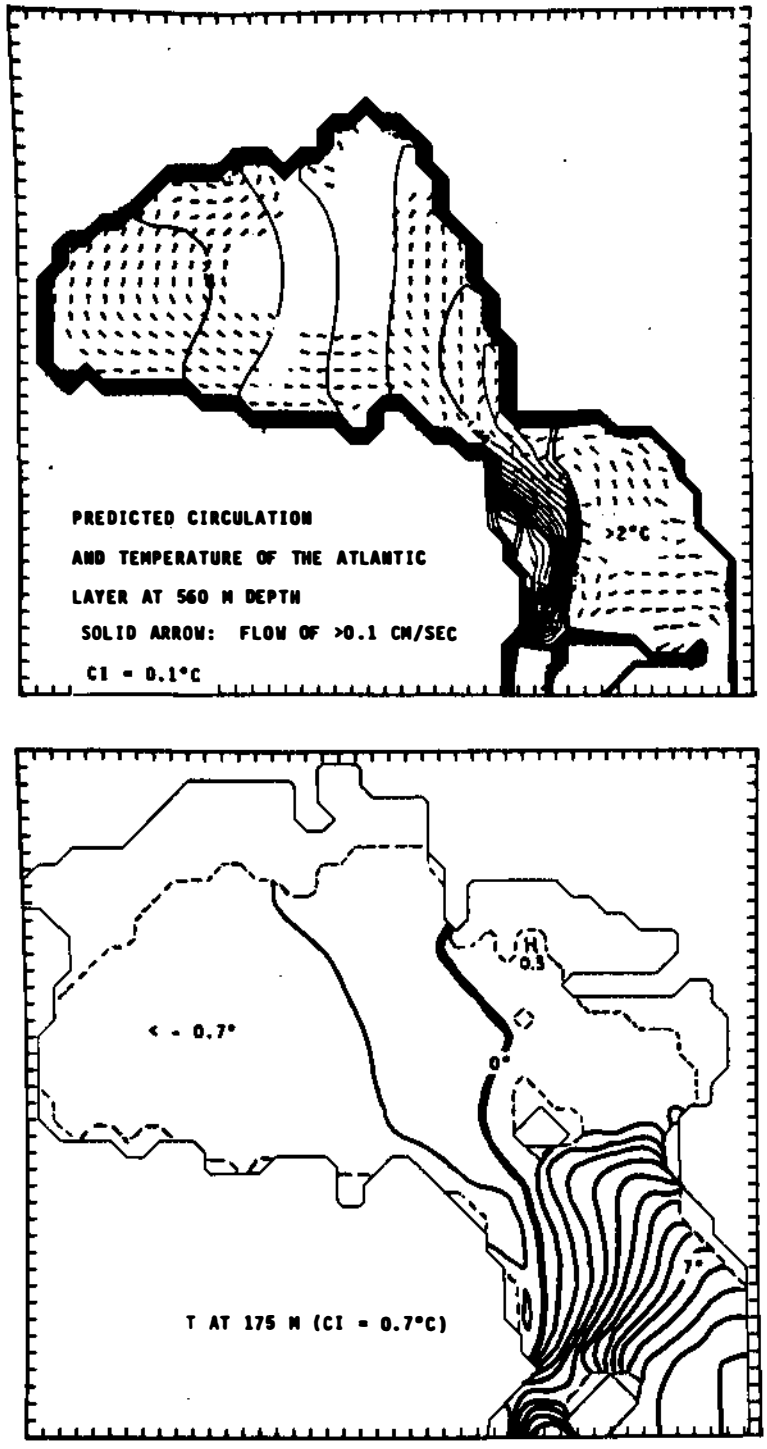


**Figure 10. An Arctic simulation of the penetration of warm intermediate water onto the continental shelf in the Kara and Barents seas. (From Semtner in press.)**

**Table 2. Plan for Modeling the Response of the Antarctic Ocean to $CO_2$ Increase**

| | |
|---|---|
| (i) | Begin with a regional model having intermediate grid size (100 km). |
| (ii) | Parameterize eddy effects as suggested by eddy resolving QG studies: $A_H$, $A_M$, $K_M$. |
| (iii) | Allow $K_H$ to depend on N and Ri. |
| (iv) | Use primitive equations with prognostic temperature and salinity and the nonlinear equation of state. |
| (v) | Specify idealized geometry but not zonal symmetry. Provide adequate vertical resolution ($\geq$ 10 levels). |
| (vi) | Include indented deep continental shelf (Weddell Sea), partially blocked channel (Drake Passage), and topography (Scotia Ridge). |
| (vii) | Prescribe seasonally varying, zonally symmetric wind forcing. |
| (viii) | Idealize the treatment of surface energy fluxes. |
| (ix) | Include thermodynamic-dynamic ice cover and (melting) ice shelf. |
| (x) | Specify NADW temperature and transport in some fashion. |
| (xi) | Try to reproduce known aspects of the general circulation (especially AABW formation and ACC transport). |
| (xii) | Consider effect of increased surface heating and precipitation (ala Gordon). |
| (xiii) | Consider effect of reduced NADW transport (ala Rooth). |
| (xiv) | Consider effect of a change in wind forcing. |

## REFERENCES

Bentley, C., 1983. The West Antarctic Ice Sheet: diagnosis and prognosis. In Proceedings, Carbon Dioxide Research Conference (pp. IV.3-IV.50). National Technical Information Service, U.S. Department of Commerce, Springfield, Virginia.

Bryan, K., S. Manabe, and R. C. Pacanowski, 1975. A global ocean-atmosphere climate model. Part II. The oceanic circulation. Journal of Physical Oceanography, 5, 30-46.

Bryden, H. L., 1979. Poleward heat flux and conversion of available potential energy in Drake Passage. Journal of Marine Research, 37, 1-22.

Cox, M. D., 1975. A baroclinic numerical model of the world ocean: preliminary results. In Numerical Models of Ocean Circulation (pp. 107-120). National Academy of Sciences, Washington, D.C.

Foster, T. D. and E. C. Carmack, 1976. Frontal zone mixing and Antarctic Bottom Water formation in the southern Weddell Sea. Deep-Sea Research, 23, 301-317.

Gordon, A. L., 1971. Oceanography of Antarctic waters. In J. Reid (ed.), Antarctic Oceanology, 1 (pp. 169-203). Antarctic Research Series, vol. 15. American Geophysical Union, Washington, D.C.

Gordon, A. L., 1983. Comments about the ocean role in the Antarctic glacial ice balance. In Proceedings, Carbon Dioxide Research Conference (pp. IV.75-IV.86). National Technical Information Service, U.S. Department of Commerce, Springfield, Virginia.

Han, Y.-J. and W. L. Gates, 1984. Preliminary analysis of the Performance of the OSU six-level oceanic general circulation model. Part II. A baroclinic experiment. Submitted to Dynamics of Atmosphere and Oceans.

Hanzlick, D. and K. Aagaard, 1980. Freshwater and Atlantic water in the Kara Sea. Journal of Geophysical Research, 85, 4937-4942.

Jacobs, S. S., A. L. Gordon, and J. L. Ardai, Jr., 1979. Circulation and melting beneath the Ross Ice Shelf. Science, 203, 439-443.

Levitus, S., 1982. Climatological Atlas of the World Ocean. NOAA Professional Paper 13 (173 pp.). U.S. Department of Commerce, Rockville, Maryland.

Manabe, S. and R. J. Stouffer, 1980. Sensitivity of a global climate model to an increase of $CO_2$ concentration in the atmosphere. Journal of Geophysical Research, 85, 5529-5554.

McWilliams, J. C., W. R. Holland, and J. H. S. Chow, 1978. A description of numerical Antarctic circumpolar currents. Dynamics of Atmosphere and Oceans, 2, 213-291.

Meehl, G. A., W. M. Washington, and A. J. Semtner, 1982. Experiments with a global ocean model driven by observed atmospheric forcing. Journal of Physical Oceanography, 12, 301-312.

Rooth, C., 1982. Hydrology and ocean circulation. Progress in Oceanography, 11, 131-149.

Semtner, A. J., Jr., in press. The climatic response of the Arctic Ocean to Soviet river diversions. Climatic Change.

Washington, W. M., A. J. Semtner, Jr., G. A. Meehl, D. J. Knight, and T. A. Mayer, 1980. A general circulation experiment with a coupled atmosphere, ocean, and sea ice model. Journal of Physical Oceanography, 10, 1887-1908.

ATTACHMENT 11

# POTENTIAL EFFECT OF $CO_2$ WARMING ON SUB-ICE-SHELF CIRCULATION AND BASAL MELTING

D. R. MacAyeal
University of Chicago

## INTRODUCTION: TWO CIRCULATION MODES

Melting below both the Ross and Ronne-Filchner ice shelves may result from the ocean circulation's having two parts, with each part ventilating separate portions of the respective sub-ice-shelf cavities (S. S. Jacobs and R. G. Fairbanks, unpublished manuscript, 1983). This viewpoint, although reflecting a considerable degree of speculation, arises from an observational water-mass census of both the Ross and Weddell seas (see S. S. Jacobs and R. G. Fairbanks, unpublished manuscript, 1983, for a detailed review), suggesting that flow below the ice shelves is divisible into two separate hydrographic and geochemical categories. The input and output water masses comprising one category are distinct from those comprising the other category because they occupy a different level of the water column and, therefore, are associated with basal melting below a different ice-shelf section. This distinction motivates the two-part-circulation hypothesis; however, current-meter data are still required for verification and to reveal the governing dynamics.

The deep mode of sub-ice-shelf circulation is characterized by S. S. Jacobs and R. G. Fairbanks (unpublished manuscript, 1983) as follows: (a) penetration of high-salinity bottom water (the Ross Sea version is called high-salinity shelf water, and the Weddell Sea version is called western shelf water) into the seafloor depressions below the ice shelves; (b) basal melting in areas far from the ice front, where this dense water mass (having a temperature several tenths of a degree Celsius above the basal melting point) is in contact with the ice-shelf base; and (c) outflow of a melt-laden offspring water mass (referred to as deep-ice-shelf water (DISW) by Jacobs and Fairbanks) at depths generally in excess of 400 m. Basal melting associated with this circulation may be restricted to approximately 10 percent of the total ice-shelf area closest to the grounding ice line and is expected to be between 0.05 and 0.5 m $year^{-1}$. Figures 1 and 2 display the dispositions of high-salinity bottom water and DISW as observed along the ice fronts of the Ross and the Ronne-Filchner ice shelves, respectively.

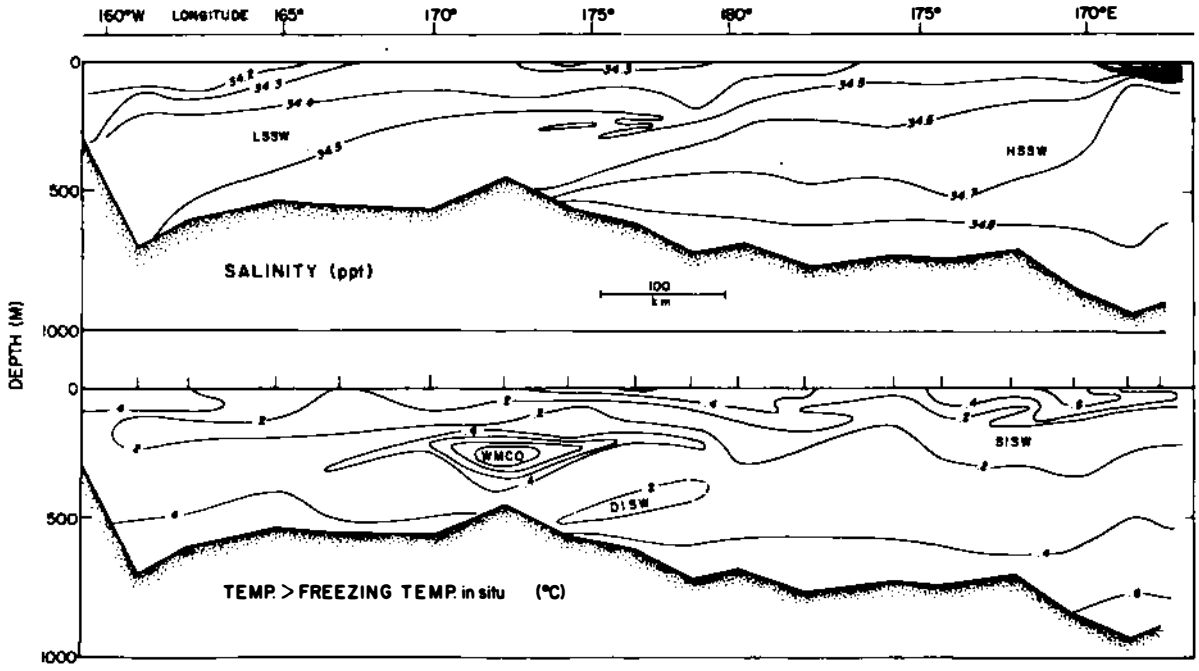


**Figure 1. Salinity and temperature (relative to the in situ freezing point) are plotted along the ice front of the Ross Ice Shelf. The deep mode of circulation consists of inflow of high-salinity shelf water (HSSW) and outflow of deep-ice-shelf water (DISW). The shallow mode of circulation consists of inflow of warm core water (WMCO) and outflow of shallow-ice-shelf water (SISW). (From Figure 6C of S. S. Jacobs and R. G. Fairbanks, unpublished manuscript, 1983.)**

The shallow mode of sub-ice-shelf circulation is characterized by Jacobs and Fairbanks as follows: (a) penetration of warm, offshore water (derived from circumpolar deep water) into sections of the sub-ice-shelf cavity having shallow ice-shelf draft; (b) melting near the ice front (meltwater derived from this warm, offshore water mass is observed below the Ross Ice Shelf at J9, but basal freezing conditions at J9 suggest that this meltwater is advected from melting sites closer to the ice front); and (c) outflow of a melt-laden offspring water mass (referred to as shallow-ice-shelf water by Jacobs and Fairbanks) at shallow depth. Basal melting associated with this mode of circulation is expected to be between 0.5 and 1.0 m/year over the 10-25 percent of the ice-shelf area closest to the ice front. As displayed in Figures 1 and 2, the inflowing is confined to cores of maximum temperature; thus, it is commonly called warm core water (WMCO) (S. S. Jacobs and R. G. Fairbanks, unpublished manuscript, 1983).

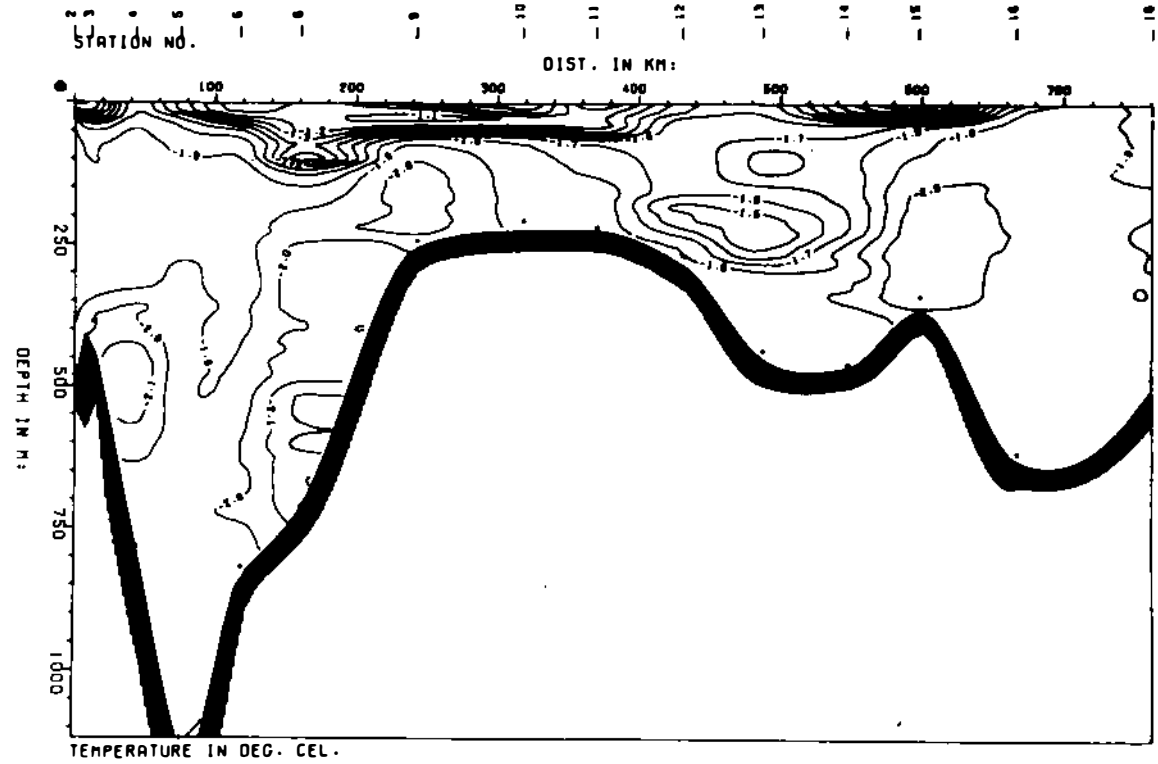


**Figure 2. Salinity and temperature plotted along the ice front of the Ronne-Filchner Ice Shelf. Characteristic water masses similar to those in Figure 1 are indicated. (From Gammelsrod and Slotsvik 1981.)**

## EVOLUTION OF WATER MASS DEDUCED FROM OXYGEN-ISOTOPE RATIOS

By far the most convincing evidence of the two modes of circulation comes from geochemical observations in the Ross and Weddell seas (S. S. Jacobs and R. G. Fairbanks, unpublished manuscript, 1983; Weiss et al. 1979). Glacial ice derived from snowfall at the surface of the West Antarctic Ice Sheet has an $H_2\,^{18}O/H_2\,^{16}O$ ($\delta d^{18}O$) ratio ranging between -35 and -45 percent. Thus, the composition of any given water mass will evolve predictably in response to dilution by fresh and isotopically light meltwater. Figure 3 indicates how the salinity and $d^{18}O$ of high-salinity shelf water (HSSW) and WMCO are altered to form DISW and shallow-ice-shelf water (SISW) by basal melting below the Ross Ice Shelf. The fact that SISW and DISW lie approximately within the composition envelopes attainable by glacial melting from the two respective parent water masses is the best evidence for two circulation modes.

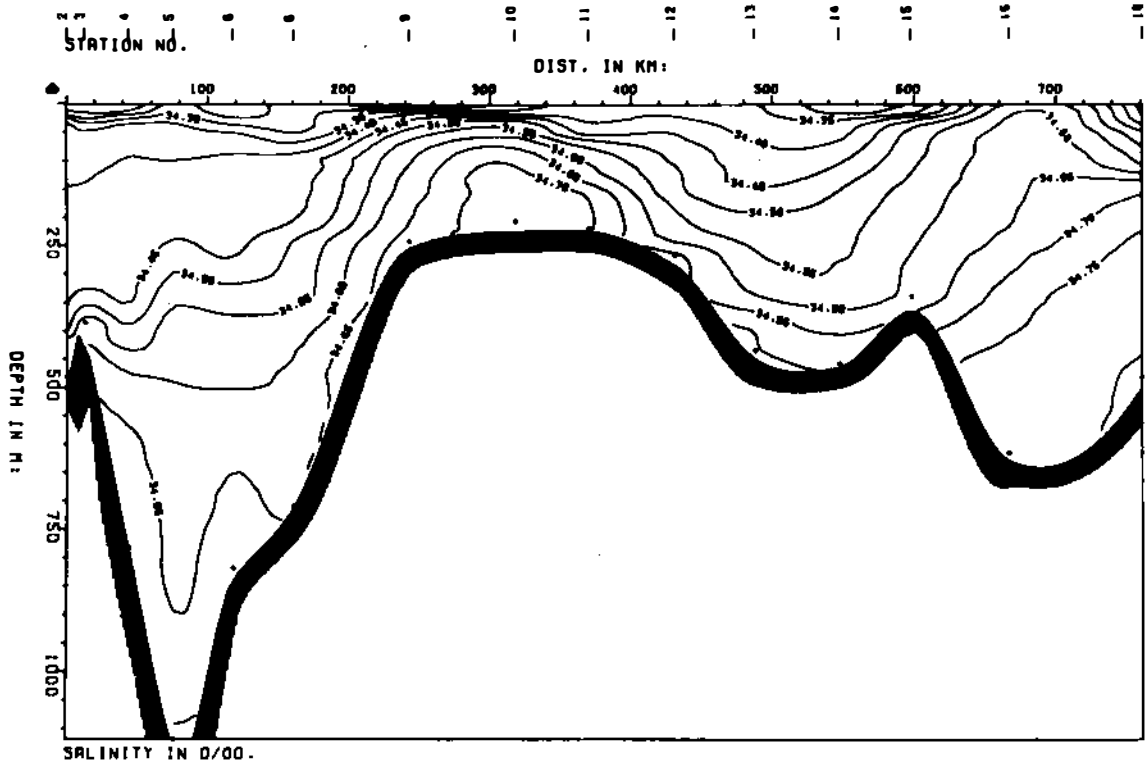


**Figure 2. (continued)**

## CONTRIBUTION OF MODELING

Numerical simulations to date have been of limited use in determining the characteristics and causes of sub-ice-shelf circulation simply because relatively little effort has been devoted to this problem. Killworth (1974), for example, has investigated a high-salinity bottom-water formation in the Ross and Weddell seas by employing a two-level model of geostrophic flow forced by the heat and salt budgets. He concluded, as did Gill (1973), that offshore advection of sea ice in winter amplifies the sea surface salt flux near the coasts and allows deep convection sufficient to produce high-salinity bottom water from 5 to 10 times in excess of its estimated demand below the ice shelves (MacAyeal 1983).

More recently, MacAyeal (1983) conducted a numerical investigation of the ocean tides below the Ross Ice Shelf. The two most promising results from his analysis are that (a) tidal fronts may form below ice-shelf sections having high draft, where DISW is presumed to originate, and (b) tidally driven barotropic circulation (tidal rectification) occurs at the ice-front site where WMCO is observed entering the sub-ice-shelf cavity.

MacAyeal's (1983) investigation of tidal-front formation was motivated by Gill's (1973) hypothesis that (a) stratification suppresses basal melting, and (b) erosion of stratification by strong

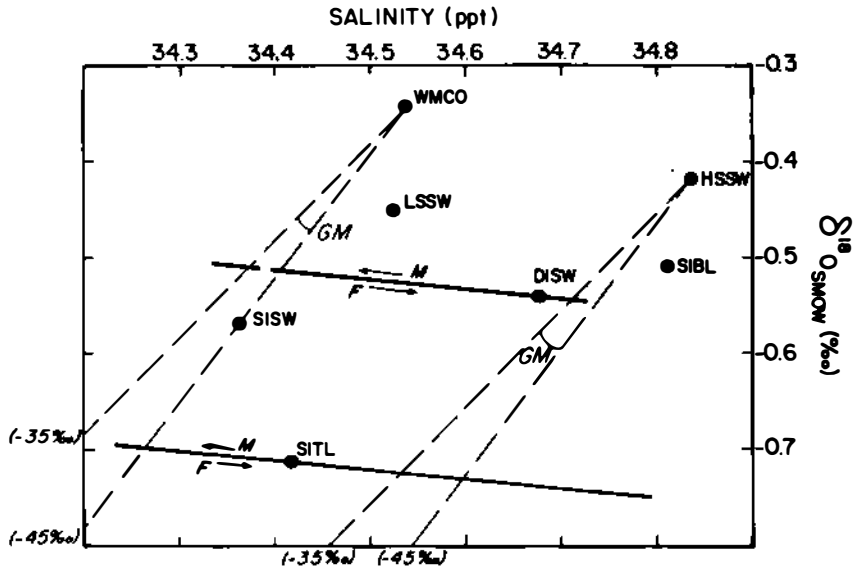


**Figure 3. The production of SISW and DISW (see Figure 1) from WMCO and HSSW by basal melting is displayed on this diagram of observed salinity versus $H_2{}^{18}O/H_2{}^{16}O$ ratio. The envelopes labeled GM represent the water-mass properties attainable by basal melting from input WMCO and HSSW. The solid lines approximately parallel to the salinity axis represent alternations by freezing and remelting of basal sea ice. (From Figure 6C of S. S. Jacobs and R. G. Fairbanks, unpublished manuscript, 1983.)**

vertical mixing is necessary to catalyze basal melting. Gill's hypothesis is supported by the observed hydrography below the Ross Ice Shelf at J9 shown in Figure 4. The available oceanic heat below J9 is isolated from the ice-shelf base by an intervening layer of cold but fresh meltwater. Strong tides observed in the southern Ross Sea (Williams and Robinson 1980) suggest that tidally induced vertical mixing can erode sub-ice-shelf stratification sufficiently to catalyze basal melting.

As shown in Figure 5, MacAyeal (1983) found that a completely well-mixed water column could be maintained near the grounding line in the southeastern part of the sub-ice-shelf cavity. Tidal fronts of the sort commonly observed in the shallow seas off northwestern Europe (Fearnhead 1975) are expected to separate the zones of vertical homogeneity from the zones of strong stratification. The important result of this numerical prediction is that the zones of strong vertical mixing correspond with sections of the sub-ice-shelf cavity where DISW is presumed to originate. MacAyeal (1983), therefore, speculates that the deep mode of circulation and conversion of high-salinity bottom water into DISW is ultimately driven by strong tidally induced vertical mixing and melting along the grounding line of the West Antarctic Ice Sheet.

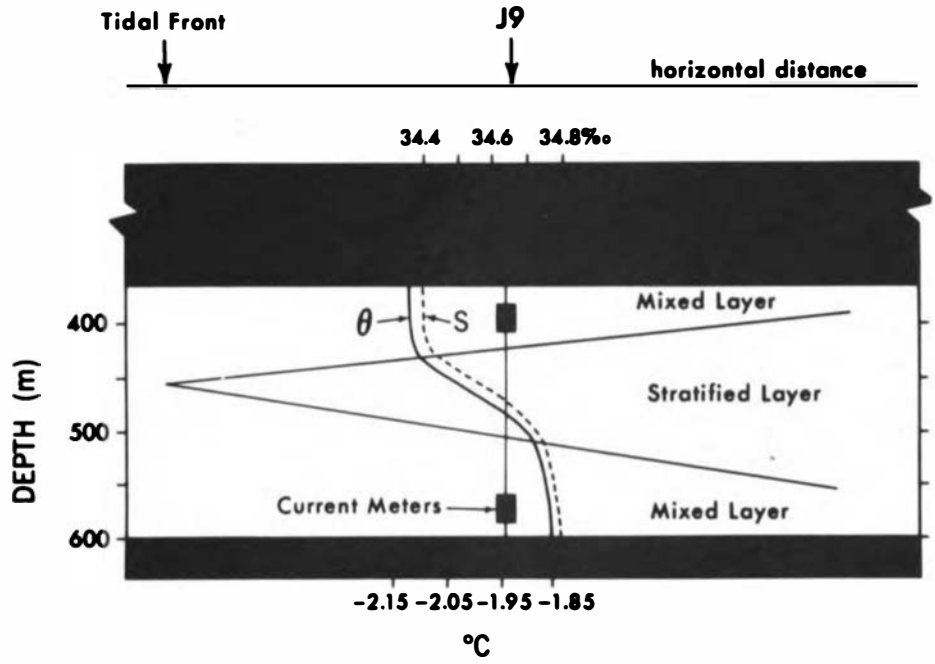


**Figure 4. The observed temperature (θ) and salinity (S) profiles below the Ross Ice Shelf at the J9 drill camp. (From MacAyeal 1983.)**

Figure 6 displays the cross-ice-front penetration of imaginary tracers resulting from the tidal rectification simulated in MacAyeal's (1983) study. Although the rate of penetration is insufficient to explain the shallow mode of sub-ice-shelf circulation, the observed inflow of WMCO corresponds with the site of strongest simulated sub-ice-shelf inflow just northwest of Roosevelt Island.

## POTENTIAL $CO_2$-INDUCED CHANGES

It is beyond the scope of this paper to present a detailed projection of how sub-ice-shelf circulation and basal melting might be altered by increased levels of atmospheric $CO_2$. The basic strategy of this projection, however, may be summarized by the following question: How will the two modes of sub-ice-shelf circulation respond to sea surface warming?

Under present conditions the deep mode of circulation is buffered from summer changes in sea surface temperature because the inflowing high-salinity bottom water is formed in winter and, therefore, is constrained to have the sea surface freezing temperature (only several tenths of a degree Celsius warmer than the melting temperature of the ice-shelf base). For $CO_2$ to alter the deep mode of circulation, the winter production of sea ice and the subsequent deep convection required to form high-salinity bottom water must be reduced dramatically.

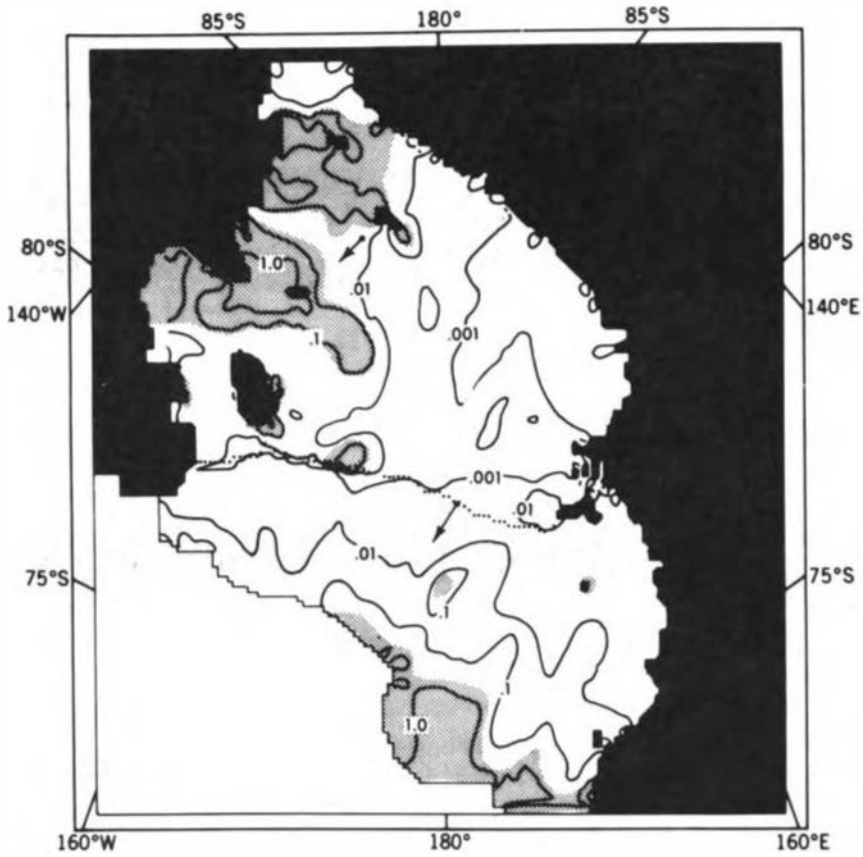


**Figure 5. Shaded regions indicate where tidal-energy dissipation is expected to cause vertically well-mixed waters. Unshaded regions indicate where stratification characterized by warm and salty water at the sea bed and cold meltwater at the ice-shelf base will suppress basal melting. Contours represent the minimum basal melting rate expected to define the position of the tidal fronts separating vertically well-mixed waters from stratified waters. Sensitivity of this position to error of the 0.05-m/year melt-rate criterion is reduced by the steepness of the minimum melt-rate gradient along the Siple Coast. The well-mixed regions predicted near the ice front and in the open part of the Ross Sea are probably incorrect because of larger basal melting rates or other sea surface bouyancy fluxes. (From MacAyeal 1983.)**

The shallow mode of circulation may increase its vigor in response to $CO_2$ warming if the southward flux of WMCO is augmented. This increase is plausible because, under present conditions, the flux may be controlled by heat losses to the atmosphere during transit across the open Ross and Weddell Seas. Warming the sea surface may reduce subsurface cooling and allow more, or warmer, WMCO to reach the ice fronts from the continental slope.

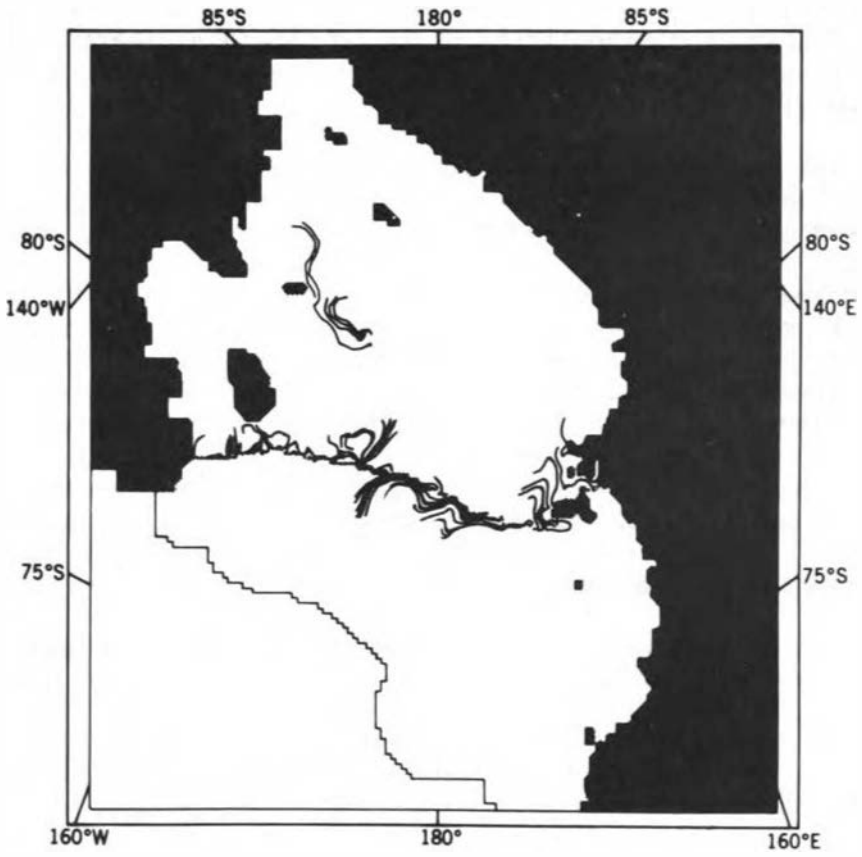


Figure 6. Tracer streak lines emitted from the ice front display how tidal rectification ventilates the sub-ice-shelf cavity. After 3 years of advection by the simulated Lagrangian-mean flow, tracers have penetrated farthest into the sub-ice-shelf cavity near the rectification site northwest of Roosevelt Island and through McMurdo Sound. Heat transport associated with the indicated water-parcel movement will cause approximately 0.5 $\pm$ 0.25 m/year basal melting in the regions penetrated by the tracer trajectories (this region comprises 10 percent of the total ice-shelf area). Hydrographic observations in the open Ross Sea indicate the presence of thermohaline circulation with areas of sub-ice-shelf inflow and outflow. This suggests that the tidally driven barotropic circulation may select sites of strong thermohaline flow associated with basal melting. (From MacAyeal 1983.)

## FUTURE RESEARCH PRIORITIES

It is unnecessary to emphasize the strong need for more observations on sub-ice-shelf circulation, so the following list of recommended priorities will concentrate on numerical modeling. Future modeling requirements may be separated into three categories: process-oriented modeling, interaction-oriented modeling, and climate-oriented modeling.

Process-oriented modeling is designed to focus on circulations and forcing mechanisms individually in order to obtain a clearer knowledge of underlying dynamics. Recommended modeling efforts of this type should include:

1. Investigation of the oceanic fronts at the margins of the continental shelf and the tidal fronts below the ice shelves;
2. Investigation of the dynamic constraints imposed by the ice fronts;
3. Renewed investigation of the production mechanism of high-salinity bottom water;
4. Investigation of basal sea-ice deposition on the ice shelves in nonmelting areas to better understand the isotopic composition of basal ice and the isotopic evolution of sub-ice-shelf water masses.

Interaction-oriented modeling focuses on the ensemble of physical processes operating in the ocean around West Antarctica in order to determine how they compete and which are most important. Recommended modeling efforts of this type include:

1. Development of a primitive-equation ocean model capable of resolving baroclinic motions on the continental shelves and able to treat ice-shelf topography;
2. The primitive-equation ocean model should be used to investigate the seasonal cycle as well as interannual variability;
3. This model should be coupled with a sea-ice model.

Climate-oriented modeling is designed to project the way that the ice-ocean-atmosphere system will respond to increased anthropogenic $CO_2$ production. Three tasks may be identified:

1. Determine which atmospheric and oceanographic variables control the ice shelves and ice sheets;
2. Run coupled ocean/ice, shelf/atmosphere models to project $CO_2$ warming scenarios;
3. Predict (for the purpose of recommending observational monitoring programs) which components of the West Antarctic oceanic system will exhibit the greatest initial and overall response to $CO_2$ warming.

## CONCLUSION

In his assessment of potential changes in the West Antarctic Ice Sheet induced by $CO_2$ warming, Bentley (1983) remarked: "Accelerated bottom melt appears to be by far the most likely mechanism by which climatic warming could affect the ice sheet rapidly.... Unfortunately, little is known about how to predict changes in ocean temperature and circulation underneath the [ice shelves].... This complex point is a critical weakness in our present ability to predict quantitatively the response of the West Antarctic Ice Sheet to $CO_2$-induced temperature

change." Bentley's assessment correctly summarizes the present scientific progress on sub-ice-shelf circulation. Progress is anticipated, however, as a result of relatively straightforward, yet previously untried, numerical modeling experiments that will accompany a growing set of observations.

## REFERENCES

Bentley, C. R., 1983. The West Antarctic Ice Sheet: diagnosis and prognosis. Proceedings, Carbon Dioxide Research Conference (pp. IV.3-IV.50). National Technical Information Service, U.S. Department of Commerce, Springfield, Virginia.

Fearnhead, P. G., 1975. On the formation of fronts by tidal mixing around the British Isles. Deep-Sea Research, 22, 311-321.

Gammelsrod, T. and N. Slotsvik, 1981. Hydrographic and current measurements in the southern Weddell Sea 1979/80. Polarforschung, 51 (1), 101-111.

Gill, A. E., 1973. Circulation and bottom water production in the Weddell Sea. Deep-Sea Research, 20, 111-140.

Killworth, P. D., 1974. A baroclinic model of motions on antarctic continental shelves. Deep-Sea Research, 21, 815-837.

MacAyeal, D. R., 1983. Rectified tidal currents and tidal-mixing fronts: controls on the Ross Ice Shelf flow and mass balance. Ph.D. thesis (287 pp.), Princeton University, Princeton, New Jersey.

Weiss, R. F., H. G. Ostlund, and H. Craig, 1979. Geochemical studies of the Weddell Sea. Deep-Sea Research, 26 (10A), 1093-1120.

Williams, R. T. and E. S. Robinson, 1980. The ocean tide in the southern Ross Sea. Journal of Geophysical Research, 85 (C11), 6689-6696.

ATTACHMENT 12

# MODELED AND OBSERVED SEA-ICE VARIATIONS IN THE WEST ANTARCTIC AND SURROUNDING REGIONS

Claire L. Parkinson
Goddard Laboratory for Atmospheric Sciences
NASA/Goddard Space Flight Center, Greenbelt, Maryland

## OBSERVATIONS

The mean latitude of the ice edge in the Southern Ocean undergoes a strong, smooth yearly cycle from its most poleward position of about 68°S in late February to its most equatorward position of about 61°S in late September, lagging the cycle of zonally averaged temperatures (60°-70°S) by about 1.5 months (Figure 1). At the winter maximum, sea ice covers roughly 20 x $10^6$ $km^2$, with the ice edge occurring between 60° and 65°S in the Bellingshausen, Amundsen, and Ross seas and between 55° and 60°S in the Weddell Sea and around much of East Antarctica. After spring and summer melt, the minimum ice coverage is roughly 4 x $10^6$ $km^2$, the bulk of the ice being in the Bellingshausen, Amundsen, Ross, and, especially, western Weddell seas (Figure 2). Typical yearly ranges for the ice coverage in the seas of the Western Hemisphere are as follows: 1-7 x $10^6$ $km^2$ for the Weddell Sea (60°W-20°E), 0.6-2.8 x $10^6$ $km^2$ for the Bellingshausen-Amundsen Sea (130°W-60°W), and 0.5-4 x $10^6$ $km^2$ for the Ross Sea (160°E-130°W).

Although the mean ice-edge position does not exhibit small-term fluctuations or interannual variability to the same extent as either the mean temperature or pressure (e.g., see Figure 1), the ice cover shows very noticeable interannual variations when viewed spatially, on a region-by-region basis. Many of these can be easily explained by atmospheric phenomena. For example, a prominent blocking high just north of the Bellingshausen Sea in July of 1973 caused warm air to be pumped into that region, leading to an unusual July retreat of the ice edge (Ackley and Keliher 1976).

Several additional recent studies further illustrate the impacts of the atmosphere on the ice, the ice on the atmosphere, or simply the concomitant changes in the respective fields (e.g., Ackley 1981; Budd 1975; Cavalieri and Parkinson 1981; Lemke et al. 1980; Parkinson and Cavalieri 1982). Significant influences of the ice on the atmosphere and oceans result from the following mechanisms: ice serves as a strong insulator, restricting exchanges of heat, mass, and momentum between ocean and atmosphere; the high albedo of ice relative to that of open ocean ensures that when ice is present there is considerably less surface absorption of solar radiation; the rejection of salt while

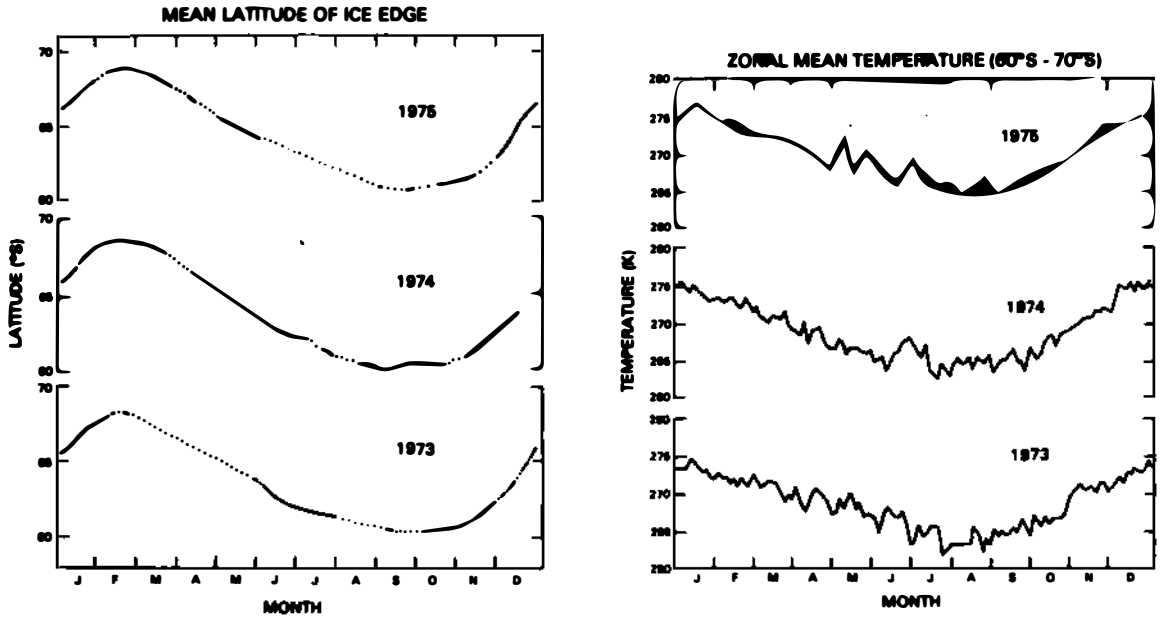


**Figure 1. Mean latitude of the Southern Ocean ice edge and zonal mean temperature across the 60°-70°S latitude band. (From Parkinson and Cavalieri 1982.)**

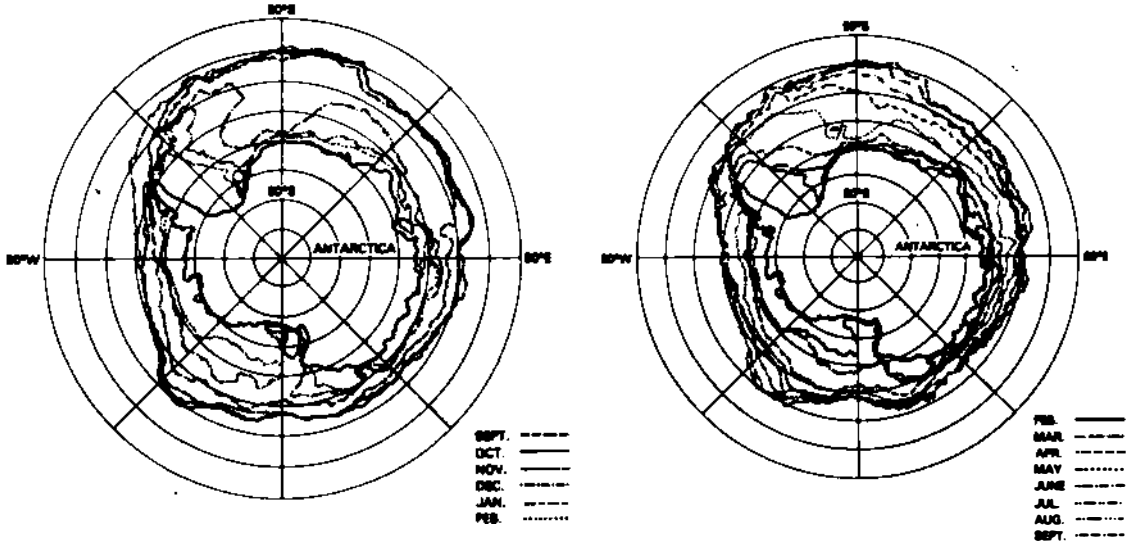


**Figure 2. Monthly ice growth and retreat in the Southern Ocean, averaged over the 4 years 1973-1976. From Nimbus 5 ESMR data (from Zwally et al. 1983a).**

ice is forming and aging contributes toward destabilizing the upper ocean, leading at times to increasing the depth of the mixed layer or to formation of bottom water.

Because of the remoteness of the Antarctic region, before the advent of satellite imagery in the late 1960s there was little possibility of detailed and consistent observational coverage of the Southern Ocean sea ice. What data existed on the large scale tended to be heavily interpolated. Although there are still difficulties, the situation has much improved. Satellite data on the Antarctic sea-ice cover in the 1970s and 1980s have included visible data from Landsat, infrared data from the TIROS N/NOAA series, and microwave data from Nimbus 5, 6, and 7. The visible and infrared data have the advantage of good spatial resolution, but the microwave data have the advantage of being unaffected by darkness or cloud cover, thereby providing the opportunity for day/night, all-season coverage. Therefore, the microwave data are probably the most appropriate for climate studies.

The most nearly complete, analyzed microwave data set covering a span of more than a few months is that compiled for the 4-year period 1973-1976 from the electrically scanning microwave radiometer (ESMR) on board the Nimbus 5 satellite. Although observations are unavailable for some months, monthly averages have been constructed for the majority of months in the 1973-1976 period (Zwally et al. 1983a). These averages reveal noticeable interannual variations in the ice cover of the West Antarctic, with the configurations of the ice covers of the Weddell, Bellingshausen, Amundsen, and Ross seas all showing significant variations from year to year. Most important, these variations are not uniform over the 4 years. For example, the winter-maximum ice area in the Ross Sea increased from 1973 to 1975, then decreased from 1975 to 1976, while the winter-maximum ice area in the Weddell Sea decreased from 1973 to 1974 and from 1975 to 1976, and increased from 1974 to 1975.

A prime example of interannual variations in the ice cover is the occurrence and nonoccurrence of the Weddell Polynya (Figure 3). This polynya, an open-water region covering from 1 to 3 x $10^5$ $km^2$ in the midst of the sea ice off Queen Maud Land, did not exist in the Southern Hemisphere winter of 1973 but did exist in the following 3 years, its position shifting westward over time. Several studies have examined this polynya over the past several years, primary ones being by Martinson et al. (1981), who explain the polynya largely on the basis of oceanographic factors, and by Parkinson (1983), who numerically examines the impact of the wind fields.

The short length of the data set and the interannual fluctuations make it difficult to detect unambiguously any long-term trends in the West Antarctic sea-ice cover; however, some overall shifts on the order of a few years have been notable. Using weekly maps of ice coverage produced by the Navy and the National Oceanic and Atmospheric Administration (NOAA), Kukla and Gavin (1981) reported a decrease in the extent of summer Antarctic sea ice of about 2.5 x $10^6$ $km^2$ between 1973 and 1980 and suggested the possibility that $CO_2$-induced atmospheric temperature increases might be the cause of the decreases in sea ice. Although emphasizing summer, Kukla and Gavin also show a

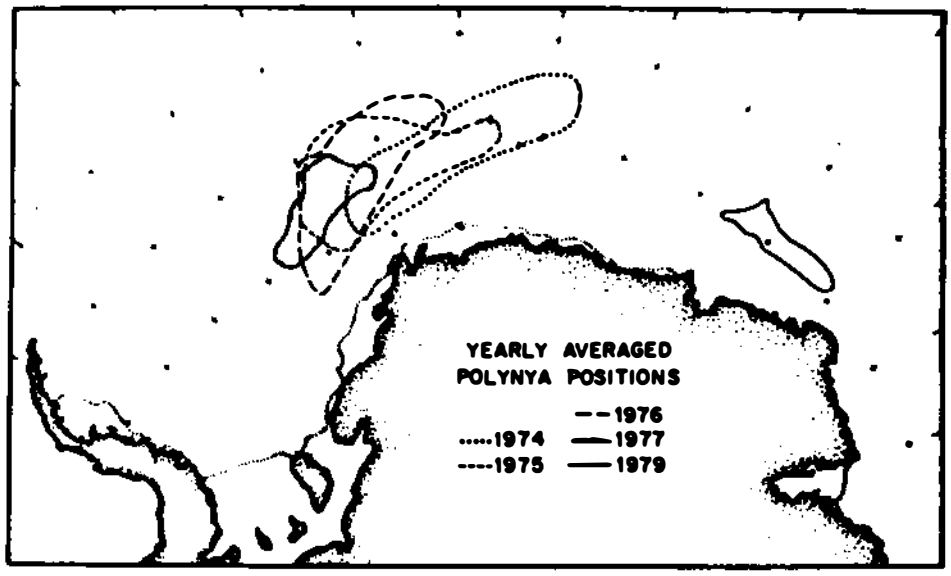


Figure 3. Average shape and position of the Weddell Polynya, 1974-1979. (Modified from Martinson et al. 1981.)

comparable decrease in the 12-month running mean (Figure 4). Such a dramatic decrease in the sea-ice cover can easily be overinterpreted. A longer data record shows that the decrease in the mid-1970s was both preceded and succeeded by periods of sea-ice increases (Figures 5 and 6), so that there is not yet any definitive evidence for a $CO_2$-induced temperature rise in the observations of the Southern Ocean sea ice (Zwally et al. 1983b).

## MODELING

Efforts at modeling the sea ice of the Southern Ocean have not been as numerous as those concerned with the Arctic and, in general, have been contained in studies that considered the Arctic and Antarctic jointly or that used models originally developed for the Arctic. Specifically, the thermodynamic calculations have derived in large part from the detailed one-dimensional (vertical) sea-ice calculations of Maykut and Untersteiner (1971) for the central Arctic and the simplification of those calculations by Semtner (1976). These calculations center on balancing incoming and outgoing energy fluxes at the air/snow, snow/ice, and ice/water interfaces. The fluxes included are solar radiation, incoming and outgoing longwave radiation, sensible and latent heat, conduction through the ice and snow layers, an ocean heat flux, and the absorption and emission of energy due to the change of state between ice and water.

The calculations of ice dynamics have similarly followed the efforts of Campbell (1964), the various modelers of the Arctic Ice Dynamics Joint Experiment (Coon 1980), and Hibler (1979), all again

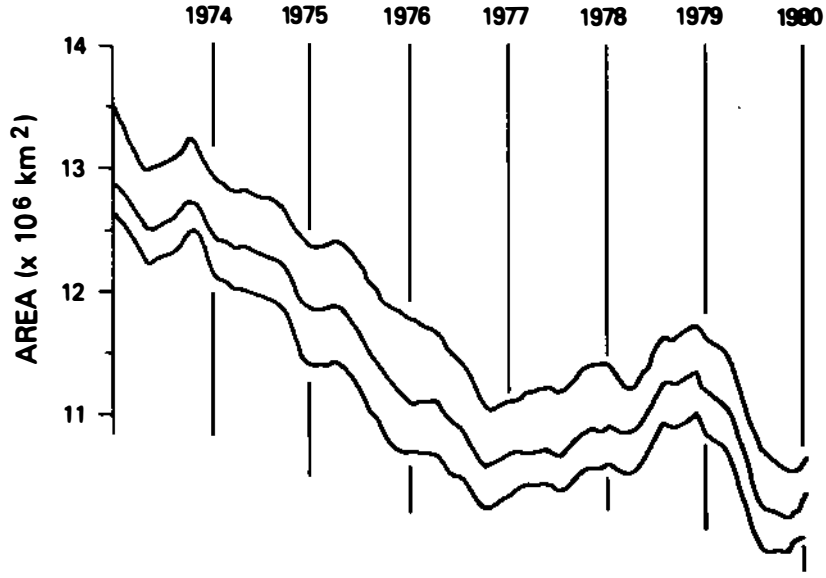


**Figure 4. Twelve-month running means of Antarctic sea-ice area, 1973-1980, for ice concentrations exceeding 1 octa (upper curve), ice concentrations exceeding 4 octas (middle curve), and the net ice area, excluding leads, polynyas, and thin dark ice (lower curve). (Redrawn from Kukla and Gavin 1981.)**

concentrating exclusively on the Arctic, and Parkinson and Washington (1979), simulating for both hemispheres. Basically, sea-ice dynamics tend to be calculated through creating a momentum balance involving the five major stresses acting on the ice: air stress, water stress, Coriolis force, dynamic topography, and internal ice resistance, with the major contrasts among the models coming in the individual formulations of those stresses.

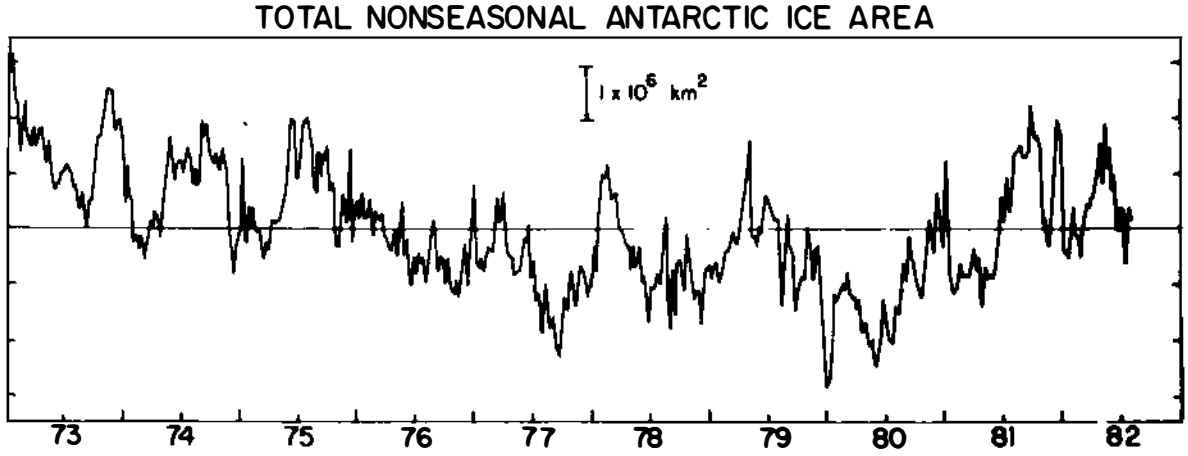


**Figure 5. Weekly departure of the Southern Ocean sea-ice area from the 1973-1982 mean for the given week. (From Chiu 1983.)**

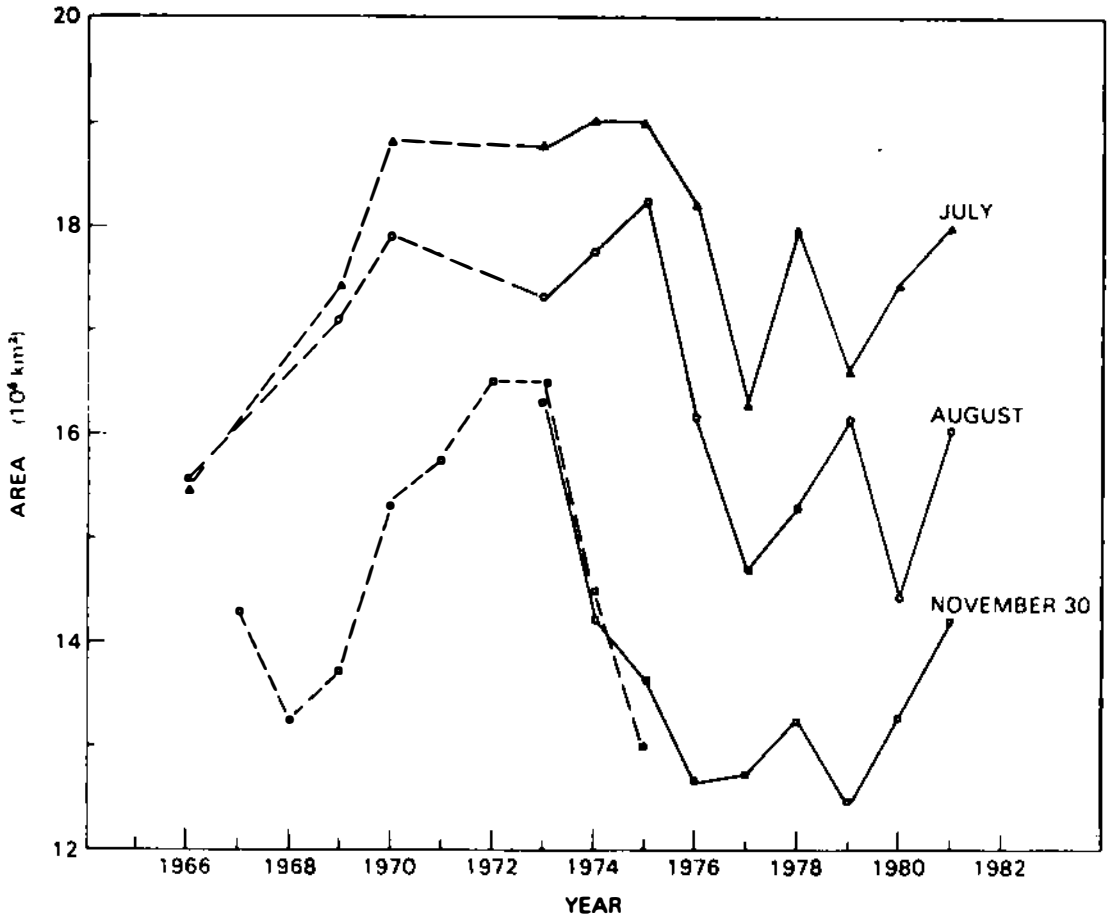


**Figure 6. July, August, and November Southern Ocean sea-ice areas from 1966 to 1982. (From Zwally et al. 1983b.)**

Since the mid-1970s, increasing attention has been paid to modeling the Antarctic ice. Pease (1974) constructed a thermodynamic model for longitude 155°E and tested it for three parameterizations of the ocean mixed layer. Washington et al. (1976) applied the Semtner (1976) one-dimensional thermodynamic calculations to full two-dimensional grids in both the Arctic and Antarctic, adding a lead parameterization based, like the ice-thickness calculations, on energy balances. Parkinson and Washington (1979) extended the Washington et al. model to include dynamics as well as thermodynamics (Figure 7). More recently, Parkinson (1983) has applied this model to examine the growth and development of the Weddell Polynya, and Parkinson and Bindschadler (1984) have applied the model to examine the impact on the Antarctic sea-ice cover of uniform atmospheric temperature increases.

In the meantime, Hibler and Ackley (1983) have applied the dynamic/thermodynamic model of Hibler (1979) to the Weddell Sea. This model employs a nonlinear viscous plastic rheology, making the calculations of ice dynamics more elaborate than those of Parkinson and Washington (1979), who incorporated internal ice resistance by

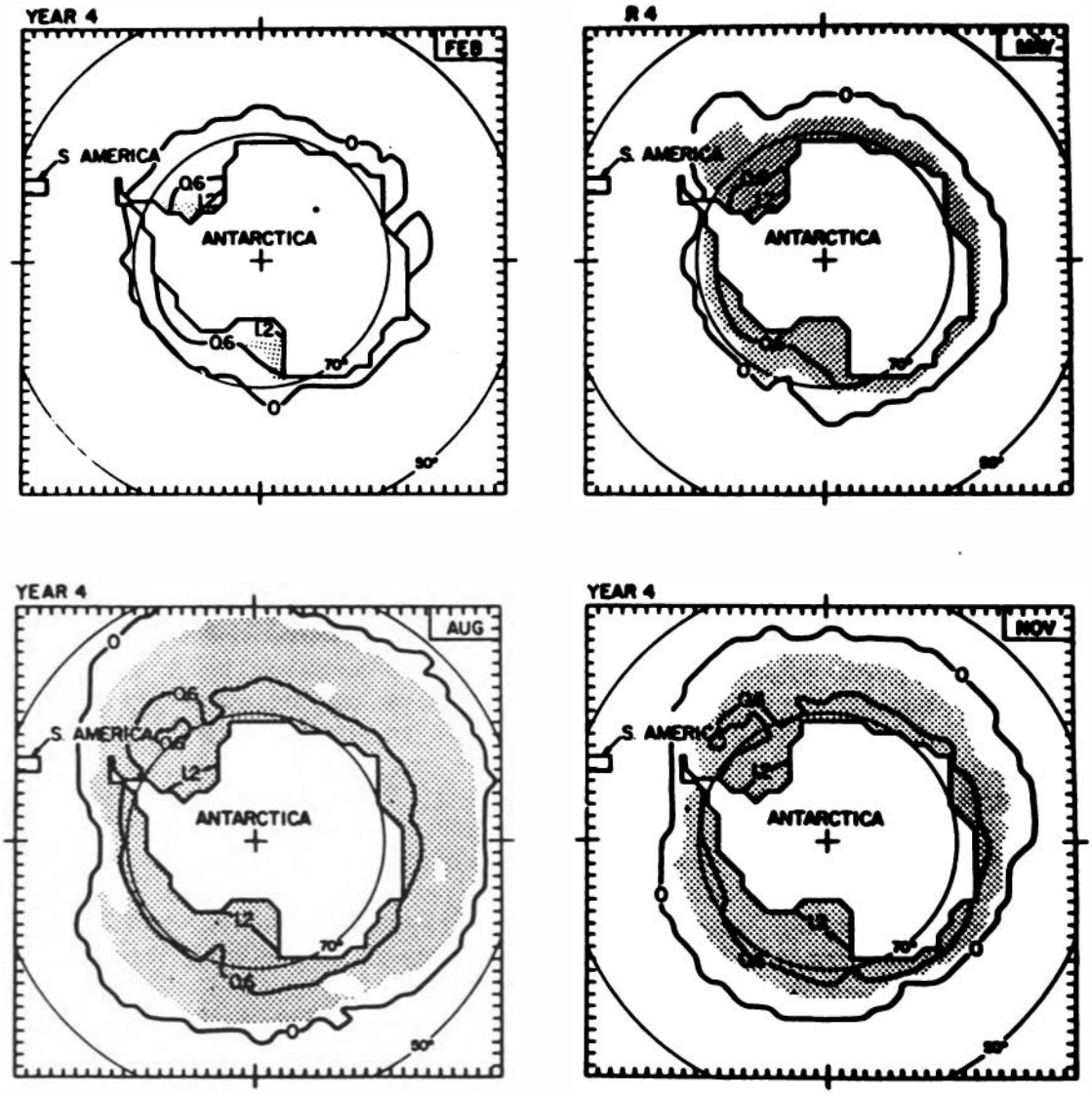


**Figure 7. Seasonal cycle of the distribution of Southern Ocean sea ice simulated by a dynamic/thermodynamic sea-ice model. Contours are ice thicknesses in meters, and stippling indicates areas of sea-ice concentration exceeding 90 percent. (Rearranged from Parkinson and Washington 1979.)**

proportionately reducing ice velocities into those grid squares where ice convergence is producing concentrations exceeding 98 percent. Hibler and Ackley find the need for dynamics in the model calculations to be strongest during the decay phase of the seasonal cycle, when the dynamics (a) move ice near the edge into warmer water and (b) increase the creation of open water within the ice pack. Both these processes enhance further ice melt. The impact of dynamics on the simulation of the seasonal cycle is illustrated in Figure 8.

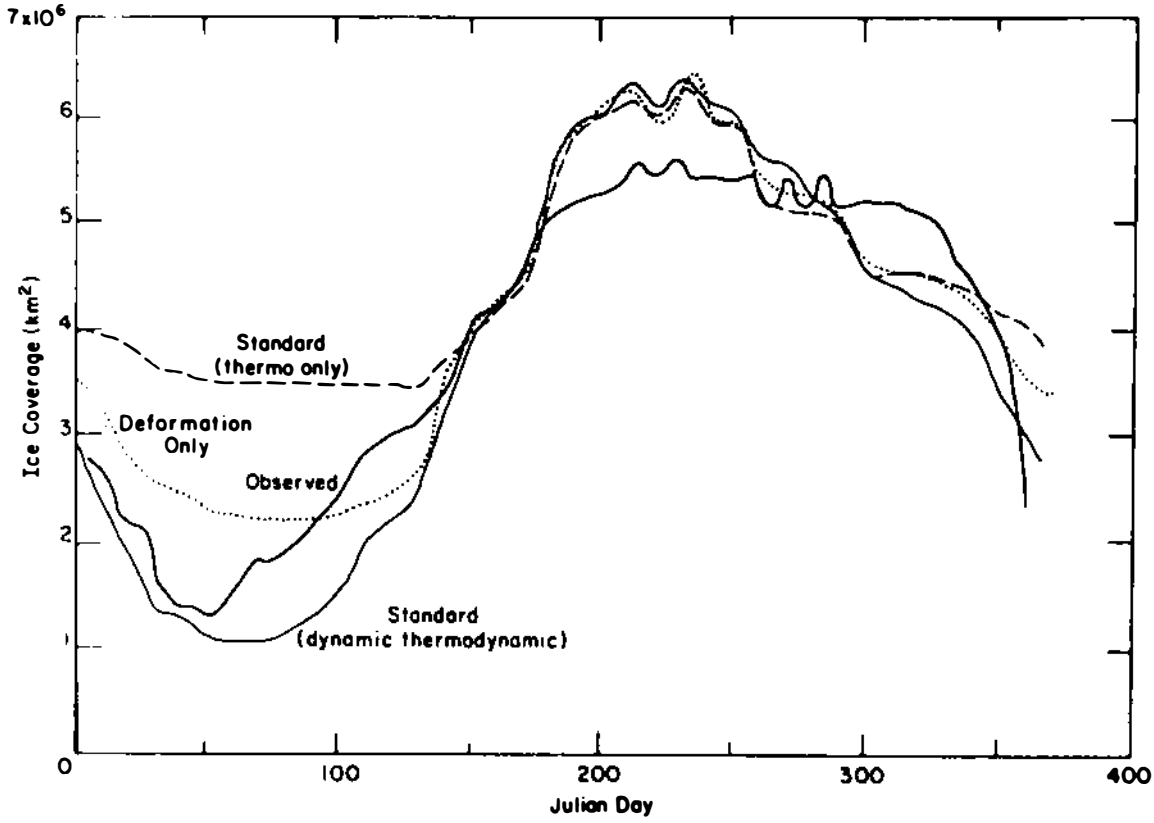


**Figure 8. Effect of ice dynamics on a sea-ice model's seasonal cycle of ice coverage in the Weddell Sea. (From Hibler and Ackley 1983.)**

Although none of these models has reproduced all the large-scale features of the Southern Ocean ice cover, they have had success in reproducing some of the major characteristics. For example, for the Parkinson and Washington model, the successes include the late February timing of minimum ice extent, the September timing of maximum ice extent, the prevalence of summer ice in the Western Hemisphere, the asymmetric pattern of winter ice, with the ice edge extending farthest equatorward at about the Greenwich Meridian, and the autumnal development of a tongue of ice in the Weddell Sea, with the subsequent formation of a Weddell Polynya (Parkinson and Washington 1979; Parkinson 1983; Parkinson and Bindschadler 1984). This model realistically simulates the emergence of the Weddell Polynya through the encircling (thermodynamically controlled) of an open-water region by ice (Figure 9).

However, in spite of the successes, there are still significant contrasts between the observed and simulated sea-ice distributions, as illustrated, for example, in Figures 10 and 11. Part of the difficulty derives from inadequate formulations of the atmospheric and oceanic boundary conditions. Improvement in those conditions could be the single most effective way of improving the correspondence between modeled and observed sea-ice distributions. However, it would not lessen a more fundamental difficulty regarding the use of these models

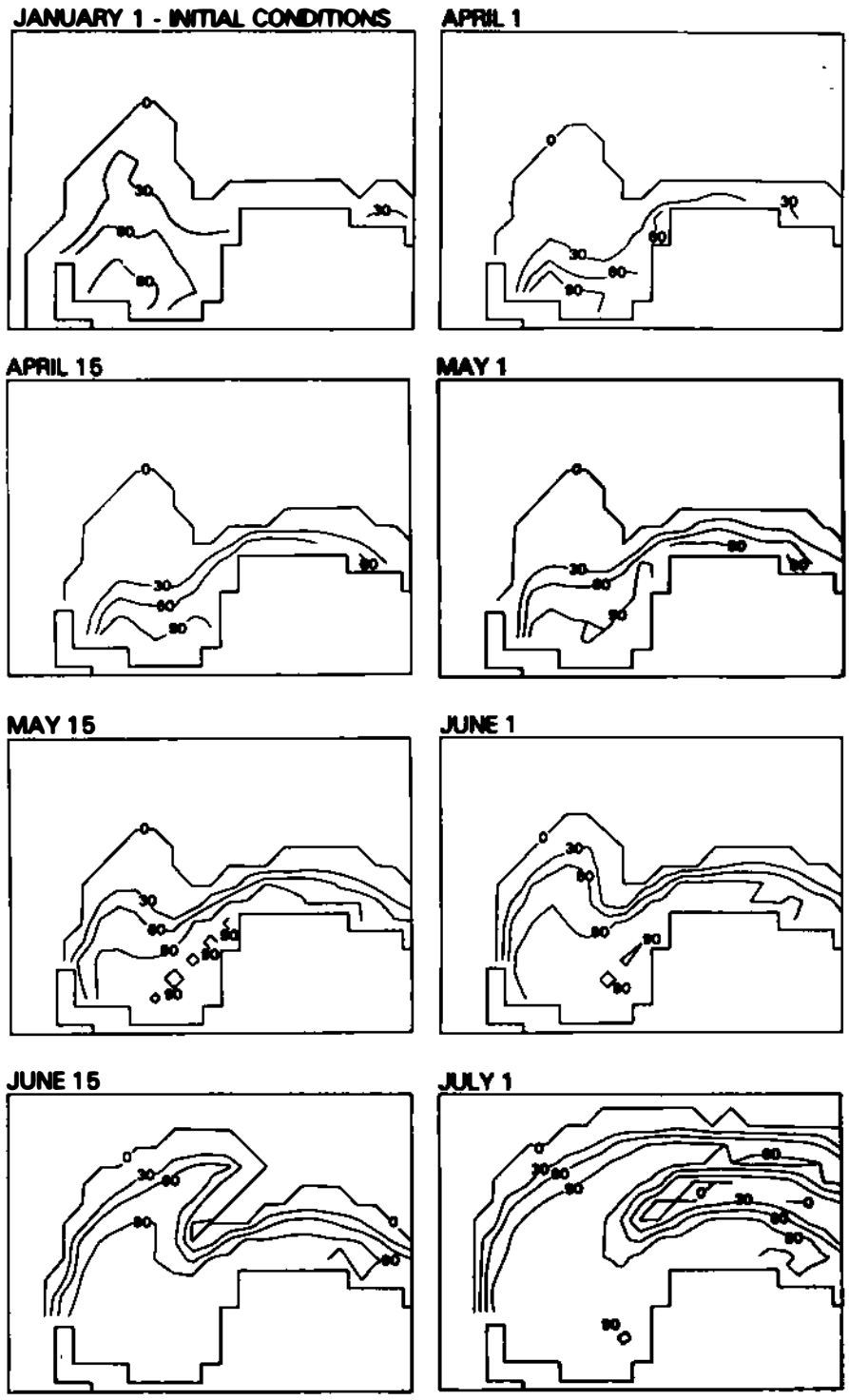


**Figure 9. Simulated development of the Weddell Polynya. Contours are drawn for sea-ice concentrations of 0, 30, 60, and 90 percent. (From Parkinson 1983.)**

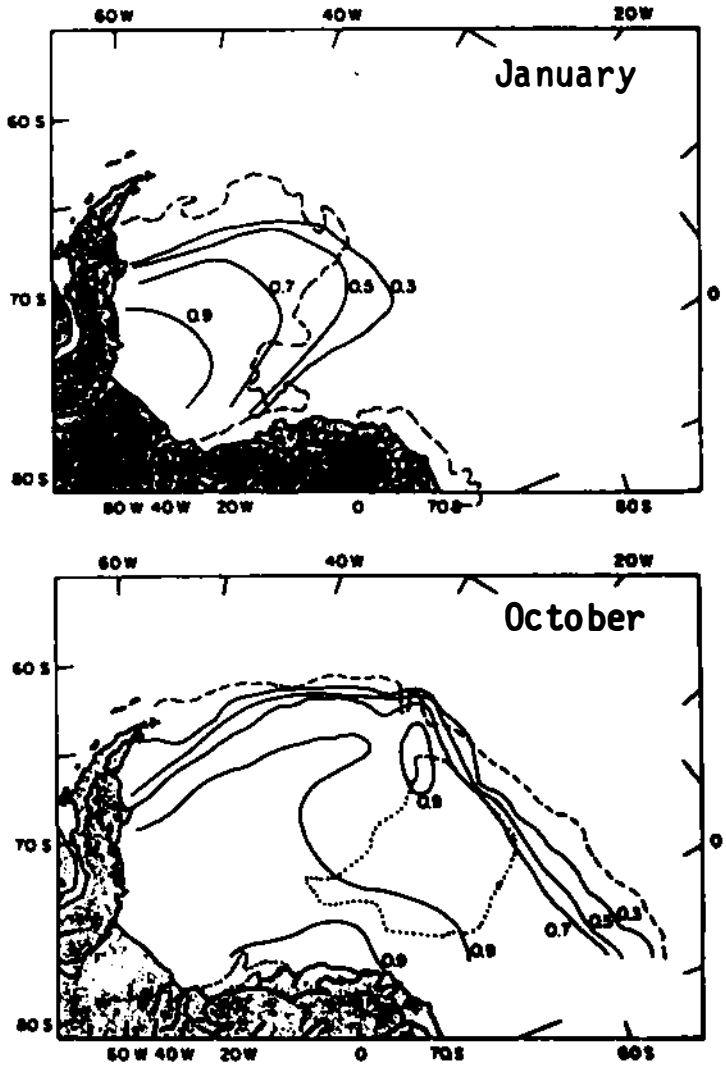


**Figure 10. January and October sea-ice concentrations computed from a dynamic/thermodynamic model of the Weddell Sea (solid lines). The dashed lines indicate the location of the observed 50 percent ice concentration contour, and the dotted lines indicate the location of observed polynyas. (From Hibler and Ackley 1983, with relabeling.)**

for examining climatic change. The difficulty is that these are all stand-alone sea-ice models, not allowing the ice conditions to feed into the oceanic and atmospheric calculations. As sea ice, ocean, and atmosphere are intricately connected in the real world, there is the need for numerical coupling of these three components of the climate system, a need that is particularly critical when trying to simulate future states.

Coupled models, however, will not necessarily produce sea-ice distributions that are improved over those of the stand-alone models. Errors in the calculated ocean and atmospheric fields in the coupled

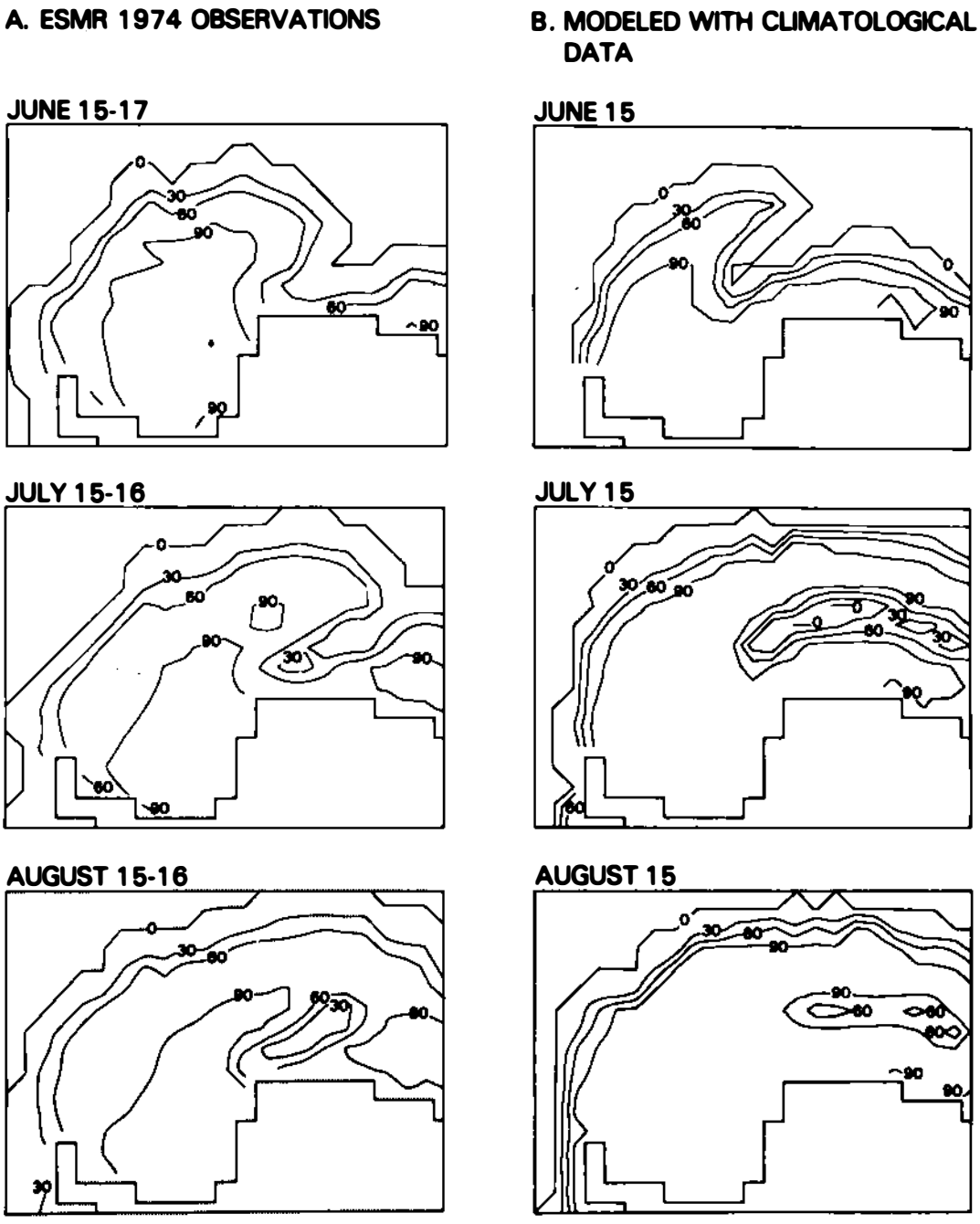


**Figure 11. Observed and simulated ice concentration contours (percentages) in the Weddell Sea in mid-June, July, and August (from Parkinson 1983). The observations have been averaged to the 200-km resolution of the model.**

models will probably adversely affect the sea-ice calculations. Indeed, the studies that have been done with coupled models (e.g., Manabe et al. 1975, 1979; Manabe and Stouffer 1980; Washington et al. 1980; Bryan et al. 1982) have tended to produce sea-ice distributions that are less realistic than those produced by uncoupled models.

For example, the simulations of Washington et al (1980), in which sea ice is treated strictly thermodynamically, result in far too little Southern Ocean ice, with no ice in April and the ice in the rest of the year restricted mainly to the Ross and Weddell seas (Figure 12). The difficulty derives from simulated sea surface temperatures in the Southern Ocean that are warmer than those observed by from 1 to 5 K, a problem also encountered by Manabe et al. (1979). The warm sea surface temperatures derive from the coarseness of the model grid and the excess diffusion of heat (Washington et al. 1980). Such compounding of difficulties can be expected in all early attempts at coupling.

Two modeling studies directly relevant to the issue of the impact of $CO_2$ increases on the West Antarctic sea ice are those of Parkinson and Bindschadler (1984) and Manabe and Stouffer (1980). By running a dynamic/thermodynamic sea-ice model of the Southern Ocean with mean monthly climatological temperatures, and then with temperatures uniformly increased by 1, 3, and 5 K in three subsequent model runs, Parkinson and Bindschadler determine that with a 5 K temperature increase the modeled winter ice cover is reduced by about 50 percent and the modeled summer ice cover vanishes everywhere except in one grid square in the Amundsen Sea (Figure 13). With a 3 K temperature increase, summer ice is restricted to the Amundsen Sea and the southwestern portion of the Weddell Sea. These results complement the

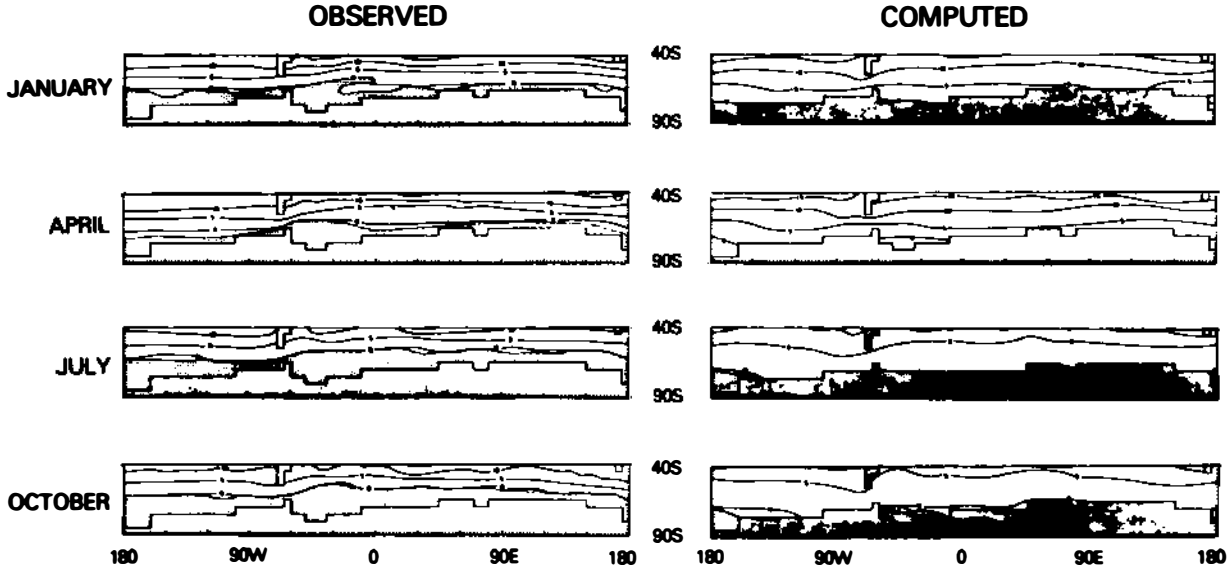


Figure 12. Observed and computed Southern Ocean sea-ice limits (stippled areas), the computed extents coming from a coupled ocean-ice-atmosphere model. (Rearranged from Washington et al. 1980, and relabeled.)

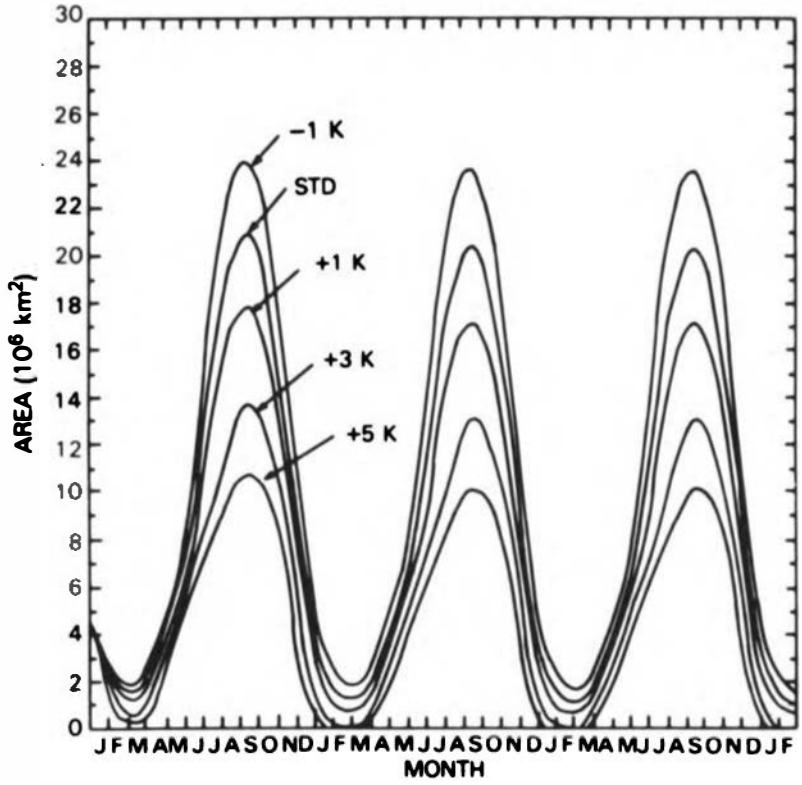


**Figure 13. Time sequences for the total ice area in the Southern Ocean as simulated with mean monthly climatological data (the standard case) and with the climatological temperatures uniformly increased by −1, +1, +3, and +5 K. (From Parkinson and Bindschadler 1984.)**

results from atmospheric climate models that a $CO_2$ doubling could be expected to increase global average temperatures by about 3 K and polar temperatures by perhaps 5 K or more. Parkinson and Bindschadler calculate a hemispherically averaged latitudinal retreat rate of the ice edge of 1.4°S per 1 K increase in temperature.

Manabe and Stouffer (1980) use a coupled ocean-ice-atmosphere general circulation model to compare results for a standard case versus a case with the concentration of atmospheric $CO_2$ increased to 4 times its present value. Antarctic sea ice in the standard case is, as in Washington et al.'s (1980) results, too sparse (see Manabe and Stouffer, 1980, Figure 11), the reason being that the simulated surface air temperatures in the region of the Southern Ocean are too low. Thus, although sea ice vanishes for much of the year in the 4 x $CO_2$ case, the simulated contrast in the two cases may still be low. Nonetheless, by including sea ice, Manabe and Stouffer have allowed the lessened amounts of sea ice resulting from increased $CO_2$ to feed back to the atmospheric calculations, thereby increasing the realism of the foundations of the climate simulations.

## REFERENCES

Ackley, S. F., 1981. A review of sea-ice weather relationships in the southern hemisphere. In Sea Level, Ice, and Climatic Change. IAHS Publication 131 (pp. 127-159). International Association of Hydrological Sciences, Canberra, Australia.

Ackley, S. F. and T. E. Keliher, 1976. Antarctic sea ice dynamics and its possible climatic effects. AIDJEX Bulletin, 33, 53-76.

Bryan, K., F. G. Komro, S. Manabe, and M. J. Spelman, 1982. Transient climate response to increasing atmospheric carbon dioxide. Science, 215, 56-58.

Budd, W. F., 1975. Antarctic sea-ice variations from satellite sensing in relation to climate. Journal of Glaciology, 15, 417-427.

Campbell, W. J., 1964. On the Steady-State Flow of Sea Ice. Report to the Office of Naval Research under Contract NR 207-352 (167 pp.). Department of Atmospheric Sciences, University of Washington, Seattle.

Cavalieri, D. J. and C. L. Parkinson, 1981. Large-scale variations in observed Antarctic sea ice extent and associated atmospheric circulation. Monthly Weather Review, 109, 2323-2336.

Chiu, L. S., 1983. Variation of Antarctic sea ice: an update. Monthly Weather Review, 111, 578-580.

Coon, M. D., 1980. A review of AIDJEX modeling. In Sea Ice Processes and Models (pp. 12-27). University of Washington Press, Seattle.

Hibler, W. D., III, 1979. A dynamic thermodynamic sea ice model. Journal of Physical Oceanography, 9, 815-846.

Hibler, W. D., III and S. F. Ackley, 1983. Numerical simulation of the Weddell Sea pack ice. Journal of Geophysical Research, 88 (C5), 2873-2887.

Kukla, G. and J. Gavin, 1981. Summer ice and carbon dioxide. Science, 214, 497-503.

Lemke, P., E. W. Trinkl, and K. Hasselmann, 1980. Stochastic dynamic analysis of polar sea ice variability. Journal of Physical Oceanography, 10, 2100-2120.

Manabe, S. and R. J. Stouffer, 1980. Sensitivity of a global climate model to an increase of $CO_2$ concentration in the atmosphere. Journal of Geophysical Research, 85, 5529-5554.

Manabe, S., K. Bryan, and M. J. Spelman, 1975. A global ocean-atmosphere climate model. Part 1. The atmospheric circulation. Journal of Physical Oceanography, 5, 3-29.

Manabe, S., K. Bryan, and M. J. Spelman, 1979. A global ocean-atmosphere climate model with seasonal variation for future studies of climate sensitivity. Dynamics of Atmosphere and Oceans, 3, 393-426.

Martinson, D. G., P. D. Killworth, and A. L. Gordon, 1981. A convective model for the Weddell Polynya. Journal of Physical Oceanography, 11, 466-488.

Maykut, G. A. and N. Untersteiner, 1971. Some results from a time-dependent thermodynamic model of sea ice. Journal of Geophysical Research, 76, 1550-1575.

Parkinson, C. L., 1983. On the development and cause of the Weddell Polynya in a sea ice simulation. Journal of Physical Oceanography, 13, 501-511.

Parkinson, C. L. and R. A. Bindschadler, 1984. Response of Antarctic sea ice to uniform atmospheric temperature increases. In Climate Processes and Climate Sensitivity, Maurice Ewing Volume 5. Geophysical Monograph 29. American Geophysical Union, Washington, D.C.

Parkinson, C. L. and D. J. Cavalieri, 1982. Interannual sea-ice variations and sea-ice/atmosphere interactions in the Southern Ocean, 1973-1975. Annals of Glaciology, 3, 249-254.

Parkinson, C. L. and W. M. Washington, 1979. A large-scale numerical model of sea ice. Journal of Geophysical Research, 84, 311-337.

Pease, C. H., 1975. A model for the seasonal ablation and accretion of Antarctic sea ice. AIDJEX Bulletin, 29, 151-172.

Semtner, A. J., Jr., 1976. A model for the thermodynamic growth of sea ice in numerical investigations of climate. Journal of Physical Oceanography, 6, 379-389.

Washington, W. M., A. J. Semtner, Jr., C. L. Parkinson, and L. Morrison, 1976. On the development of a seasonal change sea-ice model. Journal of Physical Oceanography, 6, 679-685.

Washington, W. M., A. J. Semtner, Jr., G. A. Meehl, D. J. Knight, and T. A. Mayer, 1980. A general circulation experiment with a coupled atmosphere, ocean and sea ice model. Journal of Physical Oceanography, 10, 1887-1908.

Zwally, H. J., J. C. Comiso, C. L. Parkinson, W. J. Campbell, F. D. Carsey, and P. Gloersen, 1983a. Antarctic Sea Ice 1973-1976: Satellite Passive Microwave Observations, NASA Special Publication SP-459 (206 pp.). National Aeronautics and Space Administration, Washington, D.C.

Zwally, H. J., C. L. Parkinson, and J. C. Comiso, 1983b. Variability of Antarctic sea ice and changes in carbon dioxide. Science, 220 (4601), 1005-1012.